PROCEEDINGS OF THE IRE

Published Monthly by

The Institute of Radio Engineers, Inc.

VOLUME 44 — *February, 1956* — NUMBER 2

CONTENTS

ADVERTISING SECTION

THE COVER—The growing use of transistors has brought about substantial changes in the design and manufacture of other circuit components used in transistorized equipment. The miniature IF transformers pictured in the two left-hand photographs on the cover are less than one-fifth the size of the standard models shown beside them. In the lower right, miniature transformer coils are being wound, assembled, soldered and checked for use in a pocket-size transistor radio.

Photos—*Geo. Stevens Mfg. Co., Inc.* and *Radio Industries, Inc.*

Scanning the Issue

The purpose of this page, which henceforth will be a regular feature each month, is to provide the general reader with a brief and helpful guide to the papers in the issue. These "program notes" are intended to indicate not only what is *in* the papers but also what is *behind* them—what their significance is, to whom they will be of interest and, by implication, why they are being published. These notes will be prepared by the Managing Editor with the assistance of Editorial Reviewers and others. Your comments on its usefulness are earnestly solicited by the Editorial Board.—*The Editor*

Magnetic Core Circuits for Digital Data-Processing Systems (p. 154)—The general reader who is unfamiliar with the inner workings of a digital computer will welcome this easy-to-read tutorial discussion of a promising type of computer component, the magnetic core, and how it is being used to perform storage, control and logical operations which are basic to a data-processing system. The computer specialist will be especially interested in two new interconnecting circuits which greatly increase the versatility with which data-transfer and logical operations may be carried out, and in the novel symbolism used by the authors to represent the operation of these circuits.

Long-Range Propagation of Low-Frequency Radio Waves between the Earth and the Ionosphere (p. 163)—Most of our communication services have migrated from the low end of the frequency spectrum to higher and greener pastures where they can use smaller antennas, lower transmitter power, and are relatively free of atmospheric noise. The vlf band (below 30 kc) has thus lain more or less fallow for many years. Recently, however, there has been a marked revival of interest in the low frequencies because they offer a reliable way of communicating over global distances. Equally important, they are blessed with highly stable propagation characteristics which make it possible to transmit data to distant points with unusual fidelity and precision. This promises to open the door to new and important uses of long-range systems where great accuracy is required, such as very-long-range radio navigation systems and international transmission of frequency standards. By showing that these low-frequency radio waves are propagated in the space between the earth's surface and the ionosphere in much the same manner as in a waveguide, this paper makes an important and timely contribution to our understanding of a subject which has broad implications for the future.

Artificial Dielectrics Utilizing Cylindrical and Spherical Voids (p. 171)—Microwave lenses have important applications as antennas for radars and point-to-point microwave links. In many cases these antennas must be rotated or are supported by towers. Their weight, therefore, is an important consideration. There has been considerable investigation of lens materials which are very much lighter than the usual dielectric materials and of artificially producing the desired dielectric constant by imbedding metallic objects in the material. The artificial dielectrics produced this way thus far have been somewhat limited in usefulness because they are not strong enough structurally to withstand shock and vibration. This paper proposes embedding voids in materials of greater mechanical strength, investigates the dielectric constants that result, and presents measurements that will be useful to the further development of microwave lenses.

Broadband Microwave Frequency Meter (p. 175)—At microwave frequencies certain materials exhibit a property called paramagnetic resonance which is characterized by a noticeable increase in absorption of microwave energy by the material. The frequency at which this absorption occurs may be controlled by varying the strength of an externally applied magnetic field. This phenomenon has been utilized by the authors to produce a totally new method of measuring microwave frequencies over a very wide range. This development will not only be of widespread interest and utility but may also lead to other useful applications of paramagnetic resonance absorption.

The Frequency Response of Bipolar Transistors with Drift Fields (p. 178)—The operation of junction transistors is quite well understood, but there remain some substantial gaps in our understanding of point-contact transistors. One reason is that the internal mechanisms by which a transistor functions are a great deal more complicated in the point-contact case, so much so that it becomes extremely difficult to analyze them mathematically. In this paper the author develops a simplified model of these mechanisms which can be readily analyzed and gives reasonably accurate results. Consequently, he is able to calculate one of the most important design characteristics of a transistor, namely, the frequency cutoff, thus filling in an important area of design theory not adequately covered heretofore.

Transistor Fabrication by the Melt-Quench Process (p. 185)—The fabrication process has been an especially critical factor in the development of the transistor and is, consequently, a matter of more than usual interest and importance. To obtain a transistor with the desired characteristics requires a delicate control of many interrelated factors during the manufacturing process. A factor of special interest is obtaining a close spacing between the junctions since this determines to a great extent the frequency of operation. The technique presented here of controlling this spacing solely by thermal treatment of the material during the fabrication process offers a promising method of producing high frequency transistors.

RF Bandwidth of Frequency-Division Multiplex Systems Using Frequency Modulation (p. 189)—This paper tackles one of the major problems facing designers of FM multichannel microwave systems, i.e., intermodulation distortion. Specifically, the author analyzes how much distortion is caused by limiting the bandwidths of the rf networks in the system. He succeeds in developing for the first time a simple practical procedure for obtaining a reliable estimate of the minimum bandwidth that can be tolerated for a specified system performance. Not only are the results of this work useful and important in their own right but appear capable of extension to other fields.

Design Information on Large-Signal Traveling-Wave Amplifiers (p. 200)—With a minimum of discussion, this paper presents, in a list of 10 conclusions and 24 design curves, a great deal of valuable information on how to design traveling-wave amplifiers to operate at high power levels with better efficiency.

The Polarguide—A Constant Resistance Waveguide Filter (p. 210)—By employing waveguide components instead of the usual coaxial-line com-

(*Continued on page 100A*)

Poles and Zeros

Why P & Z? Beginning with this issue, and continuing in as many succeeding ones as it appears to serve a purpose, "Poles and Zeros" will appear as a regular page of editorial comment on matters of concern to the IRE membership. Initially, as below and in the next several issues, P & Z will be devoted to the editorial program of the IRE, describing its purposes and mechanisms, acknowledging constructive criticism, keeping track of the dynamics of publication policy. Later, unless by then howled out of existence, attention is planned for other IRE vineyards where the grapes are ready for the trampling.

Choosing a title for a page of editorial comment is an indoor sport having two rules: It should have some connection with the central theme of the journal, and it should have implications beyond its literal meaning. The literal connotation has to do with the design of electrical networks (probably the most recurrent topic in the PROCEEDINGS), since poles and zeros are the roots of the polynomial used to analyze and design circuit systems. The broader implication comes from a free translation from Webster, according to which poles are extremes of opinion and zeros are middle ground, points between negative and positive. No editor could ask for more room than that!

Language. As of January 1, 1956, the Institute had 47,388 dues-paying members. All these profess a nominal interest in radio, but only a minority would insist that "radio engineer" best describes their calling. The membership statistics show a wide variety of occupations, so wide in fact that the IRE is now recognized, pre-eminently among engineering societies, as a confederation of workers in different fields.

This recognition has caused interested observers, notably the directors of other engineering societies, to ask "What can 47,388 technical specialists possibly have in common that would cause them to swarm in such numbers?" This is a good question for internal consumption. What causes the IRE to be the fastest-growing engineering society? And is the condition healthy? Sound muscle? Or elephantiasis?

There can be little doubt that large and growing membership confers real benefits, as witness the outstanding staff and facilities at headquarters, the extraordinary breadth of publication activity, the conventions, conferences and meetings covering a hundred different areas of general and special interest. There is certainly no disadvantage in size itself, so long as the individual member gets what he wants, in sufficient abundance to warrant continued support. So the question of what makes IRE tick resolves not to size, but to the values assigned by each member to his membership.

IRE membership has definite professional significance. The higher grades carry real prestige, so much so that hard work in and for the IRE is not unrelated to take-home pay. Among the tangible benefits are the PROCEEDINGS and the other IRE publications, of which more in later issues. Second only to the printed word comes the oral presentation of technical papers. By any count the IRE is the league leader for sheer volume of oral output, and it ranks high in the first division for quality.

All this, however, does not suffice to explain the IRE. Other societies have similar programs and confer similar benefits on their members, but few indeed are burgeoning in the same fashion. The explanation of the Institute's strength lies not only in these traditional values but also in the possession of a *technical language* of unique power and comprehension. To a degree unmatched among professional people (except possibly in medicine), one type of specialist can understand and respect other specialists with whom he associates in IRE because they use so many words and concepts in common. Take the concept of Q as an example, and consider Frank Lewis' excellent paper "Frequency and Time Standards" published here last September. Lewis used Q to describe conventional tuned circuits, quartz crystal vibrations, and ammonia atom resonances, with equal facility.

If we agree that language is the common denominator on which the IRE confederation rests, we must conclude that making the best possible use of language is the central responsibility in IRE management. The responsibility falls first and fundamentally on the authors of the papers, but it also lies heavy on the editors, reviewers and program committee members who exercise the power of selection.

Most important, the responsibility can be acquitted only through a dynamic publications and editorial policy, fully responsive to the needs of *all* the members, yet beneath the dignity or outside the interest of *none*. It is indeed difficult to define the correlations or need, interest and dignity among 47,388 members, but define them we must.

The editorial computer, moreover, cannot produce a valid output without an input which truly represents the IRE matrix. Few IRE members bother to make their position clear, or to take a stand, on Institute publications policy. More, many more, must do so if we are to make optimum use of oral and printed publications. The Editorial Board welcomes, and guarantees to consider carefully, all communications from members suggesting improvements in our editorial program. —*The Editor*

Herre Rinia

VICE-PRESIDENT, 1956

Herre Rinia was born at Cornwerd, Friesland, Netherlands, on March 30, 1905. He studied electrical engineering at the Delft Institute of Technology, from which he obtained his diploma in 1928.

In 1928, following his graduation, he joined the staff of the Philips Research Laboratories at Kastanjelaan, Eindhoven, Netherlands. He was employed on problems concerning radio components, facsimile, and television. When later he was promoted to group leader, he directed work on optics and caloric engines. In 1946, he was appointed co-director of research, and in this capacity he has made several visits to the United States.

He has published over fifteen technical papers, and he is the holder of over eighty patents from the United States, Netherlands, France, and Great Britain. He has made significant contributions to developments in the fields of radio and television reception, optics, and the Sterling cycle hot air engine.

He is a member of the Royal Institution of Engineers, Dutch Physical Society, English Institute of Electrical Engineers, Astronomical Society of France, and the International Television Committee. In 1947 he was awarded membership in the Koninklijke Nederlandse Akademie van Wetenschappen.

Mr. Rinia joined the IRE as a Senior Member in 1951, and in 1954 he received an IRE Fellow Award "for his creative contributions to radio engineering in Holland, and his leadership in the field of television."

The New IRE Professional Group on Military Electronics

C. L. ENGLEMAN, *Chairman*

It is safe to say that no organization related to the science of electronics can be free from an interest in the Military when close to one-half of the funds expended in the field comes from defense establishment appropriations. It therefore follows that all IRE groups have a keen interest in Military Electronics, a top weapon for defense in the security of the free world.

It is well for all of us to be interested in Military Electronics, but this is, by no means, a one-way street. It is equally desirable for the Military to be interested in the Institute of Radio Engineers and to take advantage of the vast potential assistance it offers. This is one of the major reasons for establishing an IRE Professional Group on Military Electronics. We believe the Military will show an increased enthusiasm in the IRE through a Professional Group on Military Electronics which can offer both technical and social benefits.

A major general of the U. S. Army recently wrote to me and said: "Heretofore, our electronics concept has been either a wartime concept or a peacetime concept. In war, IRE as well as other agencies mobilized promptly to support the Military. In true peacetime there has been little interest shown in the electronics problem of the Military. Few have thought of the real needs for an in-between IRE concept such as the present cold war imposes."

IRE really has no central agency for our assistance to the Military in the over-all technical aspects of national policy, regulations and coordination in the fields of manpower, education, operations, industry, the sciences, and especially in the field of international electronics where our security is at stake. In short, it is hoped that these and other deficiencies in the IRE will be improved by the new IRE Professional Group on Military Electronics (PGMIL) which was approved by the IRE Executive Committee in September, 1955. Its scope is defined as follows: "The field of interest of this group shall be concerned with the electronic sciences, systems, activities and services germane to the requirements of the Military, subject to the IRE Committee on Professional Groups. In addition, this group will aid other Professional Groups of the IRE in their liaison with and services to the Military through joint meetings and activities, and by other appropriate means, always keeping alert to the specific fields of interest of other Professional Groups."

The importance of this group to the Military is reflected in the National Administrative Committee military membership. Included are the Director of the Communications and Electronics Committee of the Joint Chiefs of Staff, the Chief of Naval Research, the Chief of the Research and Development Division of the Office of the Chief Signal Officer, the Chief of the Radar and Communications Division of the Air Research and Development Command, the Director of Engineering of the Signal Corps Engineering Laboratory, the Technical Director of the Naval Sciences Division of the Office of Naval Research, and the Technical Director of the Wright Air Development Center. The rest of the committee is composed of a distinguished group of civilian scientists and industrialists, all of whom have served with the Military and have an understanding of their problems.

Inquiries regarding membership or the formation of chapters in this new Professional Group on Military Electronics would be welcomed. Please direct all inquiries to IRE headquarters at 1 East 79 Street, New York 21, New York.

Magnetic Core Circuits for Digital Data-Processing Systems*

D. LOEV†, ASSOCIATE MEMBER, IRE, W. MIEHLE‡, MEMBER, IRE, J. PAIVINEN‡, ASSOCIATE MEMBER, IRE, AND J. WYLEN‡, ASSOCIATE MEMBER, IRE

Summary—**A magnetic core has a switching time of a few microseconds and has the ability to store binary information indefinitely without application of power. New techniques for using cores in digital data-processing systems are described. Reference is made to a system containing eight hundred cores to indicate reliability, and size and power requirements relative to a vacuum tube version.**

Three fundamental interconnecting circuits for data transfer are described. These are the single-diode loop, and a new split winding loop, and new inhibit loop. The single-diode loop permits unconditional transfer of information from one or more transmitting cores to one or more receiving cores. The split-winding loop allows conditional transfer between cores and thus permits logical operations upon isolated cores. The inhibit loop offers a reliable method for conditionally inhibiting the transfer of information from one core to another. A logical symbolism for these loops has been found useful in system design and analysis.

Units performing the functions of storage, control, and logic are explained. These are shift registers (serial, parallel, and reversible); cycle distributors and counters; negation, inclusive-or, conjunction, exclusive-or, and material equivalence (compare).

System design considerations are illustrated by two examples of half-adders.

Introduction

THE CORES considered in this paper are small toroidal ferromagnetic cores characterized by a rectangular hysteresis loop and microsecond switching time. The ability of a core to store binary information reliably and without power dissipation, and the ease with which the information can be transferred in a few microseconds make the magnetic core a useful and versatile computer component.

Magnetic-core circuits have been used to realize most of the essential functions of a digital data-processing system. These are storage[1–3] or delay, control, and logical operations.[4,5] Several new circuits are presented. These are adaptable to applications in serial, parallel, and reversible magnetic shift registers, and cycle distributors and counters. Circuits for realizing the logical functions of NEGATION, OR, AND, and EXCLUSIVE-OR are described. All of these circuits can be interconnected to provide magnetic-core digital data-processing systems which offer reliable operation with small power dissipation, space and weight saving, ruggedness, and long life.

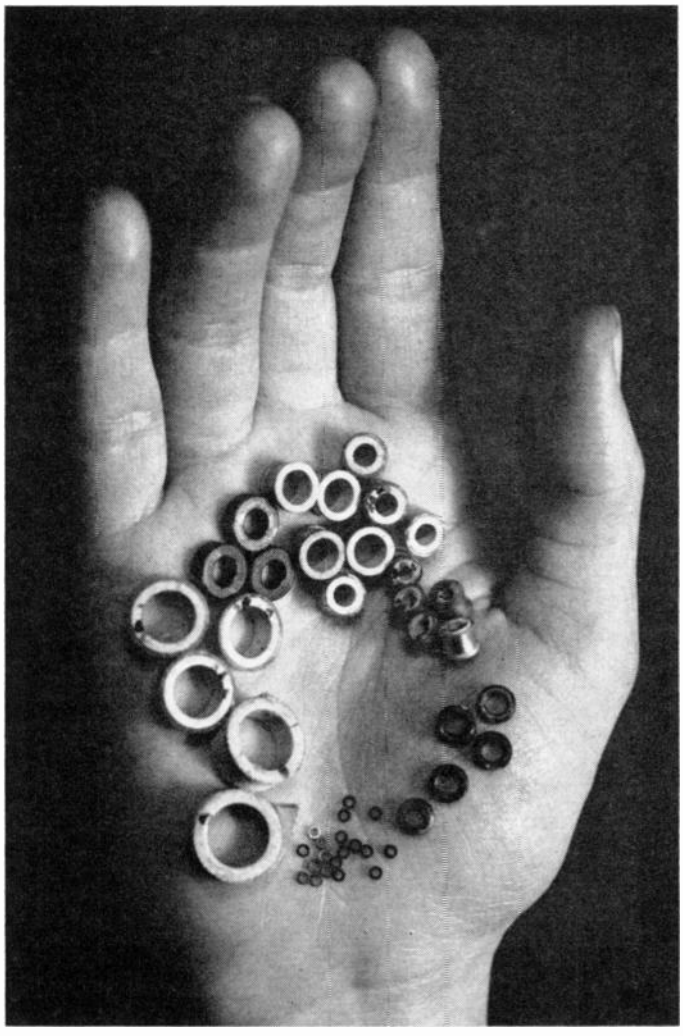

Fig. 1—Examples of cores.

The Magnetic Core

Fig. 1 shows a handful of cores of both the ferrite and metallic ribbon varieties.[6] The ferrites are characterized by high resistivity, low flux density, and large coercivity. They have gained prominence by their application in high speed coincident-current magnetic

* Original manuscript received by the IRE, April 22, 1955; revised manuscript received, September 12, 1955.

† Now Weizmann Institute, Rehevoth, Israel.

‡ Burroughs Research Center, Paoli, Pa.

[1] J. W. Forrester, "Digital information storage in three dimensions using magnetic cores," *Jour. Appl. Phys.*, vol. 22, pp. 44–48; January, 1951.

[2] I. L. Auerbach, "A static magnetic memory system for the ENIAC," *Proc. ACM*, Richard Rimbach Assn., pp. 213–222; May 2–3, 1952.

[3] A. Wang, W. D. Woo, "Static magnetic storage and delay line," *Jour. Appl. Phys.*, vol. 21, pp. 49–54; January, 1950.

[4] R. A. Ramey, "The single-core magnetic amplifier as a computer element," *AIEE Trans.*, Part I, vol. 71, pp. 342–346; January, 1953.

[5] S. Guterman, R. D. Kodis, "Circuits to perform logical and control functions with magnetic cores," *1954 IRE Convention Record*, Part 4, pp. 124–132.

[6] J. Wylen, "Pulse response characteristics of rectangular-hysteresis-loop ferromagnetic materials," *AIEE Trans.*, Part I, vol. 71, pp. 648–655; November, 1953.

memories.[7] The ultra-thin metallic ribbon cores are fabricated with $\frac{1}{8}$ to 1 mil gage alloy wrapped on ceramic bobbins. These are characterized by medium to high flux density and small coercivity. Metal cores fabricated with $\frac{1}{8}$ m 4–79 Molybdenum Permalloy ribbon, $\frac{1}{8}$ inch wide, have been used in core circuits described here.

Fig. 2(a) shows an idealized rectangular hysteresis loop, and will serve to illustrate the useful binary property of a core. The positive state of residual magnetization ($+B_r$) will be referred to as the ONE state, and the negative state of residual magnetization ($-B_r$) will be referred to as the ZERO state. Application of a pulsed magnetizing force (H) of sufficient amplitude and duration will set the core into the desired binary state. In the discussion below, the state of the core is usually sensed by the application of $-H_m$. If the core is in the ZERO state, a small change in flux density ΔB_n will result; if the core is in the ONE state, a large change in flux density ΔB_s will result. The ratio of residual to maximum flux densities, called the "squareness ratio," is a measure of the quality of a core.

Fig. 2(b) compares typical signal and noise voltage wave-forms induced in a winding on the core by the changes ΔB_s and ΔB_n, respectively. Signal-to-noise flux density ratios greater than twenty to one are obtained with commercially available cores. The signal voltage duration is usually on the order of one to ten microseconds, depending on the core material, the applied magnetizing force, and the load.

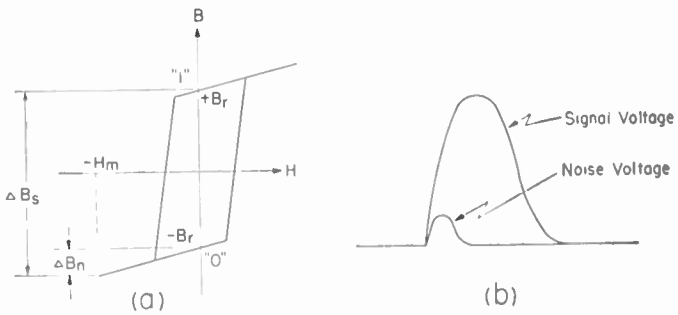

Fig. 2—(a) Idealized dc hysteresis loop. (b) Signal and noise output voltages from core.

Symbolic Representation

As a preliminary step in the design of magnetic-core systems it has been found helpful to use a simplified functional representation. Its purpose is to make the process of design easier and the functioning of the system more understandable, and to serve as a basis for circuit design.

The core is represented by a circle. A line with an arrow pointing to the circle (Fig. 3(a)) represents an input to the core, setting it to the binary state indicated just inside the circle. Open arrows imply pulses, and closed arrows indicate dc signals. Double arrowheads of either type serve to indicate that the existence of this input will hold the core to that state despite the presence of other input signals. The symbol on the input line may indicate either the time at which the input occurs (*e.g.*, t_1 is defined to mean an unconditional input at time t_1) or the data designation and the time the data may appear (*e. g.*, p $[t_3]$ is defined to mean that if p occurs, it will be at time t_3).

Lines originating at the circle represent output circuits. A signal is present on the output line when the core is switched to the state shown nearest the line inside the circle. Thus in Fig. 3(b), a signal p exists only if P_1 or P_2 exists and if the core had initially been in the ONE state. Signals q_1 and q_2 exist only when Q is applied, and then only if core had initially been in ZERO state.

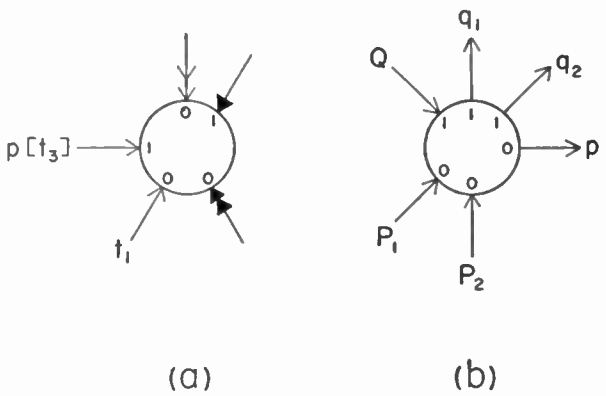

Fig. 3—(a) Core inputs, symbolic representation. (b) Core outputs, symbolic representation.

Fundamental Transfer Loops

The transfer loop is the circuit that connects two or more cores for the purpose of information transfer. The transfer loop normally includes the output windings of transmitting cores, the input windings of receiving cores, and one or more diodes.

A magnetic core may be used either as a controllable transformer or as a variable impedance. Fig. 4(a) illustrates the transformer action. Conventional dot notation is used to indicate winding polarity, with the additional definition that current into a dot terminal corresponds to a negative magnetizing force and will set the core to the ZERO state. If, in Fig. 4(a), the core is initially in the ONE state and current I_0 is applied, the core will switch to the ZERO state. The induced output voltage e_0 will correspond to a signal voltage (Fig. 2(b)) and will be relatively large. If, however, the core is in the ZERO state when I_0 is applied the core will not switch. Output voltage e_0 will correspond to a noise voltage and will be relatively small.

Fig. 4(b) illustrates the impedance concept of a magnetic core. If the core is in the ONE state when I is applied, the core will switch. A relatively large counter-emf (e) will be generated in winding N_1, and the core will look like a relatively large impedance to the driving source. If, however, the core is in the ZERO state when I is applied the counter-emf will be small and

[7] Forrester, *loc. cit.*

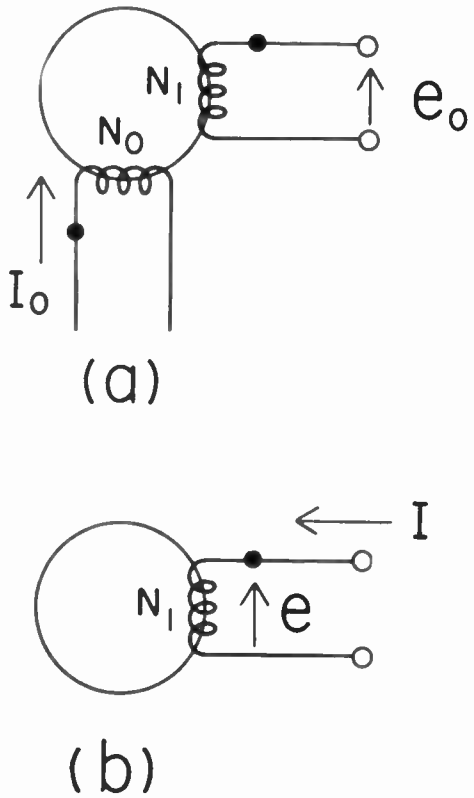

Fig. 4—(a) Core as transformer. (b) Core as impedance.

the core will appear almost as a short circuit to the driving source.

In the discussion below, cores are always assumed to be initially in the ZERO state unless otherwise noted.

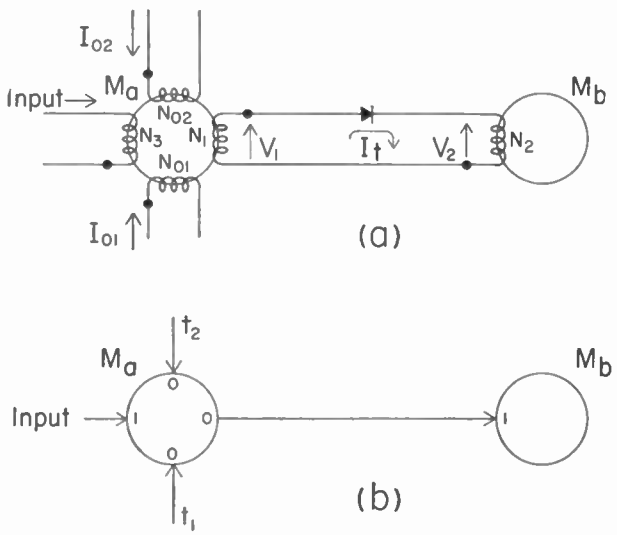

Fig. 5—(a) Single-diode transfer loop, schematic. (b) Single-diode transfer loop, symbolic representation.

Single-diode Transfer Loop

Fig. 5(a) shows schematically a single-diode transfer loop connecting core M_a to core M_b. The core is again represented by a circle. Assume that core M_a is initially in the ONE state and that M_b is in the ZERO state. To transfer the ONE from M_a to M_b, advance current I_{01} is applied through winding N_{01}. As core M_a switches to the ZERO state, the signal voltage V_1 is induced in winding N_1. This causes transfer current I_t to flow in the transfer loop. By judicious choice of the diode and proper design of windings N_1 and N_2, the transfer current I_t flowing through winding N_2 will be sufficient to switch core M_b to the ONE state. Additional receiving cores may be switched by connecting their input windings in series with the transfer loop. Note that current I_{02} applied through winding N_{02} could also have produced a ONE transfer from M_a to M_b.

After a possible transfer of a ONE to M_b, this core is in turn sensed. This sets the core to the ZERO state. Now if core M_a is also in ZERO state the next time an advance current is applied, the noise voltage is induced in winding N_1. This will not cause a sufficient current to flow in the transfer loop to switch M_b. It is thus seen that M_b is not set to a ZERO state by the transfer of a ZERO from M_a, but rather left in a ZERO state. This is clearly seen in the symbolic representation, shown in Fig. 5(b). In this example, M_b can only be set to ONE by the action of M_a at either time t_1 or t_2.

Fig. 6 will be used in connection with the discussion of the undesired "backward" flow of information; the cores and windings correspond to those shown in Fig. 5(a). Consider the case when M_b has received a ONE and M_a is in the ZERO state. The application of current I_b (Fig. 6) will switch M_b to the ZERO state and induce voltage V_n in winding N_2. Current I_n will flow in the transfer loop in such a direction as to tend to switch M_a to the ONE state. Since N_2 is normally only one-third to one-fifth of N_1, the voltage V_n will only be one-third or one-fifth of V_1 (Fig. 5(a)). The nonlinear characteristic of the crystal diode causes it to discriminate more against the smaller signal. Proper design considers this fact plus the relatively high impedance of N_1 because of the large number of turns, and guarantees that I_n is limited to such a small value as not to switch M_a.

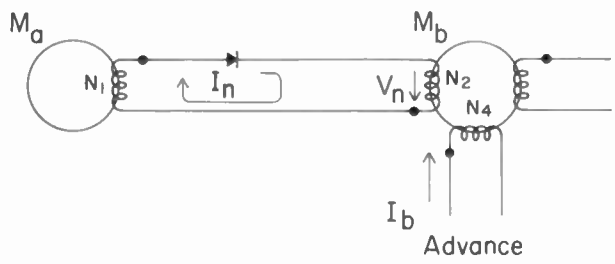

Fig. 6—Single diode transfer loop, during backward flow of information.

Although the diode plays some part in limiting noise in the transfer loop, the significant role of the diode in the single-diode transfer loop is to isolate core M_b [Fig. 5(a)] when core M_a is being set to the ONE state. An input current in winding N_3 will switch M_a to the ONE state and induce a voltage in N_1 opposite in polar-

ity to V_1. The diode prevents the flow of current in the transfer loop and thus serves to isolate M_b.

The single-diode transfer loop is the basic circuit. It permits indefinite storage of binary information without power dissipation, and unconditional transfer of that information to one or more receiving cores when an advance (or sensing) current is applied to the transmitting core.

Fig. 7 shows an operable circuit with typical values. The circuit shown will operate at data frequencies up to 50 kc.

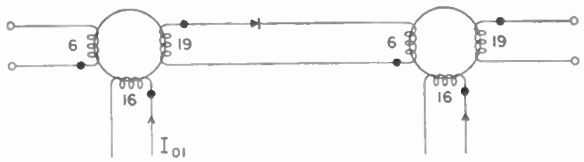

Fig. 7—Typical single-diode loop mechanization. Cores = 20 wraps, 4-79 Moly-Permalloy, $\frac{1}{8}$ mil/wrap × $\frac{1}{8}$ in × 0.2 in mean diam. I_{01} = 100 ma–125 ma, rise-time = 1 duration = 10 μ sec. Diode forward drop at 200 ma = 0.85v < E_f < 1.05v.

Split-winding Transfer Loop

Fig. 8(a) shows schematically a split-winding transfer loop connecting core M_a to core M_b. Assume that both cores are initially in the ZERO state. Transfer current pulse I_{01} is applied and divides at point X [Fig. 8(a)] into branch currents I_1 and I_2. Since M_a is in the ZERO state, winding N_1 is virtually a short circuit. The parallel paths between points X and Y offer almost equal impedance and the two branch currents are essentially equal. Current I_1 flows into a dot terminal on one winding on core M_b; current I_2 flows into a non-dot terminal on an equal winding. The net magnetizing force on M_b is nearly zero and M_b remains in the ZERO state. Small unbalances in the diodes, or the ZERO voltage induced in N_1 can be tolerated because the $B-H$ characteristic of a core is reversible for small magnetizing forces.

If core M_a is in the ONE state and M_b is in the ZERO state when I_{01} is applied [Fig. 8(a)], the ONE will be transferred from M_a to M_b. By proper design, the impedance of N_1 will be large relative to other impedances in the transfer loop and branch current I_1 will be much smaller than branch current I_2. The effect is that of a transfer current I_t, equal to one-half the difference between I_2 and I_1, flowing through a winding of N_2 turns on core M_b. The transfer current I_t sets M_b to the ONE state. Branch current I_1 clears M_a to the ZERO state.

Two important advantages offered by the split-winding transfer loop are conditional transfer of information from M_a to M_b, and the ability to perform isolated operations on either M_a or M_b. Information can be transferred from M_a to M_b only during the application of advance pulse I_{01}. At all other times one or the other of the diodes CR1 and CR2 [Fig. 8(a)] will inhibit the flow of transfer current. Because of the isolation offered by the two diodes, M_a can be switched back and forth between the ONE and ZERO states during a sequence

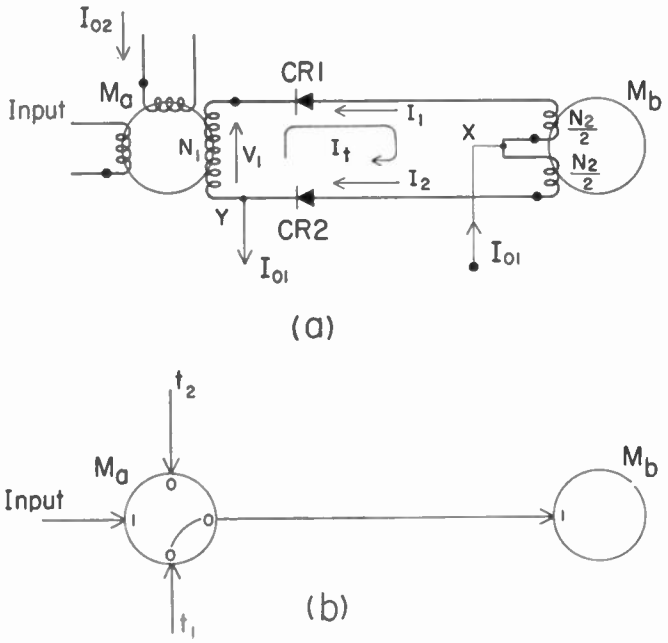

Fig. 8—(a) Split-winding transfer loop, schematic. (b) Split-winding transfer loop, symbolic representation.

of operations without affecting M_b. When desired, the results of the operations can be transferred to M_b by the application of I_{01}. The split-winding transfer loop is immune to the backward flow of information; the switching of the load core M_b by other inputs cannot send a noise current back to core M_a. This feature makes it practical for a single transmitting core in a split-winding transfer loop to switch as many as five or six receiving cores simultaneously. In general, this cannot be done with the single-diode loop because when the receiving cores are later read out they have an additive effect for the backward flow of information.

Fig. 8(b) shows the symbolic representation for the split-winding transfer loop. The connecting-line inside the circle indicates that transfer from M_a to M_b can only be produced by input t_1; input t_2 can set M_a to the ZERO state but will not produce a transfer to M_b.

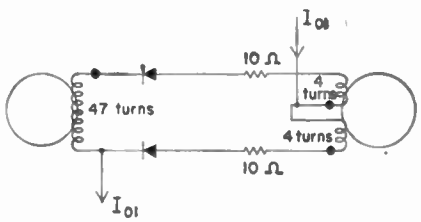

Fig. 9—Typical split-winding loop mechanization. Cores = 20 wraps, 4-79 Moly-Permalloy, $\frac{1}{8}$ mil/wrap × $\frac{1}{8}$ in × 0.2 in mean diam. I_{01} = 100 ma–125 ma, rise-time = 1μ sec, duration = 25μ sec. Diode forward drop at 200 ma = 0.85v < E_f < 1.05v.

Fig. 9 shows a circuit with typical values for use at frequencies up to 20 kc. The resistors shown are for the purpose of minimizing the effects of variation in diode forward resistance and are actually provided by the use of resistance wire for the turn winding.

Inhibit Transfer Loop

The inhibit loop shown in Fig. 10(a) is a special form of split-winding circuit interconnecting cores M_a and M_c. A ONE in M_c inhibits the transfer of a ONE from M_a to M_b, since in this case $I_1 = I_2$ when I_{01} is applied. Core M_b will thus be left in its original state. This is also true when both M_a and M_c are in ZERO state.

When M_a holds a ONE and M_c a ZERO, I_2 is greater than I_1 and therefore M_b will be set to the ONE state. Conversely, if M_a is in a ZERO state and M_c in ONE, M_b is set to ZERO. In all cases, M_a and M_c are set to ZERO by applying I_{01}.

Since normally the receiving core M_b is reset to ZERO by its own winding, the symbolism [Fig. 10(b)] need only express the inhibiting action of core M_c on the transfer of a ONE from M_a to M_b.

As will be shown later in the paper, the inhibit loop permits the synthesis of certain logical operations that might otherwise be difficult to realize. The inhibit loop also offers the isolating advantages described above for the split-winding transfer loop.

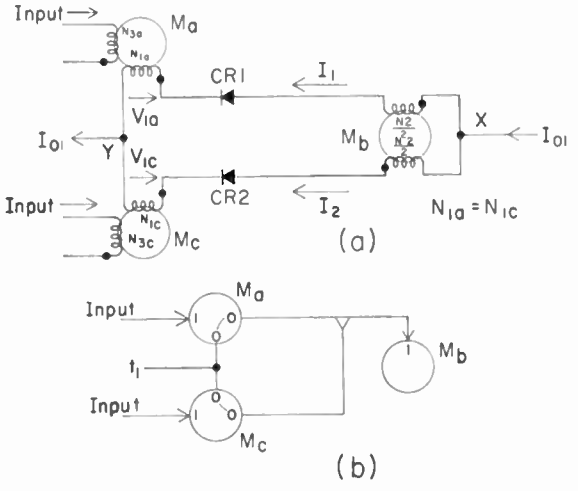

Fig. 10—(a) Inhibit loop, schematic. (b) Inhibit loop, symbolic representation.

Operating Experience

The three fundamental transfer loops described above can be designed to operate with wide variations in magnetic core, diode, and advance current characteristics. Commercially available components are used with about 90 per cent acceptance during incoming inspection. Despite the apparent requirements for diode balance in the split-winding transfer loop and core switching voltage balance in the inhibit loop, good engineering techniques have eliminated the need for any selection of components beyond the initial inspection.

All of the control, storage, and manipulative sections of a digital data-processing system can be synthesized using these three fundamental transfer loops. The simplicity, reliability, ruggedness, and expected long life of the components that were used are thus extended to the entire magnetic core system.

Advance-Current Drivers

It is required that the advance-current drivers used in core circuits: offer high impedance when in the OFF condition, and deliver current pulses of sufficient magnitude and duration to effect information transfer when in the ON condition. Vacuum-tube pentodes triggered by appropriate pulses, blocking-oscillator type circuits, and self-extinguishing thyratron circuits have served effectively as drivers for magnetic core systems. The latter two can be triggered by the output from a single core, and have been used as amplifiers where it was required that one transmitting core switch a large number of receiving cores. (The symbol for a driver is a half-circle with appropriate input and output lines; see, Fig. 15).

Magnetic Shift Registers

One of the earliest and most extensive uses of cores was in the simple magnetic shift register (MSR)[8] which accepts binary information either serially or in parallel and produces serial output.

The serial MSR can be synthesized with single diode transfer loops. The split-winding transfer loop permits the synthesis of the serial-in, parallel-out type and reversible type magnetic shift registers described below.

Serial MSR

Fig. 11 shows the symbolic representation of a serial MSR using single diode transfer loops in a two-core-per-bit configuration. Binary information initially in cores M_a and M_a' is transferred to cores M_b and M_b' respectively by advance pulse t_1. The information in M_b and M_b' is then transferred to M_a' and to "output" respectively by advance pulse t_2. For serial-in operation, new information may be inserted into M_a at any time between t_1 pulses. For parallel-in operation, the new information is placed in alternate cores at a time when these cores are not otherwise pulsed and is then shifted out serially by the alternate application of advance pulses t_1 and t_2. Serial magnetic shift registers greater than 50 bits in length have been operated with a single miniature gas tube serving for each driver.

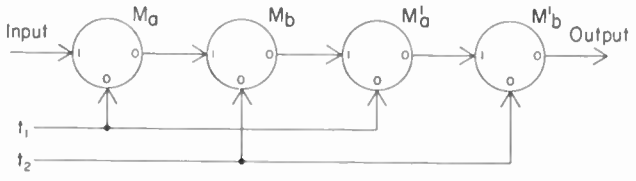

Fig. 11—Serial magnetic shift register.

In digital data-processing systems the serial MSR serves principally to provide buffer storage. Information from a drum, tape, or other source can be placed in the register when it is available and can then be delivered to the output circuit whenever desired. The serial MSR can also provide speed buffering. For example, if the input information is from a teletype transmitter, ad-

[8] Wang and Woo, *loc. cit.*

vance pulses t_1 and t_2 are pulsed at teletype rate when the register is receiving information. If the output is to a high-speed magnetic drum, t_1 and t_2 are pulsed at the drum clock-pulse rate when the MSR is delivering information to the drum.

Fig. 12 shows a serial MSR four bits in length that uses three cores for every two bits. Three interlaced advance pulses, t_1, t_2, and t_3, are required to operate this type of register. If information is assumed initially to be in cores M_a and M_b (and M_a' and M_b', etc.), t_1 will transfer one bit from M_b to M_c, t_2 will transfer one bit from M_a to M_b, and t_3 will transfer one bit from M_c to M_a' at the same time as new information is inserted in M_a. This type of MSR permits a saving in cores and diodes at the expense of additional drivers, but may be desirable in special cases.

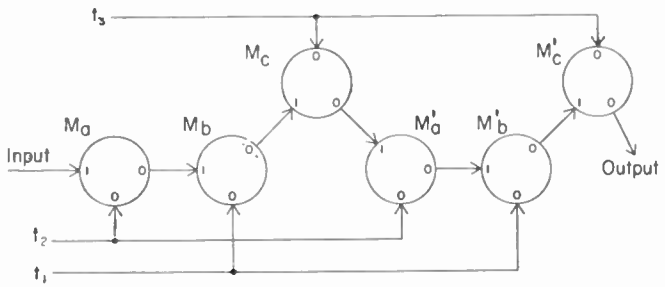

Fig. 12—Serial MSR, 3 cores per two bits.

The use of $n+1$ cores and advance pulses for every n bits may be extended indefinitely if the economics of the situation warrants it. A shift register employing 13 cores and 13 advance pulses per 12 bits of storage capacity has been used in a particular application where the expenditure of drivers was justified.

Parallel MSR

Fig. 13 shows symbolically a parallel MSR synthesized with single-diode and split-winding transfer loops. Cores M_a, M_b, M_c, . . . constitute the shift register,

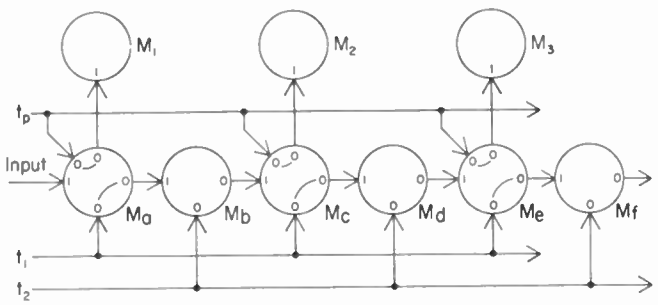

Fig. 13—Parallel MSR.

and M_1, M_2, . . . are the output cores. Information is inserted serially into the shift register at the rate at which t_1 and t_2 are firing. During the serial shifting, the split-winding loops between the register cores and the output cores prevent the transfer of information into the output. When the last bit of a word of predetermined length is inserted into M_a, the preceding bits of that word are in M_c, M_e, ... The application of advance pulse t_p will now transfer the information in parallel into the output cores.

In one application of the parallel MSR in a synchronous system, a marker pulse is inserted into the shift register at the beginning of each word. When this marker pulse reaches the last core at the end of the register it indicates that the entire word is in the register. The sampling pulse that senses this last core produces an output that is used to trigger the driver which delivers advance pulse t_p to effect the parallel transfer of the word.

Reversible MSR

Fig. 14 shows a reversible MSR synthesized with split-winding transfer loops. Information may be shifted from left to right by using advance pulses t_1 and t_2, or from right to left by using advance pulses t_3 and t_4. The reversible MSR is actually two shift registers using the same cores; the isolating reversible character of the split-winding transfer loop permits independent operation of either register. If it were desired, a third set of split-winding transfer loops could provide parallel output from the reversible MSR. Since parallel input is always possible in an MSR, this one configuration could provide a reversal of sequence of digits in a word; parallel-in to shift left or shift right and then parallel-out; or simple shift register operation.

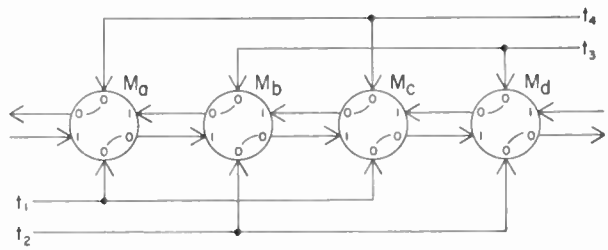

Fig. 14—Reversible MSR.

Computer Control Units

Cycle Distributor

Fig. 15 shows a cycle distributor (CD) synthesized with single-diode transfer loops in a simple shift-register configuration closed around on itself. The cycle distributor might be used to deliver various control pulses to the manipulative portion of a digital system. A single ONE is preset into core M_a and is circulated around the CD by clock pulses t_1 and t_2. As the ONE is transferred from M_a to M_b by the t_2 pulse, control output e_1 is generated. This output might be used, for example, to trigger a relay-actuating thyratron. As the ONE is transferred from M_b to M_c, output signal e_2 might, for example, set a ONE into some other cycle distributor to set it into operation. Core M_r might be used to provide a delay, with no output except to the next core in the cycle distributor. If power gain is needed in the control pulse, the CD output can trigger a current driver, as core M_r is shown doing in Fig. 13.

The number of cores in the cycle distributor and the pulse rate of t_1 and t_2 determine the period of the various control pulses.

Counters

The cycle distributor in Fig. 15 is essentially a simple counter. If, for example, the CD contained six cores, then output pulse e_1 would occur for every third t_2 pulse. Thus to obtain a count of n, a CD containing $2n$ cores would be needed.

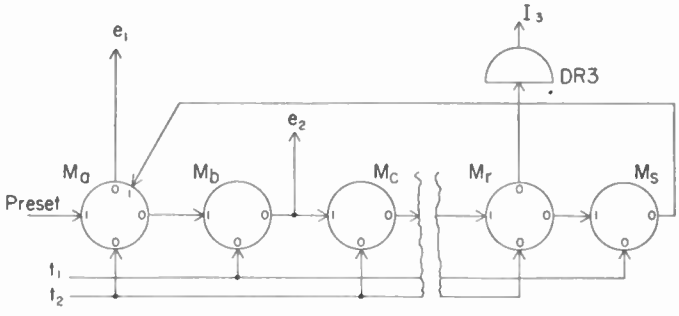

Fig. 15—Magnetic core cycle distributor.

Feedback techniques and cascaded distributors permit a reduction in the number of cores needed to obtain large counts. Fig. 16 shows, for illustrative purposes, a mod 7 counter using 12 cores.

The upper set of cores forms a modulo 3 counter. An output occurring every three "count" pulses drives the lower set of cores which are also in the form of a modulo 3 counter. The output from these cores would occur once for every nine "count" pulses were not the upper counter preset to short count by two. This produces a modulo 7 counter. Although the counting technique might seem unnecessarily complex for achieving a count of seven, it is very useful when large counts are needed.

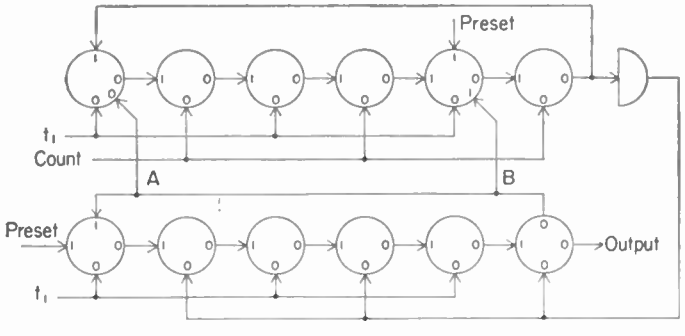

Fig. 16—Mod 7 counter.

Logical Function Units

The three fundamental transfer loops described above can be used to synthesize various logical function units. The basic functions of NEGATION, OR, AND, and EXCLUSIVE-OR, have been selected for description here. From these, more complex digital data-processing functions can be synthesized.

Negation

Fig. 17 shows symbolically the circuit providing NEGATION. Clock pulse t_1 unconditionally sets the core to the ONE state. If information pulse p occurs at time t_2 it serves to reset the core to the ZERO state without giving an output. The next shift pulse t_3 will therefore not give an output. Conversely, if a p pulse did not occur, there *will* be an output at time t_3.

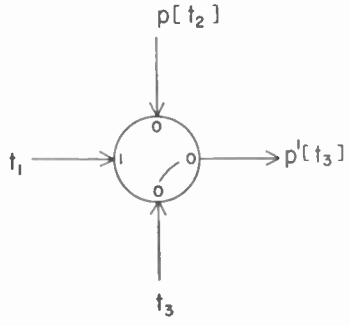

Fig. 17—Negation.

Inclusive Disjunction (OR)

Figs. 18(a) and 18(b) show schematically two methods for realizing the OR function with the single diode transfer loop. The circuit in Fig. 18(a) can be used when both transmitting cores are energized by the same advance pulse; the circuit in Fig. 18(b) is required when M_a and M_c are energized by advance pulses occurring at different times.

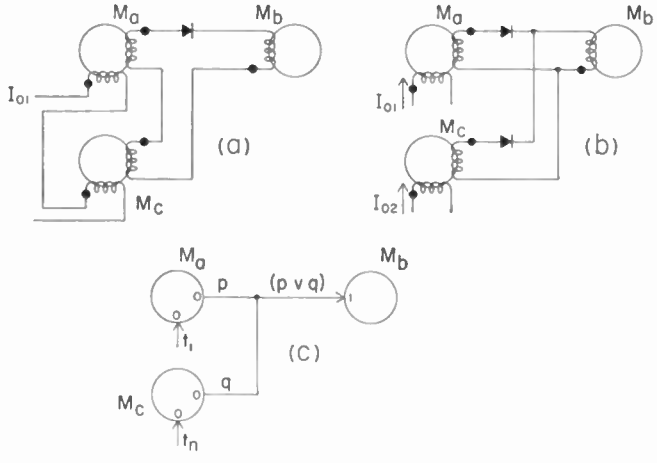

Fig. 18—Magnetic core "OR" circuits.

Fig. 18(c) shows symbolic representation for the OR circuit. Number of inputs that can be mixed into one receiving core is limited mainly by the additive effects of ZERO output voltages from transmitting cores.

The method for achieving the OR function with the split-winding transfer loop is similar to that used with the single-diode loop. With reference to Fig. 8, the outputs of two transmitting cores are mixed by connecting their N_1 windings in series.

Conjunction (AND)

The AND function can be realized with core circuits in several ways. Two that have found extensive use are illustrated symbolically in Fig. 19. Unconditional clock

pulses are indicated by t_1, t_2 and t_3. The information pulses are designated p, q and r. The information pulses need not occur simultaneously.

In Fig. 19(a), which illustrates a three-input AND function, cores M_a and M_c each perform the function of negation. Clock pulse t_1 presents ONE's in these cores, and a signal to M_b occurs at time t_3 only if q or r do not exist. A negation also takes place in core M_b, and an output is obtained from M_b at time t_1 only if p existed and if neither M_a or M_c had produced a signal at the preceding time t_3. Thus, an output is obtained if and only if p and q and r existed.

The AND circuit in Fig. 19(b) has been called the "primed-gate" and involves using the output of one core (M_a) to provide the advance current pulse for a second core, M_b. This advance current exists only if p had occurred, and can produce an output from M_b only if q had occurred. Clock pulse t_3 is needed to clear M_b for the case when q occurs and p does not.

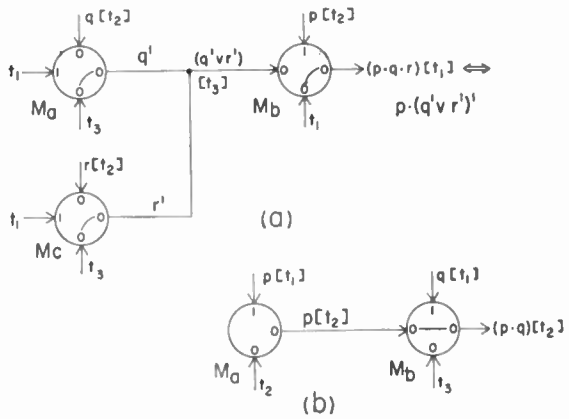

Fig. 19—Magnetic core "AND" circuits.

Exclusive Disjunction (EXCLUSIVE-OR)

Fig. 20(a) shows in symbolic form the EXCLUSIVE-OR circuit. It is synthesized with the fundamental inhibit loop and employs the previously described OR circuit to obtain an output signal indication. Fig. 20(b) is included to illustrate schematically the manner in which the double-inhibit function is realized.

In the EXCLUSIVE-OR circuit in Fig. 20(a), M_a and M_b are the input cores. If M_a contains a ONE (due to input p) and M_b contains a ZERO, advance pulse t_1 transfers the ONE to M_c. If M_b contains a ONE (due to input q) and M_a contains a ZERO, advance pulse t_1 transfers the ONE to M_d. If neither p or q occur, or if both p and q occur, balance is maintained in the branch currents in the transfer loop [Fig. 20(b)]. Both receiving cores M_c and M_d remain in the ZERO state, and it can be considered that each output served to prevent the other from causing information transfer.

The EXCLUSIVE-OR result is obtained by mixing together the outputs from M_c and M_d. An output will be obtained if p or q, but not both, had occurred.

Material Equivalence

The material equivalence (or compare) function can be realized by negating the output from the EXCLUSIVE-OR circuit described above.

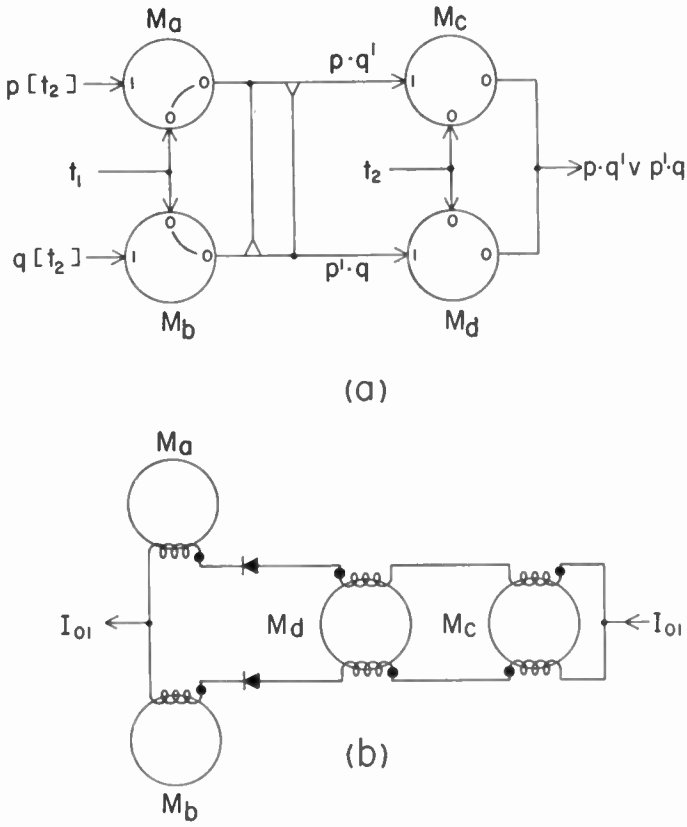

Fig. 20—Magnetic core "EXCLUSIVE-OR" circuit.

Magnetic Core Systems

Multiple Timing Sources

In combining the units previously described, due regard must be given to the sequence of pulses. In general, the operation of cores is sequential even within a single logical function unit, which is in contrast to the operation of diode logical circuits.

Information pulses originating in various units at different times must arrive at a combining unit within a prescribed time interval. There are two ways of satisfying this requirement: one method is to use delay cores in one of the information lines, and the other is to postpone the extraction of data from one of the originating units. The first scheme requires extra cores; the second requires a greater variety of shift pulses.

This is shown (Fig. 21, next page) by two versions of a half-adder. The first uses three cores and three timing pulses. The second version uses four cores, and two timing pulses. In the present example, it would not pay to save one core at the expense of an extra pulse source. However, the use of multiple timing sources does not necessarily result in a proportional increase in the number of tubes.

In any large system, a duplication of driver tubes will be necessary because of their power-handling limitations. If multiple timing sources are used, these tubes simply become distributed differently than in single or double-source systems.

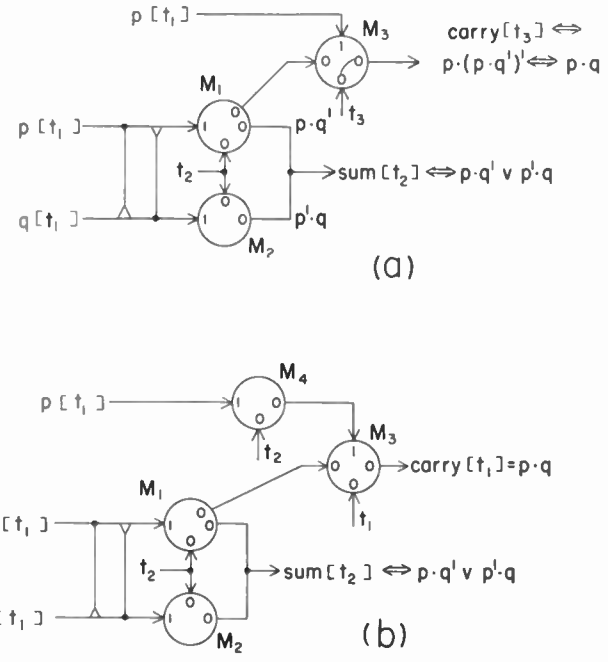

Fig. 21—Magnetic core half adders. (a) Three core, three pulse. (b) Four core, two pulse.

Systems Operation

Using the techniques described in this paper, two models of a digital data-processing system each containing 800 cores and 50 tubes have been designed and operated. An electronic version of this system required 530 vacuum tubes and dissipated 3 kilowatts. The initial design of the core system required only 500 watts, and occupied less than one-fourth the volume.

Within one month after the first magnetic core system was put into operation, a continuous error-free run of longer than 200 hours was realized. The second model has now been operated for more than 2,000 hours without component failure. Core circuits are utilized for all control, storage, and data-handling functions in the system; the tubes are used principally to supply pulse current to the circuits. Most of the basic digital computer operations are performed within this one system: AND, OR, EXCLUSIVE-OR, shift register, serial transfer, parallel transfer, counting, and control. These circuits operate at speeds ranging from 60 cps to 100 kc.

Conclusion

The magnetic core can serve as the basic component for a digital data-processing machine. Three fundamental transfer loops can be used to interconnect cores for storage, control, and logical operations. Basic functional units can in turn be interconnected into a complete system. The power saving, space reduction, reliability, and expected long life of the first models of a core system have served to establish feasibility and to encourage further development and exploitation of this new component.

Acknowledgment

Many people contributed towards the development of the techniques and applications described in this paper. The authors wish to acknowledge their indebtedness to many of their co-workers at the Burroughs Research Center, and in particular Messrs. I. L. Auerbach, G. E. Lund, and A. J. Meyerhoff.

Long-Range Propagation of Low-Frequency Radio Waves between the Earth and the Ionosphere*

J. SHMOYS†

Summary—**The problem of modes of propagation of electromagnetic waves between a perfectly conducting earth and a gradually varying ionosphere is considered. The case of exponentially varying ionospheric parameters is solved in terms of Bessel functions. The propagation constant, the angle of arrival and the group velocity are calculated for the first few modes of propagation. It is shown that the results for the phase and group velocities and angle of arrival of low-order modes obtained when the ionosphere is assumed to be a perfectly conducting sheet at a height simply related to ionospheric parameters are very close to the true values. An application of this theory to the propagation of "tweeks" is discussed.**

Introduction

THE PROBLEM considered here is that of propagation of low-frequency radio waves (frequency under 150 kc) along the surface of the earth. This problem was first treated by Watson [1] who assumed that the ionosphere is a homogeneous isotropic medium of large but constant conductivity, occupying all space above a given height over the earth's surface. In much of the subsequent work on this problem, the assumption of a sharp discontinuity between the atmosphere and the ionosphere was retained in the model used [2, 3, 4, 5, 7]. Rydbeck [6], however, considered continuous models with discontinuity in first or second derivative of the conductivity and calculated the attenuation coefficient approximately. We shall consider the ionosphere to be an isotropic medium with conductivity varying exponentially with height.

Instead of considering the problem in spherical geometry, we shall demonstrate that the error incurred by treating the earth as a plane and the ionosphere as a plane stratified medium is negligible for the parameters we shall calculate.

There are two basic approaches to the theory of propagation of radio waves between the earth and the ionosphere. One is the mode theory of Watson, also used here. The other, far simpler theory, commonly used in short wave propagation problems, is that of geometrical optics; *i.e.*, one assumes a zig-zag path connecting the receiver and transmitter. We should point out that the two theories give different results for the quantities we wish to calculate. Referring to Fig. 1, we see that in the ray theory the angle of arrival would be a function of the distance between the receiver and the transmitter, while in the wave theory it is not. Also, in the ray theory the time of travel in a constant number of hops from T to R is not proportional to the distance TR, while in the wave theory that ratio is constant. Since we are dealing with very low frequencies and propagation over large distances, we must use the wave theory.

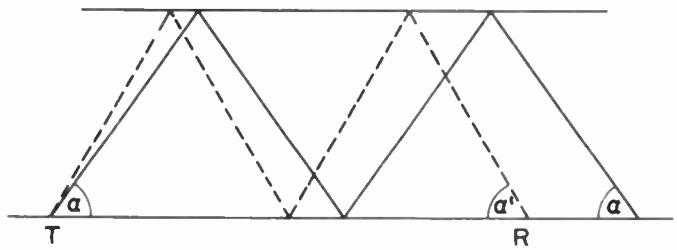

Fig. 1—Zig-zag path. T = transmitter, R = receiver.

We are concerned here not with the detailed structure of the electromagnetic field but with certain parameters characterizing the various modes of propagation, namely, group velocity, angle of arrival, and attenuation. We show that in the case of exponential variation of electron density and collision frequency we can represent the ionosphere, for most practical purposes, by a conducting sheet at a height simply related to the physical parameters of the ionosphere. The results obtained using this model are consistent with experimental results in the propagation of certain low-frequency atmospherics which have been called "tweeks."

We start from the scalar wave equation satisfied by a single-component Hertz vector. By separation of variables in spherical coordinates we reduce the problem to that of finding the eigenvalues of a certain second-order differential operator. Next we demonstrate that the eigenvalues thus obtained differ only by a negligible amount from the corresponding eigenvalues obtained for a flat earth.

Having thus formulated the eigenvalue problem we consider first the case of the lossless ionosphere. Horizontally polarized waves are shown to have certain properties independent of the actual variation of electron density with height. The case of vertically polarized waves in a lossless ionosphere presents difficulties which will be pointed out.

Next we consider the problem of propagation of horizontally polarized waves in a very lossy ionosphere. In this case we also have an infinite set of modes, although these can no longer be sharply divided into propagated and attenuated ones. The first few modes are, in general, little attenuated; higher-order modes

* Original manuscript received by the IRE, June 24, 1955; revised manuscript received, September 19, 1955.

The research reported in this article was made possible through support and sponsorship extended by the U. S. Air Force, Air Force Cambridge Research Center, under Contract No. AF 19(122)-42.

† Formerly with New York University, Inst. of Math. Sci., New York, N. Y.; now with Dept. of Elect. Engrg., Polytechnic Inst. of Brooklyn, Brooklyn, N. Y.

are heavily attenuated. Assuming exponential variation of electron density and collision frequency, we can calculate the eigenvalues of the first few modes. The group velocity and angle of arrival thus calculated are shown to be consistent with those obtained for a simpler model of the ionosphere—one in which the ionosphere is replaced by a perfectly conducting sheet at some height above the earth. This effective height is calculated in terms of ionospheric parameters.

In the case of vertical polarization in a lossy ionosphere there is an additional difficulty which makes the theory applicable only to frequencies above *ca* 25 kc.

Finally the application of our model to the problem of propagation of low-frequency atmospherics, tweeks, will be discussed.

Formulation of the Eigenvalue Problem

The electric and magnetic fields in spherical geometry (Fig. 2) can be derived from a single component Hertz

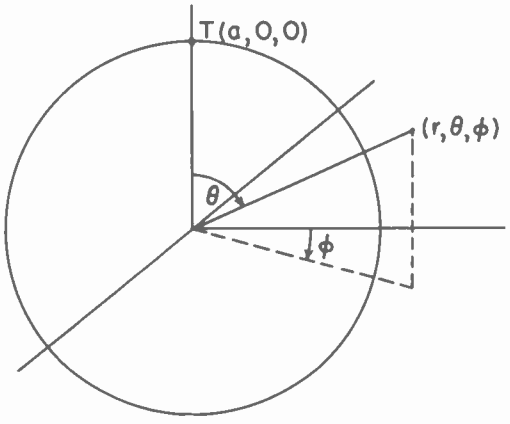

Fig. 2—Spherical geometry.

vector. Thus the vector problem is reduced to a scalar one. The equation to be solved is:

$$\nabla^2\Pi + k^2\epsilon^*\Pi = 0, \tag{1}$$

where ϵ^* is related to the complex dielectric constant as follows [10]:

1. In the transverse electric case ($E_\phi = E_r = H_\phi = 0$),

$$\epsilon^* = \epsilon; \tag{2}$$

2. In the transverse magnetic case ($H_\phi = H_r = E_\phi = 0$),

$$\epsilon^* = \epsilon - k^{-2}\epsilon^{1/2}(\epsilon^{-1/2})_{rr}. \tag{3}$$

The Hertz vector must vanish on the surface of the perfectly conducting earth ($r = a$) in case 1 while its normal derivative must vanish in case 2. At infinity, the Sommerfeld condition is to be applied.

The dielectric constant of an ionized medium of electron density N per cubic meter and collision frequency ν is

$$\epsilon = 1 - \frac{\gamma N}{\omega(\omega + i\nu)}, \qquad \gamma = 3.19 \times 10^{-3}, \tag{4}$$

where ω is the angular frequency of the field. When ω is much smaller than ν, one can approximate ϵ by

$$\epsilon \approx 1 + \frac{i\gamma N}{\omega\nu}. \tag{5}$$

In fact, for low frequencies, ω is negligible with respect to ν in the D-layer and in a large portion of the E-layer. Furthermore, since $\gamma N/\omega\nu$ is much larger than one in most of the ionosphere, we can consider the dielectric constant in those regions as purely imaginary. This is equivalent to saying that the ionosphere behaves very nearly like a conducting medium, with conductivity σ,

$$\sigma = \frac{\gamma N}{\nu}\epsilon_0, \qquad \epsilon_0 = 8.86 \times 10^{-12}. \tag{6}$$

This was the approximation made by Watson. We shall retain the form of dielectric constant given in (5).

Restricting ourselves to nondirectional sources (*i.e.*, sources radiating with the same intensity along any meridian), we can then use the method of separation of variables in spherical coordinates to reduce the three-dimensional problem to a one-dimensional one. We write

$$\Pi = R_\mu(r)P_\mu(\cos\theta). \tag{7}$$

This function satisfies the conditions of the problem if

$$u_\mu = rR_\mu \tag{8}$$

satisfies the equation

$$(u_\mu)_{rr} + \left[k^2\epsilon^* - \frac{\mu(\mu+1)}{r^2}\right]u_\mu = 0, \tag{9}$$

and the appropriate boundary conditions at $r = a$ and at infinity. Let us introduce new independent variables defined by

$$x = r - a \tag{10a}$$

$$y = a\theta. \tag{10b}$$

The differential equation (9) can be written as follows:

$$u_{xx} + \left\{k^2\left[\epsilon^*(x) + \frac{\mu(\mu+1)}{k^2a^2}\,\frac{-\frac{x}{a}\left(2+\frac{x}{a}\right)}{\left(1+\frac{x}{a}\right)^2}\right] - \frac{\mu(\mu+1)}{a^2}\right\}u = 0. \tag{11}$$

We merely split the last term of (9) into its value at the earth's surface and the remaining, variable part, shown in (11) as the second term in the square brackets. Let us look at that term. When we are close to the earth's surface x/a is small. Anticipating the analysis somewhat, we shall say that we are interested in eigenvalues μ of the order of magnitude of ka. Then the second term in the brackets is small compared to unity even for heights of a few hundred miles. At very large heights, the term

tends to the value $\mu(\mu+1)k^{-2}a^{-2}$, which is certainly bounded and which is of the order of magnitude of unity in the case we are most concerned with. The dielectric constant ϵ^* is nearly unity at the earth's surface and tends to $-\infty$ at large heights (if we assume ionization density to be monotonically increasing without bound). Thus we see that the second term has no effect at the earth's surface, and very little effect at heights up to a few hundred miles, where ϵ^* already has a large negative real part. Since ϵ^* has a large negative real part for large x, the eigenvalue problem is insensitive to the actual height dependence of ϵ^* above some large height. The same is probably true if ϵ^* tends to infinity parallel to the imaginary axis, although this case is not so clear-cut. In this investigation it will be assumed that the term in question is negligible even when ϵ^*-1 is purely imaginary. The justification for this is that (ϵ^*-1) could have been assumed to tend to infinity in some direction in the second quadrant and then the direction could be allowed to approach that of the imaginary axis—without affecting the results. Thus our problem can be simplified by omitting the second term in the bracket. We are to find the eigenvalues $\mu(\mu+1)a^{-2}$ of the operator

$$L = \frac{d^2}{dx^2} + k^2\epsilon^*(x), \tag{12}$$

with the appropriate boundary condition at $x=0$ and with a suitable behavior of the eigenfunction at infinity. With ϵ^* behaving as described above, the spectrum is discrete. The value of μ thus obtained determines the behavior of the wave function u along the earth's surface. In order to study this behavior we must turn our attention to the function $P_\mu(\cos\theta)$. Again anticipating further analysis, we take μ to be of the order of ka and therefore large. Hence we can use an asymptotic expression for $P_\mu(\cos\theta)$:

$$C_\mu(\sin\theta)^{-1/2}\cos\left[\left(\mu+\frac{1}{2}\right)\theta-\frac{\pi}{4}\right].$$

Furthermore, since μ is complex, one of the two exponentials making up the cosine is negligible, so that $P_\mu(\cos\theta)$ is approximately given by

$$P_\mu(\cos\theta) \sim \frac{D_\mu}{\sqrt{\sin\theta}}\exp\left[i\left(\mu+\frac{1}{2}\right)\theta\right], \tag{13}$$

where D_μ is a complex amplitude. So long as θ is not too large, it is a good approximation to sin θ, and we have a typical two-dimensional wave. Since $a\theta=y$,

$$P_\mu(\cos\theta) \sim a^{1/2}D_\mu y^{-1/2}e^{i(\nu+1/2)y/a}, \tag{14}$$

so that the attenuation constant α is

$$\alpha = \mathrm{Im}\left(\frac{\mu+\frac{1}{2}}{a}\right), \tag{15}$$

the wave number is

$$\beta = \mathrm{Re}\left(\frac{\mu+\frac{1}{2}}{a}\right), \tag{16}$$

and the group velocity is

$$v_g = \frac{c}{d\beta/dk}. \tag{17}$$

Had we considered the propagation of plane waves in plane stratified media; *i.e.*, the solutions of

$$\left[\frac{\partial^2}{\partial x^2}+\frac{\partial^2}{\partial y^2}+k^2\epsilon^*(x)\right]\Pi = 0 \tag{18}$$

obtained by separation of variables, we would have obtained the relation

$$(\beta+i\alpha)^2 = \mu(\mu+1)a^{-2}. \tag{19}$$

The relative error in $(\beta+i\alpha)$ is then of the order of $1/8\mu^2$, or, since μ is of the order of ka, $1/8(ka)^2$. This error is entirely negligible, since even for a wavelength of 100 km it amounts to one part of per million. We may therefore drop the spherical geometry of the original problem and consider plane wave solutions of (18). Then we set

$$\begin{aligned}\Pi &= u(x)e^{i(\beta+i\alpha)y}\\ &= u(x)e^{\Gamma y},\end{aligned} \tag{20}$$

so that u satisfies the equation

$$u_{xx} + [k^2\epsilon^*(x) + \Gamma^2]u = 0. \tag{21}$$

The eigenvalue parameter Γ has a discrete spectrum for the class of functions $\epsilon^*(x)$ considered here. The boundary conditions are different in the two polarizations, namely:

1. $u(0)=0$ for horizontal polarization (TE case)
2. $u_x(0)=0$ for vertical polarization (TM case). (22)

Because of the behavior of ϵ^* at infinity we may require u to be bounded or even square integrable.

Lossless Ionosphere—Horizontal Polarization

In the case of horizontally polarized waves propagated in a lossless ionosphere, we have, setting $\nu=0$ in (4):

$$\begin{aligned}\epsilon^* = \epsilon &= 1-\gamma N\omega^{-2}\\ &= 1-\gamma c^{-2}Nk^{-2}.\end{aligned} \tag{23}$$

Substituting this expression in the differential equation (21), we obtain

$$u_{xx} + [(k^2+\Gamma^2) - \gamma c^{-2}N(x)]u = 0. \tag{24}$$

If, as we assume here, $N(x)$ is a monotonically increasing function of the height x, then there is an infinite set of eigenfunctions $u_n(x)$ which vanish at $x=0$, tend rapidly to zero at infinity, $x=\infty$, and satisfy the equation

$$u_{xx} + [k_n^2 - \gamma c^{-2}N(x)]u = 0, \tag{25}$$

where k_n^2 are the eigenvalues of the operator $-d^2/dx^2 + \gamma c^{-2}N(x)$ and are therefore independent of k. We have then

$$\Gamma^2 = k_n^2 - k^2. \tag{26}$$

Since Γ^2 positive corresponds to attenuated waves while Γ^2 negative corresponds to propagated waves, k_n is the cutoff wave number of the nth mode. Below that wave number the wave is attenuated:

$$-\Gamma = \alpha = (k_n^2 - k^2)^{1/2}, \tag{27}$$

and above cutoff it is propagated so that

$$-i\Gamma = \beta = (k^2 - k_n^2)^{1/2}. \tag{28}$$

The group velocity is found from (17) and (28), and is

$$v_g = c\sqrt{1 - (k_n/k)^2}. \tag{29}$$

We see that the situation is pretty much the same as in the case of parallel-plate waveguide except for the actual values of the cutoff wave numbers $k_1, k_2 \cdots$, etc.

Suppose that $N(x)$ is identically zero between the ground and some small height. Then the solution of the wave equation in that strip can be written down explicitly. From (25) we have, for sufficiently small x,

$$u_n = e^{ik_n x} - e^{-ik_n x}, \tag{30}$$

so that the field is

$$\begin{aligned} \prod_n &= u_n \exp\left[i(k^2 - k_n^2)^{1/2} y\right] \\ &= \exp\left[ik_n x + i(k^2 - k_n^2)^{1/2} y\right] \\ &\quad - \exp\left[-ik_n x + i(k^2 - k_n^2)^{1/2} y\right]. \end{aligned} \tag{31}$$

Thus we obtain near the ground the decomposition of the mode field into plane waves incident on and reflected from the ground and propagated in directions making an angle ϕ with the ground, where

$$\phi = \sin^{-1}(k_n/k). \tag{32}$$

Again as for parallel-plate waveguides, we obtain the following relation between the angle of arrival and group velocity for any mode:

$$v_g/c = \cos\phi. \tag{33}$$

This relation is independent of the charge density distribution $N(x)$ and of the mode number.

Since this model of the ionosphere is unrealistic we shall not calculate the cutoff wave numbers for any specific electron distributions. The problem is essentially the same as finding the energy states of an anharmonic oscillator with potential $N(x)$. In most cases the phase integral method will give fair results even for the lowest mode. Our main interest in analyzing this case, however, is in the general properties of propagation which will carry over to some extent to the case of lossy ionosphere. Thus, in the latter case, we should expect a finite number of modes with relatively small attenuation and the rest highly attenuated; we may expect the group velocity and the angle of arrival to be related in a way analogous to (33).

Lossless Ionosphere—Vertical Polarization

The main difference between the two polarization components in the lossless case is not in the boundary condition at the ground, but in the differential equation. For vertical polarization we have

$$u_{xx} + (k^2\epsilon - \epsilon^{1/2}(\epsilon^{-1/2})_{xx} + \Gamma^2)u = 0. \tag{34}$$

The unusual simplicity of the case of horizontal polarization lay in our ability to split the coefficient of u, $(k^2\epsilon + \Gamma^2)$ into two terms; one of these, $k^2 + \Gamma^2$, was independent of x, while the other, $k^2(\epsilon - 1)$, was independent of k. Now, however, due to the extra term in (34), we cannot do this. Furthermore the extra term is singular at the zero of ϵ. This singularity did not appear in the case of horizontal polarization, where the only singularity on the real axis was at infinity. The presence of a singularity in the differential equation poses problems which will not be discussed in this paper. Apart from those difficulties we would still find that because the coefficient of u cannot be decomposed into a function of x and a function of k we lose the simple dependence of the propagation constant Γ on the wave number.

Lossy Ionosphere—Horizontal Polarization

As was pointed out above, at low frequencies the complex dielectric constant is given very closely by (5). Hence the differential equation we have to deal with is

$$u_{xx} + [k^2 + \Gamma^2 + ik\gamma N(x)/c\nu(x)]u = 0. \tag{35}$$

Again, as in the case of propagation of vertically polarized waves in a lossless ionosphere, we cannot expect the simple frequency dependence of the propagation constant given by (26) since the x-dependent term also depends on k. Since $N(x)/\nu(x)$ is a monotonically increasing function of x without bound we have a well-set eigenvalue problem, and the spectrum is discrete. If any doubts arise as to mathematical rigor, they can be overcome in most cases by writing instead of i in (35) $\exp[i(\pi/2 + \delta)]$ and allowing δ to tend to zero in the final result. In our calculations this limiting process yields the same result as taking $\delta = 0$ to begin with.

Let us now introduce the exponential model of the ionosphere. We assume that

$$N(x) = N_0 e^{x/h_N}, \tag{36}$$

$$\nu(x) = \nu_0 e^{-x/h_\nu}, \tag{37}$$

so that

$$N(x)/\nu(x) = (N_0/\nu_0)e^{x/h}, \tag{38}$$

where

$$h = (h_N^{-1} + h_\nu^{-1})^{-1}.$$

Substituting this in the differential equation (35), we obtain

$$u_{xx} + [k^2 + \Gamma^2 + ik\gamma(N_0/c\nu_0)e^{x/h}]u = 0. \quad (39)$$

In order to simplify the notation somewhat we shall introduce the following parameters:

$$G^2 = k^2 + \Gamma^2, \quad (40)$$

$$\delta = k\gamma(N_0/c\nu_0)h^2. \quad (41)$$

The latter parameter, δ, is small if the effect of the ionosphere at the ground is to be small. Eq. (39) can be solved exactly in terms of Bessel functions. By means of the substitution

$$\xi = e^{x/2h} \quad (42)$$

the differential equation is transformed into Bessel's equation [11]

$$u_{\xi\xi} + \frac{1}{\xi}u_\xi + \left[\frac{4h^2G^2}{\xi^2} + 4i\delta\right]u = 0. \quad (43)$$

Thus the solution is the appropriate cylinder function of order

$$m = 2iGh \quad (44)$$

and argument

$$\zeta = 2(i\delta)^{1/2}e^{x/2h}. \quad (45)$$

The choice of the suitable cylinder function is dictated by the required behavior at infinity. Since the field must tend to zero, the Hankel function $H_m^{(1)}(\zeta)$ must be chosen. Expressing the solution in terms of Bessel functions of order $+m$ and $-m$, we have

$$u = -i \sin m\pi H_m^{(1)}(\xi) = e^{-im\pi}J_m(\zeta) - J_{-m}(\zeta). \quad (46)$$

In order to find m, and therefore G, we have to impose the boundary condition at the ground. At the ground, however, the argument of the Bessel functions is small, so that one term of the power series expansion is sufficient to represent the Bessel function accurately; then the wave function u becomes

$$u \approx e^{iGx} - Re^{-iGx}, \quad (47)$$

where

$$R = (-i\delta)^{-2iGh}\frac{\Gamma(1 + 2iGh)}{\Gamma(1 - 2iGh)}. \quad (48)$$

we may observe that if the dielectric constant had been

$$\epsilon = 1 - \gamma N/\omega\nu, \quad (49)$$

the above analysis would still hold, but instead of $-i\delta$ we would have δ in (48).

In order to satisfy the boundary condition at $x = 0$, the reflection coefficient must be unity. The equation

$$R = 1 \quad (50)$$

has an infinite set of solutions. To order these solutions and assign to each some integer designation, we proceed as follows. First find the locus of all complex values of Gh for which the reflection coefficient has magnitude 1. It is obvious that the origin, $Gh = 0$ is on the curve. Proceeding on the curve away from the origin, the phase of the reflection coefficient increases monotonically. Points corresponding to integral multiples of 2π satisfy (50). Let us use then, the ratio between the phase, and 2π as the designation for a particular eigenvalue.

Having located one point on the curve, namely the solution of (50) corresponding to $n = 0$, let us consider this point further. $G = 0$ implies that the wave is propagated parallel to the ground with phase velocity c. Furthermore, the incident and reflected waves. both traveling in the same direction, cancel each other at the ground. Hence they must cancel each other everywhere. That this is true near the ground is obvious from (47). Hence $G = 0$ is not really an eigenvalue and we should start counting with $n = 1$.

Before proceeding with the investigation of the locus of $|R| = 1$ in the G-plane, let us see what this locus would look like if the dielectric constant were real, say as in (49). We can readily see that in that case the locus is the real axis. The absolute value of the ratio of the gamma functions in (48) is unity when G is real, since these two functions are complex conjugates. The remaining factor would be a real number raised to an imaginary power, again having magnitude one. We would still have to choose between the positive and negative real axis. This choice, however, is purely arbitrary for the purpose of determination of the propagation constant, since only G^2 appears in the equation. Let us choose the positive real axis.

The next step is to investigate locus of $|R| = 1$ in the complex G plane. Due to complexity of (48) we have to look for suitable approximations. For some values of parameter δ we may check numerically the accuracy of our approximations. Since we are interested primarily in the first few eigenvalues, the most interesting part of the curve is in the neighborhood of the origin. Let us introduce the dimensionless parameter

$$X = X_1 - iX_2 = 2Gh. \quad (51)$$

In terms of X, the equation of the curve is

$$\left|\left(\delta \exp\left[-i\frac{\pi}{2}\right]\right)^{-i(X_1 - iX_2)}\right| \cdot \left|\frac{\Gamma(1 + X_2 + iX_1)}{\Gamma(1 - X_2 - iX_1)}\right| = 1 \quad (52)$$

or

$$-X \log \delta - \frac{\pi}{2} X_1 + \operatorname{Re} \log \frac{\Gamma(1 + X_2 + iX_1)}{\Gamma(1 - X_1 - iX_1)} = 0. \quad (53)$$

Eq. (53) is the exact equation of the curve on which the absolute value of R is 1. In order to find an approximation for the curve in the neighborhood of the origin, we assume X_1 and X_2 to be small and expand the last term of (53) in a power series. Since

$$\frac{d}{dX} \Gamma(1 + X) \Big|_{X=0} = -C, \quad C = 0.577 \cdots, \quad (54)$$

(53) reduces to

$$X_2 \log \delta + \frac{\pi}{2} X_1 - 2CX_2 = 0, \quad (55)$$

or

$$\frac{X_2}{X_1} = \frac{-\pi/2}{2C + \log \delta}. \quad (56)$$

Thus we see that as a result of loss, the locus of $|R| = 1$ near the origin is pushed into the fourth quadrant. It starts as a radial line making a small angle with the real axis.

Next we can investigate the behavior of the locus far away from the origin.

For large X we can use Stirling's formula for the gamma function of large argument. When we do that we find that X_1 and X_2 satisfy the following relation:

$$\frac{X_2}{X_1} \approx \frac{-\pi/2}{\log \delta - 2 \log |X| + 2}. \quad (57)$$

Since X_1 is obviously much greater than X_2, the deviation from the real axis is not very great.

Having thus obtained approximations to the curve at both its ends, we should see how good these approximations are and what happens in the region when neither approximation is valid. For this purpose we investigated numerically the case $\log \delta = -9$ or $\delta = 1.3 \times 10^{-4}$. This value of δ is higher than those we would encounter in most cases, so that the agreement in general should be better than in this case. The results are shown on Fig. 3. Since the curve does not deviate too much from the real axis, the modes corresponding to values of G to the left of the abscissa k will be propagated with little attenuation, while those to the right will be highly attenuated.

It remains now to find on the locus to $|R| = 1$ those points which correspond to $R = 1$; *i.e.*, the points at which the phase shift is an integral multiple of 2π. For this purpose we calculate the phase; *i.e.*, the imaginary part of $\log R$, where R is given by (48). Here again the exact expression would have to be calculated numerically, but, since we are interested in the first few modes only, we shall make use of the power series expansion

$$\Phi \approx -X_1 \log \delta + \frac{\pi}{2} X_2 - 2CX_1. \quad (58)$$

This is the expression for phase Φ in the X-plane, near the origin. We need to know it on the locus $|R| = 1$, and so we make use of the relation (56), obtaining the phase in terms of X_1:

$$\Phi \approx -X_1 (\log \delta + 2C) + \frac{\pi}{2} X_1 \frac{-\pi/2}{2C + \log \delta}$$
$$\approx X_1 (A + \pi^2/4A), \quad (59)$$

where

$$A = -\log \delta - 2C.$$

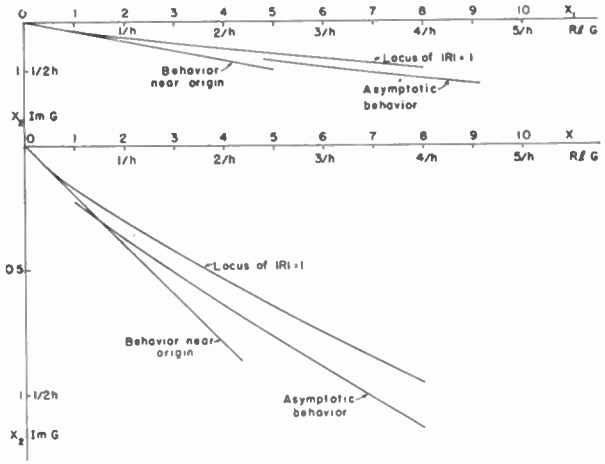

Fig. 3—Locus of eigenvalues for $\delta = 1.3 \times 10^{-4}$.

For the nth mode,

$$\Phi = 2n\pi, \quad (60)$$

so that

$$X_1 \approx 2n\pi (A + \pi^2/4A)^{-1} \quad (61)$$

and

$$X_2 \approx n\pi^2 (A^2 + \pi^2/4)^{-1}. \quad (62)$$

These two relations together with (51) and (40) give the propagation constant Γ. The numerical evaluation of the attenuation and phase constants is quite straightforward now. We wish to obtain some information, however, about the frequency dependence of the attenuation factor and about group velocity. In order to avoid unnecessary complications we shall restrict ourselves to that range of frequencies in which the particular mode in question is not heavily attenuated. In view of the fact that δ is very small we may neglect $\pi^2/4$ with respect to A^2. Thus we have

$$G_n \approx \frac{n\pi}{hA} \left(1 - i \frac{\pi}{2A}\right), \quad (63)$$

so that

$$G_n^2 = \left(\frac{\pi n}{hA}\right)^2 \left(1 - i \frac{\pi}{A}\right), \quad (64)$$

and

$$\Gamma_n^2 = -k^2 + G_n^2 \approx -k^2 + \left(\frac{\pi n}{hA}\right)^2 + i\frac{\pi^2 n^2}{h^2 A^3}. \quad (65)$$

The range of frequencies is that in which k is greater than $(\pi n/hA)$, and is not too close to it, say

$$k > 2\pi n/hA. \quad (66)$$

The imaginary part of Γ_n^2 under these circumstances is much smaller than the real part. Thus we have

$$\beta_n \approx k\left[1 - \left(\frac{\pi n}{khA}\right)^2\right]^{1/2} \quad (67)$$

and

$$\alpha_n \approx \pi^2 n^2/2h^2 A^3 \beta. \quad (68)$$

We should remember that in the above relations A is a function of frequency. From (59)and (41) we have

$$A = -\log\delta - 2C = [\log(c\nu_0/\gamma N_0 h^2) - 2C] - \log k. \quad (69)$$

If A is large, as we have assumed, the effect of frequency on A is very small and can be neglected for the sake of simplicity. We see then that in the propagation region the exponential ionosphere has the same effect on phase and group velocity as a perfectly conducting plane sheet placed at the effective height w:

$$w = Ah. \quad (70)$$

The group velocity is obtained by differentiating (67) with respect to k, neglecting variation of A

$$v_g \approx c\left[1 - \left(\frac{n}{khA}\right)\right]^{1/2}. \quad (71)$$

For k sufficiently large the attenuation coefficient should should vary approximately as k^{-1}, or proportional to wavelength.

Near the earth's surface the field can again be decomposed into two plane waves. This is a consequence of (47). Since G^2 and Γ^2 are not real, however, the plane waves are not homogeneous. But the attenuation is small and we may treat the plane waves as if they were homogeneous. The angle of arrival is then given by the same formula as in the lossless ionosphere (32), and the same relation (33) holds between group velocity and angle of arrival.

Lossy Ionosphere—Vertical Polarization

In the case of vertical polarization, besides different boundary conditions, at the ground we have a modified differential equation. If the dielectric constant is the same function of height as in the preceding section, namely

$$\epsilon = 1 + i(\gamma N_0/\omega\nu_0)e^{z/h}, \quad (72)$$

then the ϵ^* which appears in the differential equation differs from ϵ by

$$\epsilon^* - \epsilon = -k^2\epsilon^{1/2}(\epsilon^{-1/2})_{zz} = -k^2\left[\frac{3}{4}\frac{\epsilon_z^2}{\epsilon^2} - \frac{1}{2}\frac{\epsilon_{zz}}{\epsilon}\right]. \quad (73)$$

In order to simplify the treatment we shift the origin to $x = x_0$, defined by

$$(\gamma N_0/\omega\nu_0)e^{z_0/h} = 1$$
$$z = x - x_0. \quad (74)$$

In terms of z we have then

$$\epsilon = 1 + ie^{z/h}, \quad (75)$$

$$\epsilon^* - \epsilon = k^{-2}h^{-2}\left[\frac{3}{4}\left(\frac{e^{z/h}}{1 + ie^{z/h}}\right)^2 + \frac{i}{2}\frac{e^{z/h}}{1 + ie^{z/h}}\right]. \quad (76)$$

We see then that so long as kh is greater than unity, the difference between ϵ^* and ϵ is small compared to ϵ. In fact it is also small compared to $(\epsilon - 1)$.

So far we have been assuming that frequency is sufficiently low, at least in the calculation of eigenvalues. If we wish to neglect the term (76) in the differential equation, we must have $kh > 1$ and therefore sufficiently high frequency. Fortunately the approximation to the dielectric constant we have been using is valid below ca 200 kc, while $kh = 1$ corresponds to ca 25 kc. In that range the low-frequency theory used in this report should apply to the case of vertical polarization, with the effect of polarization on the differential equation neglected. We do, however, have to apply the appropriate boundary condition; *i.e.*, $u_x = 0$ at $x = 0$, so that instead of $R = 1$ we must have $R = -1$. This changes essentially nothing in our discussion of the last section, except that

$$\Phi = 2\left(n - \frac{1}{2}\right)\pi, \quad (77)$$

and all the formulas of the preceding section follow, with $(n - \frac{1}{2})$ substituted for n.

Applications

We have shown here that horizontally polarized low-frequency radio waves are propagated between the earth and the ionosphere very much as in a parallel-plate waveguide. The first few modes are propagated as if the ionosphere, instead of being a medium of gradually varying properties, were a perfectly conducting sheet located at the effective height w above the earth. This effective height w is simply related to the ionospheric parameters: the scale height of the variation of conductivity and the values of the electron density and the collision frequency at some height.

Since this model is lossless it cannot, of course, yield the attenuation coefficient. The latter can, if desired, be calculated from (65).

Let us now calculate the effective height of the ionosphere. Let us take reasonable values of electron density and collision frequency at the height of 60 km:

$$N(60) = 10^8 \text{ electrons}/m^3,$$
$$\nu(60) = 10^6 \text{ sec.}^{-1},$$

and further let us take the respective scale heights h_1

and h_2:

$$h_1 = 4 \text{ km},$$
$$h_2 = 8 \text{ km},$$

so that

$$h = (h_1^{-1} + h_2^{-1})^{-1} = 2\tfrac{2}{3} \text{ km}.$$

With these assumptions we have

$$\delta \approx ke^{-20.5}$$
$$A = -\log \delta - 2C \approx 19.3 - \log k.$$

In the low-frequency range k is of the order of $1/e$, and hence δ is indeed small and A does not vary very much with even a substantial change of k.

Finally, the effective height w is, in the neighborhood of 25 kc ($A = 20$),

$$w = Ah = 53.3 \text{ km}.$$

This height would not differ by more than a few per cent over the whole very-low and low-frequency band.

At 18 kc we would expect the ratio v_g/c to be 0.976 in the second mode ($n = 3/2$ in (71)). This is in fair agreement with the experimentally observed value 0.97 [12]. The fact that the lowest mode was not observed cannot be explained on the basis of this theory. In any case it should be clear that we deal here with low-order modes. Incidentally, the angle of arrival corresponding to the observed relative delay of about 3% is 14°. or considerably larger than that obtained by multiple-hop calculations. Perhaps it is possible to verify this figure experimentally.

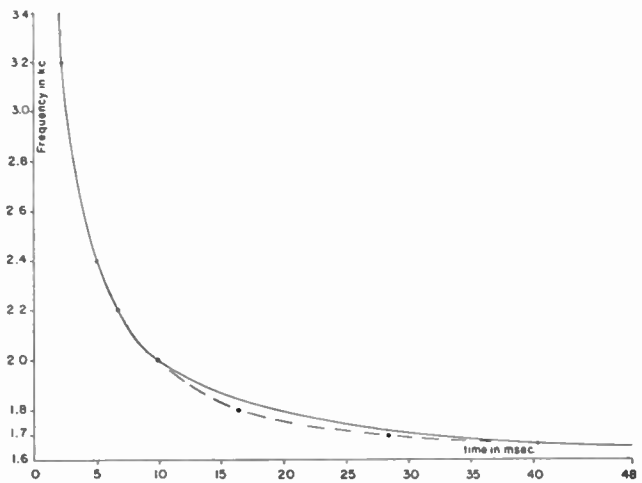

Fig. 4—Comparison of theory of tweeks with experiment. —— Experimental curve. Calculated points. $f_0 = 1.6$ kc, $d = 4{,}400$ km.

It is possible that the waveguide theory of low-frequency propagation provides an explanation of tweeks [13, 14]. Tweeks are very-low-frequency noise signals associated with lightning discharges. Following the discharge the frequency of the tweek decreases rapidly at first and then approaches an asymptotic value. This is just the behavior expected on the basis of the theory presented in this paper. The asymptotic value would correspond to the cutoff frequency of the mode. Furthermore, there is experimental evidence [13, 15] that a tweek is accompanied by its harmonics. But since the cutoff frequencies of the first few modes are integral multiples of the cutoff frequency of the lowest mode, the observed harmonics may really have been just higher frequencies arriving in a higher-order mode.

The frequency-time relation for a typical tweek was plotted by Burton and Boardman [14]; their curve is compared in Fig. 4 with computed values obtained from the parallel-plate waveguide model [using (71)]. We obtained the distance from the lightning discharge to the receiver by fitting the theoretical curve to the experimental one at 2.2 kc and assuming the cutoff frequency to be 1.6 kc. From this value of cutoff frequency the effect of height is computed to be 47 kilometers; this is in excellent agreement with the effective height calculated from our theory, 53.3 kilometers. Indeed, the general agreement between the experimental and theoretical curves is quite good.

Acknowledgment

The author wishes to express his gratitude to Professor B. Friedman for many helpful discussions.

Bibliography

[1] Watson, G. N., "The Transmission of Electric Waves Round the Earth," *Proceedings of the Royal Society*, A, vol. 95 (July 15, 1919), pp. 546–563.
[2] Schumann, W. O., "Über die Oberfelder bei der Ausbreitung Langer, Elektrisher Wellen im System Erde-Luft-Ionosphäre und 2 Anwendungen (Horizontaler und Senkrechter Dipol)." *Zeitschrift für angewandte Physik*, vol. 6 (January, 1954), pp. 35–43.
[3] Schumann, W. O., Über die Strahlung Langer Wellen des Horizontales Dipols in dem Lufthohlraum Zwischen Erde und Ionosphäre, I." *Zeitschrift für angewandte Physik*, vol. 6 (May, 1954), pp. 225–229; II. *Ibid.*, vol. 6 (June, 1954), pp. 267–271.
[4] Budden, K. G., "The Propagation of a Radio Atmospheric I." *Philosophical Magazine*, vol. 42 (January, 1951), pp. 1– ; II. *Ibid.*, vol. 43 (November, 1952), pp. 1179–1200.
[5] Budden, K. G., "The Propagation of Very Low Frequency Radio Waves to Great Distances." *Philosophical Magazine*, vol 44 (May, 1953), pp. 504–513.
[6] Rydbeck, O. E. H., "On the Propagation of Radio Waves." *Transactions of Chalmers University*, Gothenburg, Sweden, No. 34 (1954), pp. 1–170.
[7] Alpert, Ya. L., "On the Theoretical Calculation of the Field of Low-Frequency Electromagnetic Waves over the Earth's Surface." *Doklady Akademii Nauk Soyuza Sovetskikh Sotsialisticheskikh Respublik*, vol. 97 (April 23, 1954), pp. 629–632.
[8] Stanley, J. P., "Ionospheric Reflection of Long Radio Waves." *Canadian Journal of Research*, A, vol. 28 (November, 1950), pp. 549–557.
[9] Stanley, J. P., "The Absorption of Long and Very-Long Waves in the Ionosphere." *Journal of Atmospheric and Terrestrial Physics*, vol. 1 (January, 1951), pp. 65–72.
[10] Bremmer, H., *Terrestrial Radio Waves* (Amsterdam, Elsevier Publishing Company, 1949), p. 133.
[11] Magnus, W., and Oberhettinger, F., *Special Functions of Mathematical Physics*. New York, Chelsea Publishing Company, 1948.
[12] Brown, J. N., "Round-the-World Signals at Very Low Frequency," *Journal of Geophysical Research*, vol. 54 (December, 1949), pp. 367–372.
[13] Potter, R. K., "Analysis of Audio-Frequency Atmospherics." Proceedings of the IRE, vol. 39 (September, 1951), pp. 1067–1069.
[14] Burton, E. T., and Boardman, E. M., "Audio Frequency Atmospherics," *Bell System Technical Journal*, vol. 12 (October, 1933), pp. 498–516.
[15] Hepburn, F., and Pierce, E. T., "Atmospherics with Long Trains of Pulses," *Philosophical Magazine*, vol. 45 (September, 1954), pp. 917–932.

Artificial Dielectrics Utilizing Cylindrical and Spherical Voids*

H. T. WARD†, ASSOCIATE MEMBER, IRE, W. O. PURO†, ASSOCIATE MEMBER, IRE, AND D. M. BOWIE†

Summary—Artificial dielectrics utilizing three-dimensional arrays of spherical and cylindrical holes in base materials of polystyrene, Plexiglas, Teflon, and others have been investigated.

A theoretical expression relating the dielectric constant to the number and size of the spheres, and to the dielectric constants of the sphere and base materials, is derived. The analysis is restricted to spherical voids small with respect to the wavelength.

The theoretical expression (in terms of the fractional volume of the cylinders) applies also to cylindrical-void media, if the length-to-diameter ratio of the cylinders is not far removed from unity. However, for large length-to-diameter ratios, the dielectric constant depends appreciably on the orientation of the cylinder axes with respect to the electric field.

Measured dielectric constants obtained by the shorted waveguide method at 5,000 mc are shown. Values of dielectric constant in the range of 1.1 to 2.6 have been obtained. By using high-dielectric-constant base materials this range could be raised.

Introduction

THE PRACTICAL possibilities of controlling the dielectric properties of a material by embedding objects in it have been realized for some time. The material has usually consisted of some type of lightweight foamed plastic, with a dielectric constant only slightly greater than unity. The embedded objects have assumed various forms; Kock[1] investigated arrays of metallic spheres, disks, rods, and strips while Corkum[2] investigated isotropic arrays of metallic spheres and dielectric spheres. The resulting artificial dielectrics, which utilize a base material of polyfoam or styrofoam, are structurally poor and their applications are limited to devices not subject to shock or vibration.

This paper presents a study of a class of artificial dielectrics which has better mechanical properties than the ones previously considered. The improved media utilize spherical or cylindrical voids in a relatively high dielectric constant base material. Base materials of polystyrene, Plexiglas, Teflon, and others have been used with success. The measured dielectric constants were in the range of 1.1 to 2.6. These values are of interest in microwave lens applications.

Theoretical Analysis

An equation can be developed which yields the value of the dielectric constant in terms of the sphere size, sphere density (number/unit volume), and the dielectric constants of the base and sphere materials. It should be noted that the theory is restricted to a cubical lattice of spherical-shaped objects.

The polarization $\overline{P}$ that is due to the spheres is given by the expression $\overline{P}=\alpha\overline{E}'N/V$.[3] The term α is the polarizability of a sphere, $\overline{E}'$ is the effective electric field acting on a sphere, and N is the number of spheres in the volume V. The polarizability of a dielectric sphere in a dielectric of different dielectric constant is given[4] by the expression:

$$\alpha = 4\pi\epsilon_0 K_1 R^3(K_2 - K_1)/(K_2 + 2K_1) \qquad (1)$$

where K_2 is the relative dielectric constant of the sphere material, K_1 is the relative dielectric constant of the base material, R is the sphere radius, and $\epsilon_0 = 8.85\times10^{-12}$ farad/meter. The effective field $\overline{E}'$ is taken[5] to be:

$$\overline{E}' = \overline{E} + \overline{P}/3\epsilon_0 K_1 \qquad (2)$$

where $\overline{E}$ is the electric field that produces $\overline{P}$. Eq. (2) takes into account the mutual interaction of the spheres; it is an equivalent statement of the Clausius-Mosotti law.

The introduction of α and $\overline{E}'$ into the expression for $\overline{P}$ gives the following equation:

$$\overline{P} = \alpha\overline{E}'N/V = 3FC\epsilon_0 K_1(\overline{E} + \overline{P}/3\epsilon_0 K_1) \qquad (3)$$

where $C=(K_2-K_1)/(K_2+2K_1)$. Eq. (3) has been simplified somewhat by the introduction of Corkum's fractional volume concept.[2] For the array of spheres, the fractional volume is expressed as $F=4\pi R^3N/3V$.

The introduction of the effective dielectric constant K into (3) is accomplished with the aid of the fundamental relation $\overline{P}=(\epsilon_0 K-\epsilon_0 K_1)\overline{E}$. The resulting expression can be rewritten and solved for K/K_1, as follows:

$$K/K_1 = (1 + 2FC)/(1 - FC). \qquad (4)$$

Eq. (4) is the desired result. The quantity F depends only on the number and size of the spheres, while the quantity C depends only on the dielectric properties of the two materials. For the artificial media to be described, $K_2=1$ (*i.e.*, spherical voids or cavities in a dielectric), which gives $C=(1-K_1)/(1+2K_1)$. For Corkum's dielectric sphere array in air,[2] K_1 is equal to 1 and hence $C=(K_2-1)/(K_2+2)$.

* Original manuscript received by the IRE, August 22, 1955.
† Melpar, Inc., 3000 Arlington Boulevard, Falls Church, Va.

[1] W. E. Kock, "Metallic delay lenses," *Bell Sys. Tech. Jour.*, pp. 58–82; January, 1948.
[2] R. W. Corkum, "Isotropic artificial dielectric," PROC. IRE, vol. 40, pp. 574–587; May, 1952.
[3] J. C. Slater and N. H. Frank, "Electromagnetism," McGraw-Hill Book Co., Inc., New York, N. Y., p. 41; 1947.
[4] C. J. F. Bottcher, "Theory of Electric Polarization," Elsevier Publishing Co., New York, N. Y., pp. 51, 61; 1952.
[5] P. Debye, "Polar Molecules," Dover Publications, Inc., New York, N.Y., p. 11.

In any microwave application, the size of the spheres and the spacing between them adds up to an appreciable fraction of a wavelength. Since the analysis is an electrostatic one, some experimental work was necessary to determine the validity of (4). Furthermore, extensive measurements were required on cylindrical-void media, since the theoretical analysis was based on objects which are spherical in shape.

Methods of Measurement

All of the measurements to be reported were obtained by the shorted-waveguide method at a frequency of 5,000 mc. A description of the technique may be found elsewhere.[6] The waveguide was standard RG-49/U (0.874 by 1.874 inch I.D.), except for the section in which the sample of artificial dielectric was inserted. This section was modified slightly to give inside dimensions with exactly a two-to-one ratio (0.937 by 1.874 inch). A knowledge of the node shift caused by introducing the sample, the frequency, and the length of the sample is sufficient to permit a calculation of the effective dielectric constant (K). The shorted-line method offers the convenience of small samples, freedom from external influences, and adaptability to common laboratory equipment. The frequency choice of 5,000 mc permits the samples to be of a size that can be readily machined to suitable tolerances. The accuracy of dielectric constant measurements is about 1 per cent.

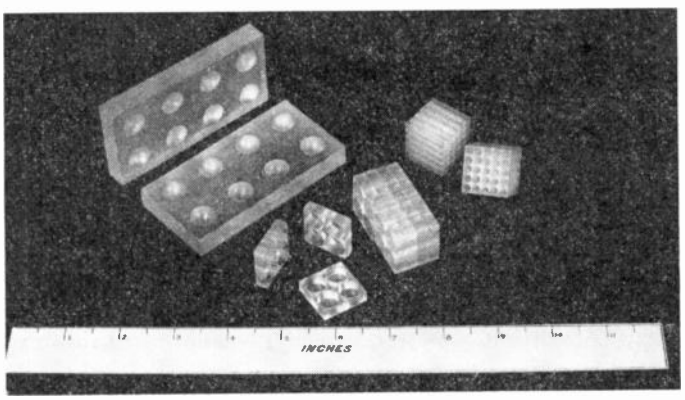

Fig. 1—Samples of materials containing spherical and cylindrical voids.

Experimental Results—Spherical-Void Medium

The sample is constructed of a number of sheets, Fig. 1, which have hemispherical depressions milled in one face. The spherical voids are obtained by placing two sheets together with corresponding hemispheres in juxtaposition. Two base dielectric materials have been used; Teflon ($K_1 = 2.02$) and an expanded material ($K_1 = 1.62$) manufactured by the Sponge Rubber Company of Shelton, Connecticut. Two lattice sizes were used; the large lattice has one row, and two rows of voids across the narrow and wide dimensions of the waveguide, respectively, while the small one has two rows across the narrow dimension and four rows across the wide dimension. In each case, the spacing between the centers of the outer spheres and the waveguide wall is one-half of the center-to-center spacing. The large lattice, with $\frac{1}{2}$-inch diameter spheres, has a fractional volume of 0.0796. The small lattice has the same fractional volume with $\frac{1}{4}$-inch spheres, and 0.268 with $\frac{3}{8}$-inch spheres.

The measured values for the dielectric media are shown in Figs. 2, 3, and 4, as a function of the length of the samples. The samples were progressively shortened by cutting off one transverse row of voids after each measurement. For the $\frac{1}{4}$-inch spheres, Figs. 2 and 3 and the upper curve of Fig. 4, the measured value does not differ by more than 2 per cent from the theoretical value calculated with (4). For this case, the diameter of the spheres is about $0.15\lambda'$ (λ' is the wavelength in the unbounded dielectric) and the spacing between the centers of the adjacent spheres is $0.28\lambda'$. Lower curve of Fig. 4 is for $\frac{1}{2}$-inch voids spaced 0.937-inch on centers. The void diameter is $0.30\lambda'$, and the spacing is $0.56\lambda'$. For this sample, in which the diameter of the void is not small compared to the wavelength, the measured value differs by less than 4 per cent from the theoretical value.

Experimental Results—Cylindrical-Void Medium

The study of the cylindrical-void medium was undertaken in an effort to alleviate the construction problem associated with spherical-void media. However, the application of (4) to a cubical lattice of cylindrical voids is questionable. It is expected that a fair accuracy will be obtained from the theory developed above, if the cylinders have a length-to-diameter ratio not far removed from unity. Under the same restriction, it is expected that the medium will be isotropic at least as long as F is small. The experimental data to be shown provide information about isotropy and the dependence of the dielectric constant on cylinder dimensions and density.

For the cylindrical-void medium, as well as for the spherical-void medium, the measured dielectric constant depends upon the length of the sample. Corkum noted this effect in his shorted-line measurements on artificial dielectrics.[2] However, the variation with length is considerably smaller for the media described in this report. This is due, undoubtedly, to the smaller difference between K_2 and K_1. The elimination of the undesired variation is accomplished by increasing the sample length until dielectric constant reaches a constant value. This value is, in every case, the one reported.

The dielectric constant as a function of the fractional volume is shown in Fig. 5 and Figs. 6 and 7 on page 174. The solid curve is calculated from (4), with

[6] T. W. Dakin and C. N. Works, "Microwave dielectric measurements," *Jour. Appl. Phys.*, vol. 18, pp. 789–796; 1947.

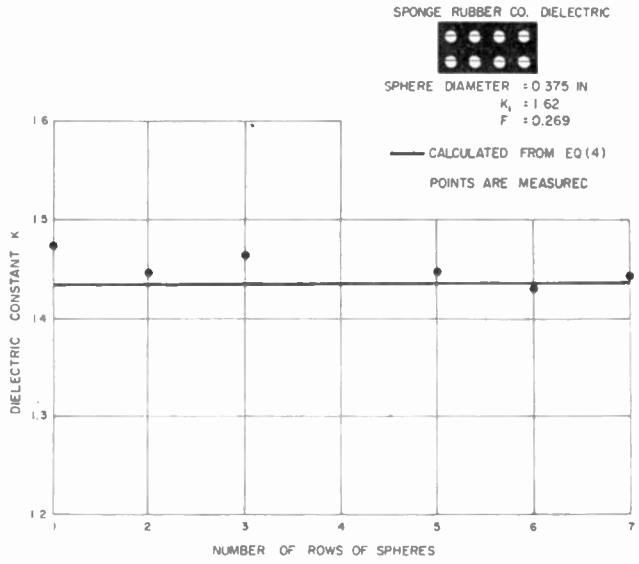

Fig. 2—Dielectric constant of Sponge Rubber Products Company material with spherical voids.

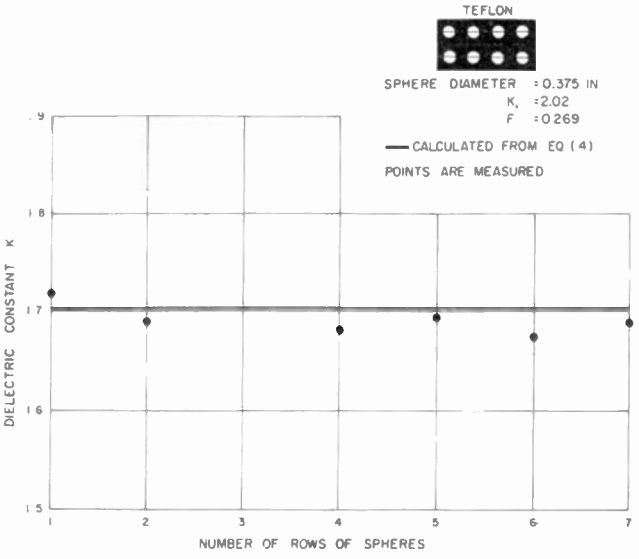

Fig. 3—Dielectric constant of Teflon with spherical voids.

$F = \pi D^2 LN/4V$ (for volume V containing N cylinders of diameter D and length L). The samples are made up of 0.936-inch square blocks which can be arranged so that the axes of all the cylinders are parallel to any one of the three principal axes of the waveguide. The length of the sample can be increased by simply introducing more blocks into the guide.

For samples containing cylinders with a high L/D ratio, Fig. 7, cylindrical voids, were created by drilling holes completely through the blocks, Fig. 1. The remaining samples were constructed in a manner similar to that of the spherical-void samples. It was felt that the anisotropic effects would be largest for large values of L/D. For Figs. 5 and 6, the base material is polystyrene ($K_1 = 2.52$); for Fig. 7, the base material is Plexiglas ($K_1 = 2.64$).

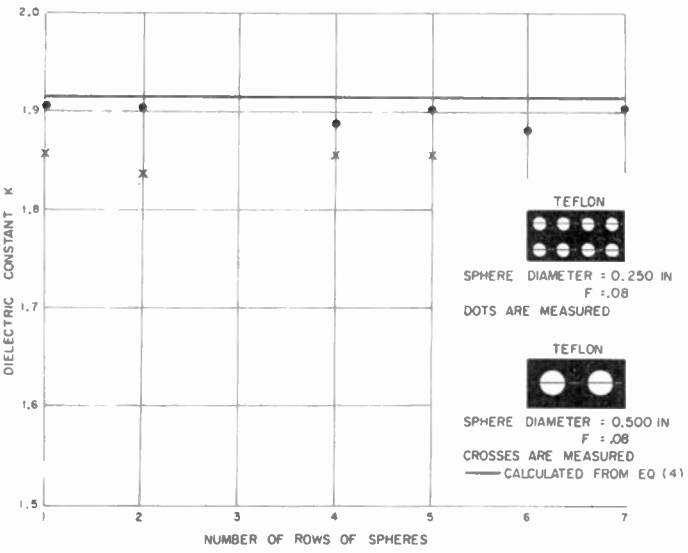

Fig. 4—Dielectric constant of two Teflon samples with spherical voids of same fractional volume but different sizes.

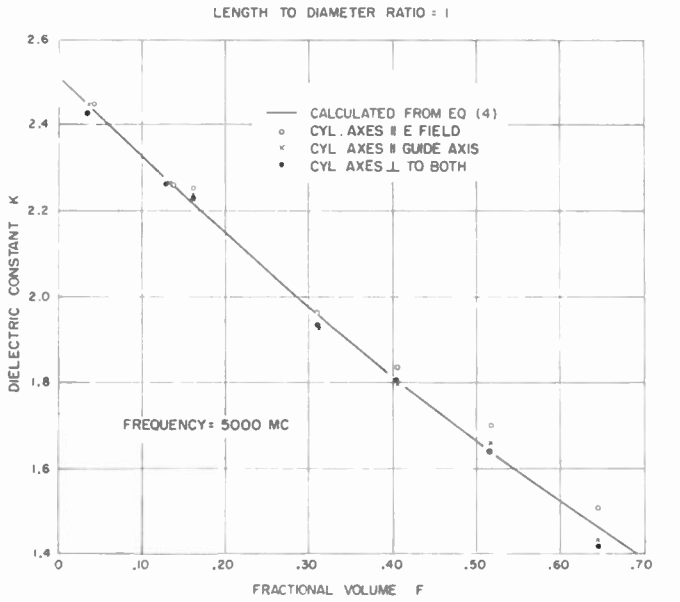

Fig. 5—Dielectric constant of polystyrene with cylindrical voids (length-to-diameter ratio = 1.0).

Discussion

The maximum fractional volume (and hence minimum dielectric constant) is limited by the geometry of the various media. For spheres, F_{max} is $\pi/6$ or 0.524. For cylinders, F_{max} depends on the length-to-diameter ratio:

$$L/D = 1, \quad F_{max} = \pi/4 = 0.785$$
$$L/D = 1/2, \quad F_{max} = \pi/8 = 0.393$$
$$L/D = 2, \quad F_{max} = \pi/16 = 0.196.$$

In practice, however, the maximum values of F are reduced slightly for mechanical reasons. The largest cylinder diameter for which data are shown is about $\lambda'/4$.

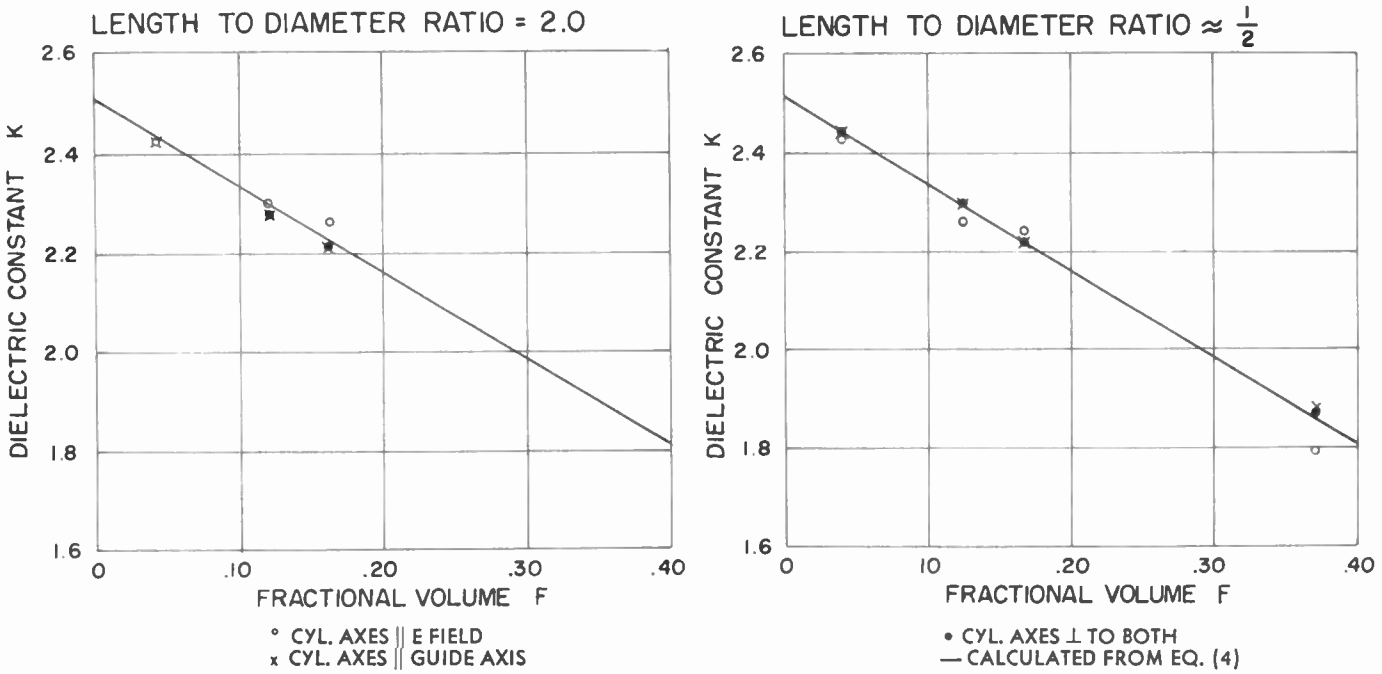

Fig. 6—Dielectric constant of polystyrene with cylindrical voids (length-to-diameter ratios = 2.0 and $\approx \frac{1}{2}$).

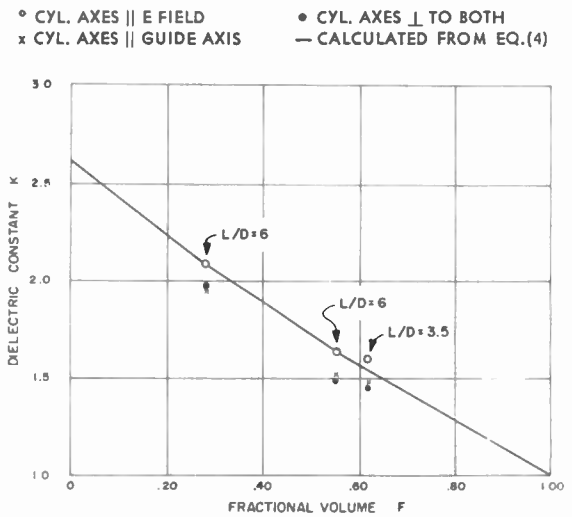

Fig. 7—Dielectric constant of Plexiglas with cylindrical voids.

The dielectric constant predicted by the spherical-object theory has been shown to apply equally well for cylindrical voids of length nearly equal to diameter. Experimental values agree with (4) to within 3 per cent for $0.5 < L/D < 2.0$, and $F < 0.4$.

For large length-to-diameter ratios, the anisotropy of the cylindrical-void media becomes appreciable. For $L/D = 6$ and F as high as 0.6, the largest deviation from the theoretical value was -12 per cent and occurred for the cylinder axes perpendicular to both the E-field and the waveguide axis.

Acknowledgment

The authors are indebted to K. S. Kelleher, who suggested the idea of void dielectrics and contributed to theoretical work. Mr. Kelleher also supervised and directed the investigation.

Broadband Microwave Frequency Meter*

P. H. VARTANIAN AND J. L. MELCHOR†

Summary—**An electronically tunable frequency meter is described for rapidly determining frequency over a wide range. The device depends on paramagnetic resonance in α,α-diphenyl β-picryl hydrazyl. It consists of a two-inch section of coaxial transmission line filled with hydrazyl and placed in a longitudinal magnetic field. Frequencies from 600 mc through X band have been displayed on an oscilloscope by sweeping the magnetic field to 4 kilogauss. Two frequencies 8 mc apart at S band have been resolved and the accuracy for a single frequency is ± 1 mc.**

The complete system is described and performance in L and S bands discussed.

Introduction

PARAMAGNETIC RESONANCE ABSORPTION was first reported by Zavoisky[1] in 1945. Although it is observable at nominal radio frequencies, paramagnetic resonance is most readily observed in the microwave region. A number of useful applications, which employ the sharp resonance line of hydrazyl, are being developed at microwave frequencies. This paper deals with the use of hydrazyl for spectrum analysis and with additional potentials of the m terial.

Paramagnetic resonance is due to transitions between the two Zeeman energy levels which are separated by an applied magnetic field. Resonance occurs at a frequency proportional to the energy separation of the two levels. Since this energy separation is proportional to the field applied perpendicular to the magnetic component of the rf field, the resonant frequency is

$$f_0 = \gamma H_0 \qquad (1)$$

where H_0 is the applied field and γ is the gyromagnetic ratio, 2.8 megacycles per oersted.

The m terial used in this experiment α,α-diphenyl β-picryl hydrazyl $(C_6H_5)_2N-NC_6H_2(NO_2)_3$ will be referred to as hydrazyl. It is a black polycrystalline powder, which can be easily packed into transmission line test sections. Hydrazyl is an organic free radical which exhibits one of the strongest and sharpest paramagnetic resonance absorption lines reported to date. For this reason it is finding use as a material for calibrating magnetic fields. Kittel, *et al.*,[2] in the original paper on hydrazyl in 1950, reported an absorption line half width of 1.35 oersteds. At that time they pointed out that the material would be useful for field calibration and stabilization. Townes and Turkevich[3] reported a line half width of 1.45 oersteds, while Cohen and Kikuchi[4] reported 1.5 oersteds. These values were for single crystals of hydrazyl and correspond to about 4.2 mc. For polycrystalline hydrazyl the line width is several times larger.

Although the absorption line itself is observable, the absorption is found to be too small to significantly alter the amplitude of the rf wave in a transmission line. However, if a small incremental magnetic field h_1 varying at some frequency f_1 is applied in addition to the dc field H_0, then when $f=f_0$ the rf energy will be amplitude modulated at the frequency f_1. If now the rf energy is detected and the output fed into an amplifier tuned to f_1, then an output as a function of magnetic field will occur only at the rf frequencies where $f=f_0$.

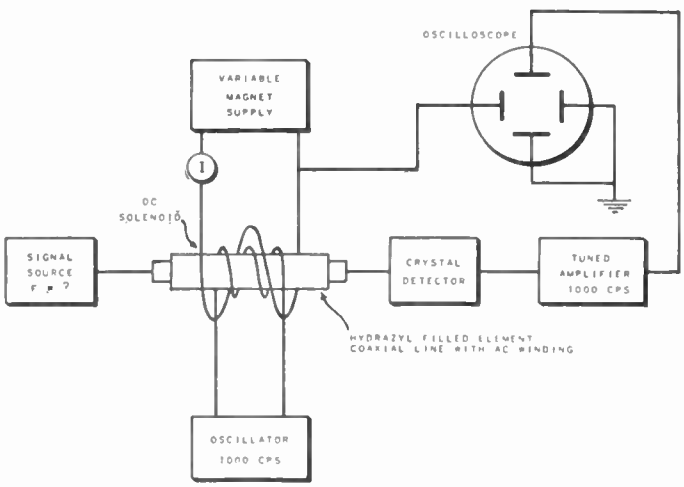

Fig. 1—Block diagram of apparatus used in electronically tunable frequency meter.

Equipment

A block diagram of the equipment is shown in Fig. 1. A 3/8-inch inside diameter 50 ohm coax test section, two inches long, is filled with hydrazyl. A small solenoid of two thousand turns is wound directly on the test section which is fitted with type N connectors at each end as shown in Fig. 2. The test section is inserted directly into the signal transmission path. In addition to the small solenoid on the coax section, the test element is inserted into a larger solenoid capable of de-

* Original manuscript received by the IRE, August 15, 1955; revised manuscript received September 15, 1955. Work performed under Signal Corps Contract No. DA-36-039-sc-31435.

† Electronic Defense Laboratory of Sylvania Electric Products Inc. Mountain View, Calif.

[1] E. Zavoisky, "Paramagnetic relaxation of liquid solutions for perpendicular fields," *Jour. Phys. U.S.S.R.*, vol. 9, pp. 211; May, 1945.

[2] A. N. Holden, C. Kittel, F. R. Merritt and W. A. Yager, "Determination of g-values in paramagnetic organic compounds by microwave resonance," *Phys. Rev.*, vol. 77, p. 147; January, 1950.

[3] C. H. Townes and J. Turkevich, "Hyperfine structure and exchange narrowing of paramagnetic resonance," *Phys. Rev.*, vol. 77, p. 148; January, 1950.

[4] C. Kikuchi and V. W. Cohen, "Paramagnetic resonance absorption of carbazyl and hydrazyl," *Phys. Rev.*, vol. 93, p. 394; February, 1954.

livering magnetic fields up to 2,000 oersteds. A power supply, designed specifically for this large solenoid, is used to supply the field current.

Power (cw) is transmitted through the coax element and detected with a PRD613M broadband detector mount. The output of the detector is fed into a tuned amplifier such as the PRD275. The amplifier is tuned to the same frequency, f_1, as the Hewlett-Packard 200AB audio generator which drives the small coil on

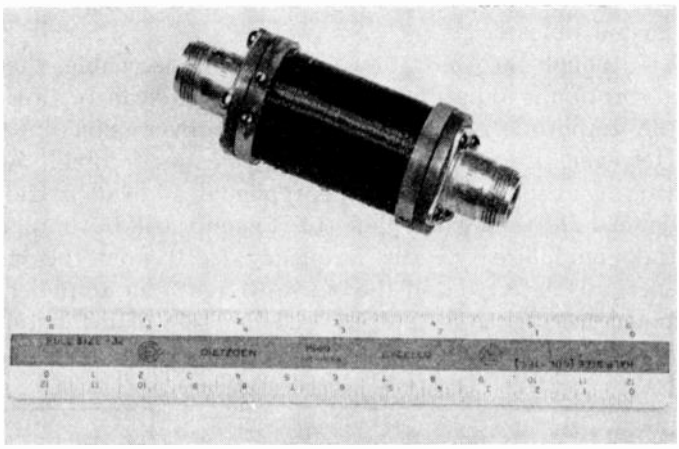

Fig. 2—Photograph of hydrazyl filled coax element.

the coax element. The output of the tuned amplifier is then applied to the vertical plates of a DuMont oscilloscope while a voltage proportional to the dc solenoid current is applied to the horizontal plates. The oscilloscope display indicates the frequencies carried by the transmission line.

The dc solenoid must be able to produce a sufficiently large field to satisfy the resonance equation (1) for the maximum frequency to be determined. It should also be long enough to produce a uniform field over the region in which the element is located.

Principle of Operation

In Fig. 3(a) the relation between the absorption line and the applied fields is shown. With an ac field of amplitude h_1 varying with frequency f_1 superimposed upon a given dc field H_1, the total field acting on the hydrazyl varies from H_1-h_1 to H_1+h_1, and for the position shown, the attenuation of the rf waves varies from α_1 to α_2. If H_1 indicates the inflection point on the absorption curve, this accounts for the first peak in Fig. 3(b). As the dc field increases to H_0, the attenuation becomes independent of h_1 and hence there is no output at f_1. At the second inflection point a large output of frequency f_1 occurs, while beyond the absorption curve no output is observed. If the amplitude of the modulating field is made small then the output as a function of H will be as shown in Fig. 3(b).

It is noted that the purpose of using a small ac magnetic field is to produce modulation of the rf wave when the resonance field H_0 is applied. Using an ac field gives two improvements over the alternate method of detecting a small attenuation in the cw wave due to the absorption line itself. In the first place, it makes it possible to use a high gain tuned amplifier which responds only to the modulation produced by the hydrazyl absorption line. This permits higher sensitivity since the ratio of signal at resonance to that off resonance is essentially infinite, while in an absolute measurement the signal at resonance is only slightly less than the off resonance signal. The second advantage of using the ac field is that greater precision in frequency determination is achieved since the null point accurately fixes the frequency, f_0. This can be seen by comparing Figs. 3(a) and 3(b).

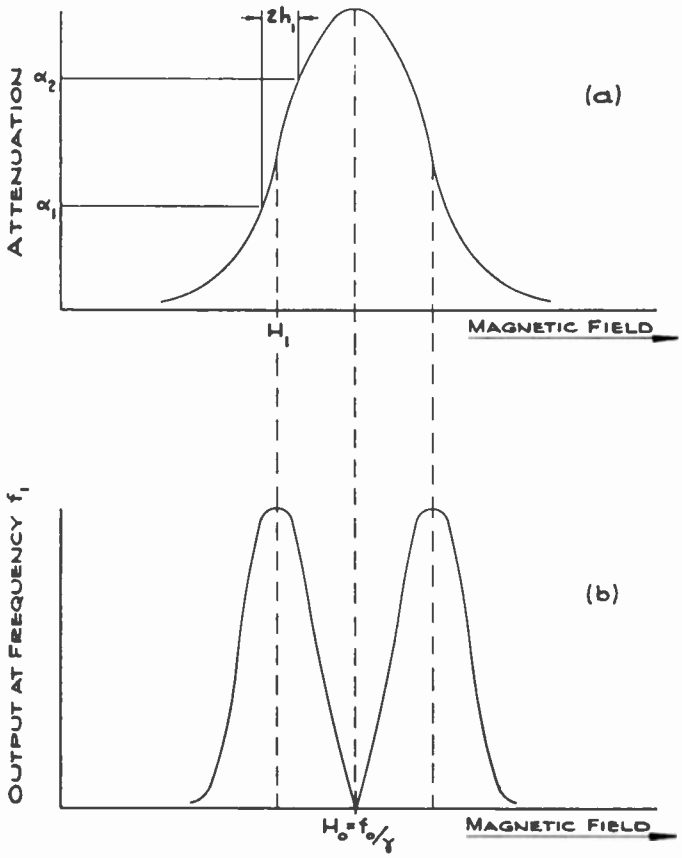

Fig. 3—(a) Paramagnetic absorption line. (b) Output signal at f_1 as a function of magnetic field for a given frequency, f_0.

Discussion of Experimental Data

In Fig. 4(a) is shown the oscilloscope trace when two frequencies, one at 1,200 mc and the second at 3,500 mc, are present in the transmission system. In Fig. 4(b) is shown an expanded view of the output from the tuned amplifier. It is the derivative of the hydrazyl absorption line and is similar in shape to the curve of Fig. 3(b). The asymmetry is due to the use of polycrystalline hydrazyl. This asymmetry is discussed by Kikuchi and Cohen.[5] The signal generator of the upper trace was set at 2,000 mc while that in the lower trace is for the identical system with the signal generator

[5] *Ibid.*, p. 394.

set at 2,008 mc. Thus the minima are separated by 8 mc. It is seen that it should be possible to determine the frequency of the unknown signal easily to within 1 mc. Since the magnetic field in a solenoid is linear with current, the ratio of signal frequency to current is a constant for a given solenoid. This constant is determined by calibrating with signals of known frequencies. Frequency determination is then reduced to a current measurement. For accurate frequency measurements, the current must be metered to within the desired precision. Measurements have been made on the line width over the entire band from 800 mc to 4,000 mc. It has been found that the line width is less than 10 mc over this entire band. The line width here is the separation of two maxima shown in Fig. 4(b). These maxima correspond to inflection points of hydrazyl absorption line.

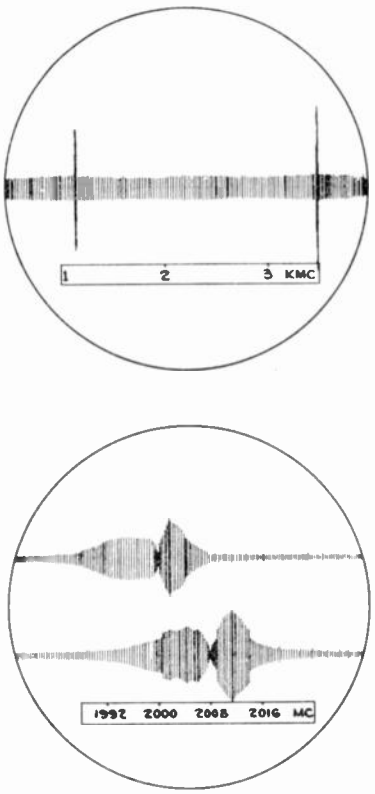

Fig. 4—(a) (Upper) Oscilloscope presentation for two signals at 1,200 and 3,500 mc. (b) (Lower) Oscilloscope presentation for two signals at 2,000 and 2,008 mc.

Measurements were also made in a transverse field produced by an electromagnet. Both the coaxial element of Fig. 2 and a hydrazyl loaded strip-line were used. Use of an electromagnet makes it possible to cover X band with a very compact field source.

With f_1 at 1,000 cps, the frequencies of cw signals and signals with very low pulse rates and high duty cycles have been measured. Alternately frequency measurements have been made for signals having higher pulse rates than f_1. For pulse signals it is necessary to choose f_1 far above or below the Fourier components of the rf envelope so that the tuned amplifier will not respond to the harmonics of the pulse envelope. It should be noted that in order to get the high frequency modulating fields into the hydrazyl the coax outer conductor must be made without a shorted turn. This can be accomplished by slotting the outer conductor longitudinally.

In the present system no special attempts have been made to achieve high signal-to-noise ratios in the tuned amplifier. Thus frequency has not been determined for signal levels below -35 dbm. The lowest microwave frequency detected with this arrangement has been 600 mc. However, hydrazyl has been studied at 25 mc[6] and there appears to be no theoretical limitation to its lowest useful frequency except the sensitivity decreases with lower frequency. Since the line width is nearly constant, the percentage accuracy decreases with frequency. To cover the frequency range 600 to 4,000 mc requires magnetic field values from 214 to 1,430 oersteds. To operate the device above S band the solenoid and power supply necessary to produce the high fields become quite large. To facilitate measurements in X band, a transverse field can be provided by an electromagnet. The use of the electromagnet has the disadvantage that the frequency is proportional to the magnetizing current only in the linear region of the magnetization curve. Otherwise a calibration curve is required. Furthermore, the dc field must be swept in only one direction (*e.g.*, sawtooth with blanking on the retrace) to avoid complications from electromagnet hysteresis effects.

Although the two observed signals shown in Fig. 4(b) are separated by approximately 8 mc, the null point between them, which is an indication of the true frequency, can be determined to within about 1 mc. However, two simultaneously incident signals of this separation could not be resolved.

References indicate that the use of single crystals will reduce the line width by a factor of 2 or 3. This permits a more accurate determination of frequency. Furthermore, a smaller line width will improve the resolution of two signals differing in frequency by a small increment. A more homogeneous dc field will also improve the line width.

The system has the same limitation as a system which depends on mixing. That is, if two signals are incident with a frequency difference equal to the tuned amplifier frequency, f_1, a signal is transmitted to the output. However, in the display, such a difference signal will be independent of magnetic field and will completely mask the oscilloscope display. Although without additional circuitry the presence of this signal is unavoidable, it can be easily identified from its display pattern. With laboratory-type testing, or when operating with a low density of incident signals, the probability of having two signals separated by f_1 will be fairly small. The limitation of spurious responses caused by two rf signals separated by f_1 can be improved by adding to the system

[6] L. S. Singer, and E. G. Spencer, "Temperature variation of the paramagnetic resonance absorption of two free radicals," *Jour. Chem. Phys.*, vol. 21, p. 939 May, 1953.

a feature which will discriminate against outputs that are independent of the rate of dc field change.

Conclusions

Paramagnetic resonance in materials such as hydrazyl is useful for a wide class of spectrum analysis applications.

The main advantage of the system is its extreme bandwidth coverage. Frequency measurements using the solenoid covered 600 to 4,000 mc. Use of electromagnet enabled measurements in X band, but hysteresis introduces nonlinear relation between current and frequency.

For the modulation frequency and amplifier used, the limiting sensitivity was found to be −35 dbm. This can be improved with a sharply tuned amplifier with a lower noise figure.

The setup as described employs standard laboratory equipment which is readily available. The system has the further advantage of simplicity. It is electronically tunable with an oscilloscopic presentation of frequency. For production-line applications, it is easily used by unskilled operators. This makes it valuable for routine testing of microwave tubes where the output frequencies may occur over broad ranges.

The Frequency Response of Bipolar Transistors with Drift Fields*

L. B. VALDES†, MEMBER, IRE

Summary—**The frequency response of bipolar transistors is calculated using a model which assumes that the spread in the transit time of minority carriers flowing from emitter to collector is the major factor in determining the frequency cutoff. The total emitter-to-collector transit time is determined by the combined effects of drift and diffusion but the spread in transit time is determined exclusively by diffusion. The analysis is adapted to point-contact transistors and checks experimental measurements of frequency cutoff in four groups of point-contact transistors having different structure and material parameters.**

Introduction

ONE OF the more important design parameters for transistors is the frequency response of the current multiplication or alpha. In bipolar transistors, where the flow of minority carriers from emitter to collector is by thermal diffusion, such as in the grown-junction or alloyed-junction *n-p-n* and *p-n-p* transistors, there is usually good agreement between calculated and experimentally measured values of frequency cutoff. However, such agreement is not found in transistors where there is an appreciable drift field, such as in point-contact transistors.[1]

This discrepancy between theory and experiment is directly attributable to the relative difficulty of the boundary-value problems involved. The diffusive flow of minority carriers in one dimension is a reasonably straight-forward problem which has been solved[2] and used to calculate the frequency response of planar junction transistors.[3,4] Fortunately, the emitter and collector boundaries in this problem can be made to fit the transistor structure if the edge effects (which are usually small) are neglected. Using superposition, it has also been shown[5] that one-dimensional diffusion theory is applicable to point-emitter junction-collector transistors, where the emitter is free to inject minority carriers away as well as toward the collector sink.

An exact solution of the carrier-flow problem in point-contact transistors is one of the most complicated boundary-value problems in all semiconductor electronics. Not only is it a three-dimensional problem but the strong drift field produced by the ohmic flow of collector current (even when the emitter current is zero) leads to nonlinear differential equations. This means that instead of attempting a straightforward solution, it is desirable to make an "educated engineering guess" and postulate a simpler structure for analysis. Then the results can be related to the actual structure and compared with experimental measurements.

* Original manuscript received by the IRE, July 18, 1955; revised manuscript received, September 23, 1955.

† Work performed at Bell Telephone Labs., Murray Hill, N. J. Now with Beckman Instruments, Inc., Fullterton, Calif.

[1] The planar structure with a built-in field across the base is discussed by H. Krömer, "Zur Theorie des Diffusions- und des Drift-transistors." *Arch. Elekt. Übertragung*, vol. 8, pp. 223–228, 363–369, 499–504; 1954.

[2] W. vanRoosbroeck, "Theory of flow of electrons and holes in semicondutors," *Bell Sys. Tech. Jour.*, vol. 29, pp. 560–607; October, 1950.

[3] W. Shockley, M. Sparks, and G. K. Teal, "*p-n* junction transistors," *Phys. Rev.*, vol. 83, pp. 151–162; July, 1951.

[4] R. L. Pritchard, "Frequency variations of current-amplification factor for junction transistors," PROC. IRE, vol. 40, pp. 1476–1481; November, 1952.

[5] R. H. Kingston, "A point emitter—junction collector transistor," *Jour. App. Phys.*, vol. 25, pp. 513–515; April, 1954.

Proposed Mechanisms

The first attempt to calculate the frequency cutoff of point-contact transistors was made by Shockley.[6] He considered this strictly as a three-dimensional drift problem in n-type germanium and by graphical field mapping estimated the spread in the transit time of holes from emitter to collector. The expression for frequency cutoff,[7] which is shown in Fig. 1, gives results which are several times larger than the measured values. It also predicts a linear dependence of frequency cutoff with emitter current, whereas, experimental results show that the frequency cutoff of alpha is almost independent of emitter current.

A second model which has been proposed[8] by J. E. Thomas considers the flow of minority carriers in the immediate vicinity of the emitter. It has been shown[9] that in an intrinsic semiconductor both holes and electrons obey the laws of ambipolar diffusion and are unaffected by the presence of a drift field. Thomas argues in a qualitative way that because of the small radius of contact, the current densities in the vicinity of a point contact are very large. Then this region is heavily conductivity modulated and the injected holes (in an n-type point-contact transistor) must diffuse away from the emitter before entering the region of high electric field. Since diffusion is a relatively slow process, the frequency response may be determined by the size of this region of ambipolar diffusion.

The strongest objections to the ambipolar diffusion model is the lack of quantitative results. In order to relate the frequency cutoff to the structure, it would be necessary to solve the three-dimensional flow problem and extend its solution to the large-signal (high-current) region. In addition, it would be desirable to consider a model for the emitter and analyze the distribution of both hole and electron currents in order to preserve the continuity of current at the boundary between the emitter p-n junction and the ambipolar region.

There is still a third model which can be used to explain the frequency behavior of the current multiplication α. Normally the flow of minority carriers in the base region of point-contact transistors is by drift. However, the diffusion mechanism cannot be ngelected entirely. For instance, even though the transit time from emitter to collector of a short pulse of minority carriers may be determined by the drift field, there will be a spreading of the pulse which is attributable to diffusion. When the transit time is large enough so that repetitive pulses overlap due to this spreading, there will be a substantial reduction in the amplitude of the alternating signal.

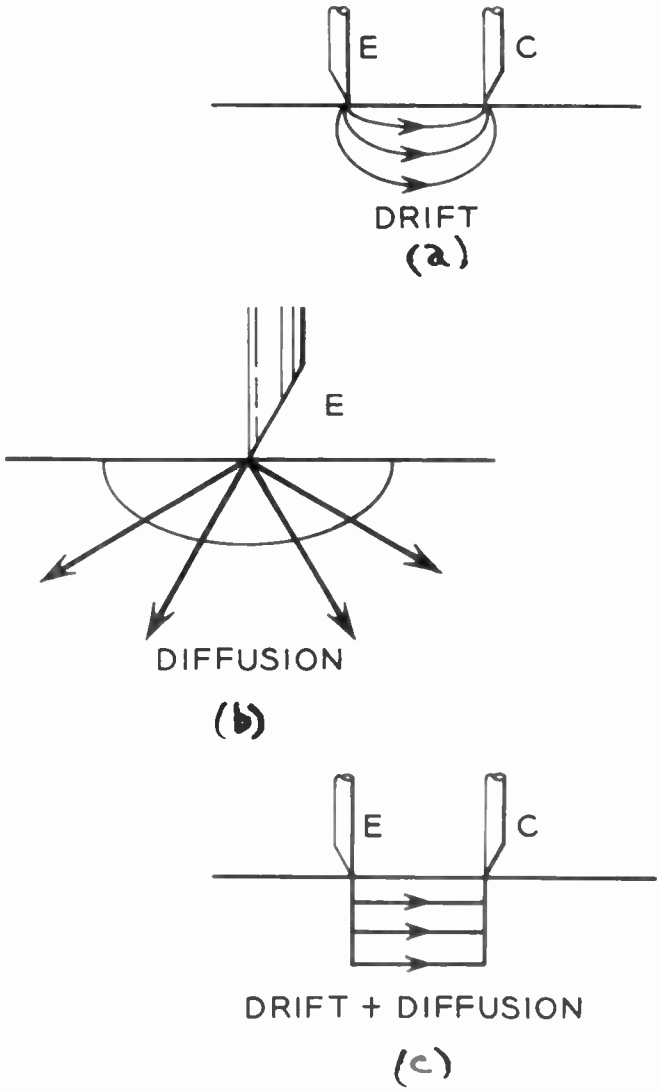

Fig. 1—Mechanism for frequency cutoff. (a) Spread in transit time from emitter to collector—$f_c = \mu_p I_e \rho / s^3$. (b) Ambipolar diffusion in quasi-intrinsic region around emitter. (c) Spread in transit time due to diffusion superposed on a drift field—one-dimensional solution.

A summary of the three proposed mechanisms is sketched in Fig. 1. Actually the remainder of this paper will be devoted to discussing these combined effects of drift and diffusion flow. Although this problem will be solved in only one dimension, it will be shown that by suitable assumptions the results are applicable to the three-dimensional flow in point-contact transistors.

Description of the Analytical Model

The model which will be solved here is shown in Fig. 2. It may be noted that an emitter in a point-contact transistor is able to inject carriers some of which initially

[6] W. Shockley, "Electrons and Holes in Semiconductors," D. Van Nostrand Co., Inc., New York, pp. 106–108; 1950.

[7] The following terms are used in Figure 1: f_c = cutoff frequency in mcps, μ_p = mobility of holes in cm²/volt-second, I_e = emitter current in amperes, ρ = resistivity of the germanium in ohm-cm, s = emitter to collector spacing in cm.

[8] J. E. Thomas, "The Frequency Cutoff of Alpha in Point-Contact Transistors," Transistor Research Conference, Pennsylvania State University; June, 1953.

[9] W. van Roosbroeck, "The transport of added carriers in a homogeneous semiconductor," *Phys. Rev.*, vol. 11, pp. 282–289; July, 1953.

will flow away from the collector. Therefore, in order to solve the flow problem, it is desirable to use a fairly simple one-dimensional model and superpose the various current components.

It is possible to use superposition when the problem can be described with linear differential equations. This will be the case if it is assumed that:

1. The semiconductor is extrinsic.
2. Small-signal theory is applicable (the conductivity of the semiconductor is not modulated by large minority carrier densities).
3. The vector magnitude of the electric (drift) field is constant within desired boundaries.
4. The mobility and diffusion constant are independent of the minority carrier concentration (this will be the case if small-signal theory is applicable).

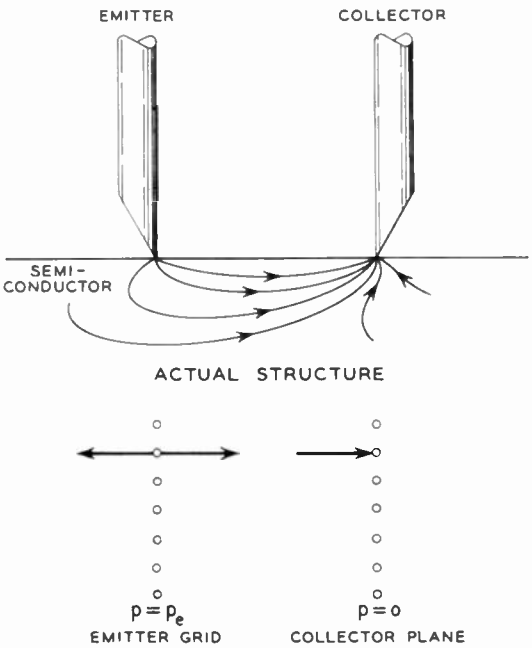

Fig. 2—Proposed one-dimensional model.

In order to represent this problem mathematically, it has been decided to use the concept of physicists' grids. These may be conceived to be like closely spaced grid wires which establish a certain minority carrier density at a particular plane in the semiconductor. Yet, they represent only a small fraction of the cross-sectional area so that carriers are able to flow through them. In an analogous way, the behavior of a physicist's grid in a semiconductor is similar to that of a vacuum tube grid which also happens to be a good electron emitter. These grids are shown in Fig. 2; however, it is desirable to define their properties more specifically for a bipolar transistor. For instance:

5. The emitter physicist's grid is free to inject minority carriers in both directions. Those carriers injected to the right will flow towards the collector.
6. The minority carrier density at the plane of the collector physicist's grid must be zero. This is because in the actual structure, the collector junction is reverse-biased.
7. The grids cannot collect minority carriers and those that flow toward a physicist's grid simply go through them. The zero minority carrier density at the collector is obtained by having the collector grid inject carriers of the same charge but negative concentration.

It can be shown that this one-dimensional model fits a point-contact transistor if all the carrier flow in the transistor is constricted very near the surface of the germanium crystal. Then the minority carriers would flow essentially along a straight line between electrodes. Even if this is not the case in an actual transistor, Shockley has shown[6] that the spread in transit-time due to carriers following different drift paths would give a much higher frequency cutoff then experimentally observed. Therefore, it is reasonable to assume that:

8. The spread in transit-time due to the minority carriers which follow different drift flow paths from emitter to collector is negligible when compared to the spread in transit-time due to diffusion effects.

This makes it possible to use the one-dimensional model for calculating the frequency response of the transport factor. In addition, it must be assumed that:

9. The diameter of the emitter and collector electrodes is small compared to the distance between electrodes.

When this assumption cannot be met in practice, reasonably good results are obtained by using the shortest distance along the surface of the semiconductor between electrodes rather than the distance between the centers of the two contact areas.

General Solution for Frequency Response

The mechanics of solving the continuity equation and obtaining the frequency dependent expressions for emitter and collector minority-carrier currents are discussed in the appendices. From these, the transport factor β for minority carriers in the base region can be calculated. The frequency cutoff is defined as the frequency at which the magnitude of β is 0.707 of its low-frequency value.

Appendix I tackles the problem where there is a constant sweeping field of magnitude E causing the flow of minority carriers toward the collector. This electric field may be produced in planar geometry by the flow of majority-carrier collector current. In this case, the frequency-dependent transport factor for a small sinusoidal signal applied to the emitter is

$$\beta = \exp\left[\left(\frac{q}{kT}\frac{E_x}{2} - \sqrt{\left(\frac{q}{kT}\frac{E_x}{2}\right)^2 + \left(\frac{1 + j\omega\tau_p}{L_p^2}\right)}\right)s\right], \tag{1}$$

where

$q/kT = 40$ volts^{-1} at 290°K.

E_x = drift field in volts/cm; positive if field is aiding carrier flow towards the collector, negative if the field is in opposition.

τ_p = lifetime of holes in n-type germanium in seconds.

L_p = diffusion length for holes in cm.

s = emitter to collector spacing in cm.

$\omega = 2\pi f$ = angular velocity.

f = frequency of the applied sinusoidal emitter signal in cps.

The dc transport factor β_0 corresponds to (1) with $\omega = 0$. Fig. 3 is a plot of values of β_0 for hole lifetimes τ_p in n-type germanium of 1 and 10 microseconds. The two cases of $E_x = 0$ are for purely diffusive flow of minority carriers toward the collector.

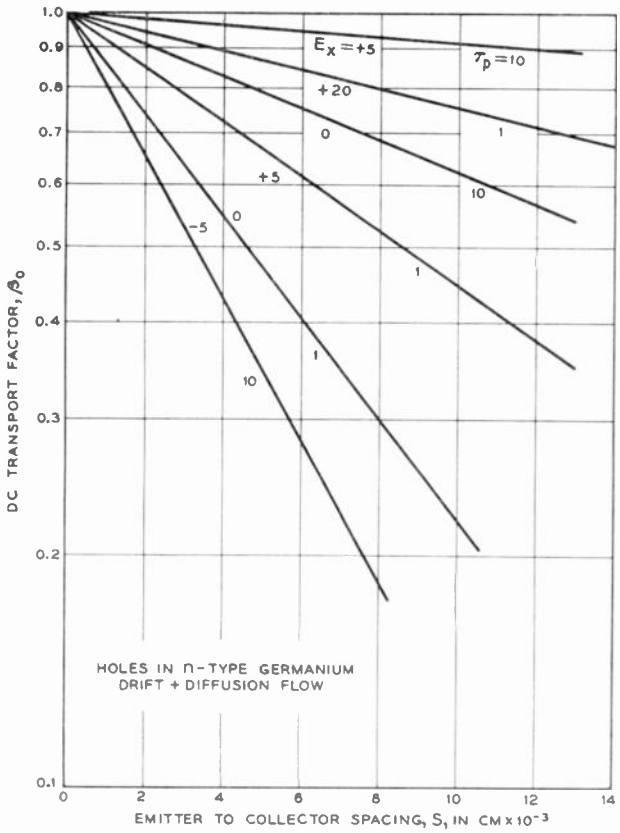

Fig. 3—Transport factor of emitter with a drift field.

The frequency cutoff can be obtained by finding the frequency at which

$$\frac{\beta}{\beta_0} = 0.707 \quad \text{or} \quad \frac{\beta}{\beta_0} = e^{-0.3465+j\theta}. \tag{2}$$

Numerical solutions to (2) have been obtained for the case of $\tau_p = 10$ microseconds, and the results are shown in Fig. 4. A hole mobility of $\mu_p = 1{,}700$ cm^2/volt-second has been used in these computations. The effect of different values of lifetime is usually secondary except with very small sweeping fields. This is illustrated in

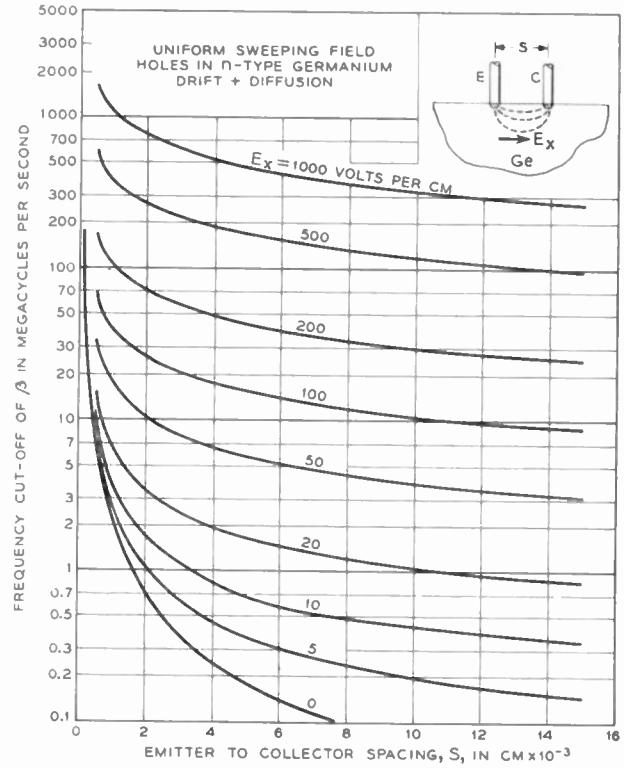

Fig. 4—Frequency cutoff with uniform drift field.

Table I, which gives a few calculated values of the frequency cutoff of β as a function of hole lifetime τ_p, sweeping field E_x, and emitter to collector spacing s.

TABLE I

s cm×10^{-3}	E_x volts/cm	τ (microseconds) 1	10	100	
2.5	0	0.98	0.47	0.34	Frequency cutoff mcps
2.5	5	1.18	0.79	0.73	
2.5	10	1.63	1.33	1.30	
2.5	20	2.95	2.76	2.73	

In bipolar transistors where the sweeping field E_x is constant, the theoretical value of the cutoff frequency f_c can be obtained from Fig. 4. However, in other devices such as point-contact transistors, the sweeping field E is produced by the flow of collector current in nonplanar geometry and increases as the distance to the collector diminishes. It is necessary, therefore, to determine the average field which minority carriers see in transit from the emitter to the collector.

Appendix II treats the problem of a variable field. It is recognized that insofar as determining the frequency response is concerned the average transit time from emitter to collector of the injected holes is the most significant characteristic. Equivalent electric field E_x was determined in Appendix II by equating transit time in actual case where field is a function of distance to transit time for same minority carriers with a constant field of magnitude E_x. This represents another "engineering" approach to the problem which is far more satifactory than substituting expression for field as a function of distance in continuity equation and attempting to solve a nonlinear differential equation.

Fig. 5 shows the results which are obtained when the electric field is expressed in terms of the resistivity ρ of the n-type germanium (in ohm-cm) and the collector current I_c (in amperes) which produces the sweeping field. Since this analysis is based on small-signal theory, the value of I_c to use is the collector current with zero emitter current. As the emitter current I_e is increased, I_c will also be larger but will then be partly composed of minority carrier current and the resistivity ρ of the material will be modulated (decreased) in the region of interest so that the drift field does not increase as rapidly as might be expected.

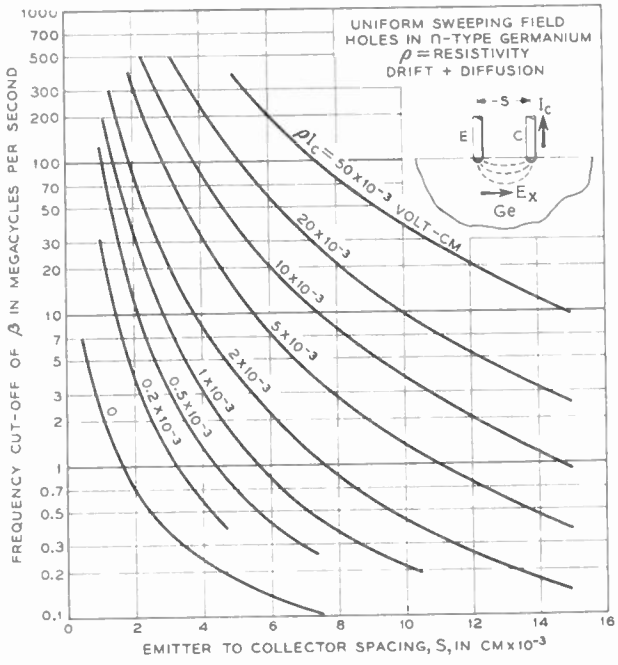

Fig. 5—Frequency cutoff of point-contact transistor structures.

Experimental Results and Conclusions

In order to check the calculated values of frequency cutoff shown in Fig. 5, examination was made of the measurements of a large number of point-contact transistors having four different sets of structural parameters. These results are presented in Table II. It is significant to note that there is good agreement between theory and experiment when all the assumptions in this analysis are considered. Furthermore, it is possible to explain many of the discrepancies in Table II if it is remembered that there is a large range of values of I_c (0, V_c) within each of the groups and that only the average value has been used in the calculations of f_c. The statistical variation in the measured values of ρ and s is not as significant because close control of these parameters was exercised.

The analysis presented here is equally applicable to any transistor which has the same structure as the model of Fig. 2. It is, nevertheless, important to remember that point-contact transistors are the most common devices which fit this description. Therefore, this paper might be construed as filling in one area of the design theory for point-contact transistors which has not been adequately described until now. While this mechanism is not considered to be exclusive, it is shown to be the dominant mechanism for determining the frequency cutoff in four different types of point-contact transistors.

TABLE II

ρ ohm/cm	1.0	2.0	5.0	7.0
s cm	2.0×10^{-3}	5×10^{-3}	5×10^{-3}	12.5×10^{-3}
$I_c(0, V_c)$ in mA	−2.0	−2.5	−1.0	−0.4
Calculated f_c in mcps	80	14	14	0.25
Measured f_c in mcps	20–80	3.0–9.0	0.6–9.0	0.1–1.0
Bias conditions (I_e, V_c)	(0.5, −7)	(1.0, −20)	(1.0, −10)	(1.5, −5)

Appendix I

Calculation of Transport Factor β with Both Drift and Diffusion Fields

The one-dimensional continuity equation for the flow of holes in n-type extrinsic semiconductors is

$$\frac{\partial p}{\partial t} = \frac{-p}{\tau_p} - \mu_p E_x \frac{\partial p}{\partial x} + D_p \frac{\partial^2 p}{\partial x^2}, \tag{3}$$

where

p = excess hole density = holes/cm³
τ_p = lifetime of holes = seconds.
μ_p = mobility of holes = 1,700 cm²/volt-seconds for germanium
D_p = diffusion constant = 44 cm²/second for germanium
x = distance = cm
t = time = seconds
E_x = electric field in the x-direction = volts/cm.

This equation, which is only applicable to small concentrations in extrinsic n-type material, has been solved by van Roosbroeck[2] for the case of

$$\frac{\partial p}{\partial t} = 0.$$

This equation also has been extended to any resistivity by van Roosbroeck,[9] but there is no need to consider the more general case here.

For the ac case the solution is

$$p = p_0 e^{+j\omega t} \exp\left[\left(\frac{q}{kT}E_x - \sqrt{\left(\frac{q}{kT}E_x\right)^2 + 4\left(\frac{1+j\omega\tau_p}{L_p^2}\right)}\right)\frac{x}{2}\right]. \tag{4}$$

In this expression the concentration at $x=0$ is $p_0 e^{j\omega t}$, the constant $q/kT = 40$ at 290°K, and the (−) sign is used before the square root because this is the only solution which is physically realizable. L_p is a constant called

diffusion length and defined as $L_p^2 = D_p\tau_p$. When the field is aiding diffusion (pointing in the $+x$ direction) E_x is a positive number.

The dc hole current density $\overline{J}_p$ is given[10] by

$$\overline{J}_p = q\mu_p E(p + p_n) - qD_p\nabla p, \tag{5}$$

where p_n is the hole density normally present in n-type germanium. The alternating current density along the $+x$ direction is

$$J_p = q\mu_p E_x p - qD_p \frac{\partial p}{\partial x}, \tag{6}$$

or, with the aid of equation (4),

$$J_p = qp\left[\frac{\mu_p E_x}{2} + \sqrt{\left(\frac{\mu_p E_x}{2}\right)^2 + \frac{D_p}{\tau_p}(1 + j\omega\tau_p)}\right]. \tag{7}$$

In this case (for current flow toward x positive) E_x is a positive number when the field is aiding and negative if the field is opposing.

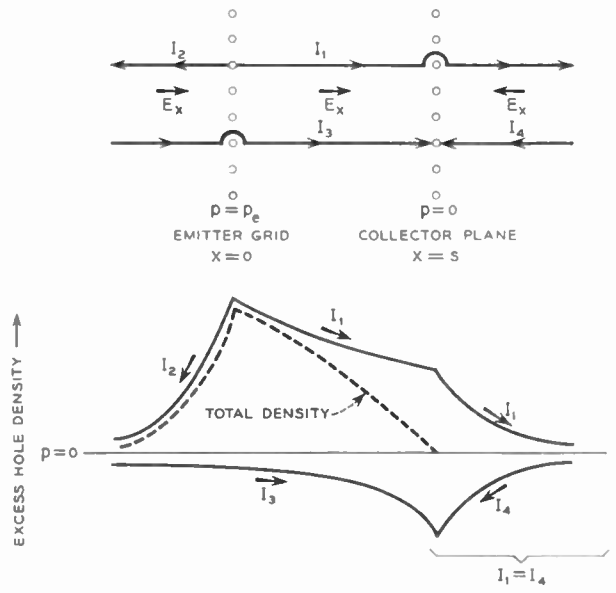

Fig. 6—Model for current flow using superposition.

The ac transport factor β can be calculated by superposition from the model of Fig. 6 which defines four components of the current flow. In this case the electrical field E_x will be taken in the direction from emitter to collector so that the field aids the flow of $I_1(x)$ at $x<s$, $I_4(x)$, and $I_3(x)$, and opposes $I_2(x)$ and $I_1(x)$ at $x>s$. The ac hole density at the emitter ($x=0$) due to I_1 and I_2 only is

$$p_e = p_{0e}e^{j\omega t}, \tag{8}$$

and at the collector ($x=s$)

$$p_c = p_{0c}e^{j\omega t}\exp\left[\left(\frac{q}{kT}E_x - \sqrt{\left(\frac{q}{kT}E_x\right)^2 + \left(\frac{1 + j\omega\tau_p}{L_p^2}\right)}\right)\frac{s}{2}\right]; \tag{9}$$

then the currents are

$$I_1(0) = qp_e[E_+], \tag{10a}$$
$$I_2(0) = qp_e[E_-], \tag{10b}$$
$$I_3(s) = qp_c[E_+], \tag{10c}$$

and

$$I_4(s) = qp_c[E_+]. \tag{10d}$$

The terms $[E_+]$ and $[E_-]$ represent the expressions within the brackets in (7) for the drift field aiding and opposing diffusion respectively.

Since the emitter current is the sum of $I_1(0)$ and $I_2(0)$ and the collector current is the sum of $I_3(s)$, $I_4(s)$, and the change in $I_1(s)$, the transport factor β (ratio of collector hole current to emitter hole current) is equal to the ratio of hole densities at the collector and emitter. Then,

$$\beta = \exp\left[\left(\frac{q}{kT}\frac{E_x}{2} - \sqrt{\left(\frac{q}{kT}\frac{E_x}{2}\right)^2 + \left(\frac{1 + j\omega\tau_p}{L_p^2}\right)}\right)s\right]. \tag{11}$$

Appendix II
Effect of a Nonuniform Drift Field

In point-contact transistors, the drift field is produced by the flow of I_c amperes of collector current. The electric field at any distance x (centimeters) away from the collector can be obtained by taking the gradient of the floating potential.[11] This gives

$$E(x) \approx \frac{I_c\rho}{2\pi x^2}\left[1 - 0.226\frac{x^3}{w^3}\right], \tag{12}$$

where w is the thickness of the slice of semiconductor and ρ is the resistivity (ohm-cm). It is apparent that in most cases the x^3/w^3 term can be neglected.

Minority carriers will flow from emitter to collector in the structure of Fig. 2 at a velocity which is given by[2]

$$v = \frac{\mu_p E}{2} + \sqrt{\left(\frac{\mu_p E}{2}\right)^2 + \frac{D_p}{\tau_p}}. \tag{13}$$

This expression includes the effects of both drift and diffusion and simplifies at large fields to $\mu_p E$. However, at fields larger than 900 volts/cm., the mobility holes of in n-type germanium varies[12] as $E^{-1/2}$ and the velocity becomes

[10] W. Shockley, *op. cit.*, p. 299.

[11] L. B. Valdes, "Effect of electrode spacing on the equivalent base resistance of point-contact transistors," PROC. IRE., vol. 40, pp. 1429–1434; November, 1952.

[12] E. J. Ryder, "Mobility of holes and electrons in high electric fields," *Phys. Rev.*, vol. 90, pp. 766–769; June, 1953.

$$v = \mu_p \left(\frac{E}{900}\right)^{-1/2} E = \mu_p \sqrt{900 \cdot E(x)}, \tag{14}$$

with $\mu_p = 1{,}700$ cm²/volt-seconds and the field given as

$$E(x) = \frac{I_c \rho}{2\pi x^2}. \tag{15}$$

The actual transit time of minority carriers from emitter ($x = s$) to collector ($x = 0$) can be obtained by integrating over the distance as

$$\text{t.t.} = -\int_0^s \frac{dx}{v}, \tag{16}$$

where v is the velocity of the carriers (a function of the distance x). In practice this can be accomplished better by subdividing the distance into regions and later adding the transit times for carrier flow across each of the regions.

Fig. 7 shows the different regions around the collector. In the nonlinear mobility region, the velocity is given by (14) and the transit time is

$$\text{t.t.}_1 = -\int_a^0 \frac{dx}{\mu_p \sqrt{900}\sqrt{E(x)}} = -\frac{1}{30\mu_p}\sqrt{\frac{2\pi}{\rho I_c}}\int_a^0 x\, dx. \tag{17}$$

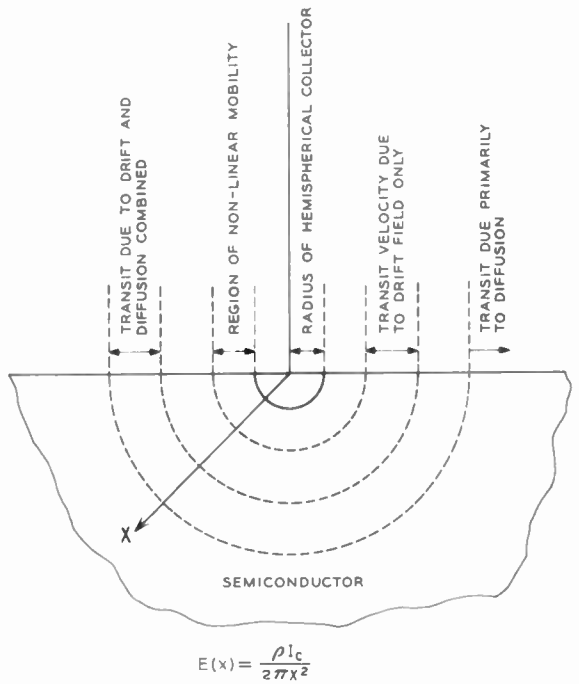

Fig. 7—Regions near transistor collector of different electric field.

The distance a is where the field equals 900 volts/cm or

$$a = \sqrt{\frac{\rho I_c}{2\pi \cdot 900}}. \tag{18}$$

When $s < a$, the emitter to collector distance s can be substituted for a and the total transit time is given by (17). At slightly larger distances (with the emitter in the region where the transit time is due only to the high drift field) a second component of transit time (t.t.$_2$) must be added to t.t.$_1$ in order to obtain the total transit time. This component is given as

$$\text{t.t.}_2 = -\int_s^a \frac{dx}{\mu_p E(x)} = -\frac{2\pi}{\rho I_c \mu_p}\int_s^a x^2 dx. \tag{19}$$

Both of these equations can be integrated in a straightforward manner.

When the emitter is in a region of sufficiently small drift field, it is necessary to use (13) to represent the carrier velocity. This defines another region although the boundary must be somewhat arbitrarily selected. In the problem solved here, it was decided that at fields greater than 20 volts/cm., the simpler expression for velocity may be used and the boundary $x = b$ was defined

$$b = \sqrt{\frac{\rho I_c}{40\pi}}. \tag{20}$$

To obtain the transit time t.t.$_3$ of holes in the region $x > b$, (13) is substituted into (16). Unfortunately this gives an expression which is not directly integrable.

The transit time t.t.$_3$ in the region where both drift and diffusion are important was obtained by expanding the velocity in power series about the two limiting conditions of very large and very small drift fields. The number of terms increases very rapidly if it is desired to get close to the critical field E_c given by

$$\mu_p E_c = \sqrt{D_p/\tau_p}, \tag{21}$$

so that a graphical method was used to match the two solutions (for $E < E_c$ and $E > E_c$) and have a continuous solution over the critical distance where the field is E_c. Obviously, at very large distances the electric field can be neglected entirely and the velocity is given by

$$v = \sqrt{D_p/\tau_p}, \tag{22}$$

so that the transit time t.t.$_4$ in such region is easily calculable.

From a numerical solution of the above equations, the transit time in each of the regions was computed for specific values of resistivity ρ, collector current I_c and electrode spacing s. The total transit time

$$\text{t.t.} = \text{t.t.}_1 + \text{t.t.}_2 + \text{t.t.}_3 + \text{t.t.}_4 \tag{23}$$

was thus obtained for the specific conditions (obviously not all of these terms were needed unless the emitter is far from the collector). This transit time was then equated to the transit time obtained for minority carriers in a constant field E_x and which is given as

$$\text{t.t.} = \frac{s}{\frac{\mu_p E_x}{2} + \sqrt{\left(\frac{\mu_p E_x}{2}\right)^2 + \frac{D_p}{\tau_p}}}. \tag{24}$$

Solving for the electric field, this gives E_x as a function of ρ, I_c, and s. Fig. 5 was drawn from Fig. 4 by using this relationship between field and collector current.

Transistor Fabrication by the Melt-Quench Process*

J. I. PANKOVE†, SENIOR MEMBER, IRE

Summary—A small cylindrical germanium crystal doped with donor and acceptor impurities of different segregation coefficients is partly melted, then caused to freeze rapidly. Due to the impurity segregation effect a p-n junction is formed at the stopping level of the liquid-solid interface. As the freezing process is accelerated, quenching occurs and impurity segregation can no longer take place. This produces a second p-n junction very close to the first junction. It is shown that most of the heat is dissipated by conduction through the crystal. Neglecting convection and radiation losses, the freezing rate in a typical structure can be greater than 0.85 cm/sec. It is found that the whole structure remains a single crystal after such a treatment.

Introduction

THIS ARTICLE discusses a novel method of making, in a germanium bar, junctions suitable for use in transistors. In this "melt-quench" process of transistor fabrication a suitably doped small bar of germanium is partially melted, then caused to freeze very rapidly. Two closely-spaced, plane-parallel p-n junctions can thus be formed in a matter of a few seconds. Since these junctions may be designed to have a variety of electrical properties, the melt-quench process promises to be applicable to the fabrication of a variety of devices. The simplicity and rapidity of this process appear attractive for exploitation in low-cost mass production of transistor devices. However, this possibility has not been fully evaluated.

A method of making n-p-n junctions by melting-back and then slowly refreezing was described by Pfann.[1] In the present paper, however, refreezing is done rapidly. So greater control of junction parameters is possible.

Principle of Junction Formation

As shown in Fig. 1, a bar of germanium containing a concentration of N_d donors and N_a acceptors is melted from the right, so that the liquid-solid interface is at X_0. At this stage in the process the impurity distribution is not altered. The detail of choosing the impurities will be described later. Let K_d and K_a be respectively the donor and acceptor segregation coefficients. For the present, consider that $N_d > N_a$ (the crystal is n-type) and that $K_d < K_a(N_a/N_d)$.

The melt is caused to freeze at first slowly, then very rapidly. During the period of slow growth, the impurities are trapped according to the rules of impurity segregation. Consequently the initial impurity concentration is such that $K_aN_a > K_dN_d$ and the recrystallized material is p-type, thus forming a p-n junction. This junction will be referred to as the "melt junction."

If the crystal were allowed to continue to grow slowly as described by Pfann,[2] the concentration of donors in the liquid would increase more rapidly than the concentration of acceptors. Eventually the donors would predominate and a second junction form.

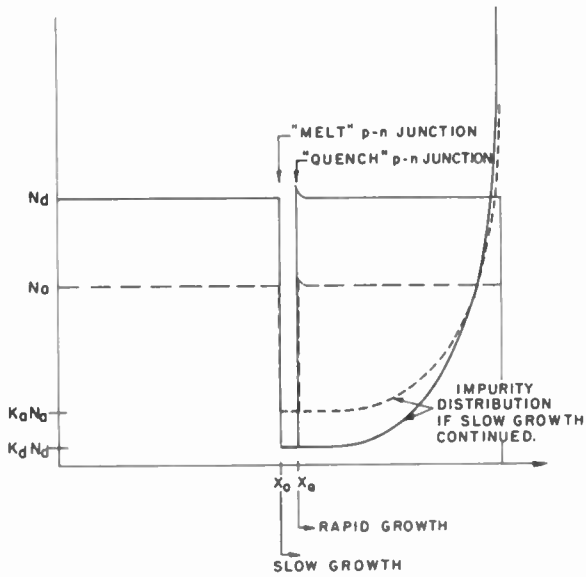

Fig. 1—Impurity distribution in the melt-quench process.

The impurity concentrations and their segregation coefficients determine the spacing between the junctions as well as the conductivity of the emitter and base regions, thus also influencing the emitter injection efficiency. While theoretically any two of these parameters may be chosen arbitrarily, in practice it is difficult to adjust them independently especially in a structure requiring high base conductivity, such as would be needed for high-frequency operation.

In the present process after a short period of slow regrowth, the crystal is caused to grow rapidly (quenched). This occurs at X_Q in Fig. 1 thus determining the spacing between junctions. Upon quenching, the impurities cease to segregate and the donors again dominate. The p-n junction produced upon quenching will be called the "quench junction." Since the thermal treatment (quenching) determines the spacing between junctions, the impurity concentration can be chosen independently to satisfy the requirements of good injection efficiency and low base resistivity. This separation of parameters

* Original manuscript received by the IRE, July 15, 1955; revised manuscript received, September 27, 1955. This paper was discussed at the IRE-AIEE Transistor Research Conference in Philadelphia, Pa., June, 1955.

† RCA Laboratories, Radio Corporation of America, Princeton, New Jersey.

[1] W. G. Pfann, "Redistribution of solutes by formation and solidification of a molten zone," *Jour. Metals* vol. 6, pp. 294–297; February, 1954.

[2] W. G. Pfann, "Segregation of two solutes, with particular reference to semiconductors," *Jour. Metals*, vol. 194, pp. 861–865; August, 1952.

controlling the junction spacing and injection efficiency allows a freedom of design not attainable in a slow growth process alone. If the slowly grown region is small compared to the quenched region, the impurity concentration in the quenched region is almost identical to the initial concentration in the crystal.

Quenching, to form the second p-n junction, is done very rapidly and it might be expected that the quenched region would be polycrystalline. This does not turn out to be the case. X-ray examination shows the quenched region to be a continuation of the single crystal.

Design Criteria

The following reasoning is applied to the design of an n-p-n unit. Analogous reasoning can be used for a p-n-p unit.

Since the unmelted region; *i.e.*, the starting material, is n-type:

$$N_d > N_a, \tag{1}$$

and the conductivity of this region is

$$\sigma_n = (N_d - N_a)e\mu_n, \tag{2}$$

where e and μ_n are respectively the electronic charge and mobility. If g denotes the fraction of the liquid that has solidified, then

$$g = \frac{x - x_0}{x_e - x_0}$$

where x_e is the length of the bar.

In the slowly freezing region the impurity distributions (n_a, n_d) are then given by

$$n_a(x) = K_a N_a (1 - g)^{K_a - 1}$$
$$n_d(x) = K_d N_d (1 - g)^{K_d - 1}.$$

But if the slowly grown region is small compared to the volume of liquid; *i.e.*, $g \ll 1$:

$$n_a(x) \cong K_a N_a$$
$$n_d(x) \cong K_d N_d. \tag{3}$$

Since the slowly grown region is required to be p-type, it is required that

$$n_a(x) > n_d(x),$$

and therefore, from (3)

$$K_a N_a > K_d N_d. \tag{4}$$

The conductivity in the p-type region is

$$\sigma_p = (K_a N_a - K_d N_d)e\mu_p, \tag{5}$$

where μ_p is the hole mobility.

Summarizing (1) and (4), the important condition to be satisfied is:

$$\boxed{N_d > N_a > \frac{K_d N_d}{K_a}}. \tag{6}$$

This result has also been presented by Pfann, but is reproduced here for completeness.

For closely spaced junctions and neglecting impurity pile-up due to segregation, the conductivity of both n-type regions is the same. Thus the units should be nearly symmetrical. For an efficient injection, σ_n/σ_p should be made high. That is,

$$\frac{\sigma_n}{\sigma_p} = \frac{(N_d - N_a)\mu_n}{(K_a N_a - K_d N_d)\mu_p} \gg 1. \tag{7}$$

Substituting (4) into (7), it is found that

$$\frac{K_d}{K_a} \ll 1. \tag{8}$$

Although (8) is satisfied by (6), the greater the inequality (8), the better the injection efficiency of the emitter will be.

The melt junction is always abrupt. The quench junction is abrupt also, but may be gradual if the growth rate is suitably controlled during the junction formation.

The Thermal Process

A theoretical model has been considered in order to gain insight into the thermal process. This model is one-dimensional, has a perfect heat sink, and for further simplicity its thermal conductivity is independent of temperature; the time constant of the heat source is negligible. Since the thermal treatment involves a varying boundary condition (motion of the liquid-solid interface), the exact heat flow problem is very difficult to solve. However, much has been learned by an approximate approach.

The power needed to melt half-way a cylinder 0.2 cm long was evaluated at 21 watts of which 19 watts are needed to supply conduction losses. The rest supplies heat of fusion. The radiation and convection losses are found negligible compared to the conduction losses.

During freezing, latent heat of fusion is liberated. Assuming all the heat is lost by conduction through the solid and that no heat is supplied externally, the process can be formulated as

$$\left(\frac{dQ}{dt}\right)_S = \left(\frac{dQ}{dt}\right)_L + HA\frac{dx}{dt},$$

where the first two terms are the rate of heat flow respectively in the solid and in the liquid, H is the heat of fusion, A the cross-sectional area through which heat flows and dx/dt is the velocity of the liquid-solid interface or the growth rate.

The present model exhibits a uniform temperature gradient at the end of the melting process. This is the initial condition for the freezing process as shown in Fig. 2. Then

$$\left(\frac{dQ}{dt}\right)_S = \left(\frac{dQ}{dt}\right)_L;$$

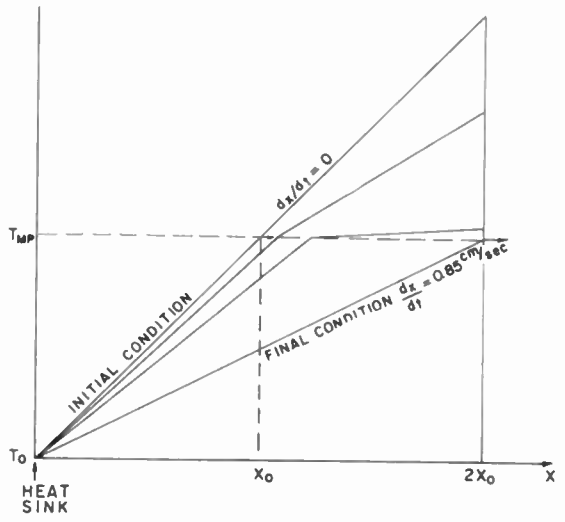

Fig. 2—Temperature distribution in cylinder during freezing process (heat loss only by conduction to heat sink).

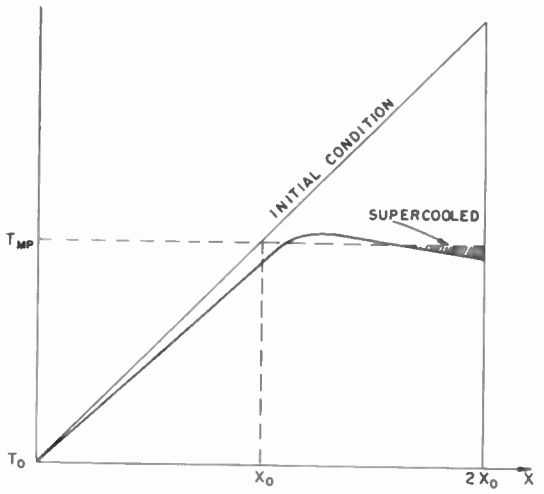

Fig. 3—Temperature distribution in cylinder during freezing process (case of supercooled liquid).

therefore the initial growth rate is zero. Obviously, at the onset of freezing the initial heat flow comes from the specific heat stored in the liquid.

The time constant for the heat diffusion process is less than 0.04 sec. Hence the temperature in the liquid drops rapidly down to the freezing temperature T_{MP}. During this time the growth rate is very low, the impurities are segregated, and the p-type layer is formed.

To take a limit case, consider the liquid-solid interface an infinitesimal distance from $x = 2x_0$, the end of the cylinder. Then the liquid is at freezing temperature T_{MP}, and $(dQ/dt)_L = 0$; then the growth rate is:

$$\left(\frac{dx}{dt}\right)_{x=2x_0} = \frac{1}{HA}\left(\frac{dQ}{dt}\right)_S = \frac{1}{HA}\,\sigma A\,\frac{dT}{dx},$$

where σ is the thermal conductivity.

$$\left(\frac{dx}{dt}\right)_{x=2x_0} = \frac{\sigma A}{HA}\,\frac{T_{MP}}{2x_0} = 0.85 \text{ cm/sec},$$

which is a very rapid growth rate.

In another limit case, if all the liquid is at T_{MP} from x_0 to the end of the crystal then the growth rate would be 1.7 cm/sec. The growth rate could be even faster in the following case.

If the heat losses at the hot end of the cylinder are appreciably greater than the losses by conduction to the heat sink alone, then the temperature at $2x_0$ will drop so rapidly that the liquid will eventually comprise two regions as shown in Fig. 3. One region will be supercooled and separated from the solid by the other region composed of hot liquid. When the nonsupercooled liquid reaches the freezing temperature (T_{MP}) the supercooled region suddenly sees the liquid-solid interface and freezes at an even greater rate than before.

Crystallographic Considerations

Since the growth is nucleated by a relatively large area single crystal it is reasonable to expect that the processed unit remains a single crystal in the region of slow growth. In the quenched region or region of rapid growth, because of the very high growth rate discussed above, it is not obvious that the crystal will remain monocrystalline. This growth rate is about 500 times greater than the rates used to pull single crystals of germanium by standard techniques. X-ray back-reflection analysis of the interior of two samples showed these to be single crystals throughout, one with stresses in the recrystallized region, the other without stress. The physical appearance and electrical behavior of good samples not X-rayed lead to no suspicion that they are other than single crystals.

It is desirable to cut the cylinders along the [111] axis, for then the (111) equilibrium face of the freezing germanium will more probably form a flat quench junction normal to the cylinder's axis. The melt junction is almost always flat and normal to the cylinder's axis as determined by the thermal gradient. [111] orientation is also desirable for obtaining a thin p-region or base layer, since crystal growth is slowed in the [111] direction.

Experimental Technique

A germanium crystal doped with donors and acceptors as discussed under design criteria is cut up into 100 mil-thick slices which are examined for their resistivity and uniformity. For this experimental work resistivities up to 0.1 ohm-cm were used. The slices are cut up into 30-mil-diameter cylinders with an ultrasonic machine-tool. It has been found that etching the crystal prior to the melt-quench process is not necessary.

The cylinders are mounted in a heat sink and placed in a helium atmosphere in contact with a heating element which may be a carbon filament or a machined graphite strip. See Fig. 4. The position of the crystal is controlled by a micrometric screw until contact is indicated by an ohmmeter labelled Ω in Fig. 4.

A timer is operated to pass a one-second pulse of current through the heating element. As the heater reaches

a temperature of 2,300 to 2,900°C, depending on the Variac setting, the crystal melts about half-way down its length. When the heating current is turned off, the crystal cools (mostly by conduction to the heat sink) at an initial rate of about 1,000°C/sec at the liquid-solid interface.

It is remarkable that in most cases surface tension can restrain the liquid to the initial cylindrical shape.

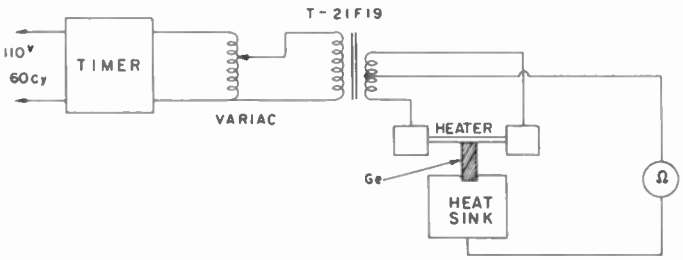

Fig. 4—Experimental setup for melt-quench process.

Graphite, copper, and forcibly-cooled copper have been used for the heat sink with the crystal stuck in a well in the case of graphite and soldered in the case of copper. The use of a heat sink is imperative in order to establish a strong longitudinal temperature gradient which causes the melting front to advance as a flat surface. Crystals supported by a thermal insulator show a lopsided melt junction.

It is possible to accelerate the cooling process by increasing the radiation losses if the crystal surface is blackened to increase its emissivity. Colloidal carbon condensed from smoke or deposited by the heater itself serves this purpose; but a coating of aquadag forms a nucleating surface and hence yields a polycrystalline region. Although radiation losses are usually negligible, they are multiplied by a factor of 10 when the crystal is blackened.

Transistors by the Melt-Quench Process

The most suitable structure for the melt-quench process is a cylinder. Hence, the resulting transistor will have axial symmetry and will comprise a pair of plane parallel junctions separated by a distance w (Fig. 5). Considering the use of such a transistor at high frequency it is reasonable to design it for operation where its power gain varies at the rate of 6 *db*/octave so that the approximate power gain can be calculated from[3]

$$\text{P.G.} = \frac{g_m}{4\omega^2 r_{bb'} C_{b'e} C_c}.$$

The base lead resistance $r_{bb'}$ can be minimized by making the connection completely surround the base layer. It is then[4]

$$r_{bb'} = \frac{\rho}{8\pi w}.$$

[3] L. J. Giacoletto, "Study of PNP alloy junction transistor from DC through medium frequencies," *RCA Review*, vol. 15, p. 506; December, 1954.

[4] J. M. Early, "PNIP and NPIN junction transistor triodes," *Bell System Technical Journal*, vol. 33, p. 526; May, 1954.

The other terms to be evaluated are:

$$C_{b'e} = 1.33 \times 10^{-9} w^2 I_e \quad \text{(mils, ma, } \mu f\text{)}$$

$$C_c = \frac{0.071\ d^2}{\sqrt{\rho V_c}} \quad \text{(mils, } \mu\mu f\text{)}$$

Hence, a 30-mil-diameter unit with $w = 0.5$ mils, $\rho = 1$ ohm cm, $V_c = 6$ volts, $I_e = 1$ ma, gives

$$r_{bb'} = 31 \text{ ohms}$$

$$C_{b'e} = 344\ \mu\mu f$$

$$C_c = 26\ \mu\mu f$$

$$\text{P.G. at 1 MC} = 29.6 \text{ db}.$$

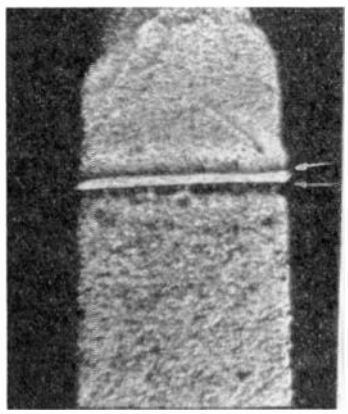

Fig. 5—Etched cross section of germanium cylinder processed by melt-quency technique. Spacing between junctions is 1.2 mils.

The present article is intended to describe the principles and techniques of the melt-quench process. Much of the evaluation has been done by direct physical observation (junction spacing, etc.) rather than by more indirect electrical measurements on completed transistors. A wide variety of structures has been made with base widths from about 0.1 mil to over 1 mil.

To give a rough estimate of the possibilities of this technique some individual measurements will be cited. An early unit of about 0.8 mil junction spacing gave the amplifier performance of Table I. This is considered promising in view of the fact that this unit had a collector-to-base current-gain factor of but 5. Its base lead resistance was 36 ohms. Other units have had current-gain factors up to 260. Measurements of junction capacitance show a dependence on voltage of $V^{-1/2}$ indicating abrupt transitions between the p- and n-type regions.

TABLE I

Characteristics of Early Experimental Melt-Quench Transistor

	Audio Frequency	455 kc
Power gain (I_e=1 ma, V_c=3v)	31.5 db	33.4 db
Power gain (I_e=2 ma, V_c=6v)		37.1 db
Input impedance	200 Ω	200 Ω
Output impedance	30 kΩ	>52 kΩ
Neutralizing capacitance		7–10 μμf

Acknowledgment

The assistance of F. H. Corregan and advice of S. G. Ellis are gratefully acknowledged.

RF Bandwidth of Frequency-Division Multiplex Systems Using Frequency Modulation*

R. G. MEDHURST†

Summary—**The radio-frequency energy distribution of a Frequency-Division-Multiplex, Frequency-Modulated Multichannel telephony system is evaluated. An estimate is obtained of the intermodulation noise generated when this spectrum is passed through an "ideal" bandpass filter with very sharp cutoff. From this it is possible to specify the minimum bandwidth of such a filter in terms of required system performance. This result provides a useful guide to the bandwidth over which control of group-delay and attenuation is necessary.**

Introduction

A MAJOR problem in the engineering of FM microwave links carrying multichannel telephony in frequency-division-multiplex lies in preventing excessive intermodulation distortion due to nonlinearity (with respect to frequency) of the radio transmission path. This nonlinearity appears in terminal and repeater circuits (amplifiers, filters, modulators and demodulators), in antenna feeders (due to antenna mismatch and feeder defects), and in the path between antennas (due to multiple reflections). Where rf networks are involved some control over the nonlinearity is afforded by the initial choice of network and by the addition of suitable equalizing sections. However, since the tolerable nonlinearity is very small, adequate equalization is by no means easy to achieve, particularly since very large numbers of channels are envisaged in present-day systems, so that the bandwidths demanded are of considerable extent.

Thus, it becomes important to know over what bandwidth control of a network characteristic has to be maintained. A rigorous solution to this problem would be obtained by considering a hypothetical characteristic (amplitude or phase) taken as constant over a certain band and operating on the sidebands outside this band in such a way as to produce maximum distortion. To make the problem more tractable, the present treatment deals with a characteristic which removes all sidebands outside the flat band (*i.e.*, with an ideal band-pass filter characteristic having infinitely sharp cutoff). While this may not be the worst that could occur, it is thought that this characteristic should be sufficiently drastic to be used for defining a bandwidth outside which it is safe to disregard network behavior, bearing in mind that a practical characteristic will, in any case, only depart comparatively slowly from its limits of equalization outside the required band.

Thus, it is proposed to estimate required bandwidth by evaluating distortion due to an ideal band-pass filter of variable pass band, having decided on a permissible distortion level substantially below that which may be contributed by a single unit of the system. The analysis requires knowledge of the rf spectral distribution when a carrier is frequency modulated by a frequency-division-multiplex signal (here idealized as a flat band of noise). This problem has been attacked by previous authors [1, 2], but not sufficiently extensively for the present requirement.

It is found that the energy distribution in the rf spectrum can be calculated in two limiting cases. When the peak frequency deviation from carrier frequency (taken arbitrarily as 11 db above rms deviation) is sufficiently large the spectrum distribution takes the form of an error function whose width can be deduced from a quasi-stationary argument. When the peak deviation is sufficiently small the spectrum follows from the first few terms of a series expansion involving the modulating signal. Both these types of spectra, together with the conditions under which they are generated, have been obtained experimentally.

It is concluded from the measurements that the spectrum has the large deviation shape when $(s/p_m)>3$ (provided that $p_0 \ll p_m$) and the small deviation shape when

$$\frac{s}{p_m} < 4\sqrt{\frac{p_0}{p_m}}$$

where p_m and p_0 are the maximum and minimum modulating frequencies respectively, and s is the peak deviation in the sense defined above.

When the deviation is such that either of these types of spectra is generated, expressions can be obtained for the distorting effect of removing all the sideband energy outside some prescribed frequency band centering on the carrier. In the case of intermediate deviations, the distortion due to spectrum truncation is evaluated for large and small deviations and the intermediate region covered by interpolation.

Spectral Energy Distribution

Peak Deviation Much Greater than Maximum Modulating Frequency

It is assumed that the multiplex signal frequency-modulating the carrier can be adequately represented by a band of random noise, of the form [3]

$$M = \frac{0.40s}{\sqrt{p_m - p_0}} \sum_{p=p_0}^{p_m} \cos(pt + \phi_p), \qquad (1)$$

where s = "peak" frequency deviation (radians/sec), taken (in accordance with the nomenclature of reference [3]) as 11 db above rms deviation,

p_m = maximum modulating frequency (radians/sec),

* Original manuscript received by the IRE, June 8, 1955; revised manuscript received September 19, 1955.

† Research Labs., General Electric Co., Ltd., Wembley, Eng.

p_0 = minimum modulating frequency (radians/sec), ϕ_p is a random phase angle

and p varies in unit steps.

In (1) M is represented by $(1+p_m-p_0)$ sinusoidal waves each of amplitude α but of different frequency and random initial phase angle. Accordingly, $\Delta = \alpha\sqrt{1+p_m-p_0}/\sqrt{2}$ and since by definition $\Delta = s$ antilog$_{10}$ $(-11/20)$, α in terms of s is given by $0.3986s/\sqrt{1+p_m-p_0}$, and, when $(p_m-p_0)\gg 1$ may be represented by $0.40s/\sqrt{p_m-p_0}$. The radian frequency components of M increase progressively in steps of one radian. Since the uniform spacing between radian frequency components is less than π radians the requirement that each initial phase angle be random insures that over any interval of 2π seconds M will be distributed in time in accordance with a Gaussian normal error law. The average chance that M exceeds s is the average chance that M exceeds its rms value by 11 decibels and this is given by $1-\text{erf}\,[1/\sqrt{2}\,\text{antilog}_{10}(11/20)] = 3.88\times 10^{-4}$. The average probability that s is not exceeded is 0.999612.

The probability that the instantaneous frequency lies between ω and $\omega+d\omega$ (ω being measured from the carrier) is proportional to

$$\exp\left\{\frac{-\omega^2}{2\Delta^2}\right\} d\omega \quad [17]$$

where Δ is the rms frequency deviation. Now, if quasi-stationary conditions hold, that is, if the peak deviation is substantially larger than the highest modulating frequency, the energy in a particular frequency band will be proportional to the fraction of the total time which the carrier spends in this band. Thus, the spectral energy distribution is

$$dW = k \exp\left\{\frac{-\omega^2}{2\Delta^2}\right\} d\omega, \qquad (2)$$

where k is a constant which can readily be evaluated in terms of the unmodulated carrier energy. This argument is based on Section 5 of [4].

The energy in a band extending from $-\omega$ to $+\omega$ is

$$2k\int_0^{\omega} e^{-\omega^2/2\Delta^2} d\omega = 2k\sqrt{2}\Delta \int_0^{\omega/\sqrt{2}\Delta} e^{-a^2} da$$

$$= 2k\sqrt{2}\Delta \sqrt{\frac{\pi}{2}}\, H\left\{\frac{\omega}{\sqrt{2}\Delta}\right\}$$

where

$$H(x) = \frac{2}{\sqrt{\pi}}\int_0^x e^{-a^2} da$$

Since $H(\infty)=1$, the energy in the band $-\omega$ to $+\omega$ expressed as a fraction of the total carrier energy is

$$H\left\{\frac{\omega}{\sqrt{2}\Delta}\right\} = H\left\{\frac{3.548}{\sqrt{2}}\,\frac{\omega}{s}\right\}$$

$$= H\left\{2.509\,\frac{\omega}{s}\right\}. \qquad (3)$$

On the assumption that 99.93 per cent of the total energy falls within the "peaks" of the frequency excursion (as defined above), Albersheim and Schafer [3] derive the formula $H[2.4\,(\omega/s)]$ for the same quantity.

Peak Deviation Much Less than Maximum Modulating Frequency

The modulated wave may be written as

$$\sin\left[\omega_c t + \sum_{p=p_0}^{p_m} \frac{a}{p}\cos(pt+\phi_p)\right]$$

where ω_c is the carrier frequency (radians/sec) and

$$a = 0.4s/\sqrt{p_m - p_0}.$$

Then, it is shown in Appendix I that when the deviation is sufficiently small, the rf spectrum becomes

$$\{e\}^{-0.04s^2/p_m p_0}\sin\omega_c t$$

$$+\frac{a}{2}\sum_{\omega=p_0}^{p_m}\frac{1}{\omega}\left[\cos(\overline{\omega_c-\omega}t-\phi_\omega)+\cos(\overline{\omega_c+\omega}t+\phi_\omega)\right]$$

$$-\frac{a^2}{4}\sum_{\omega=0}^{2p_m} F_2(\omega)\left[\sin(\overline{\omega_c-\omega}t-\psi_\omega)+\sin(\overline{\omega_c+\omega}t+\psi_\omega)\right], \quad (4)$$

where

$$F_2(\omega) = \left\{\left[\frac{2p_m-\omega}{\omega^2 p_m(\omega-p_m)}+\frac{2}{\omega^3}\log\frac{p_m}{\omega-p_m}\right]_{p_m+p_0\le\omega\le 2p_m}\right.$$

$$+\left[\frac{\omega-2p_0}{\omega^2 p_0(\omega-p_0)}+\frac{2}{\omega^3}\log\frac{\omega-p_0}{p_0}\right]_{2p_0\le\omega\le p_m+p_0},$$

$$+\left[-\frac{2p_m-\omega}{\omega^2 p_m(p_m-\omega)}+\frac{\omega+2p_0}{\omega^2 p_0(\omega+p_0)}\right.$$

$$\left.\left.+\frac{2}{\omega^3}\log\frac{p_m p_0}{(\omega+p_0)(p_m-\omega)}\right]_{0\le\omega\le p_m-p_0}\right\}^{1/2}$$

and ψ is a new random phase angle. The expressions in the square brackets have their analytical values over the ranges indicated, and are otherwise zero.

Whereas for large deviations the spectrum indicated by (2) is continuous over the frequency range $0-\infty$, in the case of small deviation a discrete component appears at the carrier frequency and discontinuities at p_0 and p_m. Also, the spectrum ceases at $\pm 2p_m$. This latter phenomenon is due to neglect of higher powers of the modulating signal than the second.

It will be shown that (2) applies when $(s/p_m > 3$ (provided that $p_0 \ll p_m$), and (4) when $s/p_m < 4\sqrt{p_0/p_m}$.

Measured Spectra

Figs. 1 to 4, and Figs. 5 to 7 (on page 192) show a series of measured rf spectra in which the ratio of peak deviation to maximum modulating frequency increases from 0.28 and 4.0. The base band in Figs. 1 to 3 was 60–1,052

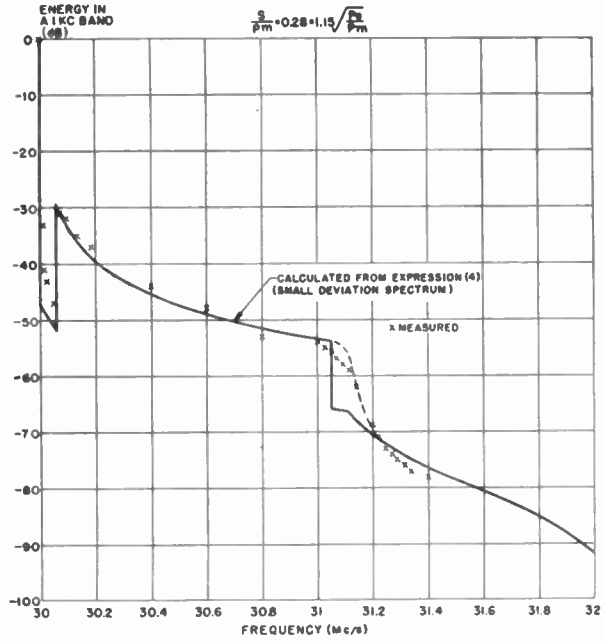

Fig. 1—Measured and theoretical spectral energy distributions. Base band 60–1,052 kc, peak deviation 0.29 mc.

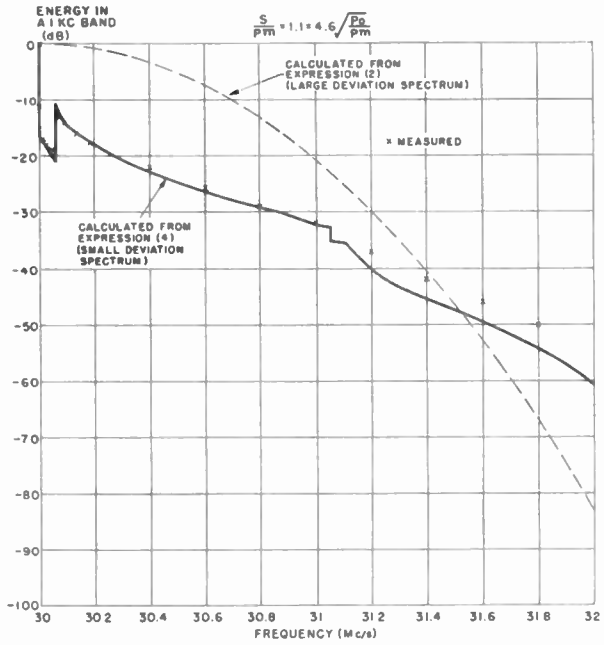

Fig. 3—Measured and theoretical spectral energy distributions. Base band 60–1,052 kc, peak deviation = 1.15 mc.

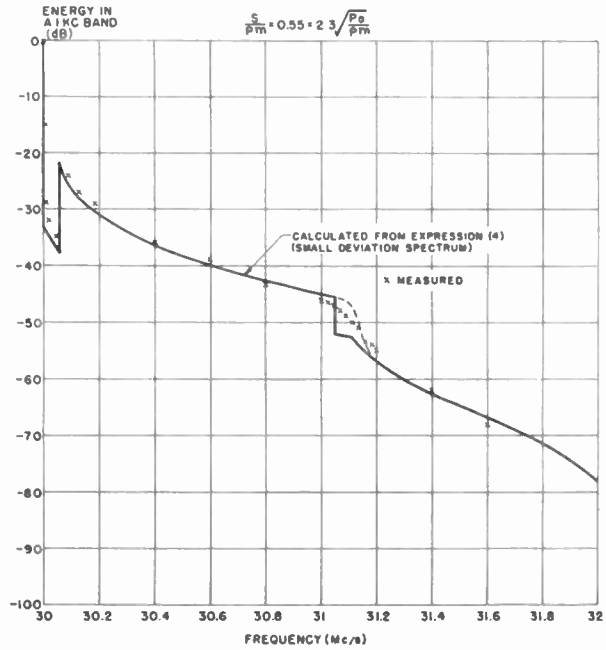

Fig. 2—Measured and theoretical spectral energy distributions. Base band 60–1,052 kc, peak deviation 0.58 mc.

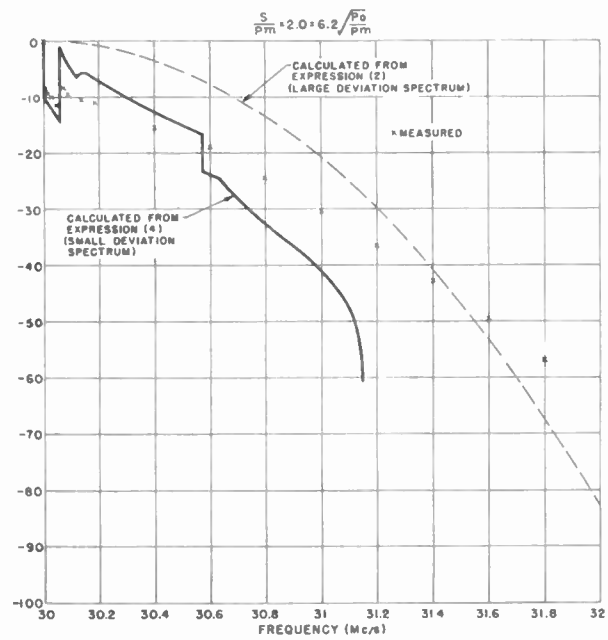

Fig. 4—Measured and theoretical spectral energy distributions. Base band 60–575 kc, peak deviation 1.15 mc.

kc, and in Figs. 4 to 7 was 60–575 kc. The carrier frequency was 30 mc. Only the upper halves of the symmetrical spectra are shown.

The measurements were made with a receiver having a nominal bandwidth of 1 kc. Energy levels thus recorded at various frequency departures from carrier were referred to the level at carrier frequency. When the deviation is small a large discrete component, additional to the "smeared out" spectrum, appears at the carrier frequency, so that at this frequency the measured energy will be substantially independent of the receiver bandwidth, whereas in the main part of the spectrum the measured energy is directly proportional to the receiver bandwidth. Thus, the relative energy levels plotted are also directly proportional to this bandwidth, when the deviation is sufficiently small.

Since the receiver bandwidth was not known accurately, the relative levels over the range 30.06–31.6 mc, in Fig. 2, were adjusted by a constant number of db to give the best fit to the theoretical curve. The adjustment required gives a measure of the effective receiver bandwidth, which came out as 1.24 kc. Justifica-

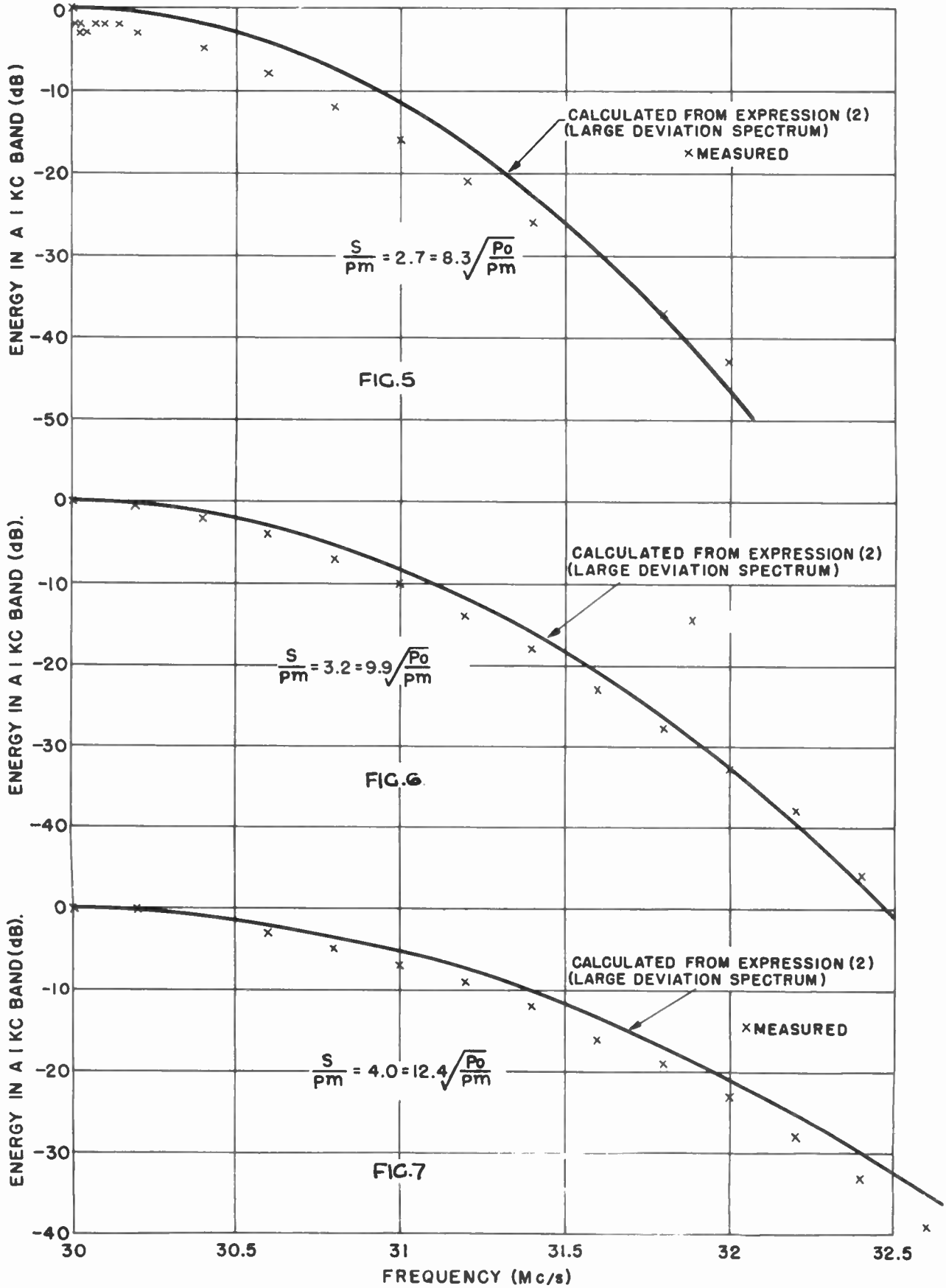

Figs. 5, 6, and 7—Measured and theoretical spectral energy distributions. Base band 60–575 kc, peak deviations 1.54, 1.83, and 2.30 mc.

tion for this procedure is provided by Fig. 1, in which the theoretical curve is constructed on the basis of the receiver bandwidth deduced from Fig. 2. The resulting fit to the measured levels is thought to be well within the experimental error.

In Figs. 1 and 2, abrupt discontinuities in the theoretical spectra are seen at 30.06 and 31.05 mc. These are a consequence of assuming a base-band spectrum having sharp cutoffs at 60 and 1,052 kc. The measured points show the discontinuity at 30.06 mc very clearly, but there is considerable smoothing of the spectrum at the higher frequency. The reason for this appears to be that while the spectrum of the flat noise-band modulation cut off very sharply at its lower end, there was substantial rounding-off at the upper end. When allowance is made for this departure from the ideal shape, using a measured filter characteristic, the dotted lines in Figs. 1 and 2 were obtained. It is seen that the trend of the measurements is satisfactorily explained.

The transitions from small to intermediate deviation spectra (between Figs. 2 and 3) and from intermediate to large deviation spectra (between Figs. 5 and 6) are well marked in this series of measurements. It remains to deduce criteria for these transitions which can be applied to other base-band conditions. It is shown in Appendix II that the deviation at which the Gaussian (large-deviation) type of spectrum ceases to be generated is a function of s/p_m only, when p_0 is much less than p_m. Thus, in consideration of Figs. 5 and 6, this spectral shape would be expected when $s/p_m > 3$, with $p_0 \ll p_m$.[1]

The criterion that the small deviation spectrum (expression 4) should be obtained is shown in Appendix II to depend on the function

$$\frac{s}{\sqrt{p_0 p_m}}, \quad i.e., \quad \frac{s}{p_m}\sqrt{\frac{p_m}{p_0}}.$$

Thus, from Figs. 2 and 3, (4) is expected to describe the spectral shape when

$$\frac{s}{p_m} < 4\sqrt{\frac{p_0}{p_m}}.$$

Previously Published Results

Calculations have been published for the cases of modulating noise bands having Gaussian [1] and flat [2] spectral distributions. In both cases, after a much more elaborate analysis than that given above, it is shown that for large deviations the rf spectra have a Gaussian shape. It is evident from the first section that any modulation having a Gaussian probability amplitude distribution with time, whatever its spectral shape, will give this limiting result.

For the small deviation FM case, Stewart [2] produces a spectrum which extends smoothly to infinity. This is obtained by putting the minimum modulating frequency identically equal to zero (so that the equivalent phase modulation spectral amplitude rises to infinity at the low end of the band) at an early stage of the analysis [5]. For the present purpose, it is sufficient to notice that while a mathematical problem has been thereby solved it seems probable that there is no physical counterpart. If the frequency modulation spectrum were to extend down to zero, *i.e.* if there were a dc term, it would appear natural to regard this term not as a phase modulation of infinite amplitude and of zero frequency (which is the source of Stewart's continuous spectrum) but as a constant frequency shift, Thus, the frequency modulation can always be regarded as having a nonzero lower bound, so that there will be a deviation small enough to satisfy the condition

$$\frac{s}{p_m} < 4\sqrt{\frac{p_0}{p_m}}.$$

The analytical background to this argument is given [5].

Stewart's approach will produce the second term of (4) (the first-order spectrum) when the limits are properly handled [5], though the analysis is quite lengthy. By the present procedure this term is written down immediately. While the autocorrelation method must also ultimately yield the third term of (4) (the second-order spectrum), it is to be expected that the analysis would be of quite formidable length.

Distortion Due to Bandwidth Limitation

We now consider the distorting effect of removing all sideband energy outside some specified frequency range, say $-p_l$ to $+p_l$.

Let the modulated carrier be

$$\sin(\omega_c t + M_{ph}) = \cos M_{ph} \sin \omega_c t + \sin M_{ph} \cos \omega_c t,$$

where

$$M_{ph} = \int M dt,$$

M = angular frequency modulation,

ω_c = angular carrier frequency.

Since M, and hence M_{ph}, consists of a number of tones whose frequencies are taken as exact multiples of unity, $\cos M_{ph}$ and $\sin M_{ph}$ can be written in the form

$$\left.\begin{aligned} \cos M_{ph} &= \sum_{p=0}^{\infty} C_p \cos(pt + \mu_p) \\ \sin M_{ph} &= \sum_{p=0}^{\infty} S_p \cos(pt + \nu_p) \end{aligned}\right\}. \qquad (5)$$

[1] If p_0 were comparable in magnitude with p_m, the more exact criteria $s/(p_m - p_0) > 3$ would be required. Then, an appropriate form for the small deviation criterion, when constructing curves such as Fig. 9, would be

$$s/(p_m - p_0) < \frac{4\sqrt{p_0/p_m}}{1 - p_0/p_m}.$$

This case does not, at present, arise in multiplex telephony practice.

After removal of sideband energy falling outside a frequency range $-p_l$ to $+p_l$, the modulated wave becomes

$$\sin(\omega_c t + M_{ph}) - \sum_{p=p_l}^{\infty} C_p \cos(pt + \mu_p) \sin \omega_c t. - \sum_{p=p_l}^{\infty} S_p \cos(pt + \nu_p) \cos \omega_c t.$$

In the notation of eq. (3) of [6],

$$\Delta_1 = -\sum_{p=p_l}^{\infty} C_p \cos(pt + \mu_p)$$

$$\Delta_2 = -\sum_{p=p_l}^{\infty} S_p \cos(pt + \nu_p).$$

Then, from (4) of the same reference, the phase modulation distortion due to truncating the rf spectrum is

$$\Delta_2 \cos M_{ph} - \Delta_1 \sin M_{ph} = -\sum_{p=p_l}^{\infty} S_p \cos(pt + \nu_p) \sum_{p=0}^{\infty} C_p \cos(pt + \mu_p) + \sum_{p=p_l}^{\infty} C_p \cos(pt + \mu_p) \sum_{p=0}^{\infty} S_p \cos(pt + \nu_p). \quad (6)$$

The two cases of deviation much larger and much smaller than the maximum modulating frequency have been evaluated in Appendices III and IV. In the first case, it is concluded that ratio of distortion to signal noise, each measured over same narrow band, in top channel (where distortion will be greatest) is given by

$$\frac{\text{Distortion}}{\text{Signal}} = 2.5 \left\{\frac{p_m}{s}\right\}^{1.5} \cdot e^{-1.57(p_m/s)^2} \left\{H\left[\frac{3.548}{s}(p_l + 0.5p_m)\right] - H\left[\frac{3.548}{s}(p_l - 0.5p_m)\right]\right\}^{1/2}, \quad (7)$$

where $H(x)$ is the error function, Very comprehensive tables exist [7]. For the small deviation case, the corresponding formula is

$$\frac{\text{Distortion}}{\text{Signal}} = 0.04\left[\frac{s}{p_m}\right]^2 [F(k)]^{1/2}, \quad (8)$$

where $k = p_l/p_m$.

$$F(k) = \frac{(k-2)(10k^2-12k+1)}{2k(k-1)^2} - \frac{6k^2-3k-1}{k^2(k-1)} \log(k-1) + 3\log\left[\frac{k^2}{k-1}\right] \log(k-1) + 6L(2) - 6L(k).$$

$L(x)$ is the Spence Integral [8–12] (see Appendix V) defined by

$$L(u) = \int_1^u \frac{\log_e x}{x-1}\, dx$$

$[F(k)]^{1/2}$ is plotted as a function of k in Fig. 8.

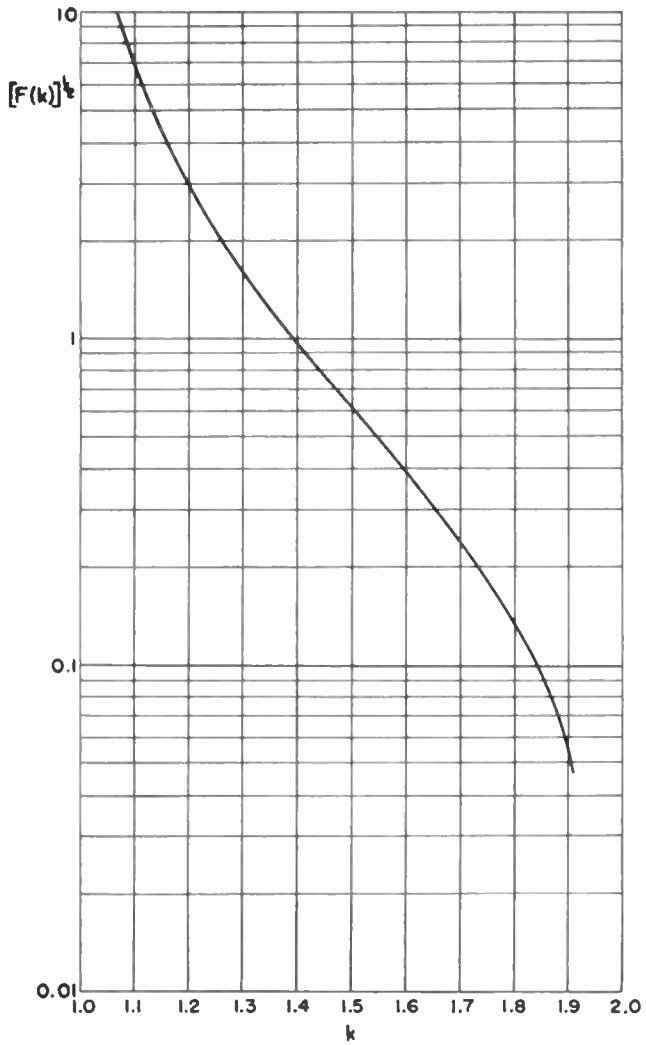

Fig. 8—Variation with k of the function $[F(k)]^{1/2}$ occurring in expression (8).

Numerical Example

If the deviation is sufficiently large or sufficiently small, operating bandwidths follow immediately from (7) or (8), once it has been decided what distortion level due to bandwidth limitation can be tolerated. For intermediate deviations it is necessary to resort to graphical interpolation.

As an example of this latter state of affairs we shall consider a 600-channel system, for which the base band extends from 0.06 to 2.54 mc. The rms deviation per channel [13] is taken as 200 kc (this being the deviation produced by a 1 mW 800 c/s tone injected at a point of zero reference level), and the rms multichannel level exceeded for not more than 1 per cent of the "busy hour" as +15 dbmo (this value is 2 db higher than than given by Holbrook and Dixon [14]: it is based on data used by the British Post Office). The equivalent noise band is supplied at such a level as to produce an rms deviation equal to the multichannel value just quoted. Thus, the peak deviation, taken as 11 db above rms, comes out as ±4.0 mc.

It is considered that a distortion level of −85 dbm (measured in a 4-kc channel at a point of zero reference level) at each repeater station, due to bandwidth limitation, will be negligible compared with other sources of distortion. This estimate is derived from a system breakdown, which need not be considered in detail here, based on CCIF required performance for cable transmission [15]. Using the rms noise level specified above, the equivalent distortion/signal ratio becomes −72 db.

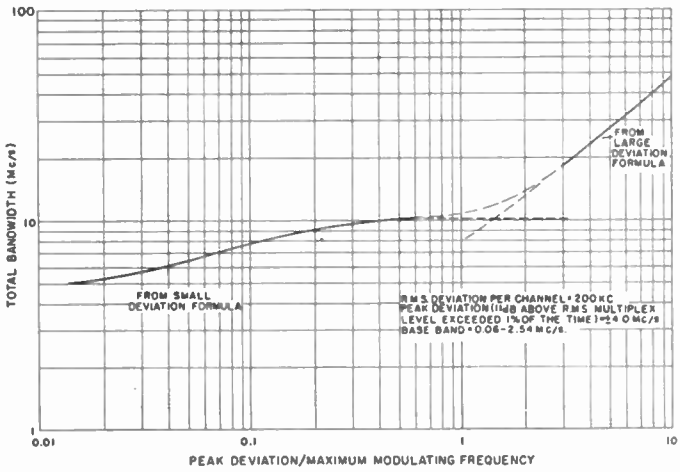

Fig. 9—Variation with deviation of the bandwidth corresponding to a distortion level of −85 dbmo (distortion/signal = −72 db) in the top channel, for a 600 channel system.

Fig. 9 shows curves obtained by plotting total bandwidth, computed from (7) and (8), against the ratio of peak deviation to maximum modulating frequency, when the distortion/signal ratio in the top channel due to bandwidth limitation is −72 db. From the trend of the curves it would appear that quite good accuracy should be obtainable when they are joined up smoothly, as shown by the heavy dotted line. The bandwidth indicated, when $s/p_m = 1.58$, is about 12 mc total. It is of interest to see how the distortion varies with variation of bandwidth. This is shown in Fig. 10, which was constructed from a number of curves similar to that of Fig. 9, but computed for different distortion levels.

Appendix I

Spectral Energy Distribution for Small Deviation Ratios

The wave frequency-modulated by flat random noise may be written as

$$\sin\left[\omega_c t + \sum_{p=p_0}^{p_m} \frac{a}{p}\cos(pt+\phi_p)\right]$$
$$= \sin\omega_c t \cos\left[a\sum_{p=p_0}^{p_m}\frac{1}{p}\cos(pt+\phi_p)\right]$$
$$+ \cos\omega_c t \sin\left[a\sum_{p=p_0}^{p_m}\frac{1}{p}\cos(pt+\phi_p)\right]$$
$$\simeq \sin\omega_c t\left[1-\frac{a^2}{2}\left\{\sum_{p=p_0}^{p_m}\frac{1}{p}\cos(pt+\phi_p)\right\}^2\right]$$

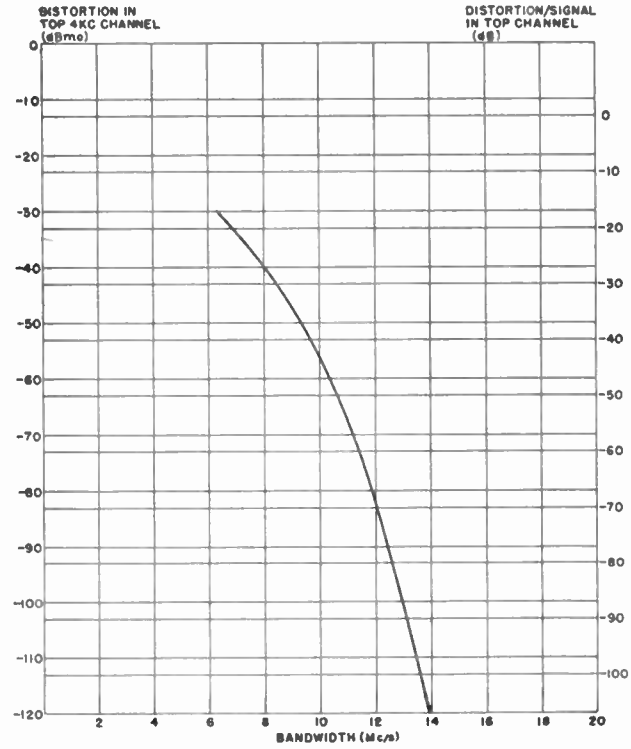

Fig. 10—Variation of distortion with bandwidth, for the same modulating conditions as in Fig. 9.

$$+ \cos\omega_c t\left[a\sum_{p=p_0}^{p_m}\frac{1}{p}\cos(pt+\phi_p)\right] \qquad (9)$$

when the deviation is sufficiently small.

Considering the term

$$\left\{\sum_{p=p_0}^{p_m}\frac{1}{p}\cos(pt+\phi_p)\right\}^2, \qquad (10)$$

the most probable amplitude of the component having frequency p has to be extracted from a product which it is convenient to write in the form [16]

$$\sum_{m=p_0+1}^{p_m}\sum_{n=p_0}^{m-1}\frac{1}{m}\cdot\frac{1}{n}\cos[(m+n)t+\phi_m+\phi_n]$$
$$+\sum_{m=p_0+1}^{p_m}\sum_{n=p_0}^{m-1}\frac{1}{m}\cdot\frac{1}{n}\cos[(m-n)t+\phi_m-\phi_n]. \qquad (11)$$

The contributions at frequency p, which must be added on a power basis, are obtained from (11) by putting $m+n$ and $m-n$ successively equal to p. Then changing the summations into integrals, the resultant amplitude of the tone of frequency p becomes

$$\left\{\left[\int_{p/2}^{p-p_0}\frac{1}{m^2}\frac{1}{(p-m)^2}\,dm\right]_{2p_0\leqq p\leqq p_m+p_0}\right.$$
$$+\left[\int_{p/2}^{p_m}\frac{1}{m^2}\frac{1}{(p-m)^2}\,dm\right]_{p_m+p_0\leqq p\leqq 2p_m}$$
$$\left.+\left[\int_{p+p_0}^{p_m}\frac{1}{m^2}\frac{1}{(m-p)^2}\,dm\right]_{0\leqq p\leqq p_m-p_0}\right\}^{1/2},$$

where the significance of the subscripts is that over the range of p indicated the expressions are to have their analytical values, and outside this range they are to be zero.

Performing the integration, this becomes

$$\left\{\left[\frac{p-2p_0}{p^2p_0(p-p_0)}+\frac{2}{p^3}\log\frac{p-p_0}{p_0}\right]_{2p_0\leq p\leq p_m+p_0}+\left[\frac{2p_m-p}{p^2p_m(p-p_m)}+\frac{2}{p^3}\log\frac{p_m}{p-p_m}\right]_{p_m+p_0\leq p\leq 2p_m}+\left[\frac{-(2p_m-p)}{p^2p_m(p_m-p)}+\frac{p+2p_0}{p^2p_0(p+p_0)}+\frac{2}{p^3}\log\frac{p_mp_0}{(p+p_0)(p_m-p)}\right]_{0\leq p\leq p_m-p_0}\right\}^{1/2}. \quad (12)$$

Then, the continuous part of (4) follows immediately writing ω for p) from (9) and (12). The carrier amplitude could be obtained by extracting the constant term from all even powers of the modulation [the first two of which appear in the first square bracket in (9)]. This leads to a series, the first two terms of which are

$$1-\frac{0.04s^2}{p_mp_0}.$$

The final result, however, follows more quickly from the integral formula for the power spectrum obtainable by autocorrelation analysis [1, 2].

The analysis is given in [5]. The discontinuous part of the spectrum is shown to be expressible in terms of the Dirac delta function as

$$\frac{1}{2}\exp\left(\frac{-\Delta^2}{p_mp_0}\right)\delta(p).$$

This is equivalent to a carrier amplitude of the form

$$\exp\left\{\frac{-\Delta^2}{2p_mp_0}\right\},$$

which, when rewritten in terms of the peak deviation s, leads to the carrier term of (4).

From expression (1) of reference [5] it would be possible to develop the whole of expression (4). However, it is shown in that reference that a very great deal of labor is involved even in arriving at the part of the spectrum corresponding to the first summation in (4), which is written down immediately by the method described at the beginning of this Appendix.

Appendix II

Criteria for Small and Large Deviation Spectra

Small Deviation

Spectra defined by (4) will be generated when the approximation assumed in (9) is valid. The basis of this approximation is that powers of the phase modulation higher than the second can be neglected. The criterion required is that the rms amplitude of the phase modulation should be small. This is

$$\left\{\frac{a^2}{2}\int_{p_0}^{p_m}\frac{1}{p^2}\,dp\right\}^{1/2}=\left\{\frac{a^2}{2}\left[\frac{p_m-p_0}{p_mp_0}\right]\right\}^{1/2}=\left\{\frac{0.16s^2}{2(p_m-p_0)}\left[\frac{p_m-p_0}{p_mp_0}\right]\right\}^{1/2}=\sqrt{0.08}\,\frac{s}{\sqrt{p_mp_0}}.$$

Thus, the necessary criterion that spectra should have the shape described by (4) is that $s/\sqrt{p_mp_0}$ should be small.

Large Deviation

Since the spectra appropriate to large deviations have been obtained (first section) from a quasi-stationary argument, it would be expected that the proper criterion in this case would be that s/p_m should be large when $p_0 \ll p_m$. A detailed analysis produces the more general criterion that $s/(p_m-p_0)$ should be large, for any p_m/p_0. This follows from consideration of the integral expression for the rf power spectrum [1, 2], which is

$$W_F(\omega)=\frac{1}{2\pi}\int_0^\infty \cos\omega\tau\cdot\exp\left\{-\Delta^2\int_0^\infty\frac{W_m(p)}{p^2}(1-\cos p\tau)dp\right\}d\tau,$$

where

$W_F(\omega)$ is the rf power spectrum,

ω is the angular frequency measured from the carrier frequency,

Δ is the rms angular frequency deviation,

$W_m(p)$ is the normalized modulating power spectrum and the carrier has been taken as having unity peak amplitude.

For $W_m(p)$, we have

$$W_m(p)=\begin{cases}\dfrac{1}{p_m-p_0} & p_0\leq p\leq p_m\\ 0 & p<p_0 \text{ and } >p_m.\end{cases}$$

Thus,

$$W_F(\omega)=\frac{1}{2\pi}\int_0^\infty\cos\omega\tau\cdot\exp\left\{-\Delta^2\int_{p_0}^{p_m}\frac{1}{(p_m-p_0)p^2}(1-\cos p\tau)dp\right\}d\tau.$$

Evaluating the integral in the exponent, and writing

$$x=(p_m-p_0)\tau,$$

$$W_F(\omega) = \frac{1}{2\pi(p_m - p_0)} \int_0^\infty \cos\left\{\frac{\Delta x}{p_m - p_0}\right\} \cdot \exp\left\{-\frac{\Delta^2}{(p_m - p_0)^2}\left[Si\left\{\frac{p_m}{p_m - p_0}x\right\} - Si\left\{\frac{p_0}{p_m - p_0}x\right\} - \frac{1 - \cos\left\{\frac{p_m}{p_m - p_0}x\right\}}{p_m x/(p_m - p_0)} + \frac{1 - \cos\left\{\frac{p_0}{p_m - p_0}x\right\}}{p_0 x/(p_m - p_0)}\right]\right\} dx,$$

where Si is the sine integral.

Expanding the exponent as a power series in x,

$$W_F(\omega) = \frac{1}{2\pi(p_m - p_0)} \int_0^\infty \cos\left\{\frac{\Delta}{p_m - p_0}x\right\} \cdot \exp\left\{\frac{-\Delta^2}{(p_m - p_0)^2}\left[\frac{x^2}{\underline{|2}} - \frac{p_m^3 - p_0^3}{(p_m - p_0)}\frac{x^4}{3\underline{|4}} + \cdots\right]\right\} dx.$$

This leads to the Gaussian distribution given as (2) of first section if only the first term in the square bracket is taken. Thus, the criterion for a Gaussian spectrum is obtained by considering the circumstances under which this is the dominant term of the bracketed series. If $\Delta/(p_m - p_0)$ is large, the exponential term will only contribute significantly to the integral when the expression in the square brackets is small. Thus, when $p_0 \ll p_m$, the criterion for the existence of a Gaussian rf spectrum is that Δ/p_m, and hence s/p_m should be large.

Appendix III

Distortion Due to Spectrum Truncation When the Deviation Ratio Is Large

When the peak deviation is substantially greater than the highest modulating frequency, C_p and S_p, defined at beginning of second section, will approach equality (below); thus (5) can bewritten, approximately,

$$\cos M_{ph} = \sum_{p=0}^{\infty} C_p \cos(pt + \mu_p)$$

$$\sin M_{ph} = \sum_{p=0}^{\infty} C_p \cos(pt + \nu_p).$$

Then (6), the phase modulation distortion, becomes

$$\begin{aligned}
&- \sum_{p=p_l}^{\infty} C_p \cos(pt + \nu_p) \sum_{p=1}^{\infty} C_p \cos(pt + \mu_p) \\
&+ \sum_{p=p_l}^{\infty} C_p \cos(pt + \mu_p) \sum_{p=1}^{\infty} C_p \cos(pt + \nu_p) \\
&= - \sum_{p=p_l}^{\infty} C_p \cos(pt + \nu_p) \sum_{p=p_l}^{\infty} C_p \cos(pt + \mu_p) \\
&- \sum_{p=p_l}^{\infty} C_p \cos(pt + \mu_p) \sum_{p=1}^{p_l} C_p \cos(pt + \nu_p) \\
&+ \sum_{p=p_l}^{\infty} C_p \cos(pt + \mu_p) \sum_{p=p_l}^{\infty} C_p \cos(pt + \nu_p) \\
&+ \sum_{p=p_l}^{\infty} C_p \cos(pt + \mu_p) \sum_{p=1}^{p_l} C_p \cos(pt + \nu_p) \\
&= - \sum_{p=p_l}^{\infty} C_p \cos(pt + \nu_p) \sum_{p=1}^{p_l} C_p \cos(pt + \mu_p) \\
&+ \sum_{p=p_l}^{\infty} C_p \cos(pt + \mu_p) \sum_{p=1}^{p_l} C_p \cos(pt + \nu_p) \\
&= - \frac{1}{2} \sum_{q=p_l}^{\infty} \sum_{r=1}^{p_l} C_q C_r \cos(\overline{q - r}t + \nu_q - \mu_r) \\
&- \frac{1}{2} \sum_{q=p_l}^{\infty} \sum_{r=1}^{p_l} C_q C_r \cos(\overline{q + r}t + \nu_q + \mu_r) \\
&+ \frac{1}{2} \sum_{q=p_l}^{\infty} \sum_{r=1}^{p_l} C_q C_r \cos(\overline{q - r}t + \mu_q - \nu_r) \\
&+ \frac{1}{2} \sum_{q=p_l}^{\infty} \sum_{r=1}^{p_l} C_q C_r \cos(\overline{q + r}t + \mu_q + \nu_r).
\end{aligned}$$

It appears safe to assume for here that μ's and ν's are mutually random. Then, the above becomes

$$\frac{1}{\sqrt{2}} \sum_{q=p_l}^{\infty} \sum_{r=1}^{p_l} C_q C_r \cos(\overline{q - r}t + \psi_{q-r}) + \frac{1}{\sqrt{2}} \sum_{q=p_l}^{\infty} \sum_{r=1}^{p_l} C_q C_r \cos(\overline{q + r}t + \psi_{q+r}),$$

where ψ is a new random phase angle. It is now easy to show that distortion component having frequency p is

$$\frac{1}{\sqrt{2}} \left\{\sum_{q=p_l}^{p_l+p} C_q^2 C_{q-p}^2\right\}^{1/2} \tag{13}$$

for any p_l.

To evaluate the C's, we may recall that the modulated wave is

$$\begin{aligned}
&\cos M_{ph} \sin \omega_c t + \sin M_{ph} \cos \omega_c t \\
&= \sum_{p=1}^{\infty} C_p \cos(pt + \mu_p) \sin \omega_c t + \sum_{p=1}^{\infty} S_p \cos(pt + \nu_p) \cos \omega_c t \\
&\simeq \sum_{p=1}^{\infty} C_p \cos(pt + \mu_p) \sin \omega_c t \\
&\quad + \sum_{p=1}^{\infty} C_p \cos(pt + \nu_p) \cos \omega_c t \text{ for } \frac{s}{p_m} \gg 1 \\
&= \frac{1}{2} \sum_{p=1}^{\infty} C_p [\sin(\overline{\omega_c - p}t - \mu_p) + \sin(\overline{\omega_c + p}t + \mu_p)] \\
&\quad + \frac{1}{2} \sum_{p=1}^{\infty} C_p [\cos(\overline{\omega_c - p}t - \nu_p) + \cos(\overline{\omega_c + p}t + \nu_p].
\end{aligned}$$

Then, using (2) and remembering that the sidebands are spaced at unit frequency intervals, we have

$$k \exp\frac{(-\omega^2)}{(2\Delta^2)} = \frac{1}{2}\left[\left(\frac{1}{2}C_p\right)^2 + \left(\frac{1}{2}C_p\right)_l^2\right] = \frac{1}{4}C_p^2.$$

k can be determined since the total energy in the rf spectrum is equal to the energy of the unmodulated carrier. Since the carrier has been taken as having unit amplitude,

$$\frac{1}{2} = 2\int_0^\infty ke^{-\omega^2/2\Delta^2}\,d\omega = 2\sqrt{2}\Delta k\int_0^\infty e^{-a^2}da$$

$$= 2\sqrt{2}\Delta k\quad\frac{\sqrt{\pi}}{2} = \Delta k\sqrt{2\pi}$$

so

$$k = \frac{1}{2\sqrt{2\pi}\Delta}$$

and

$$C_p^2 = \frac{2}{\sqrt{2\pi}\Delta}\exp\left\{\frac{-\omega^2}{2\Delta^2}\right\}. \tag{14}$$

Eq. (14) is a direct consequence of the assumption that S_p and C_p approach equality for large deviations, which has here been considered intuitively obvious. A more rigorous approach, using an integral expression for the power spectrum of cos M_{ph}, derived from the Wiener-Khintchine relation, can be shown also to lead to expression (14), when the deviation is large enough. It can also be shown, as expected, that the same limiting form results for the power spectrum of sin M_{ph}. The analysis will not be reproduced here for reasons of space. It may be remarked that, as in the second part of Appendix II, the criterion for "large deviation" appears in the form that $s/(p_m - p_0)$ has to be large.

From (13), replacing the summation by an integral, the phase modulation distortion component having frequency p becomes

$$\frac{1}{\sqrt{2}}\,\frac{2}{\sqrt{2\pi}\Delta}\left\{\int_{p_l}^{p_l+p}\exp\left(-\frac{[q^2+(q-p)^2]}{2\Delta^2}\right)dq\right\}^{1/2}$$

$$= \frac{1}{\sqrt{\pi}\Delta}\left\{\{e\}^{-(1/4)(p^2/\Delta^2)}\int_{p_l}^{p_l+p}\exp\left[-\frac{1}{\Delta^2}(q-\tfrac{1}{2}p)^2\right]dq\right\}^{1/2}$$

$$= \frac{1}{\sqrt{\pi}\Delta}\{e\}^{-(1/8)(p^2/\Delta^2)}\left\{\Delta\int_{[p_l-(1/2)p]/\Delta}^{[p_l+(1/2)p]/\Delta}e^{a^2}da\right\}^{\frac{1}{2}}\quad(\text{putting } a=\frac{1}{\Delta}(q-\tfrac{1}{2}p))$$

$$= \frac{1}{\sqrt{\pi}\sqrt{\Delta}}\sqrt{\frac{\sqrt{\pi}}{2}}\{e\}^{-(1/8)(p^2/\Delta^2)}\left\{H\left\{\frac{p_l+\frac{1}{2}p}{\Delta}\right\}-H\left\{\frac{p_l-\frac{1}{2}p}{\Delta}\right\}\right\}^{1/2}$$

$$= \frac{1}{\sqrt{2\sqrt{\pi}\Delta}}\{e\}^{-(1/8)(p^2/\Delta^2)}\left\{H\left\{\frac{p_l-\frac{1}{2}p}{\Delta}\right\}-H\left\{\frac{p_l-\frac{1}{2}p}{\Delta}\right\}\right\}^{1/2}$$

Now, the phase modulation is

$$\int M\,dt = \frac{0.40s}{\sqrt{p_m-p_0}}\,\frac{1}{p}\sum_{p=1}^{p_m}\sin(pt+\phi_p)\quad\text{from (1).}$$

Thus,

$$\frac{\text{Distortion}}{\text{Signal}} = \frac{1}{\sqrt{2\sqrt{\pi}\Delta}}\,\frac{p\sqrt{p_m-p_0}}{0.40s}\{e\}^{-(1/8)(p^2/\Delta^2)}\left\{H\left\{\frac{p_l+\frac{1}{2}p}{\Delta}\right\}-H\left\{\frac{p_l-\frac{1}{2}p}{\Delta}\right\}\right\}^{1/2}$$

$$= 2.5\,\frac{p}{s}\sqrt{\frac{p_m-p_0}{s}}\{e\}^{-1.57(p/s)^2}\left\{H\left[\frac{3.548}{s}(p_l+0.5p)\right]-H\left[\frac{3.548}{s}(p_l-0.5p)\right]\right\}. \tag{15}$$

In the top channel, when $p=p_m$,

$$\frac{\text{Distortion}}{\text{Signal}} = 2.5\left(\frac{p_m}{s}\right)^{1.5}e^{-1.57(p_m/s)^2}\left\{H\left[\frac{3.548}{s}(p_l+0.5p_m)\right]-H\left[\frac{3.548}{s}(p_l-0.5p_m)\right]\right\}^{1/2}$$

(neglecting p_0 in comparison with p_m), and this is (7).

Appendix IV

Distortion Due to Spectrum Truncation When the Deviation Ratio Is Small

In this case, (6), representing the phase modulation distortion, becomes

$$-a\sum_{p=p_l}^{p_m}\frac{1}{p}\cos(pt+\phi_p)\cdot\left[e^{-(0.04s^2/p_m p_0)}-\frac{a^2}{2}\sum_{p=0}^{2p_m}F_2(p)\cos(pt+\psi_p)\right]$$

$$-\frac{a^2}{2}\sum_{p=p_l}^{2p_m}F_2(p)\cos(pt+\psi_p)\sum_{p=p_0}^{p_m}\frac{a}{p}\cos(pt+\phi_p), \tag{16}$$

where $F_2(p)$ has the same significance as in (4).

For the deviations encountered in practice, p_l will be greater than p_m. Then, (16) becomes

$$-\frac{a^2}{2}\sum_{p=p_l}^{2p_m} F_2(p)\cos(pt+\psi_p)\sum_{p=p_0}^{p_m}\frac{a}{p}\cos(pt+\phi_p)$$

which may be written as

$$-\frac{a^3}{4}\sum_{q=p_l}^{2p_m}\sum_{r=p_0}^{p_m}\frac{F_2(q)}{r}\cdot[\cos(\overline{q-r}t+\psi_q-\phi_r)+\cos(\overline{q+r}t+\psi_q+\phi_r)].$$

This could yield terms of frequency p in three ways, first when $q-r=p$, in which case it is easy to show that the contribution is

$$-\frac{a^3}{4}\left\{\int_{p_l}^{2p_m}\left[\frac{F_2(q)}{q-p}\right]^2 dq\right\}^{1/2}, \qquad (17)$$

second when $q-r=-p$ and third when $q+r=p$. Case 2 makes no contribution since we have taken $p_l>p_m$, and case 3 also makes no contribution since $p<p_l$, as a consequence of the previous assumption.

If the restriction on p_l is slightly extended so that $p_l>p_m+p_0$, only the first term of F_2 will be required, so that (17) becomes

$$-\frac{a^3}{4}\left\{\int_{p_l}^{2p_m}\frac{1}{(x-p)^2}\left[\frac{2p_m-x}{x^2p_m(x-p_m)}+\frac{2}{x^3}\log\frac{p_m}{x-p_m}\right]dx\right\}^{1/2}.$$

This may be evaluated in terms of rational functions, logarithms and Spence Integrals. After considerable algebraic manipulation, the final result when $p=p_m$ (*i.e.*, in the top channel), is

$$-\frac{a^3}{4}\frac{1}{p_m^2}\left[\frac{(p_l-2p_m)(10p_l^2-12p_lp_m+p_m^2)}{2p_l(p_l-p_m)^2}-\frac{p_m(p_m^2+3p_lp_m-6p_l^2)}{p_l^2(p_l-p_m)}\log\frac{p_m}{p_l-p_m}+3\log\left\{\frac{p_l^2}{p_m(p_l-p_m)}\right\}\log\frac{p_l-p_m}{p_m}+6L(2)-6L\left\{\frac{p_l}{p_m}\right\}\right]^{1/2}.$$

Combining this with the expression for the phase modulation, one obtains the formula for distortion/signal in the top channel given as (8) in the second section.

Appendix V

Note on Spence Integrals

The Spence Integral, defined by

$$L(u)=\int_1^u\frac{\log x}{x-1}\,dx$$

is one of a group of integrals which, it appears, were first discussed [8] by W. Spence in 1809. It can be computed from the convergent series

$$L(1+x)=\sum_{n=1}^{\infty}(-1)^{n-1}\frac{x^n}{n^2} \qquad |x|\leqq 1$$

in conjunction with the relations

$$L(u)+L(u^{-1})=\tfrac{1}{2}(\log u)^2$$

and

$$L(u)+L(1-u)=\log u\log(1-u)-\tfrac{1}{6}\pi^2.$$

$L(u)$ has been extensively tabulated, as follows:

$u=1(1)100$, 9 places [8]
$u=0.5(0.01)1.5$, 12 places [9]
$u=0(0.01)2(0.02)6$, 7 places [10]
$u=0(0.01)2$, 9 places [12]
$u=0.5(0.001)1$, 9 places [12]

Thus, the complete coverage, to seven places or better, is $0(0.01)0.5(0.001)1(0.01)2(0.02)6(1)100$.

Lists of errors in the tables of [9] and [10] appear in [11]. A further error in [10] is noted in [12] (p. 352).

Bibliography

[1] Middleton, D., "The Distribution of Energy in Randomly Modulated Waves." *Philosophical Magazine*, vol. 42 (seventh series), (July, 1951), pp. 689–707.
[2] Stewart, J. L., "The Power Spectrum of a Carrier Frequency-Modulated by Gaussian Noise." Proceedings of the IRE, vol. 42 (October, 1954), pp. 1539–1542.
[3] Albersheim, W. J., and Schafter, J. P., "Echo Distortion in the FM Transmission of Frequency-Division Multiplex." Proceedings of the IRE, vol. 40 (March, 1952), pp. 316–328.
[4] Gladwin, A. S., "Energy Distribution in the Spectrum of a Frequency Modulated Wave, Part II." *Philosophical Magazine*, vol. 38 (seventh series), (April, 1947), pp. 229–251.
[5] Medhurst, R. G., and Stewart, J. L., discussion on reference 2, Proceedings of the IRE, vol. 43 (June, 1955), pp. 752–754.
[6] Medhurst, R. G., "Harmonic Distortion of Frequency-Modulated Waves by Linear Networks." *Proceedings of the Institute of Electrical Engineering*, vol. 101, pt. III (May, 1954), pp. 171–181.
[7] National Bureau of Standards, "Tables of the Error Function and Its Derivatives-AMS41." U. S. Government Printing Office, Washington, D. C., October 22, 1954.
[8] Spence, W., "Essay on the Theory of the Various Orders of Logarithmic Transcendents." 1809, p. 24 (2nd edn. ed. by John Herschel, 1819, has a list of last place corrections to the tables.)
[9] Newman, F. W., "The Higher Trigonometry." Cambridge, Eng., Cambridge University Press, 1892 (re-issued 1912), pp. 64–65.
[10] Powell, E. O., "An Integral Related to the Radiation Integrals." *Philosophical Magazine*, vol. 34 (September, 1943), pp. 600–607.
[11] Fletcher, A., "Note on Tables of an Integral." *Philosophical Magazine*, vol. 35 (January, 1944), pp. 16–17.
[12] Mitchell, K., "Tables of the Function $\int_0^x(-\log|1-y|)/y\,dy$ With an Account of Some Properties of this and Related Functions." *Philosophical Magazine*, vol. 40 (March, 1949), pp. 351–368.
[13] Fisher, W. C., "Transmission and Power Levels in Multiplex Equipment." *Radio-Electronic Engineering*, vol. 23 (August, 1954), pp. 10–11, 28.
[14] Holbrook, B. D., and Dixon, J. T., "Load Rating Theory for Multi-Channel Amplifiers." *Bell System Technical Journal*, vol. 18 (October, 1939), pp. 624–644.
[15] Comite Consultatif International Telephonique (CCIF), XVI^e Assemblee Pleniere, Tome III bis; Transmission sur les Lignes Maintenance, p. 121, Firenze (October, 1951).
[16] Bennett, W. R., "Cross Modulation Requirements on Multichannel Amplifiers Below Overload." *Bell System Technical Journal*, vol. 19 (October, 1940), pp. 587–610.
[17] Landon, V. D., "The Distribution of Amplitude with Time in Fluctuation Noise." Proceedings of the IRE, vol. 29, (February, 1941), pp. 50–55: see also vol. 30 (September, 1942), pp. 425–429.

Design Information on Large-Signal Traveling-Wave Amplifiers*

J. E. ROWE†, ASSOCIATE, IRE

Summary—**The large-signal traveling-wave amplifier equations have been solved and results are presented for a wide range of the traveling-wave amplifier parameters. The results have been analyzed and are presented to provide design information on large-signal traveling-wave amplifiers. Curves of saturation voltage gain and saturation efficiency are included for $C=0.05$, 0.1, and 0.2 when $QC=0$ and for $QC=0.05$, 0.125, 0.25 and 0.50 when $C=0.1$; for the space-charge cases $B=0.5$, 0.75, 1.0 and 1.5. In all cases $d=0$. A power output vs power input curve is shown for the case $C=0.1$, $QC=0.25$, $B=1$ and $d=0$. For all the cases studied the ratio of helix-to-stream radii was taken as 2. The effect of series loss along the helix is also studied for $C=0.1$, $QC=0.125$ and $B=1$: curves for variable d at fixed b and for variable b at fixed d are presented. The effect of the placement of loss is also studied.**

Introduction

THE TRAVELING-WAVE amplifier is an important and useful tube, for its high gain and inherently large bandwidth compare favorably with the characteristics of other microwave devices. In view of the many applications for a traveling-wave amplifier operating at high output levels, it seems desirable to study in detail the large-signal equations governing its behavior. Of particular interest are the variations of gain and phase shift at high output levels for different values of such parameters as space charge, electron injection velocity, loss along the helical transmission line, and gain parameter. Also of interest are the effects of space charge and loss along the helical transmission line on the saturation gain and power output. The over-all objective, of course, is to learn how to design a traveling-wave amplifier to operate at high power levels with maximum efficiency.

Partial large-signal theories of the traveling-wave amplifier have been presented by Brillouin[1] and Nordsieck[2] and a more complete theory has recently been presented by Poulter.[3]

Brillouin's approach did not include the effect of space charge or the effect of electron overtaking, which occurs in large-signal traveling-wave amplifiers. Nordsieck's theory includes the effect of electron overtaking but does not consider space charge and is limited to small values (*i.e.*, $C<0.1$) of the small-signal gain parameter C. Tien, Walker, and Wolontis[4] have recently presented large-signal calculations using Nordsieck's equations with a space-charge term added. However, their work does not consider the effect of large values of the small-signal gain parameter C.

Equations have been derived describing the large-signal operation of the traveling-wave amplifier, including the effect of ac space charge and attenuation along the helical slow-wave structure. The equations constitute a system of nonlinear partial-differential-integral equations valid with reasonable approximations for all values of the parameters which are encountered in typical high-power traveling-wave amplifiers.[5] The parameters which appear in the equations and on the graphs are the relative injection velocity b, the gain parameter C, the loss parameter d, the input-signal level to the helix A_0, and the space-charge parameters QC and B. The space-charge range parameter B, which measures the space-range of effectiveness of the space-charge forces, is defined by $B=\beta b'$ where b' is the electron stream radius and β is the propagation constant of the rf wave on the helix. For all the cases calculated the ratio of helix-to-stream radii a'/b' was taken as 2. Mathematical definitions of all parameters will be found at the end of this paper.

Voltage Gain and Tube Length at Saturation

In order to determine the optimum injection velocity for particular C and QC values, the voltage gain and tube length in undisturbed wavelengths at saturation are plotted vs b in Figs. 1 and 2.

The drop-out point of the voltage-gain curve is quite sharp, as it is in the linear case, and the value of b at which this drop of the gain to a very small value occurs is approximately that value of b for which the small-signal gain goes to zero. For these large values of b the saturation tube length is very short, which is to be expected since the electron velocity is much greater than the wave speed and hence the interaction between the wave and the stream is negligible.

In Fig. 1 the gain curve for $C=0.2$ is shown dotted in the vicinity of $b=2.0$ because the total velocity of some electrons approaches zero near saturation for this case. This means that these electrons have stopped moving

* Original manuscript received by the IRE, May 2, 1955; revised manuscript received September 26, 1955.

† Department of Electrical Engineering, University of Michigan, Ann Arbor, Mich.

[1] L. Brillouin, "The traveling-wave tube (discussion of waves for large amplitudes)," *Jour. Appl. Phys.*, vol. 20, pp. 1196–1206; December, 1949.

[2] A. Nordsieck, "Theory of the large-signal behavior of traveling-wave amplifiers," PROC. IRE, vol. 41, pp. 630–637; May, 1953.

[3] H. Poulter, "Large signal theory of the traveling-wave tube," Stanford University, Electronics Research Laboratory, Technical Rept. No. 73, January, 1954.

[4] P. Tien, L. Walker, and V. Wolontis, "A large-signal theory of traveling-wave amplifiers," PROC. IRE, vol. 43, pp. 260–277; March, 1955.

[5] The derivation of the generalized large-signal equations is presented in a paper to be published in the TRANS. IRE (Electron Devices).

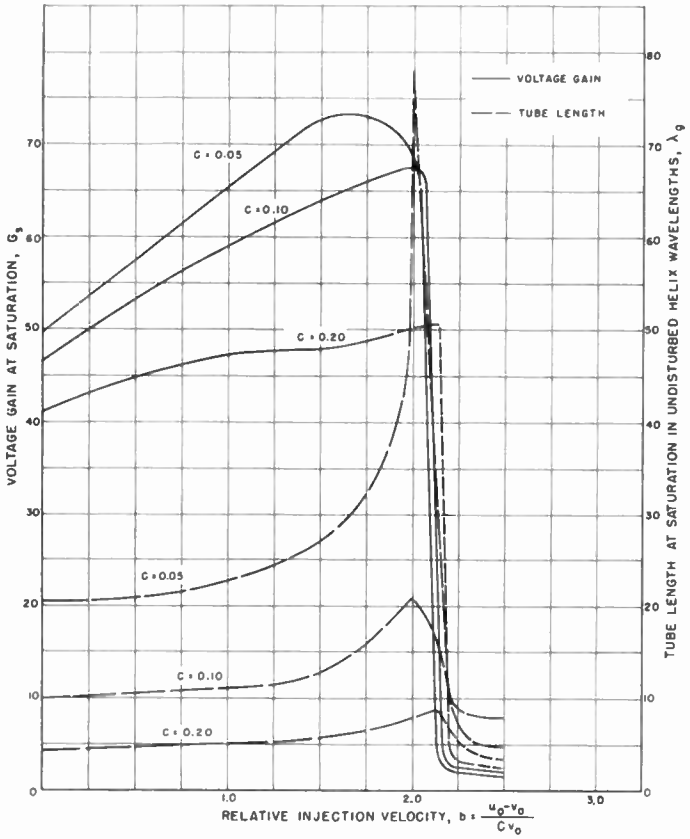

Fig. 1—Voltage gain and tube length at saturation vs relative injection velocity. $QC=0$, $d=0$, $A_0=0.0225$.

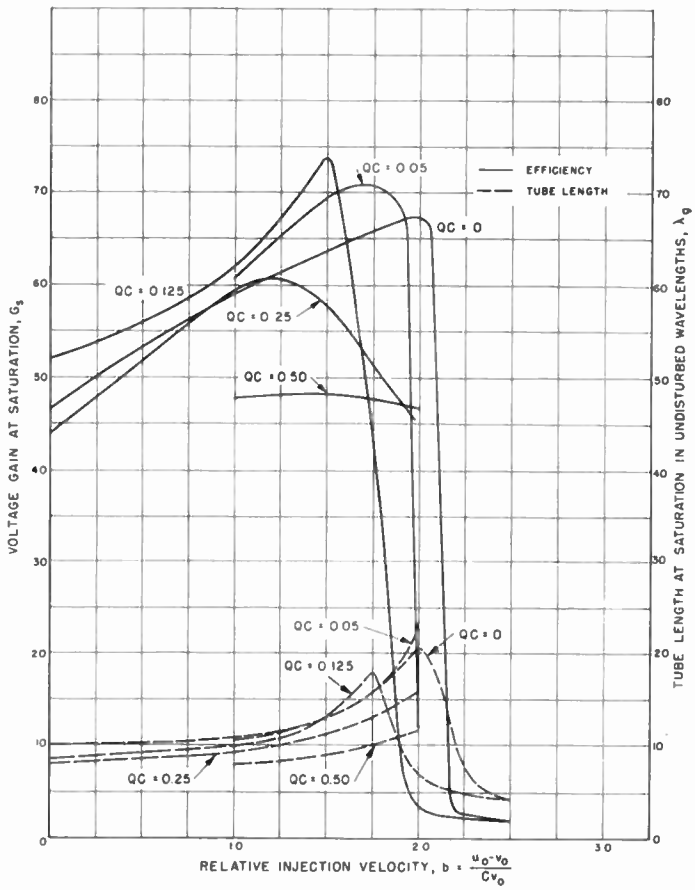

Fig. 2—Voltage gain and tube length at saturation vs relative injection velocity. $C=0.1$, $d=0$, $A_0=0.0225$, $B=1$.

relative to the rf field and eventually will move backward relative to the rf field. For values of C as large as 0.2 neglect of space charge leads to appreciable errors and hence these particular results are of questionable physical significance.

In comparing saturation gains for different values of C from Fig. 1 it is necessary to keep the tube length constant. For a tube 20 wavelengths long the saturation gain is 50 when $C=0.05$ and 67.5 when $C=0.10$.

Maximum saturation gain for $C=0.1$ and $QC=0$ occurs at $b=2.0$, which amounts to an 18.2 per cent increase in velocity or a 40 per cent increase in the stream voltage V_0 over that for maximum small-signal gain. As b is increased the tube length at saturation would be expected to be greater, since the electrons advance in phase with respect to the wave faster and hence it takes a greater distance for them to build up comparable ac velocities. Also, the expected saturation gain should be greater for larger b, since the kinetic energy in the stream is greater by an amount proportional to b^2.

In Fig. 2 gain curves are shown for $C=0.1$ and several values of the space-charge parameter QC. For QC up to 0.5 it is noticed that the b for maximum saturation gain is less than that for $QC=0$. However, for larger values of QC it is expected that the b for maximum saturation gain will increase as in the linear theory. The "optimum" relative injection velocity vs the small-signal space-charge parameter is shown in Fig. 3 for two

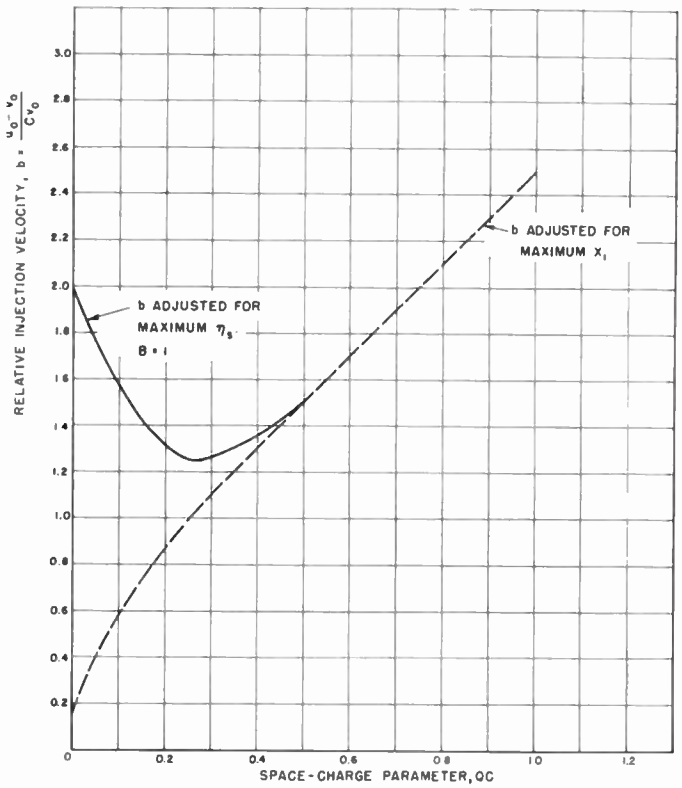

Fig. 3—"Optimum" relative injection velocity vs small-signal space-charge parameter. $C=0.1$, $d=0$.

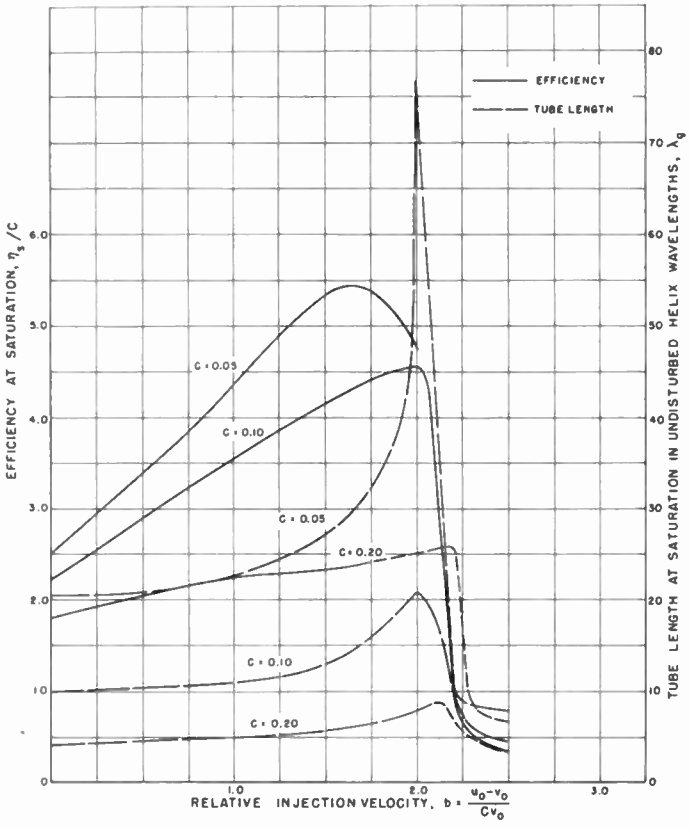

Fig. 4—Efficiency/C and tube length at saturation vs relative injection velocity. $QC=0$ $d=0$, $A_0=0.0225$.

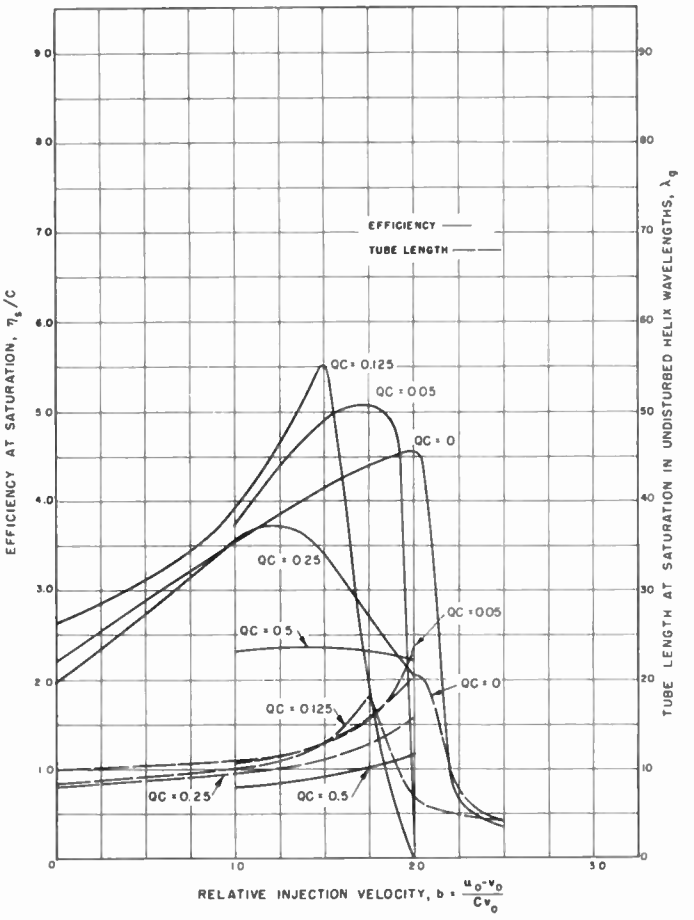

Fig. 5—Efficiency/C and tube length at saturation vs relative injection velocity. $C=0.1$, $d=0$, $A_0=0.0225$, $B=1$.

different definitions of "optimum" conditions: (1) b adjusted for maximum small-signal gain, and (2) b adjusted for maximum saturation gain. It is noticed that at $QC=0.5$ the curves intersect, which is an "absolute optimum" condition since the tube length is then a minimum for any desired gain. Also, the saturation gain with small values of QC has increased over that for $QC=0$, but as QC is increased further the gain decreases, as is expected for large values of space charge. A qualitative explanation of this phenomenon is given in the following section.

Efficiency and Tube Length at Saturation

For the same data as discussed above, saturation efficiency and tube length may be plotted vs the velocity parameter b. The saturation efficiency η_s is:

$$\eta_s = 2C\,A_{\max}^2(y). \tag{1}$$

Efficiency/C is plotted vs relative injection velocity with C and QC as the respective parameters in Figs. 4 and 5. The efficiency curves are seen to be quite similar to the voltage-gain curves, and efficiency increases with C as is expected since larger C values correspond to greater coupling between the circuit and the stream.

In Fig. 6 the maximum saturation efficiency is plotted vs C for $QC=0$. For each value of C the efficiency is maximized by optimizing the velocity parameter b. Fig. 6 indicates that not much is gained in efficiency by increasing the gain parameter C beyond 0.10 or 0.12 for

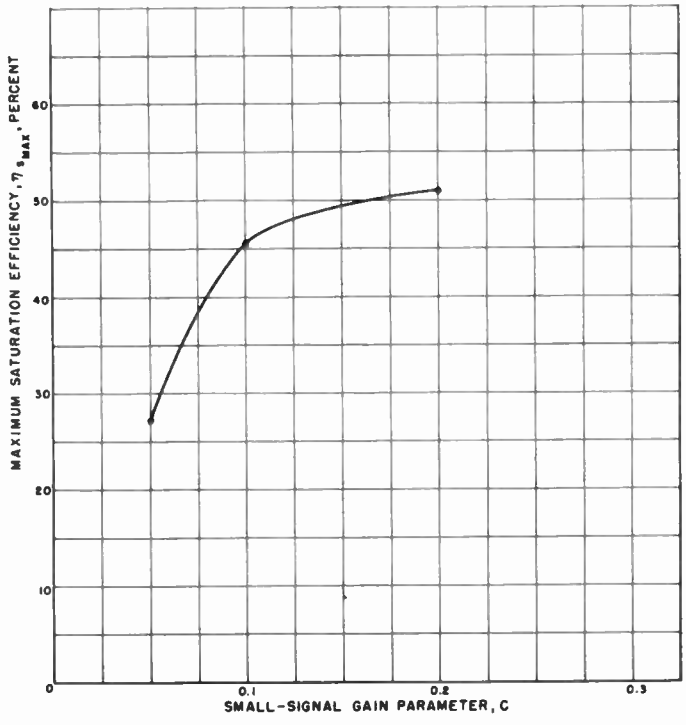

Fig. 6—Maximum saturation efficiency vs small-signal gain parameter. $QC=0$, $d=0$.

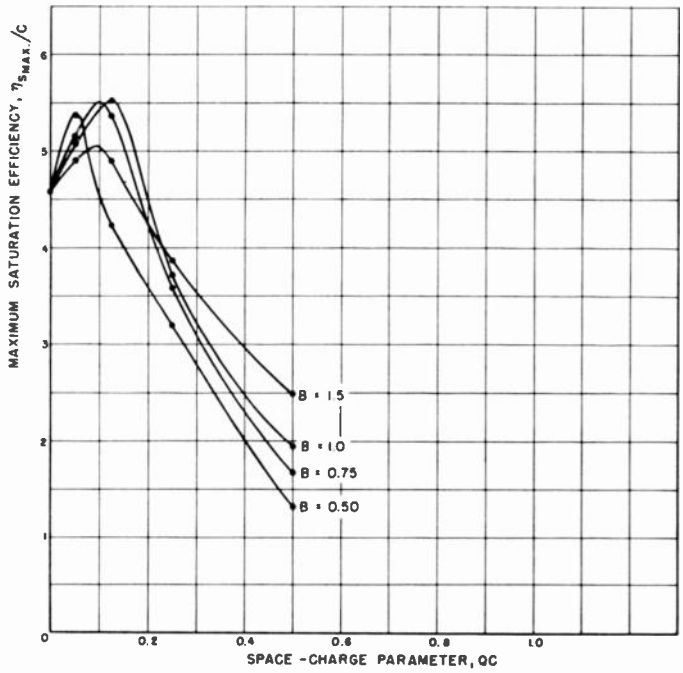

Fig. 7—Maximum saturation efficiency/C vs small-signal space-charge parameter with stream diameter as the parameter. $C=0.1$, $d=0$, $A_0=0.0225$.

small values of space charge. The computed points are shown on the curves where there are not sufficient data to determine the curve uniquely.

The maximum saturation ecffiiency divided by C is plotted against the small-signal space-charge parameter QC in Fig. 7 for several values of the space-charge range parameter B, which is proportional to the stream radius. The variation of saturation efficiency with QC for constant B as indicated in Fig. 7 might be interpreted qualitatively as follows: For small values of QC, up to approximately 0.125, the maximum saturation efficiency increases with QC, as might be expected since the charge density and the space-charge forces in the stream are very small and the increase in charge density associated with increasing QC appears as increased power output. However, for larger values of QC it is probable that the strong short-range space-charge forces inhibit the bunching severely enough to overcome the effect of the increased charge density.

The variation of efficiency with B for fixed QC might be explained as follows: Consider the efficiency variation with QC for the $B=1.0$ curve of Fig. 7. The power output and efficiency of a tube are determined by the absolute value of the space-charge density in the electron stream, which is proportional to ω_p/ω; a given QC may be obtained by either a relatively large value of ω_p/ω and a small value of B or a small value of ω_p/ω and a larger value of B as shown in Fig. 8. Since the space-charge term in the large-signal equations has as its coefficient a term proportional to the absolute value of the space-charge density and since this term represents the space-charge force acting on the electrons and hence

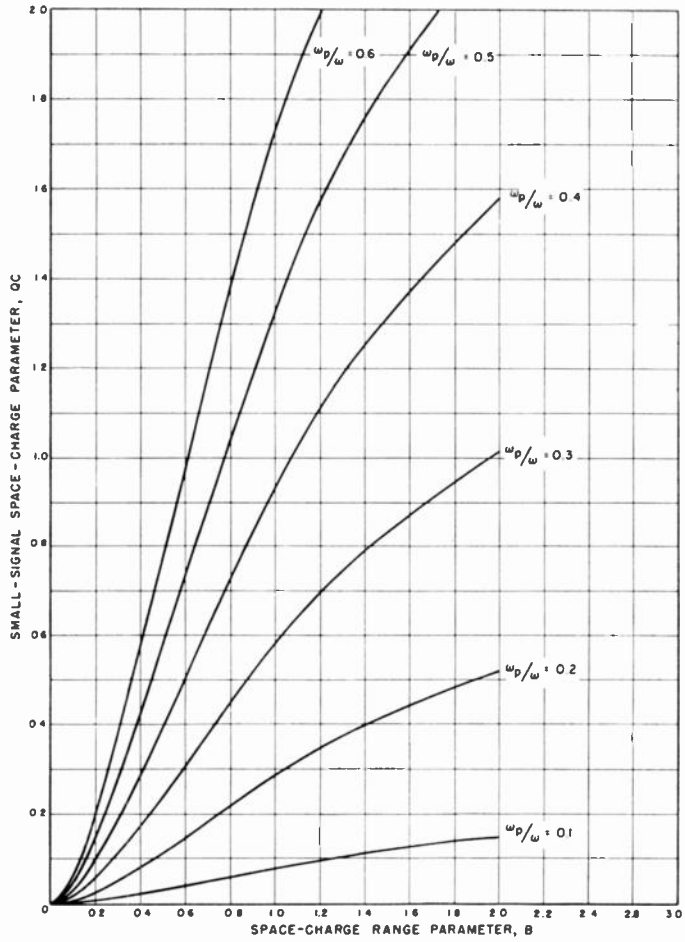

Fig. 8—Small-signal space-charge parameter vs space-charge range parameter for constant values of the absolute space-charge density. Ratio of helix-to-stream radii is $2C=0.1$.

influences the motion of the electrons in the stream, it might be expected that the efficiency would vary with ω_p/ω for fixed QC and variable stream diameter as shown in Fig. 7. In all these calculations it has been assumed that the electric field does not vary across the stream.

Variable Input-Signal Level

The input-signal level for all calculations heretofore presented has been the same, *i.e.*, 30 db below CI_0V_0. This value of A_0 was selected so that the input boundary conditions could be calculated from the linear theory.

The purpose of these calculations, however, is to analyze the operation of high-power amplifiers. For the value of A_0 used here the saturation gain is between 30 and 40 db, but it has been found experimentally that the maximum gain in a loss-free region must be limited to approximately 20 db if the standing-wave ratio at the output transducer is of the order of 1.5:1. Hence, where higher gains are necessary, added external attenuation must be placed on the helix and consequently the saturation gain and power output are reduced. Thus it is not practical to build high gain and high power output in the same tube; instead, a short low-gain loss-free tube should be used when high power output is desired.

To shed some light on the tube characteristics under such conditions, solutions are presented for larger values of the input-signal level A_0. These solutions are shown in Figs. 9 and 10 with ψ, the input-power level below CI_0V_0, having values of 5, 7, 10, 15, 20, 25, 30, and 40 db. The case selected for this investigation is $C=0.1$, $QC=0.25$, $b=1.25$, and $B=1$.

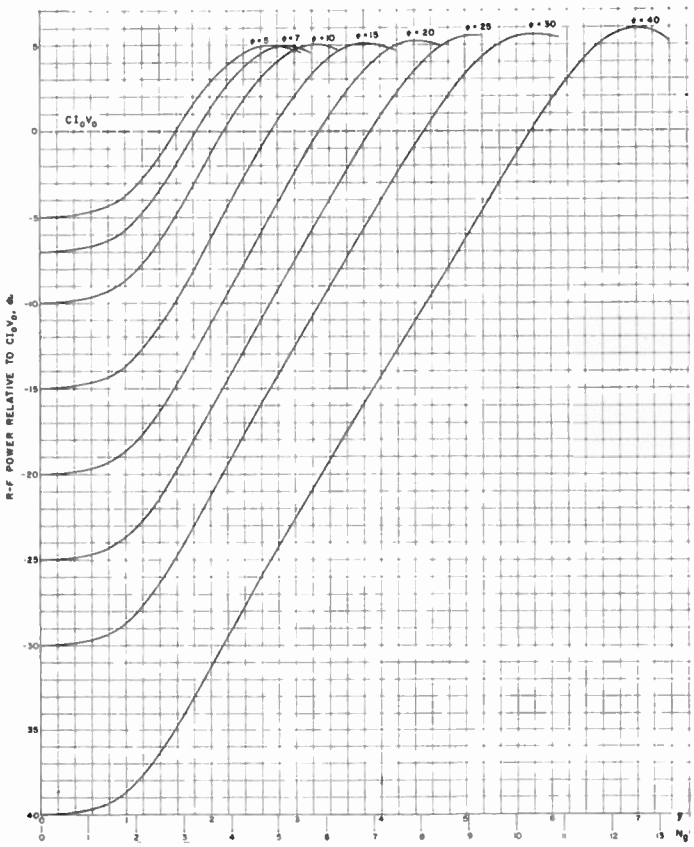

Fig. 9—RF power relative to CI_0V_0 vs distance with ψ, the input power level in db below CI_0V_0, as the parameter. $C=0.1$, $QC=0.25$, $d=0$, $b=1.25$, $B=1$.

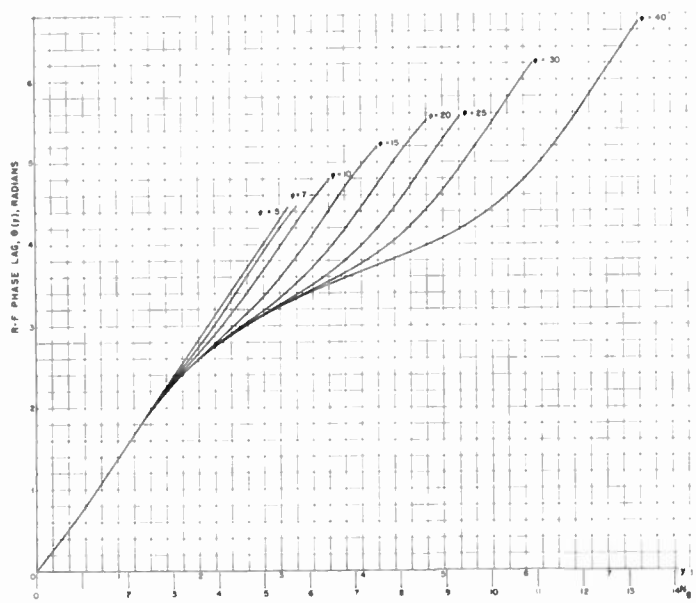

Fig. 10—RF phase lag of the wave relative to the electron stream with ψ, the input power level below CI_0V_0, as the parameter. $C=0.1$, $QC=0.25$, $d=0$, $b=1.25$, $B=1$.

The input boundary conditions on the entrance phase of the electrons relative to the rf wave at the helix input and the ac velocity of entering electrons are taken to be the same for all values of A_0. The value of $A'(y)$ at the input of a lossless helix is always zero since the stream cannot influence the wave amplitude until it has become bunched. However, the value of $\theta'(y)$ at the input for large input-signal levels is open to question. The value of $\theta'(y)$ gives an apparent phase velocity of the total wave at the input which results when the three small-signal-theory waves are combined. Since no theory is available to calculate a more accurate value of $\theta'(y)$, the value given by the linear theory is used. This is tantamount to assuming that $\theta'(0)$ is independent of signal level, which is not considered to be a serious deviation from the truth. The insensitivity of the solutions to small errors in $\theta(y)$ and $A(y)$ further justifies the assumption.

Some additional information on the operation of large-signal amplifiers when the input-signal level is varied may be obtained from Figs. 9 and 10; in addition data are shown for the case $C=0.1$ and $QC=0.125$. Since the saturation level is relatively independent of ψ, one curve is a plot of the input-signal level vs the saturation length, shown in Fig. 11. It can be seen that the optimum tube length is very nearly a linear function of the input-signal level for a wide range of ψ.

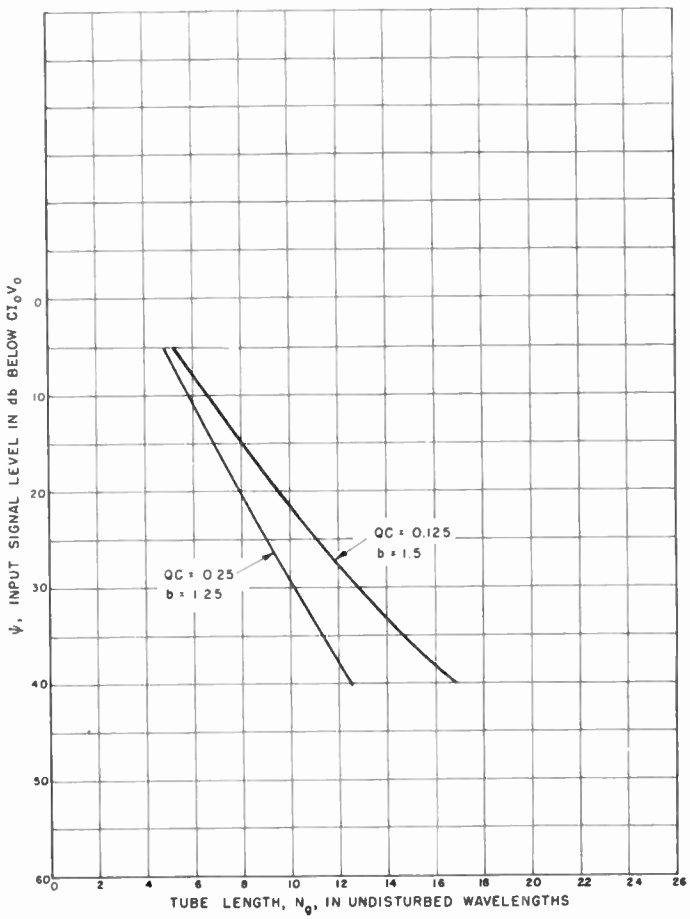

Fig. 11—ψ, input-signal level in db below CI_0V_0, vs tube length at saturation in undisturbed wavelengths. b is adjusted for maximum saturation gain. $C=0.1$, $d=0$, $B=1$.

Fig. 12 is a plot of the phase shift at saturation, relative to that for a very small input-signal level, vs the input-signal level for a fixed tube length. The tube length chosen is $N_g = 5.5$ (*i.e.*, $y = 3$); from the figure it can be seen that the tube would saturate at approximately $y = 3$ for $\psi = 7$ db. This curve indicates the amount of incidental phase modulation that would accompany a change in the input-signal level or amplitude modulation of the input signal. Clearly if the tube is to be amplitude-modulated it must be operated well below saturation and with small amplitudes of modulating voltage if linearity is desired.

For the same tube length, *i.e.*, $N_g = 5.5$, a power-output vs power-input curve prepared from the data of Fig. 9 is shown in Figs. 13(a) and 13(b). The power levels are plotted on a linear scale in Fig. 13(a) and on a logarithmic scale in Fig. 13(b). In the small-signal region the power output is seen to be a linear function of the input power as expected; however, as the input power is increased still further the output power reaches a maximum and then decreases.

Fig. 13(b) indicates that for this case the saturation power output is approximately 5 db below that which would be obtained if the output were still linearly re-

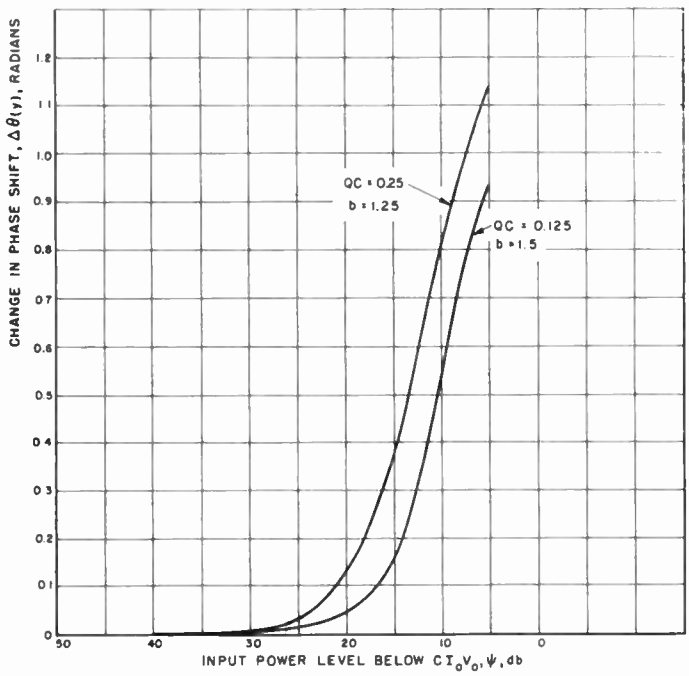

Fig. 12—Change in phase shift at saturation vs ψ for fixed tube length with variable input-signal level. $C = 0.1$, $d = 0$, $N_g = 5.5$, $B = 1$.

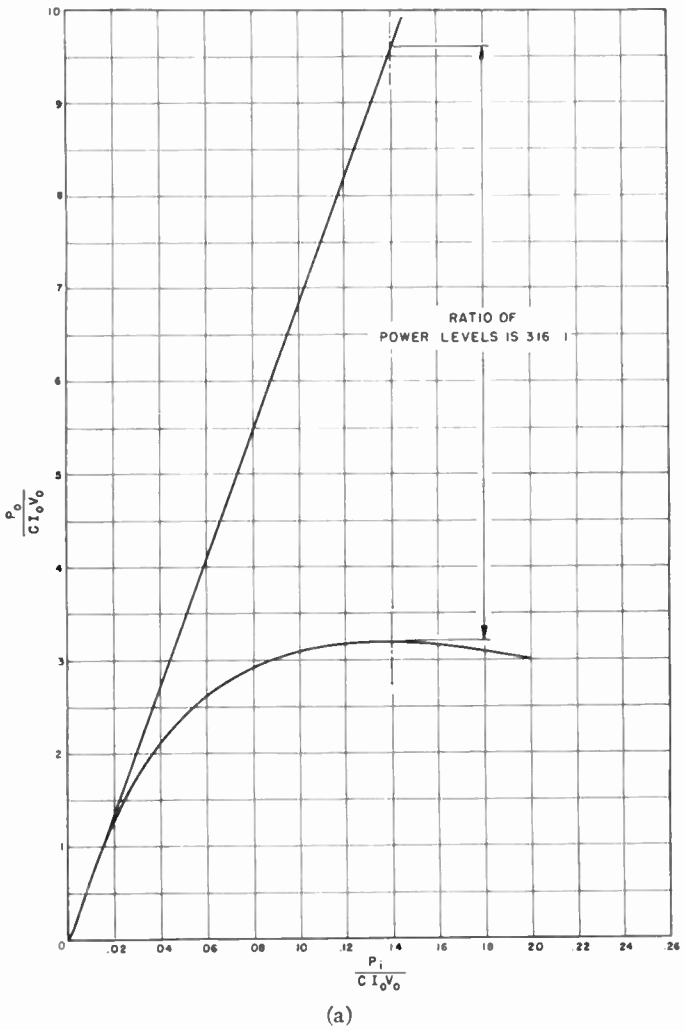

(a)

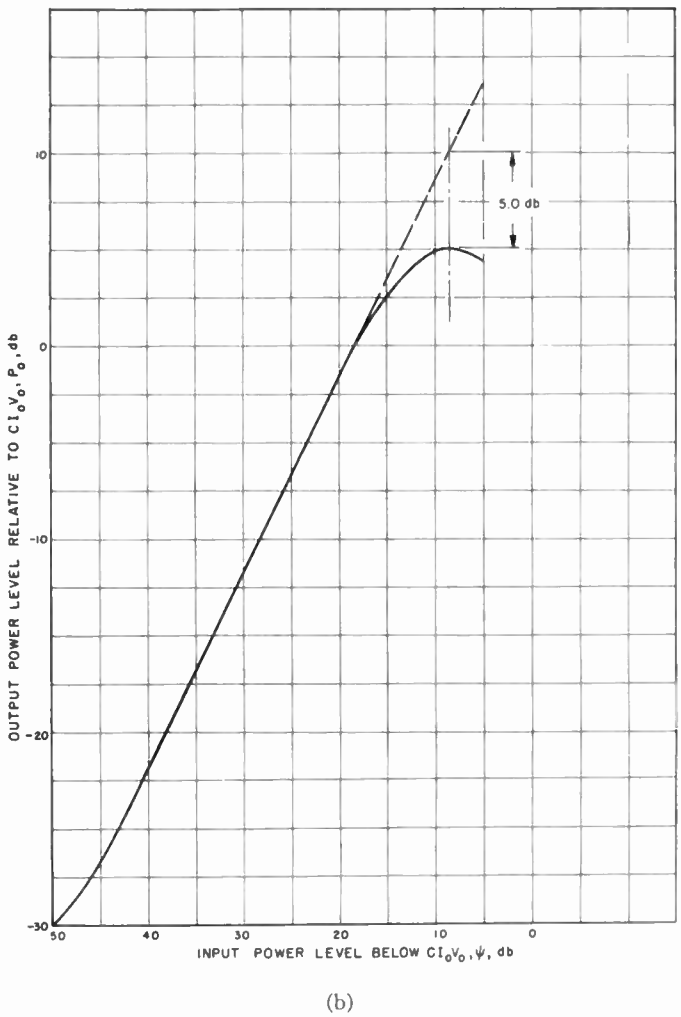

(b)

Fig. 13—(a) Output power level relative to CI_0V_0 vs input power level relative to CI_0V_0 for fixed tube length. $C = 0.1$, $QC = 0.25$, $d = 0$, $b = 1.25$, $N_g = 5.5$, $B = 1$. (b) Output power level relative to CI_0V_0, P_0, vs input power level below CI_0V_0, ψ, for fixed tube length. $C = 0.1$, $QC = 0.25$, $d = 0$, $b = 1.25$, $N_g = 5.5$, $B = 1$.

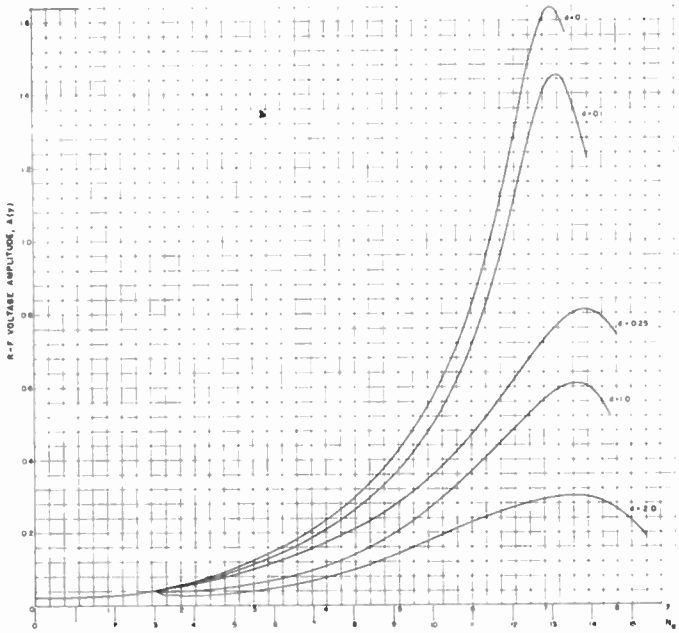

Fig. 14—Amplitude of the rf voltage along the helix with loss as the parameter. $C=0.1$, $QC=0.125$, $A_0=0.0225$, $b=1.5$, $B=1$. $d=0$ for $0\leqq y\leqq 1.6$ for all curves.

lated to the input and that the power output departs slowly from the straight-line value. When $QC=0.125$ it was found that there is an increase in the output due to the presence of space charge, and the saturation power output was only 3.75 db below the small-signal value, but for larger QC the output decreases. Hence for values of $QC>0.25$ it is expected that the saturation power output should be more than 5 db below the extrapolated linear output value. Experimentally it has been found that when $C=0.1$ and $QC=0.25$ the best that can be achieved for saturation power is 5 to 6 db below the value predicted by the linear relation.[6] Furthermore, it has been verified experimentally that as QC is increased beyond 0.25 the saturation power drops further below the extrapolated linear output.

Effect of Series Loss Along the Helix

As was pointed out above, it is necessary to add series loss along the helix in high-gain amplifiers in order to insure stable operation. To assist in determining the effect of the amount and placement of this loss on the saturation gain and efficiency, solutions are presented for several values of the loss factor d at $C=0.1$, $QC=0.125$ and $B=1$. The values of d selected are 0.1, 0.25, 1.0, and 2.0, which, for $C=0.1$, correspond to losses of approximately 0.56, 1.36, 5.45, and 10.9 db per undisturbed wavelength λ_0 respectively. In addition, the effect of the placement of loss and the reduction of the optimum value of b in the presence of loss is discussed for $d=2.0$.

The power flow along a lossy helix is given by

$$P_{0L}(y) = \text{Re}\,\frac{1}{2}VI^*$$

[6] J. J. Caldwell, Jr., Hughes Research Development Labs. (private communication).

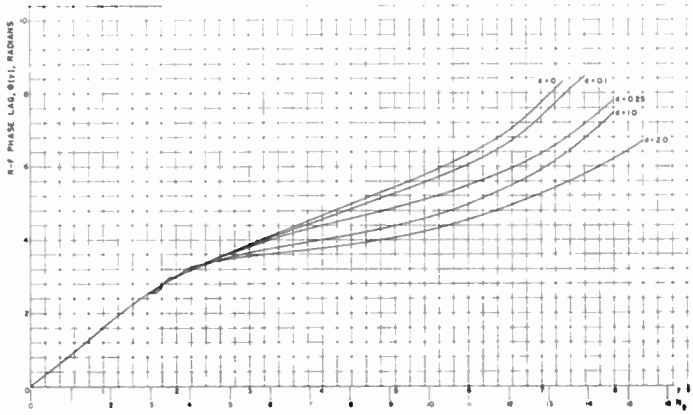

Fig. 15—RF phase lag of the wave relative to the electron stream vs distance along the helix with loss as the parameter. $C=0.1$, $QC=0.125$, $A_0=0.0225$, $b=1.5$, $B=1$. $d=0$ for $0\leqq y\leqq 1.6$ for all curves.

$$= \text{Re}\,\frac{VV^*}{2Z_0{}^*_L}, \tag{2}$$

where $Z_{0L}=Z_0(1-jCd)$, the characteristic impedance of the lossy helix. The voltage along the helix is defined by

$$V(y,\phi) \triangleq \text{Re}\left[\frac{Z_0I_0}{C}A(y)e^{-j\phi}\right]. \tag{3}$$

Substitution of the defining expressions for Z_{0L} and the voltage gives for the power flow along the lossy helix,

$$P_{0L}(y) = \frac{2CI_0V_0}{1+jCd}A^2(y). \tag{4}$$

Variable Loss Factor d for Fixed Injection Velocity b

The solution selected for investigation is $C=0.1$, $QC=0.125$, $B=1$, and that value of b which gives maximum saturation gain when $d=0$, *i.e.*, $b=1.5$. The method is to integrate for a distance of approximately three undisturbed wavelengths from the input with $d=0$ and then to carry out solutions from this point to saturation for the values of d listed above. The results are presented in Figs. 14 and 15.

Since the region in the vicinity of the point where the loss is first applied is of particular interest, this region has been expanded in Figs. 16 and 17 for the variables $A(y)$ and $\theta(y)$. It can be seen that in the cases where $d=1.0$ and 2.0 the signal level on the helix diminishes in amplitude for approximately one undisturbed wavelength after the loss is applied and then as the stream is continually being bunched resumes increasing in amplitude. This temporary decrease in rf signal amplitude indicates that energy is being put back into the stream and appears as an increase in the kinetic energy of the stream. Hence the electrons are accelerated, which lessens the interaction between the wave and the stream so that the signal level on the helix drops until the stream becomes rebunched sufficiently to give energy back to the helix wave.

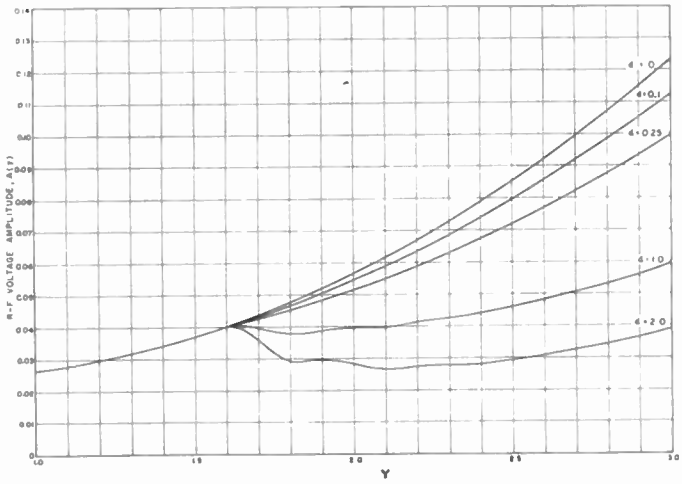

Fig. 16—Expanded portion of Fig. 14.

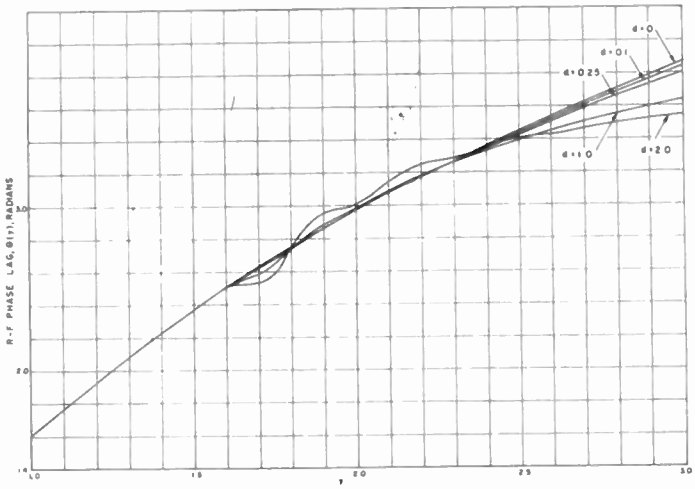

Fig. 17—Expanded portion of Fig. 15.

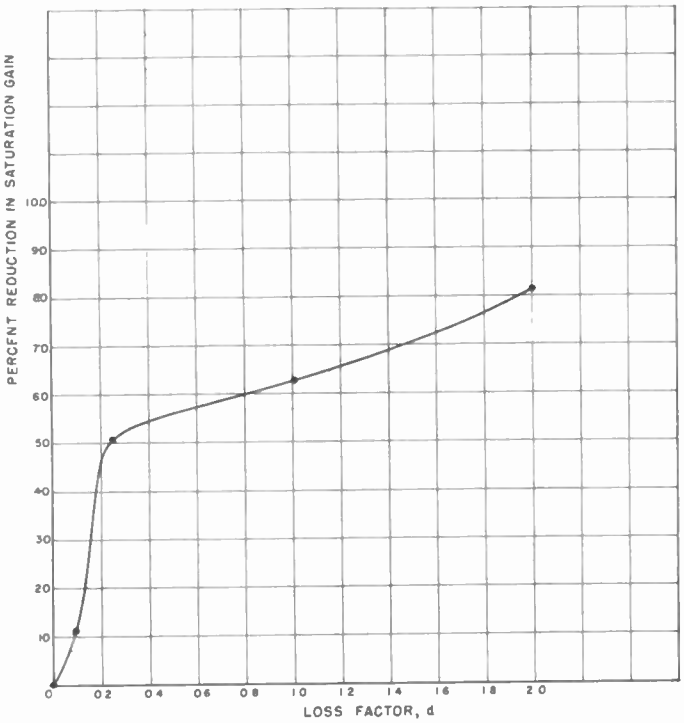

Fig. 18—Per cent reduction in sturation gain vs loss factor for fixed injection velocity. $C=0.1$, $QC=0.125$, $A_0=0.0225$, $b=1.5$, $B=1$. $d=0$ for $0 \leqq y \leqq 1.6$.

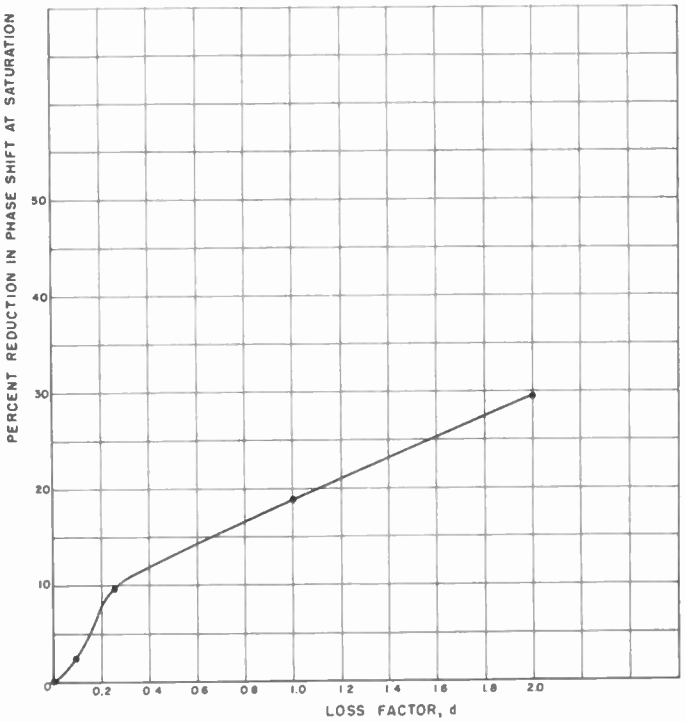

Fig. 19—Per cent reduction in phase shift at saturation vs loss factor for fixed injection velocity. $C=0.1$, $QC=0.125$, $A_0=0.0225$, $b=1.5$, $B=1$. $d=0$ for $0 \leqq y \leqq 1.6$.

The slowing of the rf wave due to the presence of series loss also contributes to a decreased interaction between the wave and the stream. The axial phase velocity of the wave in the presence of small amounts of loss is

$$v_{0L} = \frac{\omega}{\beta} = \frac{v_0}{\left(1 + \frac{C^2 d^2}{2}\right)}. \qquad (5)$$

From the loss curves for constant injection velocity shown in Fig. 14, the per cent reductions in saturation gain and phase shift are calculated and plotted in Figs. 18 and 19. For low values of loss the per cent reduction in saturation gain increases rapidly, but for values of d greater than 0.2 (1.09 db/λ_q) the per cent reduction increases more slowly.

Fig. 18 agrees well with the experimental results of Cutler and Brangaccio[7] for small values of the loss factor d, but they differ by nearly a factor of 2 for larger values of d. This disagreement was expected because the gain parameter for their tube was much smaller (approximately $C=0.025$) than the $C=0.1$ used in the calculations. Furthermore, the QC for their tube was approximately 0.50, whereas it was 0.125 in these calculations.

Variable Injection Velocity b for Fixed Loss Factor d

As discussed above, the effect of series loss along the helix is to decrease the wave velocity and thus reduce the interaction between the wave and the stream. The

[7] C. C. Cutler and D. J. Brangaccio, "Factors affecting traveling-wave tube power capacity," TRANS. IRE, vol. ED-3, pp. 9–24; June, 1953.

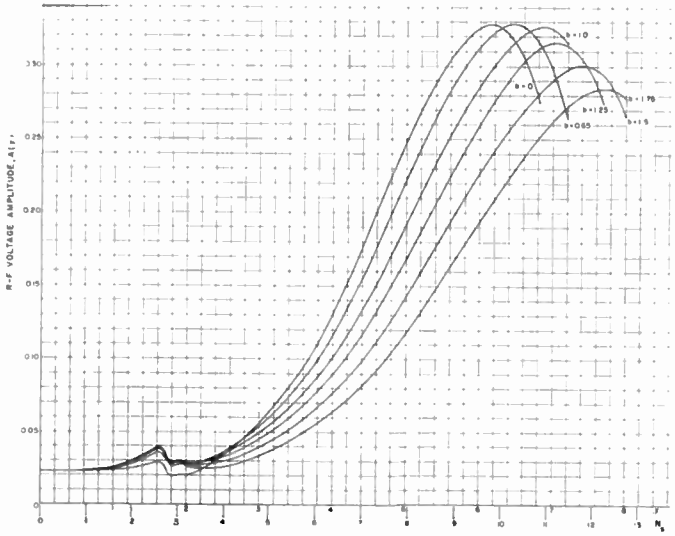

Fig. 20—Amplitude of the rf voltage along the helix for fixed loss with relative injection velocity as the parameter. $C=0.1$, $QC=0.125$, $A_0=0.0225$, $B=1$. $d=0$ for $0\leqq y\leqq 1.6$; $d=2.0$ for $y>1.6$

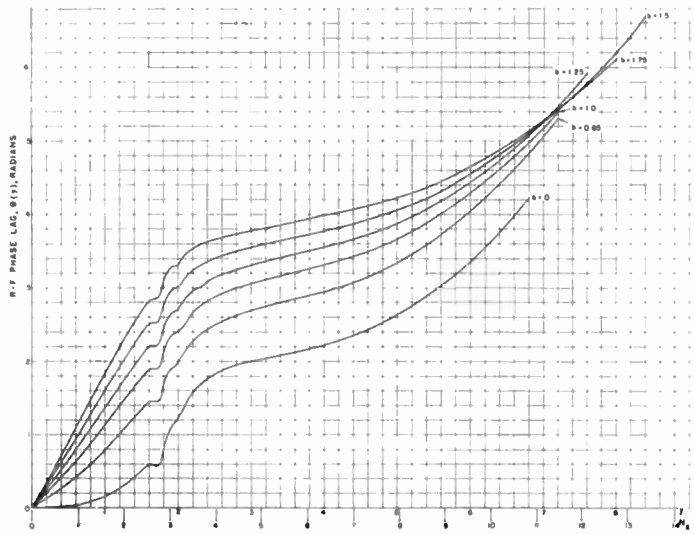

Fig. 21—RF phase lag of the wave relative to the electron stream for fixed loss with relative injection velocity as the parameter. $C=0.1$, $QC=0.125$, $A_0=0.0225$, $B=1$. $d=0$ for $0\leqq y\leqq 1.6$; $d=2.0$ for $y>1.6$.

larger the value of d, the greater the decrease in wave velocity. In order to determine the amount by which the velocity is decreased and also the b associated with maximum saturation gain in the presence of loss, solutions have been carried out for several values of b with fixed loss. The value of d selected is 2.0 (10.9 db/λ_g). The results of these computations are in Figs. 20 and 21.

The optimum injection velocity is reduced by the presence of loss as pointed out above. The saturation voltage gain is plotted vs the velocity parameter for the case $C=0.1$, $QC=0.125$, and $B=1$ in Fig. 22, from which it is seen that the optimum b at $d=2$ is 0.65 as compared to 1.5 for $d=0$, a reduction of 8.5 per cent in velocity above synchronism. The saturation gain is seen to vary only slightly for b between 0 and 0.65. Hence it would seem desirable to change the helix pitch under the attenuator of a traveling-wave amplifier in order to realize an increased gain. This is especially true if the loss per wavelength is large. In the above-mentioned case an improvement in the saturation gain in the lossy region of 1 db would be realized. The reduction in optimum b would obviously be less for smaller values of loss.

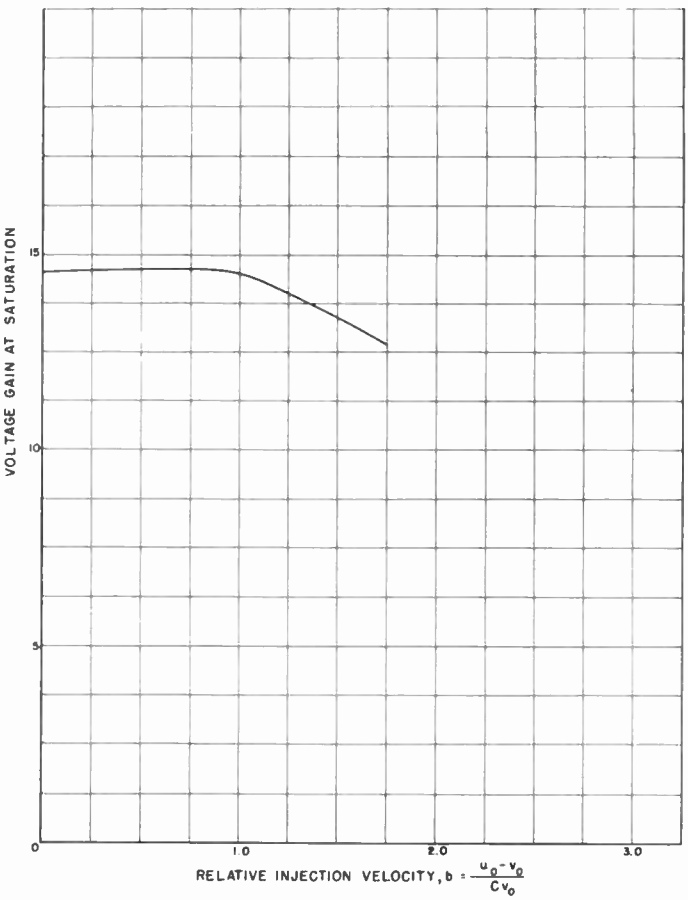

Fig. 22—Voltage gain at saturation vs relative injection velocity for fixed loss factor. $C=0.1$, $QC=0.125$, $A_0=0.0225$, $B=1$. $d=0$ for $0\leqq y\leqq 1.6$. $d=2$ for $y>1.6$.

Effect of Position of Loss for Fixed Loss Factor d and Fixed Injection Velocity b

In his development of the linear theory Pierce[8] found that the loss should be applied at least a distance corresponding to $CN_g=0.2$ from the input, since at that value of CN_g the signal on the helix is just beginning to increase. It should be noted that Pierce's curve is plotted for the special case $QC=b=0$.

In order to determine the effect of the placement of loss on a large-signal amplifier, the loss was introduced at $CN\cong 0.2$ and $CN\cong 0.4$ for the case $C=0.1$,

[8] J. R. Pierce, "Traveling Wave Tubes," D. Van Nostrand, New York, 1950.

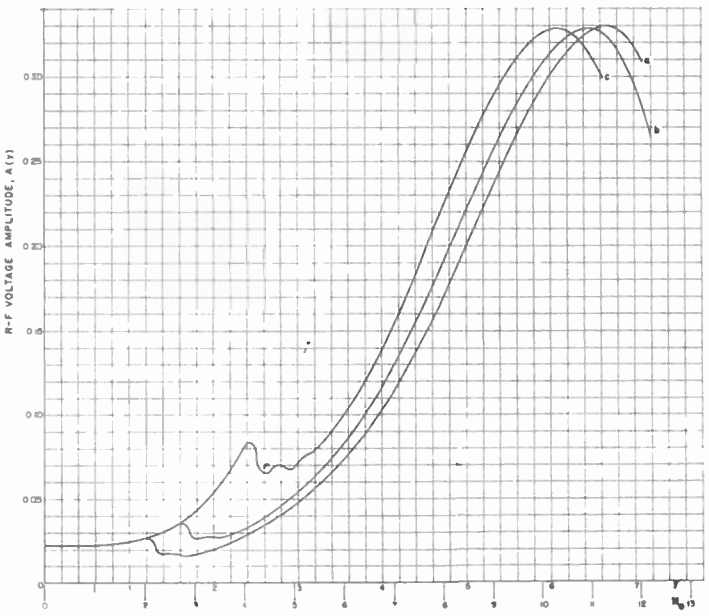

Fig. 23—Amplitude of the rf voltage along the helix for fixed loss with point of loss initiation as the parameter. $C=0.1$, $QC=0.125$, $A_0=0.0225$, $b=0.65$, $B=1$. *a*) $d=0$ for $0\leqq y\leqq 1.2$; $d=2.0$ for $y>1.2$. *b*) $d=0$ for $0\leqq y\leqq 1.6$; $d=2.0$ for $y>1.6$. *c*) $d=0$ for $0\leqq y\leqq 2.4$; $d=2.0$ for $y>2.4$.

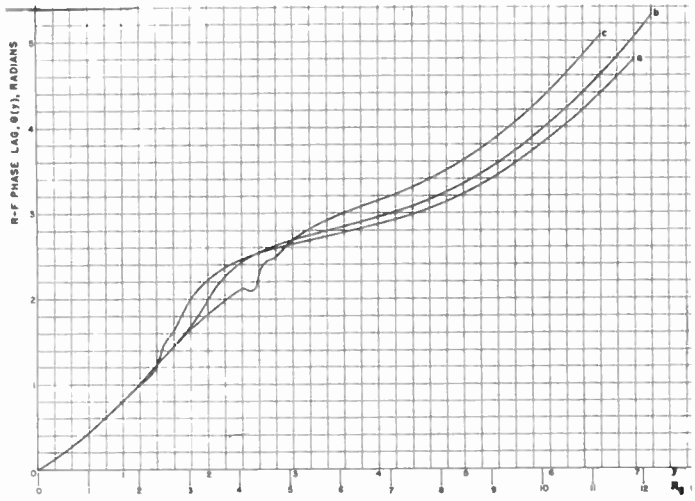

Fig. 24—RF phase lag of the wave relative to the electron stream for fixed loss with point of loss initiation as the parameter. $C=0.1$, $QC=0.125$, $A_0=0.0225$, $b=0.65$, $B=1$. *a*) $d=0$ for $0\leqq y\leqq 1.2$; $d=2.0$ for $y>1.2$. *b*) $d=0$ for $0\leqq y\leqq 1.6$; $d=2.0$ for $y>1.6$. *c*) $d=0$ for $0\leqq y\leqq 2.4$; $d=2.0$ for $y>2.4$.

$QC=0.125$, $b=1.5$, $B=1$, and $d=2.0$ (10.9 db/λ_q). A solution had already been obtained for these same conditions with the loss applied at $CN\cong 0.3$. The three solutions are presented for comparison in Figure 23 and Figure 24.

Conclusions

In the preceding sections of this paper, solutions of the large-signal traveling-wave amplifier equations have been presented for several values of the gain parameter C, the space-charge parameter QC, the loss factor d, the velocity parameter b, and the space-charge range parameter B. Solutions are also shown for variable input-signal level. From the graphs presented the following characteristics are notable:

1. The optimum relative injection velocity b increases with C for zero space charge ($QC=0$). Typically, for $C=0.1$ and $QC=0$ the optimum b is 2.0.
2. When $QC=0$ and $C=0.1$ the optimum b decreases with increasing QC up to $QC=0.25$, for which the optimum b is 1.25. However, as expected the optimum b increased with QC beyond that point and at $QC=0.50$ the b's for maximum small-signal gain and for maximum saturation gain were equal.
3. In the absence of space-charge forces, the saturation gain was found to increase, as in the linear theory, with increasing C for fixed tube length. For zero space charge the maximum saturation efficiency increases rapidly with C up to approximately $C=0.1$; beyond this value the increase in efficiency is slower.
4. The drop-out of each voltage-gain vs relative-injection-velocity curve is quite sharp, as in the small signal case, and the value of b at which this drop of the gain to a very small value occurs is approximately that value of b for which the small-signal gain goes to zero.
5. At $C=0.1$ the optimum tube length for QC between 0 and 0.25 is between 10 and 20 undisturbed wavelengths when A_0 is 30 db below CI_0V_0 and varies approximately linearly with A_0.
6. For small values of space charge and $C=0.1$, the saturation gain and efficiency both increase with increasing QC up to about $QC=0.125$ and then both decrease as QC increases further.
7. For a typical case, $C=0.1$, $QC=0.25$, and $B=1$, the saturation power output is approximately 5 db below the value predicted by the linear theory for the same input-signal level. The difference would be still greater for larger QC.
8. The presence of series loss along the helix has two important effects. First, the loss reduces the value of b for optimum gain, for example from 1.5 to 0.65 in the case of $d=2.0$ (10.9 db/λ_q) for $C=0.1$, $QC=0.125$, and $B=1$. Second, a series loss as high as $d=2.0$ reduces the saturation gain to 18.3 per cent of its value for $d=0$ where $C=0.1$, $QC=0.125$, $B=1$, and $b=1.5$.
9. The point at which loss is introduced at a distance of $CN\cong 0.2$, 0.3, or 0.4 from the input has little effect on the saturation gain for $C=0.1$, $QC=0.125$, $B=1$, and $b=0.65$.
10. The curves prepared from the computed large-signal traveling-wave amplifier data also shed a considerable amount of light on many other details of the high-level operation of the traveling-wave amplifier.

List of Symbols

A_0 the amplitude of the rf voltage initially impressed on the helix.
$A(y)$ the normalized amplitude of the rf voltage along the helix.
$A'(y)$ the first space derivative of the normalized rf voltage amplitude $A(y)$
a' mean helix radius, m.
$B=\beta b'$ space-charge range parameter, radians.
b $(u_0-v_0)/Cv_0$, the relative injection velocity.
b' electron stream radius, m.
C the gain parameter defined by $C^3=|\eta|Z_0I_0/2u_0^2$.
C_h the capacitance per section of the equivalent transmission line, farads/m.
d 0.01836 l/C, the loss factor.
G_s $A_{max.}(y)/A_0$, the saturation gain.
I_0 the dc stream current, amp.
L_h the inductance per section of the equivalent transmission line, henries/m.
l the series loss expressed in db per undisturbed wavelength along the helix.
N_q helix length measured in undisturbed wavelengths, λ_q.
QC $(1/4C^2)(\omega_q/\omega)^2/(1+\omega_q/\omega)^2$, small-signal space-charge parameter.
R plasma frequency-reduction factor.
u_0 $(2\eta V_0)^{1/2}$, the dc stream velocity, m/sec.
$V(y, \phi)$ rf voltage along the helix, volts.
v_0 $1/\sqrt{L_hC_h}$, the undisturbed phase velocity of the equivalent transmission line, m/sec.
y $C\omega z/u_0$, normalized distance along the tube.
Z_0 $\sqrt{L_h/C_h}$, the characteristic impedance of the lossless equivalent transmission line, ohms.
z distance measured along the tube, m.
β propagation constant of the rf wave on the helix, radians/m.
η q/m, the charge-to-mass ratio for the electron, coulombs/kg.
$\theta(y)$ the rf phase angle (or lag) of the wave on the helix relative to a hypothetical traveling wave whose phase velocity is the initial stream velocity u_0, radians.
$\theta'(y)$ first space derivative of the rf phase lag $\theta(y)$.
λ_q v_0/f, the undisturbed helix wavelength, meters.
ϕ the phase of the fundamental-frequency rf wave on the circuit relative to the phase of the wave at the input to the helix, radians.
ψ the input power level, to the helix, below CI_0V_0, db.
ω angular frequency of the wave impressed on the helix, radians/sec.
ω_p^2 $|\eta|\,|I_0|/\pi\epsilon b'^2u_0$, radian plasma frequency for an electron, radians/sec.
ω_q/ω $(\omega_p/\omega)R$, normalized effective plasma frequency.

Acknowledgment

The author wishes to express his appreciation to Professors W. G. Dow and Gunnar Hok of the Electrical Engineering Department at the University of Michigan, who devoted considerable time and offered valuable suggestions during the course of the work. The Mathematics Group at the Willow Run Research Center, in particular Messrs. R. T. Dames and L. Razgunas, rendered invaluable assistance in the programming and running of the problem on MIDAC. Appreciation is also due to Miss Priscilla L. Woodhead for her excellent work in preparing the figures.

The Polarguide—A Constant Resistance Waveguide Filter*

R. W. KLOPFENSTEIN†, senior member, ire, and J. EPSTEIN†, senior member, ire

Summary—**A new type of waveguide filter is described which utilizes circular waveguide components. Through the use of circular polarization a particularly compact structure has been achieved. The features of the filter include constant input resistance, high power handling ability, and high efficiency. Although intended primarily for use as a vestigial sideband filter in the uhf television frequency range, the new filter should find application throughout the frequency range in which waveguide techniques are applicable.**

* Original manuscript received by the IRE, June 17, 1955; revised manuscript received, August 12, 1955.
† RCA Laboratories' Division, Radio Corporation of America, Princeton, N. J.

Introduction

VESTIGIAL sideband filters are used in television broadcasting to prevent the radiation of spurious signals outside the assigned channel. Many currently used filters employ coaxial-line components to achieve the required transmission characteristic and as a consequence are limited in power handling ability. The object of the development described here was to design and construct a uhf vestigial sideband filter which would have constant input resistance, high power handling capacity, and high efficiency.

A design using waveguide components has been evolved which satisfies these requirements. The name "Polarguide Filter" will be used throughout this paper for this type of structure. A perspective sketch of the components of the system is shown in Fig. 1. A circular waveguide is excited with a linearly polarized wave (TE_{11}). This wave is then converted to a circularly polarized wave by means of a circular polarizing section.

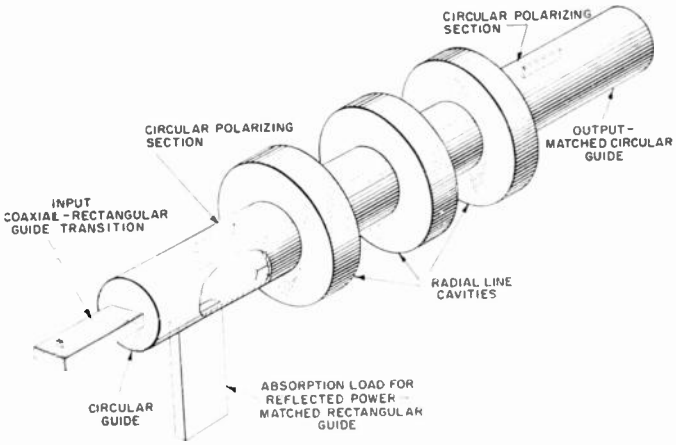

Fig. 1—Polarguide filter.

Required transmission characteristic is obtained by way of resonant radial line cavities. Cavities act electrically as series connected elements. Since load side of guide is matched, any reactance introduced by cavities reflects a certain amount of incident power. Reactance vs frequency characteristics of cavities are designed to obtain required transmission response of filter. Reflected energy passes through circular polarizing section again and is reconverted to a linearly polarized wave in space quadrature with input wave. This wave is completely absorbed by a terminated waveguide coupled to circular guide. Energy transmitted through cavities is passed through a second circular polarizing section which converts it to a linearly polarized wave having desired transmission characteristics.

A microwave model filter based on these principles has been built. The measured attenuation characteristic conforms to the FCC specification for a NTSC color television signal in all respects. The measurements also indicate that power efficiencies exceeding 95 per cent can be realized throughout the uhf television band.

Polarguide Filter can readily be adapted for operation as a filterplexer. Filterplexer performs function, combining picture and sound signals into a common load, as well as that of a vestigial sideband filter.

System Aspects of the Polarguide Filter

The bridge type of vestigial sideband filter and filterplexer with coaxial transmission line components has been used in vhf and uhf television practice for a number of years.[1] A line diagram of a coaxial transmission line type of bridge filter is given in Fig. 2(a). This may be thought of as a diagram showing connections to the inner conductor of coaxial line components.

The operation of the Polarguide Filter is directly analogous to that of the coaxial transmission line filter. The difference between the two types of filters resides in the types of components used and their physical arrangement. The Polarguide Filter has been developed for use in uhf television service and is capable of handling very large powers (on the order of 100 kilowatts nominal). One type of coaxial transmission line filter currently used in uhf television practice is rated for a nominal input power of 12.5 kilowatts. The Polarguide Filter has been developed with the exclusive use of waveguide components, and the physical arrangement is such that only a single cavity chain is required as opposed to the double cavity chain of the coaxial transmission line type of filter. This elimination of redundancy is possible because the function of the two identical transmission lines of Fig. 2(a) are served by decoupled orthogonal TE_{11} modes in a single circular waveguide.

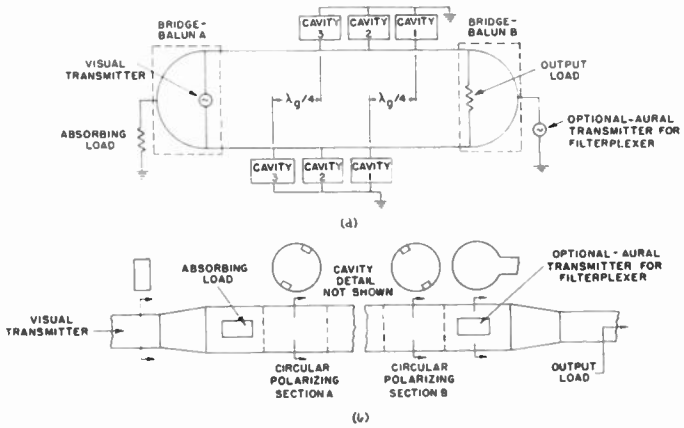

Fig. 2—Sketch showing comparison between coaxial transmission line filter and Polarguide Filter. (a) Coaxial line filter; (b) circular waveguide filter.

The function of the bridge-balun is performed simply by a section of circular waveguide with four outputs. Two of these outputs are brought out through transitions to rectangular waveguide while the other two feed directly into a continuation of the circular waveguide without transition. Referring to Fig. 2(b), the visual transmitter is fed into the circular waveguide from a rectangular waveguide through a tapered transition. This excites the TE_{11} dominant mode in the circular guide. The absorbing load is coupled through a side port in the circular waveguide to the orthogonal TE_{11} dominant mode. The two outputs, which are TE_{11} modes with polarization at an angle of 45° with respect to those just discussed, continue through circular waveguide to the filter section. The relations between the polarization vectors in the circular waveguide bridge-balun are shown in Fig. 3. The balance and decoupling in the circular waveguide bridge-balun are independent of frequency although the impedance match will gener-

[1] I. E. Goldstein and H. E. King, "Diplexers and the VHF filterplexer," *Broadcast News*, vol. 71, pp. 48–53; Sept.–Oct., 1952.

ally be frequency sensitive. Thus, a simple piece of circular waveguide forms a superior, broad-band bridge-balun with extremely high power handling ability. The output circuitry of the Polarguide Filter is exactly the same as the input circuitry.

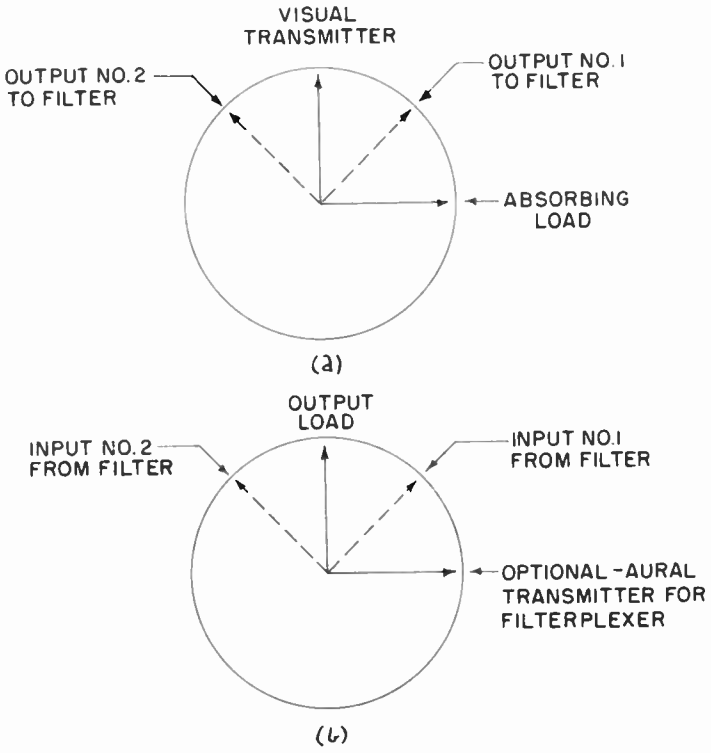

Fig. 3—Decoupled TE_{11} modes in circular waveguide as a bridge-balun. (a) Input bridge-balun A. (b) output bridge-balun B.

Before reaching the cavity section a differential in electrical length of 90° (or some odd multiple thereof) must be introduced between the two outputs of the bridge-balun section. This can be accomplished in a number of ways (dielectric slabs, lumped loading, etc.), but in this model of the Polarguide Filter the differential loading was accomplished through the introduction of metal fins in the plane of polarization of one of the modes. This takes place in the section marked "Circular Polarizing Section A" in Fig. 2(b). The output from this section consists of two equal magnitude modes in space and time quadrature when the output is matched.

After passing through the cavity section the circularly polarized wave is reconverted to a linearly polarized wave by a second circular polarizing section marked "Circular Polarizing Section B" in Fig. 2(b).

The cavities used in the Polarguide Filter are of the radial transmission line type excited by a rotating phase wave in a principal mode (mode which can be propagated at all frequencies). These cavities are series coupled to the circular waveguide through a circumferential gap and are tuned to be parallel resonant at a reject frequency below the lower band edge. Waveguide transformers perform the function of series resonating the individual transformer-cavity combinations at picture carrier frequency so that the entire cavity section is matched at this frequency. One of the advantages of the cavity structure used here is that practically all of the power dissipated in the filter is dissipated in exterior metal walls. Thus, forced cooling means can be readily applied if required.

The quantities of primary interest in connection with filters such as the Polarguide Filter are the variation of the input impedance with frequency and the transfer characteristic. This type of filter is inherently constant resistance input—a feature limited only by the impedance bandwidth of components such as the input transitions, absorbing load, and circular polarizing sections. It should be mentioned, however, that in order to obtain the constant resistance feature it is necessary that rotational symmetry be maintained rather closely in the cavity structure. A vernier adjustment of the electrical symmetry of the cavities can be provided through tuning probes suitably disposed in the individual cavities.

Although some work has been done to determine the number of cavities required to obtain certain symmetrical types of bandpass response functions,[2] there seems to be no general theory indicating the number of cavities necessary to obtain the dyssymmetrical response of interest here (see Fig. 6). Intuitively one would feel that the individual cavities should be highly reflecting at frequencies spaced throughout the reject band and that they should have very little attenuation and reflection at the picture carrier frequency. A certain amount of mathematical experimentation has indicated that the response curve required here can be achieved with three cavities of the type mentioned.

An equivalent circuit of the filter is shown in Fig. 4.

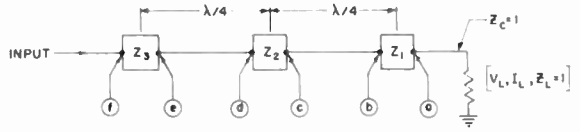

Fig. 4—A pseudo-equivalent circuit of the Polarguide vestigial sideband filter. Z_1, Z_2, and Z_3, are normalized cavity impedances.

The fraction of the *incident* power, in magnitude and phase, that reaches the ouput load gives the transfer characteristic of the filter. In Fig. 4 the transmission line characteristic impedance has been taken as unity for convenience. The filter characteristic can be determined through the usual transmission line equations and is given by

$$\frac{I_{out}}{I_{inc.}} = \frac{V_{out}}{V_{inc.}} = \frac{-2}{1 + (1 + Z_1)(1 + Z_2 + Z_2Z_3) + Z_3}, \quad (1)$$

[2] M. Dishal, "Concerning the minimum number of resonators and minimum unloaded Q needed in a filter," TRANS. IRE, vol. PGVC-3, June, 1953, pp. 85–117.

where the Z_n are the cavity impedances numbered consecutively from the output terminals of the filter to the input. It has been assumed that the spacing between the cavities is an odd multiple of guide quarter wavelengths and that this spacing does not change significantly over the frequency band of interest.

A typical calculated response curve is shown in Fig. 5. The choice of 15,000 for the cavity Q's corresponds to a conservative estimate of the practical Q realizable with cavities of the radial transmission line type at Channel 72 of the uhf television band.

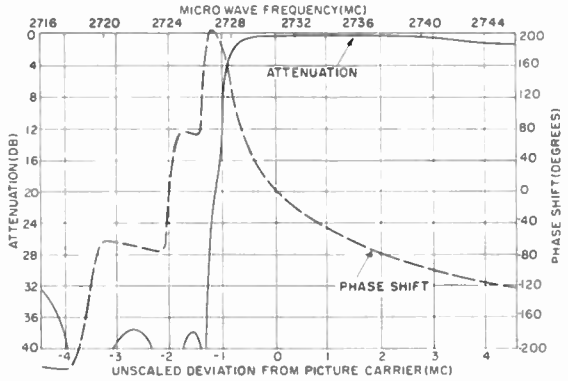

Fig. 5—Calculated amplitude and phase response of Polarguide vestigial sideband Filter for cavity $Q = 15{,}000$.

In order to obtain an estimate of the extent to which the nonlinearity of the phase characteristic of Fig. 5 could be eliminated by improved design, an idealized attenuation characteristic was assumed and the phase shift associated with the corresponding minimum phase shift network was computed.[3] This is shown in Fig. 6.

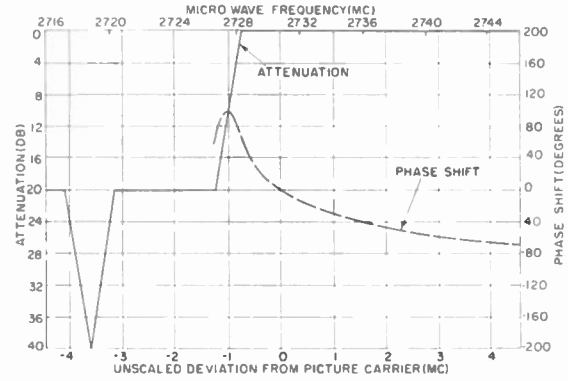

Fig. 6—Minimum phase shift response for idealized amplitude response of vestigial sideband filter.

It is seen that the idealized attenuation characteristic leads to some improvement in linearity of the phase characteristic but not enough to justify much additional complication of filter design. However, some improvement might be expected if design parameters were altered to allow wing response in Fig. 5 to come up to about 20 db instead of 32 db maximum obtained there.

[3] D. E. Thomas, "Tables of phase associated with a semi-infinite unit slope of attentuation," *Bell Sys. Tech. Jour.*, vol. 26, pp. 882–885; October, 1947.

A microwave model of the Polarguide vestigial sideband filter has been constructed and tested. The filter simulated was intended for operation at Channel 72 of the uhf television broadcast band (818–824 mc) and a three-tenths wavelength scale (ten-thirds frequency scale) was applied for purposes of the microwave model construction.

Fig. 7 shows a photograph of the completely assembled microwave model of the filter with the associated measuring equipment used in determining its characteristics. At the far left of the assembly is a tapered symmetrical waveguide load. This load required no special tunable matching means and introduced a mismatch of less than 0.2 db on uniform circular waveguide over the frequency band used. Near the input of the load is shown a tunable voltage pickup probe which was used with a crystal detector to measure the output of the filter when under test. Then proceeding from left to right are shown first a short section of guide which contains a septum, the output circular polarizing section, the cavity section, and the input circular polarizing section. The vertical section of rectangular waveguide contains a load which was used as the absorbing load in the filter. This load was coupled to the circular waveguide through a side port in the circular guide and was matched by three tuning probes which are just visible on the far side of the load. A tapered transition from rectangular to circular waveguide was inserted between the absorbing load and the measuring section which was a section of slotted rectangular waveguide. The tapered transition was tuned by means of three tuning probes which are shown in the photograph.

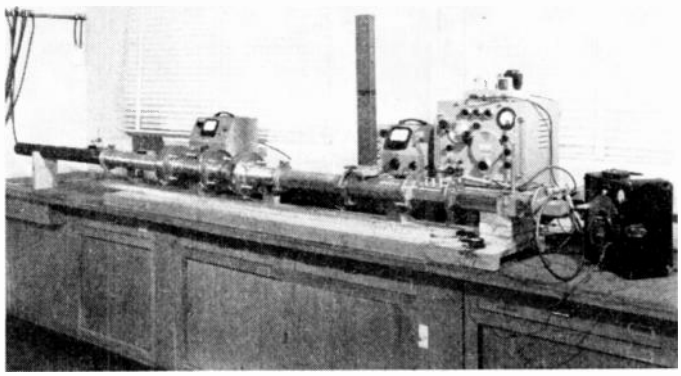

Fig. 7—Completely assembled microwave model of Polarguide vestigial sideband Filter.

Fig. 8 shows the attenuation of the filter plotted vs frequency over the band of frequencies of interest. It will be observed that this characteristic satisfies the requirements for the transmission of an NTSC color television signal in all respects. The phase characteristic of the filter was not determined experimentally since it was felt that preliminary calculations were adequate

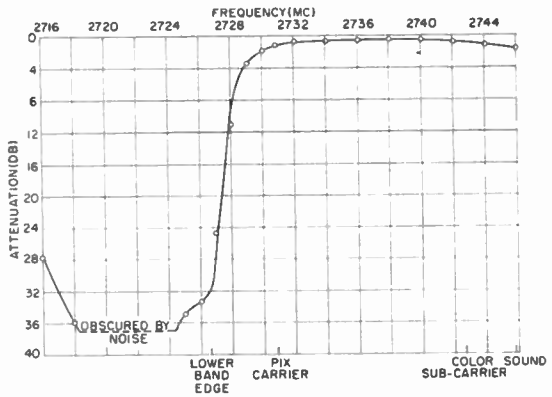

Fig. 8—Measured response for microwave model of Polarguide vestigial sideband Filter.

to determine the acceptability of filter performance in this respect.

A plot of the input voltage standing wave ratio (V_{min}/V_{max}) of the filter is shown in Fig. 9. As is shown, the vswr exceeds 0.9 throughout the pass band, and is not lower than 0.85 throughout the reject band. This illustrates the constant resistance input characteristic which is inherent in filters of this type.

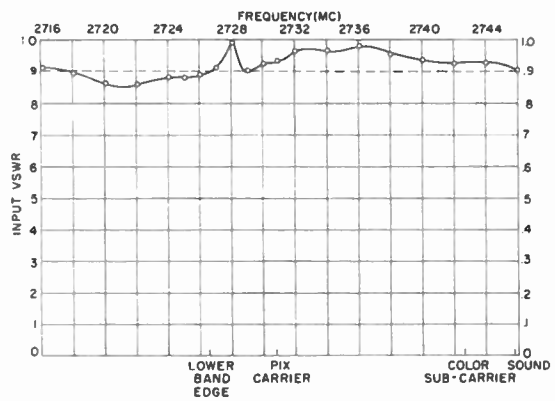

Fig. 9—Measured input voltage standing wave ratio of microwave model of Polarguide vestigial sideband Filter.

Circular Polarizing Sections

The general theory of the operation of circular polarizing sections, and, in particular, that of metal fin circular polarizing sections, has been previously described in the literature.[4] Of the many available types of circular polarizers in circular waveguide, the metal fin type was thought best adapted to this problem due to its power handling ability and broad bandwidth characteristics.

The operation of the metal fin type of circular polarizing section depends upon the fact that a metal fin introduced into a circular waveguide produces a different change in phase velocity for a wave polarized in the direction of the fins than it does for a wave polarized in the perpendicular direction. For a thick fin some change is introduced for both polarizations, but the change is in opposite directions so that the differential in phase delay is larger than the phase delay of either of the polarizations separately. Fig. 10 shows the experimentally determined change in cutoff frequency for the two TE_{11} mode polarizations in a fin loaded circular waveguide for various fin dimensions. The differential phase delay for a given section of fin loaded waveguide can be calculated directly from this data.

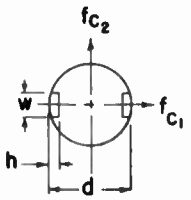

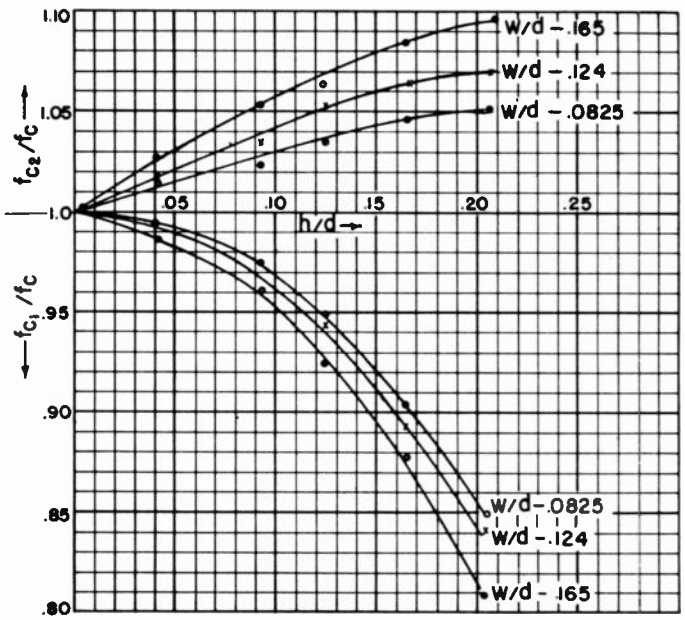

Fig. 10—The dependence of the ratio of the cutoff frequencies of mode I and mode II to the cutoff frequency of the unperturbed guide as a function of the fin dimensions.

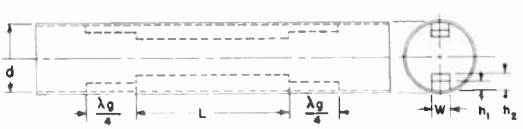

Fig. 11—Circular polarizing section used in Polarguide Filter.

A cross section drawing of a typical circular polarizing section is shown in Fig. 11. The two quarter-wavelength stepped sections are for the purpose of impedance matching. The step height of the matching sections is determined experimentally, and so long as the fins are not too thick, the same step will produce an impedance match for both mode polarizations. A photograph of the circular polarizing section used in the microwave model is shown in Fig. 12.

[4] A. G. Fox, "An adjustable wave-guide phase changer," Proc. IRE, vol. 35, pp. 1489–1498; December, 1947.

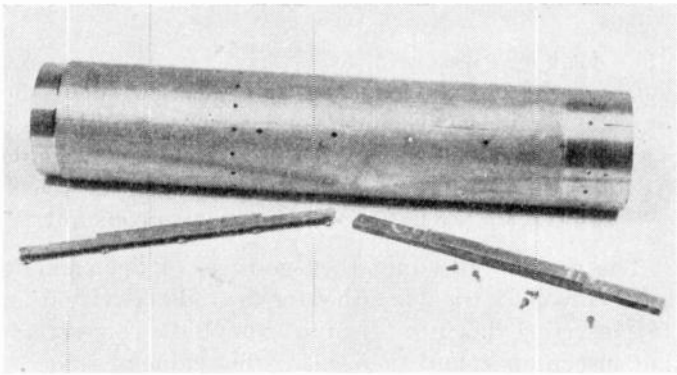

Fig. 12—A disassembled view of the circular polarizer.

It should be mentioned that the total differential phase delay of a fin type circular polarizing section is not quite equal to the sum of the phase delays introduced by the stepped sections and the central fin section. This is due to the fact that additional phase delays are introduced by the discontinuity susceptances at the steps. Therefore, the initial design will have to be modified slightly by reducing the length of the central section. The proper correction is readily determined by a single experimental measurement of the phase delay through the polarizer as initially designed.

A figure of merit which may be used to evaluate the performance of a circular polarizer is the circularity bandwidth. This is the band of frequencies over which the circularity ratio stays within prescribed limits. Under the assumptions that the fin sections introduce no reflections in the band of interest and that the arithmetic mean of the cutoff frequencies of the two orthogonal modes is equal to the cutoff frequency of the unperturbed guide, it can be shown that the circularity bandwidth is independent of fin dimensions as such and depends only on the phase velocity in the unperturbed guide.

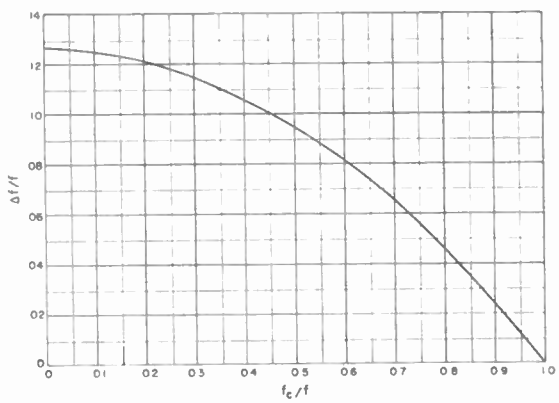

Fig. 13—Bandwidth versus f_c/f for circularity ratio of $0.9<R<1.1$.

Fig. 13 shows the bandwidth within which the circularity stays within ten per cent of unity as a function of the ratio of the cutoff frequency of the unperturbed circular guide to the operating frequency. For the present application, the cutoff frequency of the guide was 85 per cent of the operating frequency so that the circularity remained within 10 per cent of unity over a 3.5 per cent band.

Radial Transmission Line Cavities

A large variety of cavity structures are suitable for use with filters of the Polarguide type. In particular, any cavity whose structure is invariant with respect to rotations relative to the waveguide axis of multiples of 90 degrees is suitable. This requirement is dictated by the consideration that any filter element must have the same characteristics for the two orthogonal modes present in the circular waveguide.

The radial transmission line type of cavity was used here because it satisfies the symmetry requirement, has a relatively high volume to surface ratio (and, hence, high Q potentiality), and because such cavities can be readily designed from available theory.[5]

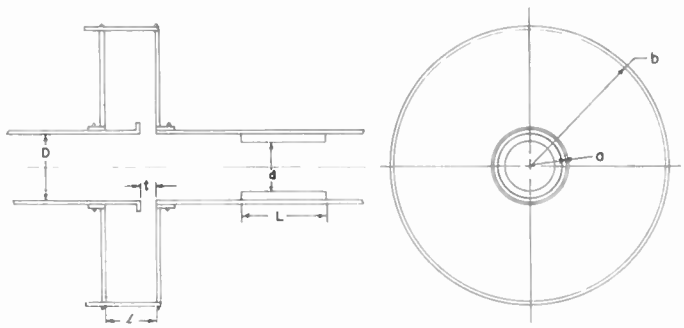

Fig. 14—Typical filter element including radial transmission line cavity with capacity lip and high impedance waveguide transformer.

A sketch of a typical filter element cross section is shown in Fig. 14. The capacity lip serves to resonate the cavity at the desired parallel resonant frequency while the waveguide transformer series resonates the entire structure at picture carrier frequency. Fig. 15 shows an open wire transmission line model of the filter element while a lumped circuit element model is shown in Fig. 16. The pertinent design parameters are shown on these last two figures, and the design of the cavity structure will consist of determining the corresponding quantities for the radial transmission line cavity.

The normalized input susceptance of the cavity is given by[5]

$$B/Y_0 = -1.3778\,\frac{a\lambda_g}{l\lambda}\,\frac{G_2(ka)}{G_1(ka)}\,\frac{\cos\left[\theta(kb)-\psi(ka)\right]}{\sin\left[\theta(kb)-\theta(ka)\right]}, \quad (2)$$

where the notation of reference 5 has been used. λ_g is the guide wavelength on the circular waveguide, and G_1, G_2, θ, and ψ are related to the first kind of Hankel function and its derivative:

[5] R. W. Klopfenstein, "Circular polarization in waveguides and cavities," *RCA Rev.*, vol. 15, pp. 291–311; September, 1954.

$$G_1(x) = \sqrt{J_1^2(x) + N_1^2(x)} = \left| H_1^{(1)}(x) \right|,$$
$$\theta(x) = \arctan \left[N_1(x)/J_1(x) \right] = \operatorname{Arg} H_1^{(1)}(x),$$
$$G_2(x) = \sqrt{J_1'^2(x) + N_1'^2(x)} = \left| H_1^{(1)\prime}(x) \right|,$$

and

$$\psi(x) = \arctan \left[-J_1'(x)/N_1'(x) \right] = \operatorname{Arg} - jH_1^{(1)\prime}(x). \quad (3)$$

These functions are directly tabulated in available tables.[6]

In the present application it was desired to design the radial cavities to have a specified susceptance slope at a given frequency. That is, regarding all the parameters as fixed except the outer radius b of the cavity, it was desired to determine this radius so that the cavity had a specified susceptance slope. While it would be possible to do this directly from (2), the resulting differentiated expression is quite intractable numerically.

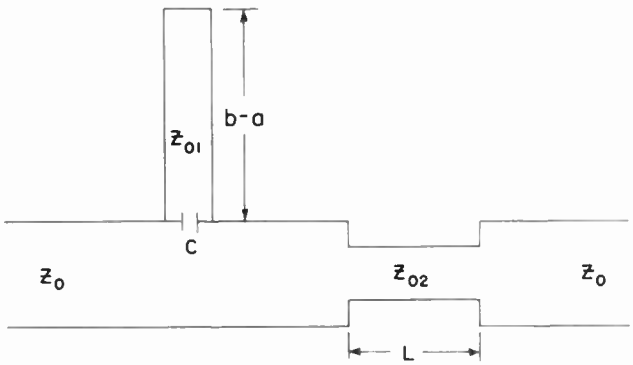

$$f_p = \frac{1}{2\pi C \bar{z}_{01} \tan K(b-a)}$$

$$S = \frac{dB}{df} \simeq \frac{K(b-a)}{f_p}\left(\frac{\bar{z}_0}{\bar{z}_{01}}\right)\csc^2 K(b-a)$$

NORMALIZED MHOS/MEG.

$$f_s \simeq f_p + \frac{1}{S\left(\frac{\bar{z}_{02}}{\bar{z}_0} - \frac{\bar{z}_0}{\bar{z}_{02}}\right)\sin KL}$$

Fig. 15—Open wire transmission line model of typical filter element.

An alternative procedure results through the introduction of asymptotic forms for the Hankel functions in (2). It is then found that

$$B/Y_0 = -1.3778 \frac{a\lambda_g}{l\lambda} \cot \phi, \quad (4)$$

and

$$s = d(B/Y_0)/df$$
$$= \frac{2.5347}{(kl)f_c}(\lambda_g/\lambda)\phi \csc^2 \phi\left[1 + (\lambda_g/\lambda_c)^2(\sin 2\phi/2\phi)\right], \quad (5)$$

[6] Mathematical Tables Project and MIT Underwater Sound Laboratory, Scattering and Radiation from Circular Cylinders and Spheres, Tables of Amplitude and Phase Angle. Published by U.S. Navy Dept., Office of Research and Inventions, July, 1946.

where

$\phi \cong k(b-a)$,
f_c, λ_c = the cutoff frequency and wavelength of the circular waveguide,
λ_g = the guide wavelength in the circular waveguide
λ = the free space wavelength, and
$k = 2\pi/\lambda$ = the free space propagation constant.

The design procedure then consists of determining an effective electrical length ϕ for the radial cavity from (5), inserting this into (4) to determine the corresponding susceptance, and then, using this value of susceptance, entering (2) to obtain the outer cavity radius b.

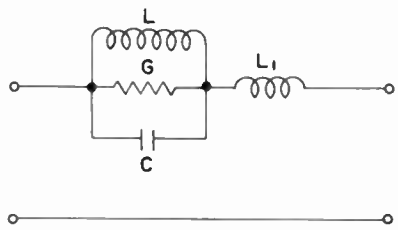

$$f_p = \frac{1}{2\pi\sqrt{LC}}$$

$$S = \frac{dB}{df} \simeq 4\pi C \times 10^6 \quad \text{MHOS/MEGACYCLE}$$

$$Q = \frac{Sf_p}{2G}$$

$$f_s \simeq f_p + \frac{\sqrt{LC}}{SL_1}$$

Fig. 16—Lumped circuit element model of typical filter element.

This procedure is quite accurate, and involves only the assumption that the susceptance slope corresponding to a given susceptance is the same for a radial transmission line as for the corresponding uniform transmission line.

The Q of the radial transmission line cavity can be obtained by integrating the power losses on the side walls and cylindrical terminating walls. It is convenient to do this by introducing asymptotic forms in the Bessel function expressions for the electromagnetic fields.[6] When this is done it is found that

$$Q = \frac{60\pi}{\rho} \frac{A\phi}{1 + \frac{A(1 + \cos^2 \phi)}{1 + (\sin 2\phi/2\phi)}}, \quad (6)$$

where A is a shape factor of the cavity equal to $l/(b-a)$, and ρ is the surface resistivity of the metal from which the cavity is constructed in ohms per square.

An assumption implicit in all of the results given above is that only the principal mode is propagated in the radial transmission line. This can be insured by keeping the dimension l below one-half wavelength. This is, in fact, the consideration which serves to limit the Q attainable with a cavity of this type.

The circular waveguide transformer shown in Fig. 14 is used to series resonate the entire structure at a frequency slightly above the parallel resonant frequency of the radial-cavity capacity-lip combination. Although other tuning means such as irises and probes would be equally satisfactory for this purpose, the waveguide transformer was chosen because of its high power handling capabilities and because it has the required symmetry of structure.

Three cavities of the radial transmission line type were used in the model constructed of the Polarguide vestigial sideband filter. The microwave cavities were constructed as a series load on circular waveguide having an inner diameter of 3.000 inches and an outer diameter of 3.250 inches. The main circular waveguide including the capacity ring and its supporting cylinder was constructed of brass while the side plates and outer shorting cylinder of the radial transmission line cavity were constructed of copper. The outer shorting cylinder consisted of two lengths of copper strap secured to the side plates by means of hose clamps. The side plates were secured to the main waveguide by means of hose clamps and slotted bushings.

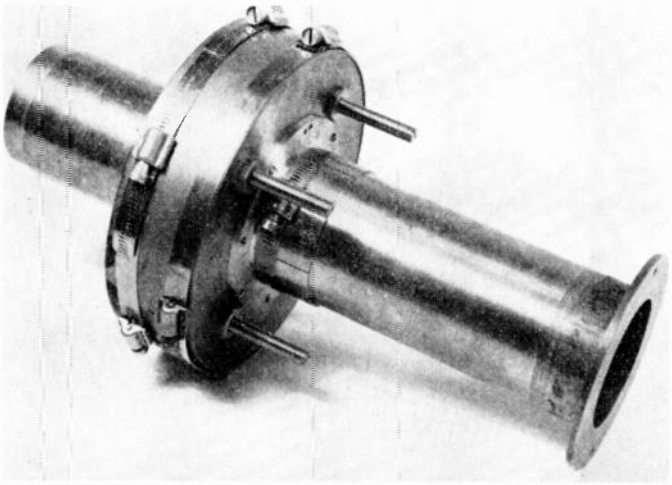

Fig. 17—Typical assembled cavity.

A photograph of a typical assembled cavity is shown in Fig. 17. In Fig. 18 a photograph of the same cavity disassembled to show its components is given. The parts shown in Fig. 18 fit together as shown from left to right. The aluminum cylinder to the right of the photograph is the high-impedance waveguide transformer. Its outer surface has been knurled so that it forms a sliding friction fit when inserted in the circular waveguide. The capacity lip was brazed to the circular guide before machining.

The four 5/16-inch diameter brass probes shown in Figs. 17 and 18 provide a vernier adjustment which compensates for small dissymmetries arising from unavoidable lack of mechanical precision. If this symmetry is not maintained reflected energy from the cavity will be elliptically polarized, and the input of the filter will become mismatched. The degree of such mismatch will be largest when the cavity is highly reflecting, i.e., at the parallel resonant frequency of the cavity.

The probes are located equiangularly around the cavity and spaced radially one quarter-wavelength from the outer short circuiting cylinder. They, thus, have maximum effect being located approximately at a voltage maximum. With the probes used it was possible to maintain a high degree of electrical symmetry over the band of frequencies of interest. The probe penetration should be small in order to retain a high Q figure for the cavity, however, so that the availability of probe correction does not entirely remove the problem of mechanical precision in obtaining constructional symmetry. It does alleviate this problem considerably though, and as seen from Fig. 18 the probe correction required in a cavity of reasonably precise construction is quite small.

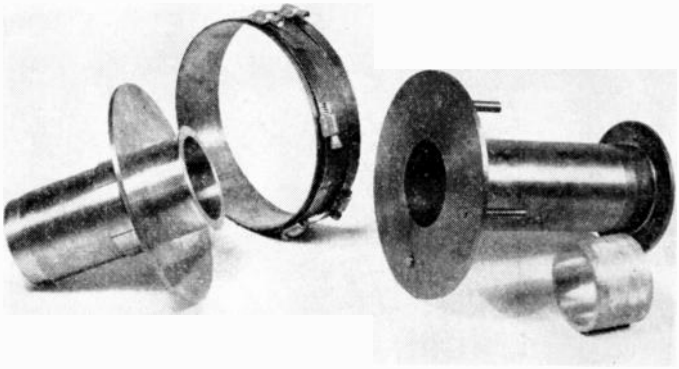

Fig. 18—A typical cavity disassembled to show its component parts.

An experimentally determined impedance characteristic of one of the model cavities is shown in the Smith chart of Fig. 19. It is compared with the corresponding impedance characteristic calculated for the lumped circuit element model of the cavity shown in Fig. 16, and it is seen that a rather close comparison is obtained.

Conclusions

The application of waveguide principles has led to the development of a new type of constant-input-resistance filter. The development of this filter was motivated primarily by the need for a filter with the ability to handle high continuous powers in uhf television broadcasting. The filter should prove useful throughout the frequency range in which waveguide techniques are applicable, however.

Through the use of circular polarization in circular waveguide transmitting dominant mode a particularly compact structure has been achieved. Cavities of the radial transmission line type have been developed for use with this filter.

A microwave model of a vestigial sideband filter was constructed and tested. The performance of this model was satisfactory in all respects. Conservative estimates

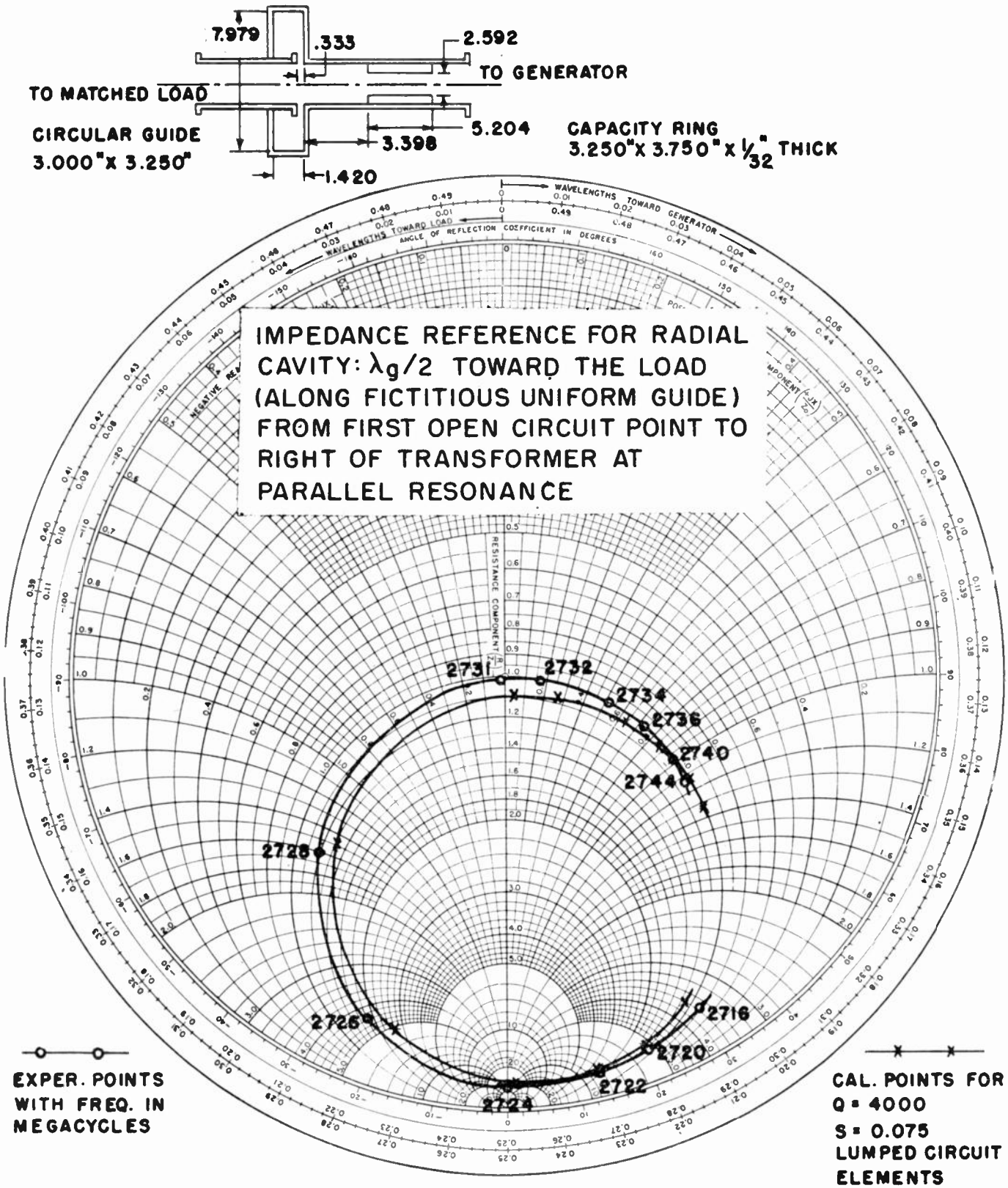

Fig. 19—Impedance plot for typical cavity used in the microwave model of the Polarguide vestigial sideband Filter.

indicate that a nominal input power on the order of 100 kilowatts can be handled without excessive heating or voltage breakdown throughout the uhf television frequency range. It is estimated that picture-carrier efficiencies exceeding 95 per cent will be readily achievable with the radial transmission line type of cavity.

Acknowledgment

The authors would like to express their sincere appreciation to O. M. Woodward who provided the data on which the design of the circular polarizers was based as well as contributing many useful ideas in regard to other aspects of the filter development.

Frequency Stability of Point-Contact Transistor Oscillators*

C. C. CHENG†, ASSOCIATE, IRE

Summary—**Frequency-stability properties of oscillators using point-contact transistors are investigated both analytically and experimentally. Point-contact-transistor "two-terminal" oscillators are analyzed by means of nonlinear differential equations of the Van der Pol type. Duality relationship is demonstrated between oscillators using the voltage-controlled, negative-impedance, base-input characteristics and oscillators using the current-controlled, negative-impedance, emitter-input or collector-input characteristics. As a result, the general stability criteria derived for the former can be applied directly to the latter. Stabilization techniques are derived according to theoretical analysis. Experimental results confirming the theoretical findings are also included.**

Introduction

ALTHOUGH available literature on transistor-circuit analysis contains much information on linear circuit problems, the field of nonlinear transistor circuits has not been explored to any great extent. In many cases, nonlinear transistor circuits have been treated as linear problems by the use of the "sectionalized" method. This simplified method of linearization is often very convenient, and useful results are frequently obtained for applications such as switching circuits. The sectionalized method, however, fails to solve problems of a more complex nature, such as the frequency-stability problems of nonlinear transistor oscillators.

This paper describes a method of solving more complex transistor-circuit problems by the use of nonlinear-circuit theory. The paper also describes the frequency-stability criteria for point-contact transistor oscillators. These oscillators are treated as "two-terminal" devices having negative-impedance characteristics. The input characteristic of a point-contact transistor is "shaped" so that simple nonlinear differential equations of oscillation can be derived and oscillator-frequency stability is improved. Solution of the differential equations leads to frequency-stability criteria for the oscillators.

Input Characteristic of Point-Contact Transistors

An important feature of point-contact transistors is their negative-impedance input characteristics. Fig. 1(a) shows a typical circuit used for analysis of the base-input characteristics, which are shown in Fig. 1(b). The *S*-shaped base-input curve represents a voltage-controlled negative-impedance characteristic. This input characteristic can be "sectionalized" and "linearized," as shown in Fig. 1(c). Similar data for *N*-shaped, current-controlled, negative impedance emitter-input and collector-input characteristics are shown in Figs. 2 and 3.

* Original manuscript received by the IRE, August 15, 1955.
† Formerly with RCA Tube Division, Harrison, N. J.

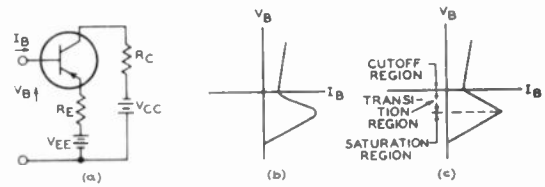

Fig. 1—Typical circuit (a) used for analysis of base-input characteristic, (b) of point-contact transistor. "Linearized" characteristic is shown in (c).

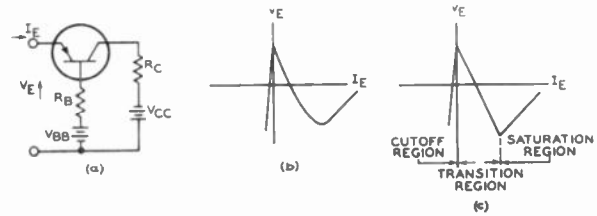

Fig. 2—Typical circuit (a) used for analysis of emitter-input characteristic, (b) of point-contact transistor. "Linearized" characteristic is shown in (c).

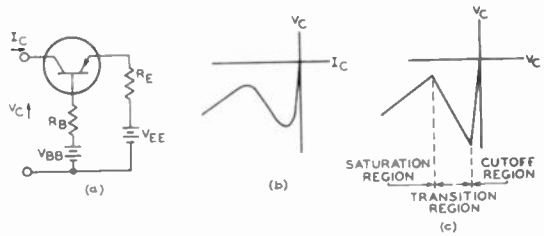

Fig. 3—Typical circuit (a) used for analysis of collector-input characteristic, (b) of point-contact transistor. "Linearized" characteristic is shown in (c).

Circuits using these negative-impedance input characteristics may be analyzed by treatment of each region as a separate linear circuit. This "sectionalized" method has often been used for analysis of switching circuits using point-contact transistors.[1,2] Because point-contact transistor oscillators depend on transition-region characteristics, this method fails to predict the performance and another method of evaluation is required.

Modification of Input Characteristics

The input characteristics of a point-contact transistor may be represented mathematically by a power series:

$$i = a_0 + a_1 v + a_2 v^2 + \cdots + a_n v^n \qquad (1)$$

(voltage controlled)

or

$$v = b_0 + b_1 i + b_2 i^2 + \cdots + b_n i^n. \qquad (2)$$

(current controlled)

[1] R. L. Trent, "Idealized Negative Resistance Characteristics of the Transistor," *The Transistor—Selected Reference Material on Characteristics and Applications*, Bell Telephone Labs., Inc.; 1951.

[2] A. W. Lo, "Transistor trigger circuits," PROC. IRE, vol. 40, pp. 1531–1541; November, 1952.

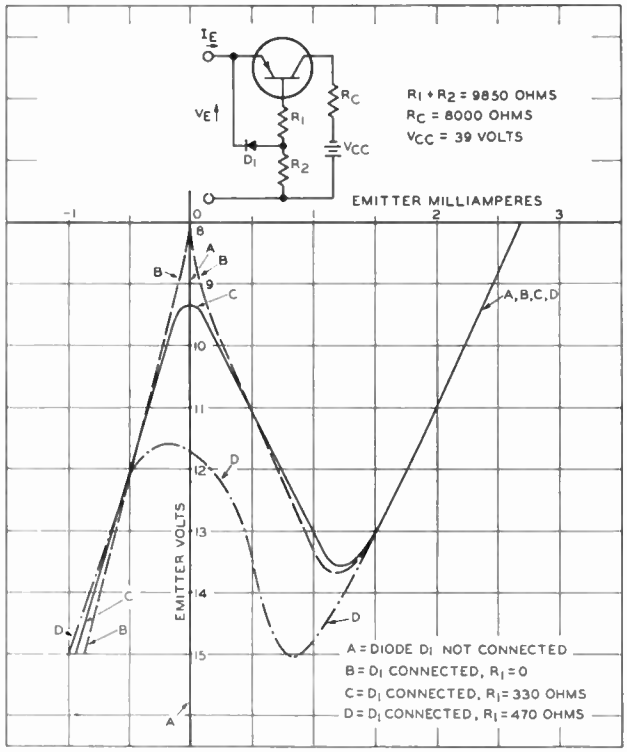

Fig. 4—"Shaping" of emitter-input characteristic by adjustment of circuit components.

However, the analysis of oscillators using the input characteristics represented by (1) and (2) is very complicated. Nonlinear-circuit theory[3–5] indicates that the analysis of oscillators can be simplified by the use of simple input characteristics, such as

$$i = a_1 v + a_3 v^3, \qquad a_1 < 0 \tag{3}$$

or

$$v = b_1 i + b_3 i^3, \qquad b_1 < 0. \tag{4}$$

These characteristics can be obtained from (3) and (4) by deletion of even-power terms and terms including powers greater than 3. Oscillators using the "shaped" input characteristics represented by (3) and (4) also contain fewer harmonics, especially even harmonics, and have better frequency-stability performance then oscillators using the original input characteristics represented by (1) and (2). (The interdependence of frequency drift and harmonic content of an oscillator has been treated previously.[6–9])

[3] B. Van der Pol, "The nonlinear theory of electric oscillators," PROC. IRE, vol. 22, pp. 1051–1086; September, 1934.
[4] J. J. Stoker, "Nonlinear Vibrations in Mechanical and Electrical Systems," Interscience Publishers, Inc., New York, N. Y.; 1950.
[5] N. W. McLachlan, "Ordinary Non-linear Differential Equations in Engineering and Physical Science," Oxford University Press, New York, N. Y.; 1950.
[6] D. C. dePackh, "The first order behavior of separable oscillators," *Trans. AIEE*, vol. 72, part I, pp. 450–455; September, 1953.
[7] J. Groszkowski, "The interdependence of frequency variation and harmonic content, and the problem of constant-frequency oscillators," PROC. IRE, vol. 21, pp. 958–981; July, 1933.
[8] H. A. Thomas, "Theory & Design of Valve Oscillators," Chapman & Hall Ltd., London, Eng.; 1951.
[9] W. A. Edson, "Vacuum Tube Oscillators," John Wiley & Sons, Inc.; 1953.

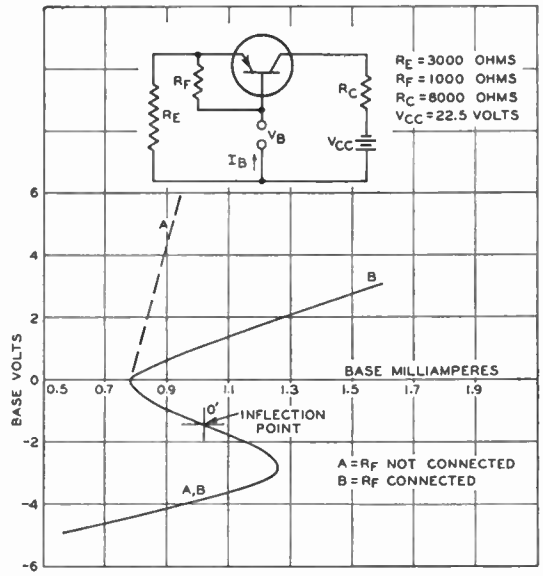

Fig. 5—"Shaping" of base-input characteristic by addition of feedback resistor, R_F, in circuit.

The emitter-input characteristic of a point-contact transistor can be "shaped" to the form represented by (4) by the addition of a diode, D_1, between the emitter and the node between two base resistors, R_1 and R_2, as shown in Fig. 4. Adjustment of the values of R_1 and R_2 shapes the emitter-input characteristic into the desired skew-symmetrical form. The base-input characteristic can be shaped into the desired form by the addition of a feedback resistor, R_F, of appropriate value between the base and the emitter, as shown in Fig. 5.

The curves shown in Fig. 5 are expanded and redrawn in Fig. 6 with the origin shifted to the inflection point of the input characteristic, O'. The shifted input characteristic, B, in Fig. 6 can be represented by the simple power series given in (3), where the constant a_1 is equal to the slope of curve B at the new origin

$$a_1 = \left.\frac{\partial i}{\partial v}\right|_{v \to 0} = \frac{-1}{3.65 \times 10^3} \text{ mho},$$

and the value of the constant a_3 is obtained from either of the following conditions:

$$\text{at} \quad i = 0, \qquad v = v_m, \qquad a_3 = \frac{-a_1}{v_m^2}$$

$$\text{at} \quad \frac{\partial i}{\partial v} = 0, \qquad v = v_0, \qquad a_3 = \frac{-a_1}{3v_0^2}$$

$$\left(a_3 = \frac{1}{20.2 \times 10^3} \text{mho/volt}^2\right).$$

The equation for curve B, therefore, is given by

$$i = \frac{-1}{3.65 \times 10^3} v + \frac{1}{20.2 \times 10^3} v^3. \tag{3a}$$

Eq. (3a) is plotted as curve C in Fig. 6. Because this curve is a good approximation of curve B, (3a) can be used to represent curve B for analysis.

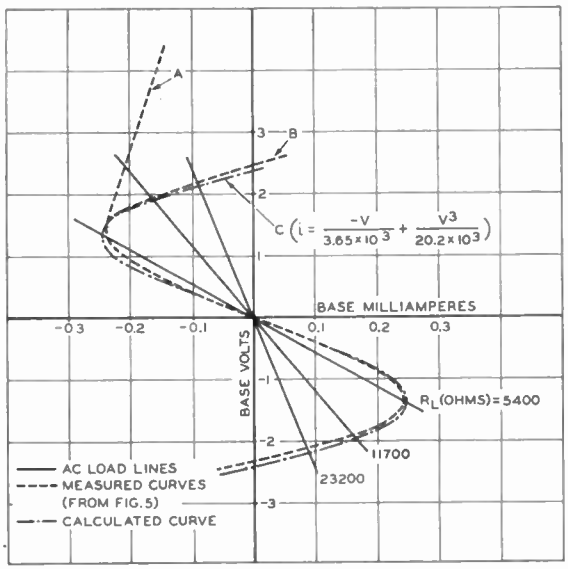

Fig. 6—Mathematical representation of "shaped" base-input characteristic.

Analysis for Oscillator Using Voltage-Controlled Input Characteristics

The oscillator shown in Fig. 7, which contains a parallel resonant circuit in the base circuit, has a shaped input characteristic which may be represented by (3). The input current, i, is given by

$$i = -[i_R + i_L + i_C] = -\left[\frac{v}{R} + \frac{1}{L}\int v\,dt + C\frac{dv}{dt}\right]. \quad (5)$$

When (3) and (5) are combined, the following expression is obtained:

$$C\frac{dv}{dt} + \left[\frac{1}{R} + a_1 + a_3v^2\right]v + \frac{1}{L}\int v\,dt = 0. \quad (6a)$$

This expression may be differentiated, as follows:

$$\frac{d^2v}{dt^2} + \frac{1}{C}\left[\frac{1}{R} + a_1 + 3a_3v^2\right]\frac{dv}{dt} + \frac{v}{LC} = 0. \quad (6b)$$

Eq. (6b) is the conventional nonlinear differential equation of oscillation.[3–5]

If the value of the quantity

$$-\sqrt{\frac{L}{C}}\left(\frac{1}{R} + a_1\right)$$

is small, the solution of (6b) for the sinusoidal oscillatory voltage v is as follows:

$$v = 2\sqrt{\frac{-(a_1 + 1/R)}{3a_3}}\sin\left[1 - \frac{L}{16C}\left(a_1 + \frac{1}{R}\right)^2\right]\frac{t}{\sqrt{LC}}$$
$$= A\sin[1-\delta]\omega_0 t$$
$$= A\sin\omega t, \quad (7)$$

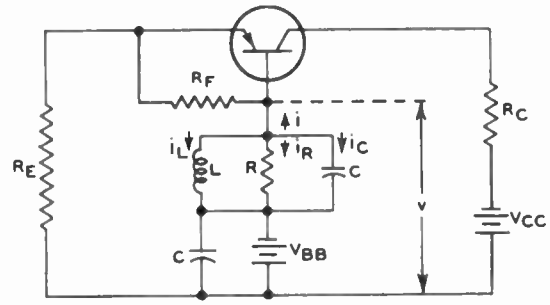

Fig. 7—Transistor oscillator containing parallel resonant circuit in base circuit and using voltage-controlled input characteristics.

where

$A = 2\sqrt{\frac{-(a_1 + 1/R)}{3a_3}}$ = the amplitude of the oscillatory voltage,

$\omega_0 = \frac{1}{\sqrt{LC}}$ = the natural angular frequency of the tank circuit,

ω = the angular oscillating frequency. (8)

The difference between the angular frequency of oscillation and the natural angular frequency of the tank circuit, $\omega - \omega_0$, is equal to $-\delta\omega_0$, where

$$\delta\omega_0 = \frac{L}{16C}\left[a_1 + \frac{1}{R}\right]^2\frac{1}{\sqrt{LC}}. \quad (9)$$

Eq. (7) indicates that the frequency of oscillation depends not only on the external circuit elements, L, C, and R, but also on the slope of the input characteristics at the operating point, a_1, which represents the negative conductance of the transistor. If the value of a_1 varies and the external circuit elements are constant, then the frequency drift is determined as follows:

$$\frac{\partial\omega}{\partial a_1} = -\omega_0\frac{\partial\delta}{\partial a_1} = -\frac{1}{8C}\sqrt{\frac{L}{C}}\left(a_1 + \frac{1}{R}\right). \quad (10)$$

Eq. (10) shows that the rate of change of oscillator frequency also depends on the external elements, L, C, R, and the negative conductance a_1.

The ratio $\partial\omega/\partial a_1$ should be minimized for optimum frequency stability. A minimum value is obtained by the use of a tank circuit having a small L/C ratio and a low value for the quantity $-[a_1+(1/R)]$. The value of $\partial\omega/\partial a_1$ is limited, however, by the availability of practical components for L and C and the load resistor R necessary to provide the required amplitude of oscillation. If the value of the quantity $-[a_1+(1/R)]$ is reduced (*i.e.*, if the ac load line approaches the negative conductance curve tangentially, as shown in Fig. 6), the frequency stability of the oscillator is improved. In addition, because the amplitude of oscillatory voltage, A, is proportional to the square root of the quantity $-[a_1+(1/R)]$, as shown in (8), the amplitude of oscillation becomes smaller.

The required value of load resistance, R, for a fixed minimum amplitude of oscillation, A, is obtained from (8), as follows:

$$\left(\frac{1}{R}\right)_{\min} = -a_1 - \frac{3a_3}{4}A_{\min}^2. \tag{11}$$

Substitution of this value in (10) yields

$$\frac{\partial\omega}{\partial a_1} = -\frac{1}{8C}\sqrt{\frac{L}{C}}\left(\frac{3a_3}{4}A_{\min}^2\right). \tag{12}$$

The Q of the parallel tank circuit is given by

$$Q = R\sqrt{\frac{C}{L}}. \tag{13}$$

Because R has a fixed value determined from (11), the tank circuit should have a high Q and a small L/C ratio to reduce oscillator-frequency drift caused by variation of the input characteristic.

If the negative conductance a_1 varies with temperature [*i.e.*, $(\partial a_1/\partial T) \neq 0$], the frequency of oscillation will also vary with temperature [*i.e.*, $(\partial\omega/\partial T) \neq 0$]. Oscillator frequency can be kept constant during temperature changes [*i.e.*, $(\partial\omega/\partial T) = 0$] with external circuit elements having appropriate temperature coefficients.

If the external elements L and R are constant, but C varies with temperature, the oscillator frequency will vary as follows:

$$\frac{\partial\omega}{\partial T} = -\frac{\omega_0}{2C}\left\{\left[1 - \frac{3L}{16C}\left(a_1 + \frac{1}{R}\right)^2\right]\frac{\partial C}{\partial T} + \frac{L}{4}\left(a_1 + \frac{1}{R}\right)\frac{\partial a_1}{\partial T}\right\}. \tag{14}$$

The required condition for frequency stability is then

$$\frac{\partial C}{\partial T} = \frac{-4LC(a_1 + 1/R)}{16C - 3L(a_1 + 1/R)^2}\frac{\partial a_1}{\partial T}. \tag{15}$$

If C and R are constant, but L varies with temperature, the frequency drift is given by

$$\frac{\partial\omega}{\partial T} = -\frac{\omega_0}{2L}\left\{\left[1 + \frac{L}{16C}\left(a_1 + \frac{1}{R}\right)^2\right]\frac{\partial L}{\partial T} + \frac{L^2}{4C}\left(a_1 + \frac{1}{R}\right)\frac{\partial a_1}{\partial T}\right\}. \tag{16}$$

The condition for stability then becomes

$$\frac{\partial L}{\partial T} = \frac{-4L^2(a_1 + 1/R)}{16C + L(a_1 + 1/R)^2}\frac{\partial a_1}{\partial T}. \tag{17}$$

Eqs. (15) and (17) illustrate the design criteria which the external circuit components must satisfy to protect the oscillator frequency against variation of the input characteristic due to temperature fluctuations.

Oscillator Using Current-Controlled Input Characteristics

The oscillator circuit shown in Fig. 8, which contains a simple series resonant circuit in the emitter circuit, uses the current-controlled emitter-input characteristics. This oscillator can be analyzed directly by the same method given for the oscillator shown in Fig. 7. The analysis can be further simplified, however, by use of the principle of duality. The dual relationship and analytical results for the two oscillators are shown in Appendix I. It is important to note that frequency stability is obtained in oscillators employing voltage-controlled input characteristics by the use of a parallel tank circuit having a high Q and a small L/C ratio. A series tank circuit having a high Q and a large L/C ratio should be used for oscillators employing current-controlled input characteristics.

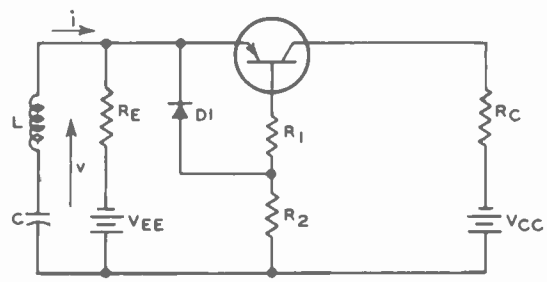

Fig. 8—Transistor oscillator containing simple series resonant circuit in emitter circuit, using current-controlled input characteristics.

Illustrative Example

The use of the design criteria given in the paper may be illustrated by consideration of a 125-kilocycle oscillator using the circuit shown in Fig. 7. Dc operating conditions are chosen to provide an input characteristics similar to that shown in Fig. 6. The circuit elements used are as follows:

$$R_E = 3{,}000 \text{ ohms}$$
$$R_C = 8{,}000 \text{ ohms}$$
$$V_{CC} = 22.5 \text{ volts}$$
$$V_{BB} = 1.45 \text{ volts}$$
$$C = 6{,}820 \text{ micromicrofarads},$$
$$L = 237 \text{ microhenries},$$
$$f_0 = 125 \text{ kilocycles}$$
$$a_1 = \frac{-1}{3.65 \times 10^3} \text{ mho}$$
$$a_3 = \frac{1}{20.2 + 10^3} \text{ mho/volt}^2.$$

The oscillatory voltages for three selected load conditions are given by

$$v = 1.54 \sin 2\pi(1.25 \times 10^5)(1 - 2.85 \times 10^{-5})t \quad \text{for } R = 5{,}400 \text{ ohms}$$
$$= 2.25 \sin 2\pi(1.25 \times 10^5)(1 - 12.5 \times 10^{-5})t \quad \text{for } R = 11{,}700 \text{ ohms}$$
$$= 2.54 \sin 2\pi(1.25 \times 10^5)(1 - 19.7 \times 10^{-5})t \quad \text{for } R = 25{,}200 \text{ ohms}.$$

The amplitude of oscillation is determined by three methods: (a) from analytical equations, (b) from experiments, and (c) from direct interpolation of the curves shown in Fig. 6. Results obtained by the use of each method are given in Table I, next page:

TABLE I

Load Resistor R (ohms)	Amplitude of Oscillation (Peak Volts)		
	From Analysis	From Measurement	From Interpolation
5,400	1.54	1.45	1.4
11,700	2.25	2.1	1.9
25,200	2.55	2.3	2.2

In the interpolation method, the oscillation is assumed to occur between the two intersections of the ac load line with the input characteristic. However, because the actual oscillatory path[4,5] may be different from the assumed one, results obtained from this method are only approximate.

The frequency of oscillation under various loading conditions is obtained both by measurement and by analysis. If f_s is used to denote the frequency of oscillation when R equals 25,200 ohms, and f_l to denote frequency of oscillation at other loading conditions, the difference between f_l and f_s is equal to Δf. Values of Δf obtained by both methods are compared in Table II:

TABLE II

R (ohms)	Δf (cycles per second)	
	From Analysis	From Measurement
5,400	+21	+22
11,700	+9	+8
25,200	0	0

The frequency stability of an oscillator can be improved by the use of proper loading and proper shaping of input characteristics, as illustrated by the frequency-drift data given in Table III below:

TABLE III

R_L	Frequency Drift P.P. M/°C.	
	Input Characteristics Not Shaped	Input Characteristics Shaped
5.4 kilohms	25.0	3.5
11.7 kilohms	36.0	8.8

Other Applications

The design methods discussed in this paper can also be applied to oscillators using new devices such as the double-base diode[10] or junction transistors operated in the "DCC" mode[11] provided the circuit designs use the skew-symmetrical input characteristics described.

Acknowledgment

The author wishes to thank his colleagues at the RCA Tube Division for their suggestions, criticisms, and assistance, and particularly A. Zinisky for supplying experimental results.

[10] J. J. Suran, "Double base expands diode applications," *Electronics*, vol. 28, pp. 198–202; March, 1955.
[11] M. C. Kidd, W. Hasenberg, and W. M. Webster, "Delayed collector conduction, a new effect in junction transistors," *RCA Rev.*, vol. 16, pp. 16–33; March, 1955.

Appendix I

Duality relationship between circuits shown in Figs. 7 and 8.

Oscillator Circuit	Fig. 7	Fig. 8
Power Series representing input characteristics	$i = a_1 v + a_3 v^3$ (voltage-controlled)	$v = b_1 i + b_3 i^3$ (current-controlled)
Circuit equation	$-i = C\frac{dv}{dt} = \frac{1}{L}\int v dt + \frac{v}{R}$	$-v = L\frac{di}{dt} + \frac{1}{C}\int i dt + ir$
Dual relationship	i	v
	v	i
	C	L
	L	C
	$1/R$	r
	a_1	b_1
	a_3	b_3
Nonlinear differential equation	$\frac{d^2v}{dt^2} + \frac{1}{C}\left[\frac{1}{R} + a^1 + 3a_3v^2\right]\frac{dv}{dt} + \frac{v}{LC} =$	$\frac{d^2i}{dt^2} + \frac{1}{L}\left[r + b_1 + 3b_3i^2\right]\frac{di}{dt} + i/LC = 0$
Solution (sinusoidal oscillation)	$v = 2\sqrt{\frac{-(a^1+1/R)}{3a_3}}\sin\left[1-\frac{L}{16C}(a_1+1/R)^2\right]\frac{t}{\sqrt{LC}}$	$i = 2\sqrt{\frac{-(b_1+r)}{3b_3}}\sin\left[1-\frac{C}{16L}(b_1+r)^2\right]\sqrt{LC}$
Q of the external resonant circuit	$Q = R\sqrt{\frac{C}{L}}$	$Q = \frac{1}{r}\sqrt{\frac{L}{C}}$
Criterion for frequency stabilized oscillators	High Q Small L/C ratio Small $[-(a_1+1/R)]$	High Q Small C/L ratio Small $[-(b_1+r)]$.

Prediction of Pulse Radar Performance*

W. M. HALL†, SENIOR MEMBER, IRE

Summary—**A method of calculating the range performance of a pulse radar is presented which is simple, yet which leads to more consistent results than do other methods commonly used. The factors entering into the calculation are discussed in detail, and graphs are given which greatly simplify the procedure.**

Introduction

A PROCEDURE for the calculation of the range performance of a pulse radar is presented below. It takes into account a number of factors which affect the range perfomance of a radar that are frequently overlooked, and as a result has been found to give results that are very consistent with actual tests, even when applied to radars having vastly different characteristics. Because of this, it is particularly useful for the calculation of the relative performance of two radars or the calculation of the percentage change in range corresponding to a given change in radar parameters. Such calculations are frequently much more important than the calculation of the absolute range of a radar, which at best is a rather indefinite number.

To present the procedure, the terms appearing in the "Radar Equation" are discussed in detail one at a time. A sample calculation is then carried through. Reference is made to the bibliography for a great deal of the background material on radar performance. However, certain previously published information has been repeated herein, in order to provide a reasonably complete set of data for the calculation of radar range.

The Radar Equation may be written:

$$R^4F^2(10^{0.2\alpha R}) = \frac{P_t G^2 \lambda^2 \sigma}{(4\pi)^3 (KT)(1.2/\tau)(NF)(S)}.$$

R = Range, in meters, of which the radar is capable.

F = Propagation factor, to take into account the effect of interference of reflections from the ground surface. In effect, G/F is the resultant gain of the antenna system, including the image antenna below the ground, in the given direction.

α = Attenuation constant of the medium, in db/meter.

P_t = Peak transmitter power of a pulse radar, in watts.

λ = Wavelength, in meters.

σ = Cross section of equivalent isotropically reradiating target, in square meters.

KT = Boltzmann's constant × absolute temperature, $= 4 \times 10^{-21}$ watts/(cycles per second).

τ = Pulse duration in seconds. $1.2/\tau$ is a frequency bandwidth in cycles per second equal to 1.2 times the reciprocal of the pulse duration τ.

NF = Noise figure of the receiver.

S = Integration factor; a factor to account for the effects of integration, introduction of extra noise samples, required probability of detection, etc. It is the ratio of signal power, required for detection, to noise power in the bandwidth $1.2/\tau$. The noise power in the bandwidth $1.2/\tau$ is given by the product of terms (KT) $(1.2/\tau)$ (NF). (S is sometimes quite inappropriately called Scan Loss, implying that if the antenna were not scanning, a signal precisely equal to noise could be detected.)

G = Antenna gain, relative to an isotropic radiator, in the direction of the target.

The various terms in the above equation are discussed in more detail below.

Range and Propagation Factor

(R^2F) is the ratio of power density one meter from the equivalent center of radiation of a point source at the antenna to power density at the target, attenuation being neglected. One reason for expressing this factor thus is the availability of plots of contours for over-water coverage of surface radars in Radiation Laboratory Report No. 22 [1]. In the absence of ground reflections $F = 1$. If the free space coverage pattern is known, the pattern above a plane reflecting surface can be approximated readily.

The range capability is proportional to the equivalent field intensity at unit distance in a given direction. The field intensity will be the vector sum of the field intensity E_d of the direct ray, and the field intensity E_r of the reflected ray.

For an antenna located near the earth's surface, the coverage pattern in the vertical plane will have a lobe structure, with the range at the maxima equal to the sum of the free space range plus ρ times the free space range at the same angle below the horizon, and the range at the minima equal to the difference. ρ is the coefficient of reflection of the surface. Over rough, irregular terrain, at microwave frequencies, ρ is very small. Over smooth water it is nearly -1 for horizontal polarization, but for vertical polarization it is complex, and varies with angle, approaching -1 as the grazing angle approaches zero [2].

Hence, for small grazing angles and either polarization, a minimum range occurs along the horizon line and at elevation angles corresponding to

$$\frac{H}{D} = \frac{n\lambda}{2h}$$

* Original manuscript received by the IRE, August 1, 1955; revised manuscript received September 21, 1955.

† Raytheon Manufacturing Co., Wayland, Mass.

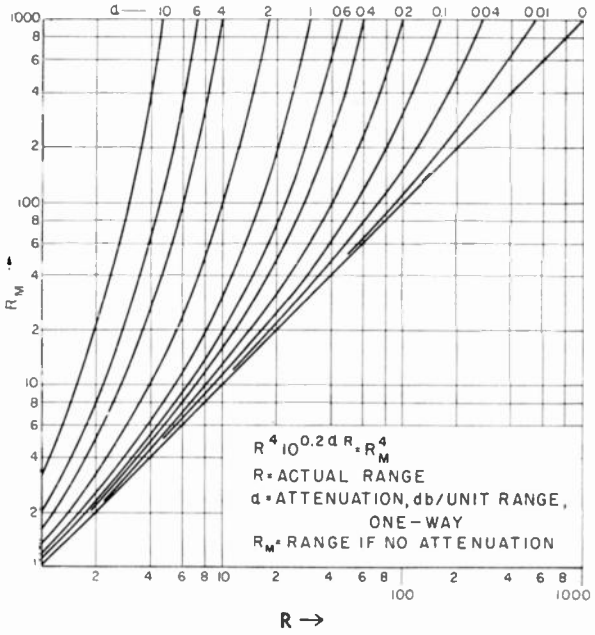

Fig. 1—Effect of atmospheric attenuation on range.

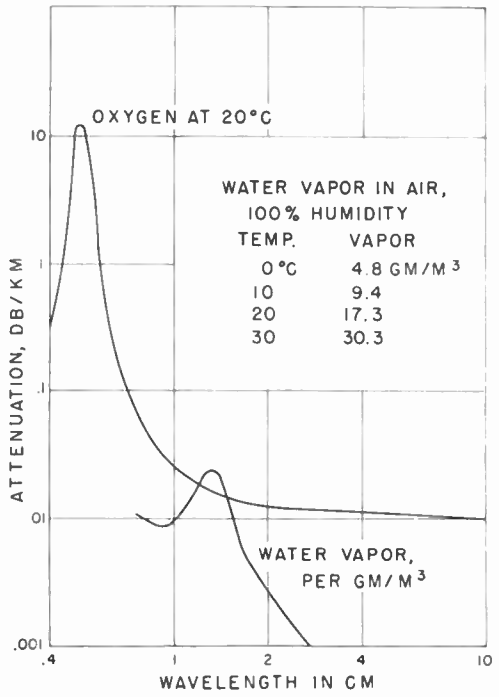

Fig. 2—Attenuation due to oxygen and water vapor (from reference 3).

where

H = height of target above plane surface.
D = horizontal range to target.
h = height of center of radiation of antenna.
λ = wavelength.
n = an integer.

The maxima occur at angles midway between the above.

For long range operation, where curvature of the earth must be considered, the computation is far more complicated. "Trapping" and similar phenomena may also greatly affect the range. Further discussion will be found in Kerr [2], and Radiation Laboratory Report No. 22 [1].

Attenuation

Attenuation, if appreciable, makes the direct calculation of range somewhat difficult, because of the manner in which it enters into the equation. A simple procedure is to compute the range in the absence of attenuation, and then introduce the effects of attenuation by the use of Fig. 1. An excellent survey of attenuation and related problems is found in the Air Force Surveys in Geophysics, No. 23, Weather Effects on Radar, December, 1952 [3]. Representative figures for attenuation at low altitudes are given in Figs. 2 and 3.

Antenna Gain

The gain G is uniquely related to the *effective* area A_e of the aperture of the antenna by:

$$G = \frac{4\pi A_e}{\lambda^2}.$$

A_e is a measure of the cross section of the beam intercepted by the antenna as a receiver. For a simple parabolic reflector, giving a pencil beam, its value, in the direction of maximum gain, is about 0.5 to 0.7 times the actual aperture area. The gain of a small dipole is 1.5. For the usual shapes of either pencil or fan beams, the gain is generally equal to about $25{,}000/(\theta_h \times \theta_v)$, where θ_h and θ_v are the horizontal and vertical beamwidths to the one-way half-power points, in degrees. The beamwidth, in degrees, is in turn equal approximately to $70\lambda/D$, where D is the width of the antenna aperture.

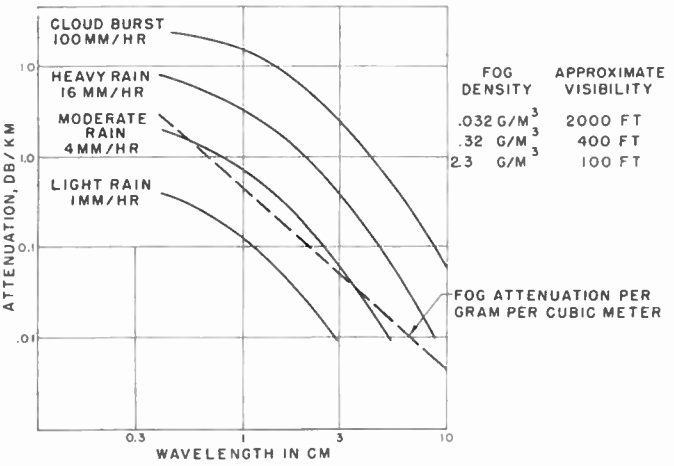

Fig. 3—Attenuation due to rain and fog (from references 2 and 15).

Boltzmann's Constant and Absolute Temperature

Boltzmann's constant K times the absolute temperature T is equal to the mean noise power per cycle per second, at the input to the receiver, caused by thermal fluctuations in the circuit.

Noise Factor

The noise factor NF is a measure of the ratio of the equivalent total noise at the input to the receiver to the limiting value given by KT. It should include attenuation in the transmission line from the antenna to the receiver, loss in the duplexer, conversion loss in the mixer, the effect of noise introduced by the local oscillator, mixer, and intermediate amplifier, etc.

Transmitter Power

As the radar equation is written above, P_t is the power radiated by the antenna averaged over the duration of the pulse τ. It is less than the peak power at the output of the transmitter-proper by an amount equal to the duplexer and transmission line loss.

Bandwidth

The bandwidth $1.2/\tau$ represents the bandwidth passing substantially all of the power in a pulse of duration τ, and is taken to be the optimum bandwidth prior to the detector, for maximum sensitivity of the receiver. The exact bandwidth for optimum performance actually depends on the spectrum of the pulse and the shape of the frequency response characteristic of the receiver [7]. If the bandwidth of the receiver is not equal to $1.2/\tau$, its effect on the radar performance is taken into account in the factor S.

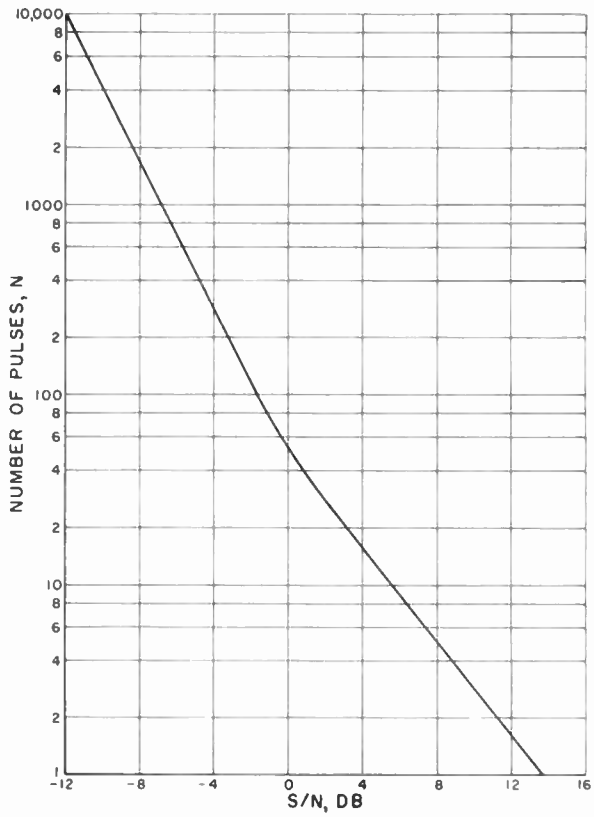

Fig. 4—Input S/N vs number of pulses integrated, $P_D=0.5$; $P_N=10^{-10}$.

Integration Factor

Most of the above terms are fairly definite quantities to which numerical values can be assigned. This is not true of the target area σ and the integration factor S. This is because the detection of a signal in the presence of noise is a statistical procedure, involving probability of false alarm and probability of detection, as well as factors of operator training, fatigue, etc., and local ambient conditions. The target area also fluctuates, in general, because of the effects of interference among the reflections from various portions of the target. In the following discussion, the assumption is made that the fluctuation of the signal is at such a rate that the signal has approximately the same magnitude on successive pulses, as contrasted to the noise, which is random.

The integration factor S may be expressed (on a db scale) as the sum of a group of contributing factors:

$$S = S_O + S_N + S_A + S_B + S_C.$$

S_O is an operator and degradation factor. This is a term generally added to the equation to account for the difference between "theoretical" and observed radar performance. However, it is a legitimate factor to include, as the ability to detect targets certainly depends on the particular operator and the environmental conditions. It also serves as a factor to account for degradation of the equipment below optimum. For a good operator and a *PPI*, under good conditions, a figure of 2 or 3 db appears reasonable; a somewhat larger figure, up to 10 db or more, should be used under more difficult ambient conditions. Another aspect of the "Operator Factor" is discussed in connection with a discussion of Probability of Detection.

S_N is the basic ratio of signal to noise required for the detection of N pulses integrated under ideal conditions [7, 11, 13, 14]. A value for S_N can be found from Fig. 4. This curve is premised on the concept of a threshold voltage set at some factor times rms noise. The sum of the signal and noise must exceed this threshold for the signal to be detected; if the noise alone exceeds this threshold a false alarm results. Fig. 4 is calculated for a probability of detection (P_D) of 0.5, and a probability of false alarm (P_n) of 10^{-10}. There are approximately 10^{10} microseconds in three hours, so if the maximum range presented corresponds to the time interval between transmitted pulses, and there is no integration, so that a separate signal can be detected on each pulse, a probability of false alarm of 10^{-10} means about one false alarm every three hours for one microsecond pulses. Experience indicates that the curve of Fig. 4 is a reasonable one to apply to the usual operating conditions.

The effect of changing the probability of false alarm and the probability of detection is shown in Fig. 5. The data on this curve is calculated for one pulse, but the departures from the reference point indicated may be used as a correction to the curve of Fig. 4, without serious error, for up to about 100 pulses integrated. It is adequate for the general purpose of radar performance prediction.

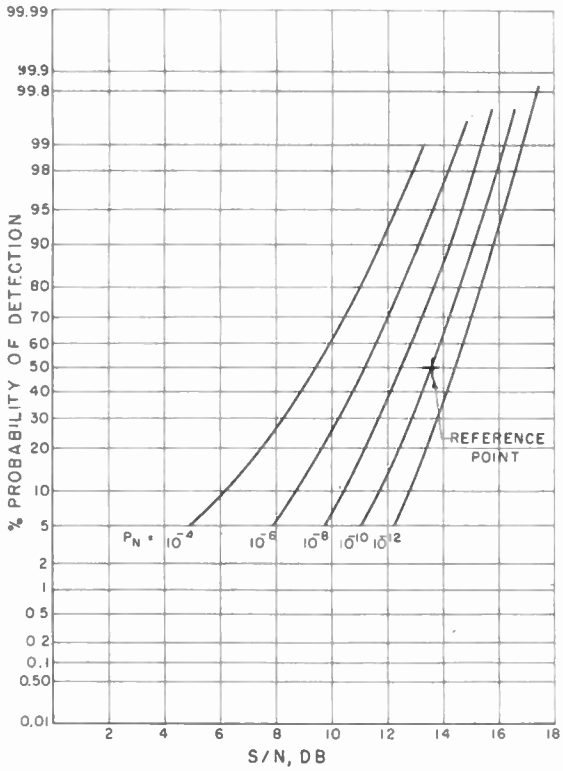

Fig. 5—Probability of detection P_D vs S/N for various false alarm probabilities P_N. (One pulse.)

The departure of the curve of Fig. 4 from a straight line having a slope of 10 db per decade represents the "Integration Loss," which is the system loss that is suffered if the energy is distributed over N pulses instead of being concentrated in one pulse. This is plotted in Fig. 6, and will be referred to in connection with other S factors below.

S_A is an antenna beam-shape factor, used in scanning radars, to allow for the fact that not all of the pulses received between the half-power points are the same strength. If N in the previous term is the number of pulses between the one-way half-power points, then $S_A = 1.6$ db. This is derived and discussed by Blake [4].

S_B is an IF bandwidth factor. If the IF bandwidth is too wide, it permits an excess of noise to reach the output of the receiver. If it is too narrow, it combines noise received prior to and subsequent to the signal with the signal, and results in a degradation of performance. A bandwidth B of about $1.2/\tau$ is considered optimum. If $B\tau = 1.2$ there will be one independent sample of noise or of signal-plus-noise, in the time τ. Now if $B\tau = 1.2k$, with $k > 1$, the receiver will, in effect, take k independent samples in that time. The IF bandwidth loss for n pulses integrated will accordingly be the loss in db corresponding to $N = (B\tau/1.2) \times n$, minus the loss in db corresponding to $N = n$ (Fig. 6). To help visualize this consideration, it may be pointed out that the detectability of a signal in the presence of noise is in general a function of the ratio of signal-plus-noise to *fluctuation* of noise, rather than of the ratio of signal-plus-noise to *mean* noise. Arguments similar to those which follow in connection with collapsing loss indicate similar IF bandwidth loss if $B\tau = 1.2/k$.

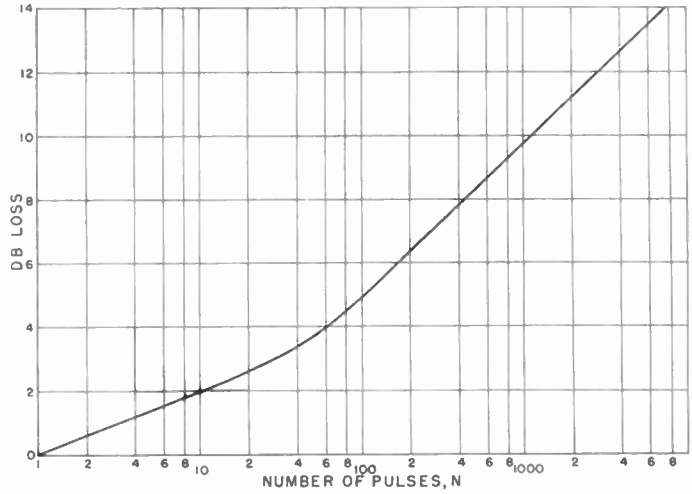

Fig. 6—Loss curve for integration factor calculation.

S_C acounts for the inclusion of samples of noise alone with samples of signal-plus-noise. It is called a collapsing loss because it applies to the superposition—"collapsing"—of information on the radar scope. Into this term are lumped the effects of such factors as sweep speed on the cathode ray tube indicator, video bandwidth, mixing of outputs from two or more channels not all of which contribute signal, or the superposition on one *PPI* of the output from all elevations of a radar which scans in three dimensions. S_C is a function of number of signal samples (pulses) and number of extra noise samples.

Define a collapsing ratio ρ as:

$$\rho = \frac{m+n}{n}$$

where n is the number of signal-plus-noise samples and m is the number of additional noise samples. The collapsing loss S_C can then be found from the curve of Fig. 6. It is equal to the loss in db corresponding to $N = m+n$ minus the loss corresponding to $N = n$. This calculation applies only if the combination of the detector and integrator has a square law characteristic; for example, if a square law detector is followed by a substantially linear integrator or adder, or if a linear detector is followed by an integrator such as a cathode ray tube in which the intensity of the excitation of the phosphor is approximately proportional to the square of the applied voltage. The reasoning is as follows.

The voltage at the input to the detector, for a single pulse, is $E_i = (E_s^2 + E_n^2)^{1/2}$, where E_s and E_n are the components of voltage due to signal and noise respectively. The output, being proportional to the square of the input, is $E_o = E_s^2 + E_n^2$. The sum of the outputs for a series of n signal-plus-noise pulses and m additional noise pulses is:

$$E_o = E_{s1}^2 + E_{s2}^2 + \cdots + E_{sn}^2 + E_{n1}^2 + E_{n2}^2 + \cdots + E_{n(m+n)}^2.$$

The output is seen to be proportional to the total signal power, regardless of how many of the pulses contain signal. Consequently the behavior is the same as if all the pulses contained signal, and the signal energy per pulse were reduced by a factor $n/(m+n)$. The collapsing loss is therefore equal to the change in total signal energy required with $(m+n)$ pulses instead of (n) pulses. If the detector-integrator combination is other than square law, this argument does not hold. The collapsing loss is very much greater in the case of a linear system. The "integration loss" resulting from distributing the energy over N pulses instead of concentrating it in one pulse is, on the other hand, substantially independent of the detector law.

If the video bandwidth is less than is needed to pass the pulse, it results, in effect, in integrating additional samples of noise which occur at times just prior to or subsequent to the signal pulse. The collapsing ratio in this case is:

$$\rho_{\text{eff.}} = \frac{(1.2/\tau) + B_v}{B_v}$$

where B_v is the video bandwidth.

For slow sweep-speeds, the spot size, if greater than the product of pulse duration and writing speed, has a similar effect of integrating additional noise samples. The effective collapsing ratio, for this case, is

$$\rho_{\text{eff.}} = \frac{d + s\tau}{s\tau}$$

where d is the spot diameter and s the sweep speed. A minimum value to use for spot diameter is about 1 millimeter, which corresponds to the resolution of the eye at normal viewing distances.

The collapsing loss is a function of the over-all effect of these various factors. If any one of the above terms predominates, the others may be ignored entirely.

It should be noted that restricting the video bandwidth to a value just sufficient to pass the pulse will not compensate for the effects of an over-wide IF amplifier. A *PPI*, or any other conventional indicator, has the effect of "integrating" over a period equal to at least the duration of the pulse, which is no more nor less than the restricted bandwidth in the video amplifier would do. This effect has already been taken into account in the evaluation of the effect of the IF bandwidth; restricting the video bandwidth has no further effect.

Target Area

Except in the case of simple point targets, such as corner reflectors or spherical objects, a radar target is composed of complex surfaces, the reflections from which interfere, with the result that slight changes in aspect result in drastic changes in equivalent reflecting area. The target area is therefore a statistical thing, fluctuating with time. In case of distributed targets such as rain, sea clutter, or ground surface, "area of the target" is also a function of beamwidth and pulse length.

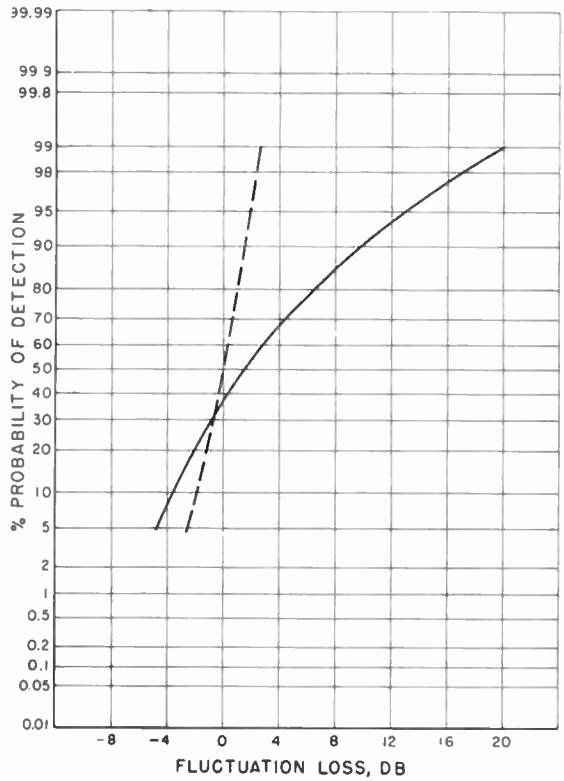

Fig. 7—Fluctuation loss for Rayleigh distribution of fluctuating target. Dotted curve shows loss for non-fluctuating target.

At microwave frequencies the equivalent echoing area of almost any airplane target has approximately an exponential distribution (corresponding to a Rayleigh distributed amplitude) at frequencies such that all the hits within one beamwidth of an ordinary scanning radar may be about the same strength, and on successive antenna scans may be independent. The corresponding energy distribution is exponential, the probability of the energy in one sample exceeding a value σ being $\exp(-\sigma/\sigma_0)$, where σ_0 is the mean value.

Two possible procedures may be followed to handle this fluctuation. If the mean area is known, it may be used in the radar equation, and an additional S-factor introduced to correspond to any specified probability of detection. Or the target area used in the calculation may be modified to correspond to any given probability of detection. The effect on the calculation is of course the same. The correction to use in either case is shown in Fig. 7. Shown also in Fig. 7 is the variation in signal to noise ratio required for different probabilities of detection of a nonfluctuating target. The relation between range and probability of detection for a fluctuating target is shown in Fig. 8, in which the range is arbitrarily normalized to unity at the range at which the probability of detection, and therefore the "blip-scan ratio" is 0.5.

One of the great difficulties in predicting the maximum range of a radar on any given airplane target is that the equivalent area of the target, as given in any table, practically never specifies whereabouts on the

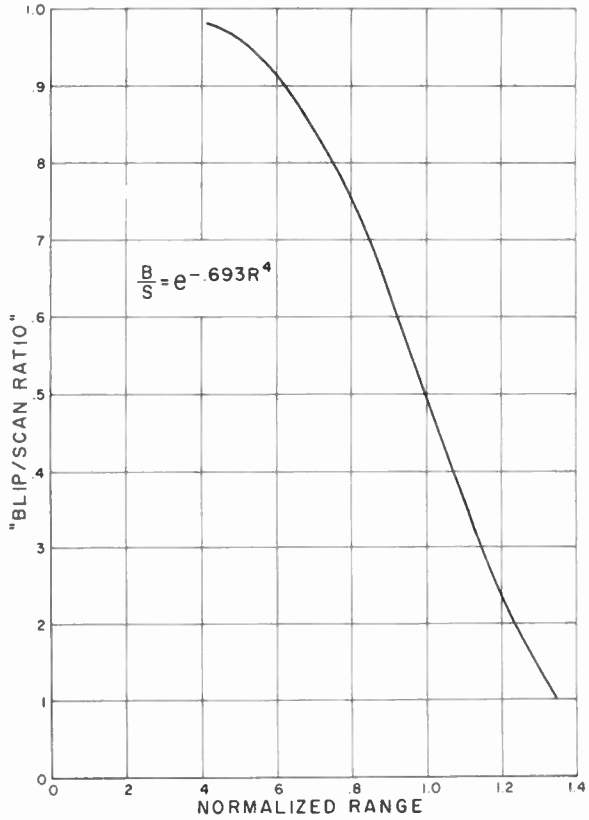

Fig. 8—Probability of detection vs range, fluctuating target.

distribution curve it falls. The original Radiation Laboratory measurements specified a target area which satisfied the radar equation if the target could be seen in perhaps one out of a dozen looks. Other figures represent a probability of detection of 50 per cent, others 80 per cent. Caution is recommended. The mean target area for different airplanes varies from a fraction of a square meter to 50 or more square meters. Some idea of the target size for other targets may be had from the following.

For distributed targets the radar cross section is equal to the area or volume illuminated within one beamwidth and pulse length times the reflectivity per unit area or per unit volume of the illuminated target. Thus for ground viewed by an airborne radar the radar cross section σ of the ground will be the reflectivity K of the ground times the cross section of the beam illuminating the ground within one pulse length. Referring to Fig. 9,

$$\sigma = K \cdot \theta_h \cdot R_g \cdot \left(\frac{h}{R_g} \cdot \frac{c\tau}{2} \right) = K \cdot \theta_h \cdot h \frac{c\tau}{2}$$

where R_g is the ground range, θ_h is the horizontal beamwidth, h is the height above ground of the radar, and c is the velocity of propagation ($c/2 = 150$ meters per microsecond). The mean coefficient of reflection of the ground may be about 0.01, with cities, mountains, etc., considerably larger. This equation indicates that if the coefficient of reflection is independent of angle of incidence the effective target area is independent of range, but is directly proportional to the height of the antenna above the surface. Over a water surface, however, the coefficient of reflection may vary drastically with angle, resulting in greatly increased signal return from close-in areas; *i.e.*, areas for which the grazing angle is large [2].

For rain or clouds:

$$\sigma = R^2 \cdot \theta \cdot \phi \cdot \frac{c\tau}{2} \cdot \rho$$

where θ and ϕ are the horizontal and vertical widths of the beam filled with rain, and ρ is the reflectivity in square meters per cubic meter of the rain. Note that θ and ϕ may be less than the beamwidth of the radar antenna pattern if the entire beam is not filled with rain.

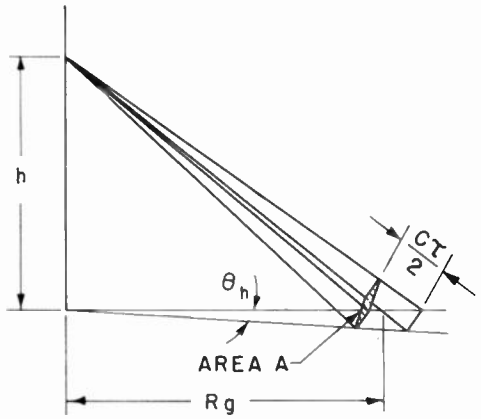

Fig. 9—Distributed ground target.

Substituting this relation in the original radar equation leads to the following form for the radar equation for weather radars:

$$R^2(10^{0.2\alpha R}) = \frac{P_T G^2 \lambda^2 \theta \phi (c\tau/2) \rho}{(4\pi)^3 (KT)(1.2/\tau)(NF)S}.$$

Representative reflection coefficients for rain are shown in Fig. 10. For further information, reference is made to Kerr [2] or to Atlas *et al.* [3].

The target area of a sphere, with diameter large with respect to wavelength, is equal to the cross-section area of the sphere, πr^2. For a corner reflector, with edges of length a, the area depends on the aspect, and has a maximum [5]:

$$\sigma = \frac{4}{3} \frac{\pi a^4}{\lambda^2}.$$

Experience with shipborne radars indicates that the usual nun and can buoys can be represented with fair reliability as approximately one square meter target area, centered about one meter above the water surface.

Probability of Detection

The term "probability of detection," as used above means the probability of the operator seeing the target on any one antenna scan. As a practical approximation, it is numerically equal to the "Blip-Scan Ratio," which

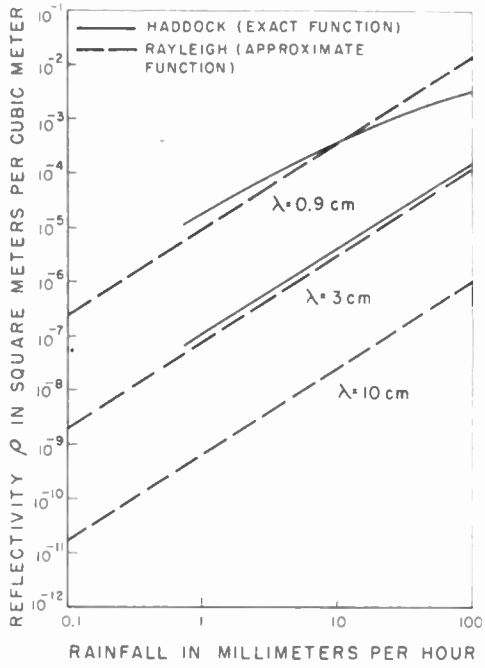

Fig. 10—Reflection coefficient of rain (from reference 3).

is the ratio of the number of times a target is seen to the number of times it is scanned by the antenna.

Under adverse conditions there is a possibility of the operator missing a target even when brightly painted on the indicator. In this case the "probability of detection" may be described as the product of the probability of the target appearing times the probability of the operator detecting it when it does appear. There is some experimental evidence that the probability of the operator detecting a target that is painted solidly on the indicator may be as low as 0.1 under some conditions.

The "cumulative probability of detection," is the probability that a new target will be detected by the time it reaches a specified point. It is a function of the probability of detection on each individual scan and the number of scans.

The cumulative probability of detection on the nth scan is:

$$\text{C.P.D.}_n = 1 - (1 - P_1)(1 - P_2) \cdots (1 - P_i) \cdots (1 - P_n)$$

where P_i is the probability of detection on the ith scan.

An interesting and very important point can be made in the case of the detection of fluctuating targets: increasing the scan rate of an antenna may greatly increase the cumulative probability of detection in a given elapsed time, even though the increased scan rate results in an appreciable decrease in the probability of detection on any one scan.

Example

As an example, the range of a hypothetical air-search radar will be computed.

Assumed System Parameters

Transmitting power	P_T	600 kw
Antenna gain	G	29 db
Wavelength	λ	25 cm
Pulse length	τ	2.6 cm
Noise figure	NF	11 db
IF bandwidth	B	1 mc
Scan rate		10 rpm
Horizontal beamwidth	θ	3.5°
Pulse repetition rate		400 pps
Indicator scale		40,000 yards/inch

The range for 90 per cent probability of detection of an aircraft target having a mean reflecting area of 6 square meters is desired. For reference, the free space range on a nonfluctuating target of 1 square meter will be computed.

All the numbers to enter in the range equation are available in the above table except the integration factor S. Referring to the preceding discussion of integration factor:

$$S = S_O + S_N + S_A + S_B + S_C.$$

The operator factor S_O is arbitrarily set at 2 db, and the antenna scanning loss S_A is 1.6 db. The number of pulses per beamwidth, as calculated from the above data, is 23. S_N, from Fig. 4, is accordingly 2.6 db. The bandwidth, pulse length product, $B\tau$, is 2.6. The IF bandwidth loss S_B is therefore the difference between the loss for $2.6\times23=60$ pulses and 23 pulses (Fig. 5): $S_B=4-2.7=1.3$ db. At the assumed sweep speed of 40,000 yards per inch there are 3.7 pulse intervals τ per millimeter of radial sweep on the face of the indicator. The collapsing ratio ρ is therefore $(3.7+1)/1=4.7$ and the collapsing loss S_C is accordingly the difference between the loss for $4.7\times23=108$ pulses and 23 pulses (Fig. 5): $S_C = 5.1 - 2.7 = 2.4$ db.

Totalling the above,

$$S = 2 + 2.6 + 1.6 + 1.3 + 2.4 = 9.9 \text{ db} = 9.8 \text{ times}.$$

This means that the received signal must be 9.9 db above rms noise for 50 per cent probability of detection. Solving the radar equation:

P_T	6×10^5	$(4\pi)^3$	2×10^3
G	8×10^2	KT	4×10^{-21}
G	8×10^2	$1.2/\tau$	4.6×10^5
λ	2.5×10^{-1}	NF	1.26×10^1
λ	2.5×10^{-1}	S	$.98=10^1$
σ	1×10^0		
	$2{,}400\times10^7$		45.5×10^{-11}

$$R^4 = \frac{2{,}400 \times 10^7}{45.5 \times 10^{-11}} = 53 \times 10^{18}$$

$$R = 0.85 \times 10^5 \text{ meters} = 93{,}000 \text{ yards} = 46.5 \text{ miles}.$$

This is the range, for $P_D = 0.5$ on a nonfluctuating target of one square meter cross section. The range on a nonfluctuating target of 6 square meters will be $6^{1/4} \times 46.5 = 73$ miles. The fluctuation loss (Fig. 7) for 90 per cent probability of detection of a fluctuating target is 9.8 db. The range will therefore be reduced by $9.8/4 = 2.45$ db $= 1.76$ times, to 41.5 miles. The effect on range of considering other probabilities of detection, or blip-scan ratios, is shown in Fig. 8.

The above ranges should be expected over heavily wooded irregular terrain, over which there is a minimum of interference of direct and reflected rays. Over water or smooth ground, the range should be increased considerably, but with "holes" in the pattern, or a much wider spread in range for different probabilities of detection, as a result of the destructive interference at certain angles of elevation.

Attenuation is negligible for good weather at this frequency, so is not considered in this calculation.

The foregoing analysis has discussed only the performance of search-type pulse radars. However, the general principles established can be readily applied to other problems, such as tracking radars, range-gated doppler radars, automatic alarm systems, etc. *CW* radars may also be included, by identifying a time equal approximately to the reciprocal of the receiver bandwidth with the time τ of a pulse in pulse radar case, and identifying ratio of post-detection smoothing or integrating time to this time with the number of pulses n.

The mathematics which has been involved is based almost entirely on the work of Rice [9]. In addition to the specific references in the text, the bibliography contains a few references to recent articles on radar performance and the general problem of signal detection; however, it makes no attempt to be complete, and several pertinent studies have been omitted because of their classification.

Bibliography

[1] Hutner, R. A., Parker, F., Howard, B., Dodson, H., and Gill, J., *Transmission at Low Altitudes Over Sea Water*. R. L. Report No. 22, Radiation Laboratory. Cambridge, Massachusetts Institute of Technology, September, 1943.

[2] Kerr, D. E., *Propagation of Short Radio Waves*. Radiation Laboratory Series, Vol. 13, New York, McGraw-Hill Book Company, Inc., 1951.

[3] Atlas, D. *et al. Weather Effects on Radar*. Air Force Surveys in Geophysics, No. 23. Cambridge, Air Force Cambridge Research Center, December, 1952.

[4] Blake, L. V., "The Effective Number of Pulses per Beamwidth for a Scanning Radar." Proceedings of the IRE, Vol. 41, (June, 1953), p. 770 and Addendum, Proceedings of the IRE, Vol. 41 (December 1953), p. 1785.

[5] Ridenour, L. N. *Radar System Engineering*. Radiation Laboratory Series Vol. 1, New York, McGraw-Hill Book Company, Inc., 1947.

[6] Payne-Scott, R., "The Visibility of Small Echoes on Radar PPI Displays." Proceedings of the IRE, Vol. 36 (February, 1948), p. 180.

[7] Page, I. H., *Detection of Radar Echoes*. NRL Reprint No. 36 53, Anacostia, D. C., Naval Research Laboratory, March, 1953.

[8] Lawson, J. L. and Uhlenbeck, G. E., *Threshold Signals*. Radiation Laboratory Series, Vol. 24, New York, McGraw-Hill Book Company, Inc., 1950.

[9] Rice, S. O., "Mathematical Analysis of Random Noise." *Bell System Technical Journal*, Vol. 23 (October, 1944), p. 282 and Vol. 24 (January, 1945), p. 46.

[10] Kac, M., and Siegert, A. J. F., "On the Theory of Noise in Radio Receivers with Square Law Dectectors." *Journal of Applied Physics*, Vol. 18 (April 1947), p. 383.

[11] Sherwin, C. W., *The Detection of Pulsed Signals in Noise*. Report R-26, Control Systems Laboratory. University of Illinois, September 27, 1952.

[12] Sherwin, C. W., *Further Considerations in the Detection of Pulsed Signals in Noise*. Report R-30, Control Systems Laboratory. University of Illinois, January 30, 1953.

[13] Drukey, D. L., with the collaboration of Levitt, L. C., Wolcott, N. M., *Radar Range Performance*, Hughes Aircraft Company, Technical Memo No. 277, Culver City, California, April 15, 1954.

[14] Kaplan, E. L., "Signal-Detection Studies, with Applications." *Bell System Technical Journal*, Vol. 34 (March, 1955), p. 403.

[15] Mueller, G. E., "Propagation of 6-Millimeter Waves." Proceedings of the IRE, Vol. 34 (April, 1946), p. 181P.

Methods of Sampling Band-Limited Functions*

R. S. BERKOWITZ†, ASSOCIATE MEMBER, IRE

Summary—**A family of signals is considered which lie within a bandwidth of W cps. Methods are discussed of experimentally obtaining suitable discrete numbers at the rate of $2W$ per second to describe completely any given member of the family. An "Educated Direct" sampling method is presented and compared with previously known sampling methods.**

* Original manuscript received by the IRE, October 10, 1954; revised manuscript received September 9, 1955.

† Assistant Professor of Electrical Engineering, Moore School of Electrical Engineering, University of Pennsylvania, Philadelphia, Pa. The work reported in this paper was done under contract with the U. S. Department of Defense, Washington, D. C.

I. Introduction

CONSIDER THE family of signals $V(f_1, W)$ specified to lie frequency-wise entirely within a band of width W cps extending from f_1 to $f_1 + W$ cps. It is well known that all such signals are directly determinable in terms of suitable discrete numbers given at a rate $2W$ numbers per second. Here we are interested in methods of *experimentally obtaining* such numbers at the rate $2W$ per second to describe completely any given member of the family.

The main feature of this paper is the presentation of an "Educated Direct" sampling method which is described in detail and compared with previously known sampling methods. Sections II and III contain the basic theoretical ideas needed to describe sampling techniques; Sections IV, V, and VI contain outlines of three methods of obtaining samples that have been discussed or implied in the literature; Section VII contains an exposition of the Educated Direct method; and Section VIII consists of a practical appraisal of the relative merits of the different methods presented.

II. Low-Frequency Case

In the special case where the lower limit frequency f_1 is zero cps, the discrete numbers describing any member $v(t)$ of the family $V(0, W)$ are the values of instantaneous samples of $v(t)$ taken at times $t=t_0+n/2W$ seconds where t_0 is an arbitrary fixed time. Thus $v(t)$ at all times is given by [1–3]

$$v(t) = \sum_{-\infty}^{\infty} v\left(t_0 + \frac{n}{2W}\right) \frac{\sin\left[2\pi W(t - t_0) - n\pi\right]}{2\pi W(t - t_0) - n\pi}, \quad \text{for family } V(0, W). \tag{1}$$

III. Representations of General Bandpass Functions

Consider the general case of functions of the family $V(f_1, W)$. Three possible general representations of such functions are [4]

$$v(t) = v_c(t) \cos 2\pi(f_1 + W/2)t + v_s(t) \sin 2\pi(f_1 + W/2)t, \tag{2}$$

$$v(t) = v_c'(t) \cos 2\pi f_1 t + v_s'(t) \sin 2\pi f_1 t, \tag{3}$$

$$v(t) = v_c''(t) \cos 2\pi(f_1 + W)t + v_s''(t) \sin 2\pi(f_1 + W)t: \tag{4}$$

$v_c(t)$ and $v_s(t)$ are each of family $V(0, W/2)$. Each is thus specified by its discrete values spaced $1/W$ seconds apart. Thus both of these functions are needed to completely specify $v(t)$.

The functions $v_c'(t)$, $v_s'(t)$, $v_c''(t)$ and $v_s''(t)$ are each of class $V(0, W)$ and thus each must be specified by discrete values spaced $1/2W$ seconds apart. It is readily shown that *any one* of these four functions contains sufficient information to completely specify the original function $v(t)$. This can be done by showing that the functions $v_c(t)$ and $v_s(t)$ of (2) can both be completely specified by any one of the four primed functions. This will be demonstrated in the sequel for v_c' and v_c''. Similar demonstrations would hold for v_s' and v_s''.

Comparing (2) and (3), there results:

$$v_c'(t) = v_c(t) \cos \pi W t + v_s(t) \sin \pi W t, \tag{5}$$

giving

$$v_c'\left(\frac{n}{2W}\right) = v_c\left(\frac{n}{2W}\right) \cos n\frac{\pi}{2} + v_s\left(\frac{n}{2W}\right) \sin n\frac{\pi}{2}, \tag{6}$$

and hence, letting $n=2m$ and $2m+1$, respectively,

$$v_c\left(\frac{m}{W}\right) = (-1)^m v_c'\left(\frac{2m}{2W}\right) \tag{7}$$

$$v_s\left(\frac{m}{W} + \frac{1}{2W}\right) = (-1)^m v_c'\left(\frac{2m+1}{2W}\right). \tag{8}$$

Eqs. (7) and (8) specify samples of $v_c(t)$ and $v_s(t)$ taken at the rate of $1/W$ per second each; thus $v_c(t)$ and $v_s(t)$ are both completely determined in terms of samples of $v_c'(t)$. This completes the demonstration for $v_c'(t)$.

It is similarly shown that in terms of $v_c''(t)$, there results

$$v_c\left(\frac{m}{W}\right) = (-1)^m v_c''\left(\frac{2m}{2W}\right) \tag{9}$$

$$v_s\left(\frac{m}{W} + \frac{1}{2W}\right) = -(-1)^m v_c''\left(\frac{2m+1}{2W}\right). \tag{10}$$

Comparing the above with (7) and (8) there results, incidentally,

$$v_c''\left(\frac{n}{2W}\right) = (-1)^n v_c'\left(\frac{n}{2W}\right). \tag{11}$$

The point of the above discussion is the fact that the band-pass function $v(t)$ can be expressed in terms of discretely spaced samples of the low-pass functions $v_c(t)$ and $v_s(t)$; $v_c'(t)$; $v_c'(t)$; $v_s'(t)$; or $v_s''(t)$. The remaining parts of this paper will present methods of determining such low-pass function sample values from measurements on the bandpass function $v(t)$.

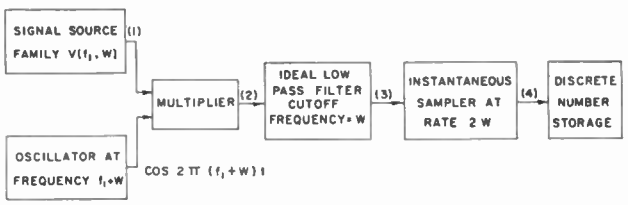

Fig. 1—Frequency conversion method of obtaining samples.

IV. Frequency-Conversion Method

A possible procedure for obtaining suitable sample values to specify a band-pass function would utilize the conventional methods of detection of single-side-band suppressed carrier signals [5]. Consider block diagram of Fig. 1. At point 2 there will be the sum of two signals, one of family $V(0, W)$ and the other of family $V(W+2f_1, W)$. The signal at point 3 will be $v_c''(t)$, of family $V(0, W)$ and therefore expressible in terms of discrete samples obtained at point 4. Note, that as in the low-pass case, $2W$ samples per second are required to specify $v(t)$.

The original signal $v(t)$ can be reconstructed from the discrete samples by the method indicated schematically in Fig. 2. The signal at point 1 in Fig. 2 would be the same as that at point 3 in Fig. 1; that at point 2 in Fig. 2 would be the same as that at point 1 in Fig. 1.

Now while the scheme of Fig. 1 is thus simply shown to be theoretically correct, there are several serious

practical defects. One is the difficulty of constructing an adequate multiplier. Another is the difficulty of constructing a suitable low-pass filter without introducing amplitude and phase distortion that would obscure possible significant properties of the stated original function $v(t)$.

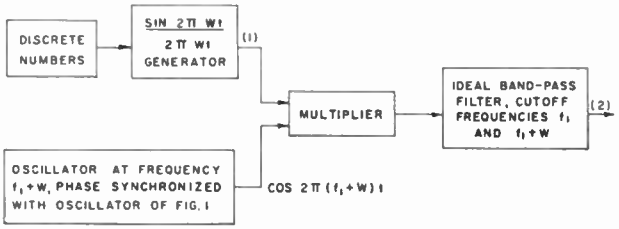

Fig. 2—Reconstruction of continuous signal from sample values.

Note that some of these difficulties could be avoided in the case where the frequency f_1 is much greater than W. The trick would be to insure that the oscillator signal at frequency f_1+W is much greater in amplitude than the signal $v(t)$, replace the multiplier of Fig. 1 by a simple adder and then use envelope detection to obtain the required low-frequency signal. In this case the main practical difficulty would be the elimination of distortion in the detection process.

V. Amplitude—Phase Sampling

This method is based on (2) expressing $v(t)$ in terms of low-pass functions $v_c(t)$ and $v_s(t)$ of family $V(0, W/2)$. Thus, functions $A(t)$ and (t) can be defined as follows:

$$v_c(t) = A(t)\cos[(t)]; \quad v_s(t) = A(t)\sin[(t)], \tag{12}$$

so that

$$v(t) = A(t)\cos[2\pi(f_1 + W/2)t - (t)]. \tag{13}$$

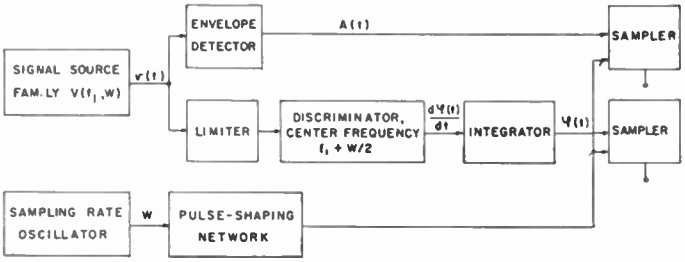

Fig. 3—Amplitude Phase method of obtaining samples.

Synchronously spaced samples of $v_c(t)$ and $v_s(t)$ can thus be expressed in terms of corresponding synchronous samples of functions $A(t)$ and (t) so that the latter samples thus serve to specify the function $v(t)$. To obtain these samples, (13) suggests a system as indicated in Fig. 3. Note that this method is valid only if the bandwidth of the signal is much less than the center frequency.

VI. Simple Direct Sampling

By definition, any $v(t)$ of the family $V(f_1, W)$ will also be included in the family $V(f_1', W')$ if the following conditions are satisfied:

$$f_1' \leqq f_1, \quad W' \geqq W + f_1 - f_1'. \tag{14}$$

It follows that $v(t)$ can be expressed in terms of low-pass functions $\mu_c(t)$ and $\mu_s(t)$, $\mu_c'(t)$, $\mu_c''(t)$, $u_s'(t)$ or $\mu_s''(t)$ having properties as indicated for the low-pass functions $v_c(t)$, etc., in Section III above, only with f_1 replaced by f_1' and W replaced by W'. Now if f_1' *is an integral multiple of* W' $(f_1' = kW')$, we have, from equations similar to (2), (3) and (4):

$$\mu_c\left(\frac{m}{W'}\right) = (-1)^m v\left(\frac{2m}{2W'}\right);$$

$$\mu_s\left(\frac{1}{2W'} + \frac{m}{W'}\right) = (-1)^{k+1} v\left(\frac{2m+1}{2W'}\right) \tag{15}$$

$$\mu_c'\left(\frac{n}{2W'}\right) = (-1)^{kn} v\left(\frac{n}{2W'}\right) \tag{16}$$

$$\mu_c''\left(\frac{n}{2W'}\right) = (-1)^{(k+1)n} v\left(\frac{n}{2W'}\right). \tag{17}$$

Thus the low-pass functions which can specify $v(t)$ are obtainable by direct instantaneous sampling of $v(t)$ itself. However, the required rate of $2W'$ samples per second will in general be greater than the theoretical $2W$ values per second necessary to specify $v(t)$.

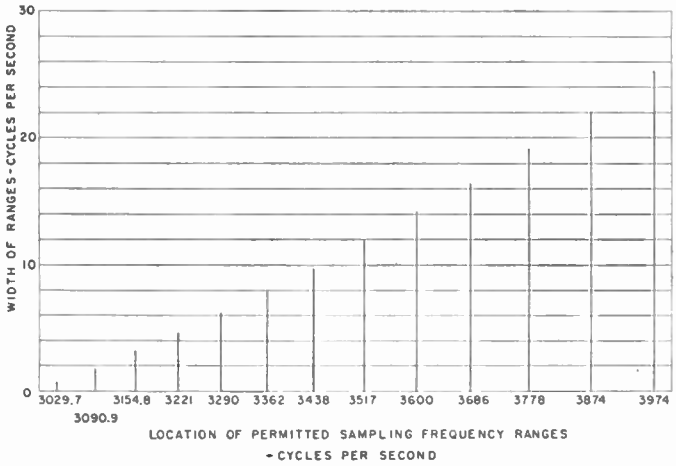

Fig. 4—Location and width of permitted sampling frequency ranges for Simple Direct sampling method in the case where $W = 3$kc; $f_1 = 151.5$ kc.

In fact, W' must be in one of the ranges determined from (14) and expressed as follows (where $f_1 = W(k+\alpha)$, k an integer, α less than unity):

$$\frac{\alpha + r}{k + 1 - r} \leqq \frac{W' - W}{W} \leqq \frac{\alpha + r}{k - r},$$

$$r = 0, 1, 2, 3, \cdots, k. \tag{18}$$

An illustration of these relations is given in Fig. 4 for the case where $W = 3$ kc, $f_1 = 151.5$ kc.

VII. Educated Direct Sampling

At this point a procedure for direct sampling will be pointed out that will be valid when the low-frequency limit f_1 is much greater in magnitude than the bandwidth W. This procedure is independent of whether f_1 is or is not an integral multiple of W.

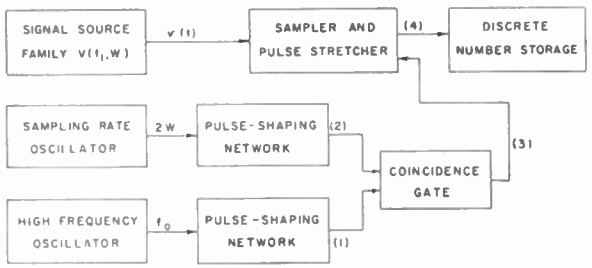

Fig. 5—Educated Direct method of obtaining samples—diagram.

Consider the block diagram of Fig. 5 and the corresponding waveforms in Fig. 6.

At point 1 are narrow pulses of fixed amplitude occurring at times $t=m/f_0$, $m=$integer. At point 2 are rectangular pulses of repetition rate $2W$ and duration greater than $1/f_0$. Hence, at point 3 there will be a series of uniform narrow pulses occurring at times:

$$t_n = \frac{n}{2W} + \Delta_n \tag{19}$$

where n is an integer and $|\Delta_n| < (1/f_0)$ and is such that:

$$\cos 2\pi f_0 t_n = 1, \qquad \sin 2\pi f_0 t_n = 0. \tag{20}$$

The sample values at point 4 will then be

$$v_n = v(t_n). \tag{21}$$

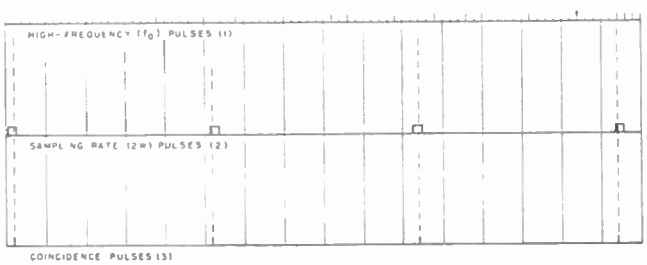

Fig. 6—Educated Direct method of obtaining samples—pertinent waveforms.

The frequency f_0 is taken equal to f_1 or to f_1+W. Now if $f_0=f_1$, we have from (3), (19), (20), and (21),

$$v_n = v_c'\left(\frac{n}{2W} + \Delta_n\right); \qquad f_0 = f_1. \tag{22}$$

That is, the samples of $v(t)$ are taken at times when $v_c'(t)=v(t)$. Now we make use of the fact that $v_c'(t)$ is of family $V(0, W)$. Since f_0 is assumed much greater than W and since Δ_n is less than $1/f_0$, $v_c'(t)$ will not change appreciably in a time Δ_n and we will have:

$$v_c'\left(\frac{n}{2W} + \Delta_n\right) = v_c'\left(\frac{n}{2W}\right) = v_n, \qquad f_0 = f_1. \tag{23}$$

Thus the low-pass function $v_c'(t)$ is completely specified by the samples at point 4 in Fig. 5. Similarly, if the oscillator frequency is taken equal to f_1+W, we will have

$$v_n = v_c''\left(\frac{n}{2W}\right) \text{ for } f_0 = f_1 + W. \tag{24}$$

Similarly, sample values specifying $v_s'(t)$ and $v_s''(t)$ could be obtained by the above block diagram by shifting the oscillator phase by $\pi/2$. To obtain $v_c(t)$ and $v_s(t)$, it would be necessary to set f_0 equal to $f_1+W/2$, and generate sets of pulses synchronized with both $\cos 2\pi f_0 t$ and $\sin 2\pi f_0 t$. The first set would be used with even-numbered pulses from the sampling rate oscillator to obtain samples specifying $v_c(t)$; the second would be used with the odd-numbered pulses to obtain samples specifying $v_s(t)$.

VIII. Practical Considerations

In the above sections four methods of obtaining discrete samples to specify bandpass functions have been outlined. These are:

Frequency-Conversion—FC—Section IV.
Amplitude-Phase—AP—Section V.
Simple Direct—SD—Section VI.
Educated Direct—ED—Section VII.

Let us examine the relative merits of these methods from the point of view of mechanization requirements.

A. Rate at Which Samples Must Be Taken and Stored

In methods FC, AP, and ED, samples can be taken at the theoretical rate of $2W$ per second. In methods FC and ED, voltage amplitudes are sampled at this rate while in method AP both voltage and phase values are taken simultaneously at the rate W per second. Method SD requires, in general, a sampling rate greater than $2W$.

B. Effect of Frequency Band Location

Methods AP and ED are valid only when the low-frequency limit f_1 is much greater than the bandwidth W. Method FC will also be easiest to mechanize when this condition is satisfied. Method SD is probably best when f_1 is smaller than W.

C. Frequency Accuracy Requirements

Consider the case where the signal under study is narrow-band (for example the intermediate frequency output of a high-stability receiver). Methods FC and ED require an oscillator, at approximately the frequency of the signal, having enough stability to ensure that frequency variations are much smaller than the signal bandwidth. Method AP requires no high frequency oscillator but at least equivalent accuracy in measurement of instantaneous frequency of the signal.

In all three of the above methods the sampling-rate oscillator variations need only be small compared to the bandwidth W. In method SD, no high-frequency oscillator is required but the accuracy requirements on the sampling rate oscillator are quite severe. From (18), in the case where $k \gg 1 (f_1 \gg W)$ and $r \ll k$, the permissible range of sampling rates would be of approximate magnitude.

$$2W \cdot (\alpha + r) \cdot \left(\frac{W}{f_1}\right)^2. \tag{25}$$

Variations in sampling rate should be small compared to the above quantity.

D. Requirements on Sampling Time

Generally, the time required to obtain samples should be small enough so that the quantity sampled remains essentially constant during this time. Thus, for methods FC and AP, sampling time need only be small with respect to the reciprocal of the bandwidth of the signal (*i.e.* $\Delta t_s \ll 1/W$) while for the other two methods (SD and ED) the sampling time must be small compared with the reciprocal of the highest frequency in the signal (*i.e.* $\Delta t_s \ll 1/(f_1 + W)$).

E. Form of Output Samples

In methods FC, SD and ED, the sample values obtained specify a single low-frequency function that contains all the information of the given band-pass signal. In method AC, however, two functions are obtained which must be used in conjunction to reproduce the information present.

F. Numerical example

Consider the case where the signal has a bandwidth of 3 kilocycles centered about a frequency of 153 kc. The requirements on the different sampling methods can be indicated in Table I.

TABLE I

REQUIREMENTS ON DIFFERENT SAMPLING METHODS FOR SIGNAL HAVING 3 KC BANDWIDTH, CENTERED AT 153 KC

	FC	AP	SD	ED
1. Sampling Rate	6 kc	3 kc 2 quant.	>6 kc	6 kc
2. Sampling Rate accuracy	$\ll$3 kc	$\ll$3 kc	$\ll$10 cps*	$\ll$3 kc
3. High Frequency oscillator frequency	154.5 kc	—	—	154.5 kc
4. High Frequency oscillator accuracy	$\ll$3 kc	—	—	$\ll$3 kc
5. Sampling time	$\ll$300 μsec	$\ll$300 μsec	$\ll$6 μsec	$\ll$6 μsec

* See Fig. 4 for acceptable ranges of sampling frequencies.

ACKNOWLEDGMENT

The author would like to acknowledge the value of several discussions with Dr. R. M. Showers of the Moore School Faculty concerning the work in this paper.

BIBLIOGRAPHY

[1] Bennett, W. R., "Spectra of Quantized Signals." *Bell System Technical Journal*, Vol. 27 (July, 1948), pp. 446–472.

[2] Shannon, C. E., "Communication in the Presence of Noise." PROC. IRE, Vol. 37 (January, 1949), pp. 10–21.

[3] Ville, J., "Signaux Analytiques a Spectra Borne." *Cables and Transmission*, Vol. 4 (January, 1950), p. 9 and Vol. 7 (January, 1953), p. 44.

[4] Goldman, S., *Frequency Analysis, Modulation and Noise*. New York, McGraw-Hill Book Co., Inc., 1948.

[5] Terman, F. E., *Radio Engineers' Handbook*, 1st ed. New York, McGraw-Hill Book Co., Inc., 1943, pp. 578, 659.

[6] Goldman, S., *Information Theory*. New York, Prentice-Hall, Inc., 1953.

The Rubber Membrane and Resistance Paper Analogies*

J. H. OWEN HARRIES†, SENIOR MEMBER, IRE

Summary—**Part I of this paper sets out a theoretical and experimental analysis of the rubber membrane analogy. Part II describes and analyzes the resistance paper analogy.**

Both analogies have errors which are investigated by comparison with exactly computed solutions. Precautions which ought to be taken in using the analogies are described.

Introduction

THE INTERNAL electric and magnetic fields, space charges and electron trajectories found in discharge tubes are not, in general, analytically calculable except for simple and often trivial electrode shapes, such as infinite parallel planes and infinite cylinders. Designers of advanced types of vacuum tubes therefore proceed largely by cut-and-try in the light of broad theory and, on occasion, by reference to analogies such as the well-known rubber membrane model [1–9], the electrolytic tank, which is sometimes used to feed information to a computing machine [10] for the calculation of trajectories, and resistance paper models [11, 12]. Of these three analogies the rubber membrane model is at first sight perhaps the most attractive to a tube designer because it purports to show both nonrelativistic electron trajectories and space charge effects [6]. The resistance paper model is simple and to a limited extent effective, but yields only the potential field in the absence of space charge; the electron trajectories have to be computed separately, as is the case with the electrolytic tank.

The author has had occasion to compare the results obtainable from the rubber membrane and resistance paper analogies with corresponding and exact solutions obtained sometimes by analytical methods and sometimes by numerical computation using the calculus of finite differences. These comparisons revealed that the regions of reasonable validity of these analogies in their published forms are much more restricted than one is led to believe from a study of the literature. The present paper is an attempt to delineate the regions of validity and to suggest useful procedures.

I. The Rubber Membrane Model

1. *The Limitations and Usefulness of the Classical Theory*

The classical theory [13, 14] of a sphere traveling over a surface has been invoked by previous authors to study the rubber membrane model. However, we shall show by experiment that this classical theory does not apply to the trajectories of balls traveling over a rubber membrane. On the other hand, a study of the classical theory yields the useful information that the equations of motion contain so-called "spin" terms, the existence of which in the general case prevents the trajectory of a ball over a surface from being a valid analogy to that of an electron. The spin terms are absent only if the surface is a plane. In order to both delineate the extent to which the classical theory yields useful information, and to enable this theory to be tested by experiment, it will be helpful briefly to recapitulate part of E. J. Routh's classic work [14].

The classical theory assumes that the sphere makes contact with the surface at a point only, and that the frictional force is a constant multiple of the normal reaction. Neither of these assumptions is true [15, 16]. This theory also states that if the frictional force is sufficiently great, no loss of energy due to friction occurs, and the ball rolls on the surface without sliding. This motion is called "pure rolling." The equally unrealizable case of zero friction is that of the movement of a body over an infinitely smooth surface which is known as "pure sliding" and is without loss by friction. When the friction is intermediate between zero and the value needed to produce "pure rolling," the theoretical sphere both slides and rolls, and loss of energy then appears due to friction.

The general equations of motion for the classical case of pure loss-free rolling upon any shape of surface can be shown [14] to be

$$\frac{du}{dt} = \frac{a^2}{a^2 + k^2} X + \theta_3 v + \frac{k^2}{a^2 + k^2} \theta_1 a\omega_3$$

$$\frac{dv}{dt} = \frac{a^2}{a^2 + k^2} Y - \theta_3 u + \frac{k^2}{a^2 + k^2} \theta_2 a\omega_3 \qquad (1)$$

where the system of moving axes illustrated in Fig. 1 is employed. In (1) the forces are denoted by X and Y and the motion of the axes GA, GB, GC are determined by the angular velocities θ_1, θ_2, and θ_3 of these axes about their instantaneous positions. The velocity components of the center of gravity G parallel to these axes are u, v and w; ω_1, ω_2 and ω_3 are the instantaneous angular velocities of the body about these axes. We have $w = 0$. F and F' are the components of the friction on the sphere parallel to the axes GA and GB, respectively. The radius of the sphere is denoted by a, and k is the radius of gyration about a diameter. The mass is assumed to be unity.

Only if the second and third terms on the right hand side of (1) (sometimes called the "spin" terms) are zero will the analogy to an electron trajectory be perfect.

* Original manuscript received by the IRE, May 12, 1955; revised manuscript received August 29, 1955.

† Consulting Engineer, Warwick, Bermuda.

This will be true if $\theta_1\omega_3$, $\theta_2\omega_3$ and θ_3 are zero. Now the classical theory states that if the axes GA, GB are taken to be tangents to an imaginary surface formed by producing all the normals of the actual surface a distance equal to the radius a of the sphere, then we can describe $\theta_1, \theta_2, \theta_3$ and $d\omega_3/dt$ in terms of the shape of this imaginary surface at any instantaneous position of the sphere.

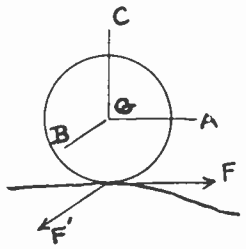

Fig. 1—A sphere traveling over a surface in the presence of friction.

Let ρ_1 and ρ_2 be the radii of curvature of the normal sections of the imaginary surface through the above tangents. Let χ_1 and χ_2 be the angles which the radii of curvature of the lines of curvature of the imaginary surface at the center of the sphere (G in Fig. 1) make with the normal. The classical theory then shows that

$$\theta_1 = -\frac{v}{\rho_2} \tag{2}$$

$$\theta_2 = \frac{u}{\rho_1} \tag{3}$$

$$\theta_3 = \frac{u}{\rho_1}\tan\chi_1 + \frac{v}{\rho_2}\tan\chi \tag{4}$$

$$\frac{d\omega_3}{dt} = \frac{uv}{a}\left(\frac{1}{\rho_2} - \frac{1}{\rho_1}\right). \tag{5}$$

These equations and (1) indicate that only if ρ_1 and ρ_2 are infinite, that is, only if the surface is a plane, does the analogy hold strictly.

Although this particular analysis refers only to the unreal case of pure loss-free rolling, it will be clear that, even if more realistic assumptions were used instead of those of point contact, and if a frictional force is used which is a constant multiple of the normal reaction and sufficient to produce pure rolling, we will find "spin" terms in the equations and must again conclude that they are only absent if surface is a plane.[1] To this extent classical theory of pure rolling may be usefully invoked.

2. *An Experiment to Test the Classical Theory*

The classical theory has an appearance of reality when (unlike the case quoted above) the frictional force, though not zero, is not sufficiently great for "pure rolling" to occur with no energy loss due to friction. On the other hand, in the presence of frictional loss, the classical equations cannot, of course, lead to an analogy with electron trajectories because these trajectories are assumed to be without any loss analogous to friction. Nevertheless, the question arose at the beginning of the investigation described in this paper as to whether the classical case showing frictional loss does, or does not, describe the trajectories of actual balls traveling over a rubber membrane with losses due to friction. If it does, then the errors of the rubber membrane analogy will be calculable for specific cases from the classical theory. Unfortunately, the following experiment shows that the classical theory fails in this respect.

The classical equations of motion when loss of energy exists due to friction leads to a simple analytical solution [13] for the case when the sphere rolls on an inclined plane. It is, therefore, possible in this instance to compare experimentally the classic theory and an observed result. A further advantage of this case for this purpose is that the solution of the differential equation for the rubber membrane when it is arranged as an inclined plane satisfies the Laplacian exactly.

This inclined plane case is illustrated in Fig. 2. The sphere rotates around G and travels down a plane which is inclined at an angle α for a distance x in a time t.

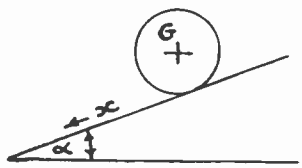

Fig. 2—A sphere traveling down an inclined plane.

According to the theory the frictional force is a fixed fraction μ of the normal reaction and it can then be shown that

$$x = g(\sin\alpha - \mu\cos\alpha)\frac{t^2}{2} \tag{6}$$

when g is the acceleration due to gravity. Hence, we have

$$\mu = \tan\alpha - \frac{2x}{gt^2\cos\alpha} \tag{7}$$

which shows that the classic theory requires that x/t^2 be constant for all values of t and x. The sphere according to this part of the theory both slides and rolls; that is, there exists a relative velocity S of the surface of the sphere and the surface over which it moves which is equal to $\dot{x} - \dot{\theta}a$. θ denotes the angle through which the sphere turns as it rolls.

The apparatus used for a test of the classical theory is illustrated diagramatically in Fig. 3. A photograph of the apparatus is shown in Fig. 4. A rubber membrane (latex sheet approximately 0.008 inch thick) was stretched evenly over the flat surface of a glass surface

[1] Walker (see reference [17]) and others appear to assume that if the relative heights of the boundaries in the rubber membrane are kept "small," the spin terms will then be negligible. In the author's opinion this is a dangerous assumption. There is no definition of "small."

plate. The surface plate was supported on three adjustable supports upon a second flat sheet of plate glass which was in turn supported on three further adjustable supports. This second glass sheet was accurately levelled so that the angle of inclination of the rubber, and its level in the dimension at right angles to the inclination, could both be set by means of a toolmaker's height gauge to better than 0.001 inch. These precautions were found to be essential.

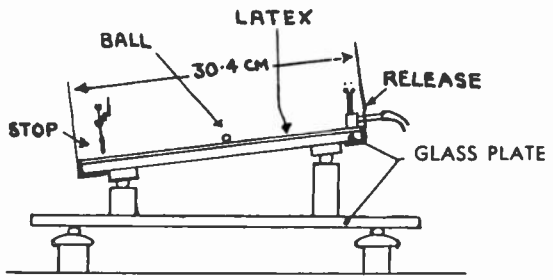

Fig. 3—Apparatus for the measurement of the trajectories of balls down an inclined plane. The two glass plates are each resting on three adjustable supports.

The ball was held until released by air suction against a vertical slit approximately 0.75 millimeter wide. The slit separated two copper contacts which were short-circuited by the metal ball until the air suction ceased and the ball moved away from the release point. This mechanism was found to hold the ball before release so that it was resting on the membrane and so that it was

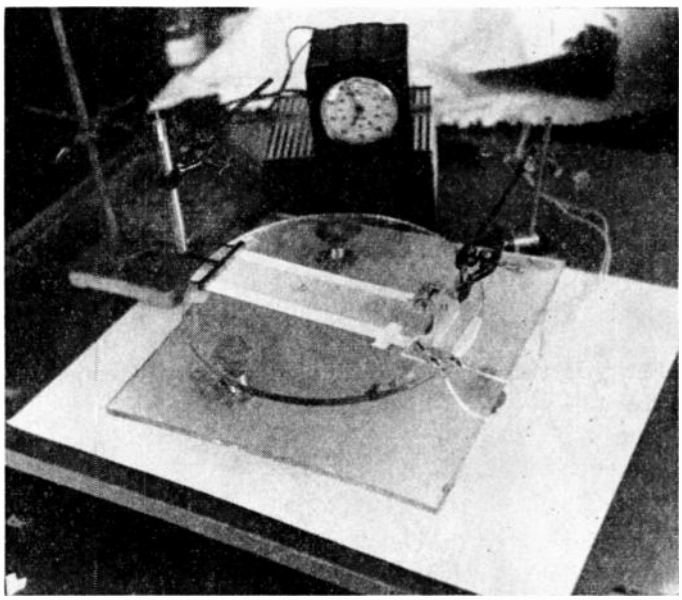

Fig. 4—A photograph of apparatus for measuring the trajectories of balls (see Fig. 3).

neither dropped nor pushed when it was released. At the end of the run the ball was arranged to strike a vane which was pivoted and balanced on dead center. As shown in Fig. 6 the ball, on arriving at the vane, caused it to close an electrical contact to a pool of mercury. The two contacts on the release mechanism and the two contacts on the vane were connected in parallel and to the input of a thermionic valve switch which actuated a clutch on a synchronous motor-type timer. This method of measuring the lapse of time was chosen after a consideration of various other methods. The photographic method using intermittent exposures which has been used by previous authors [3, 6] was found to produce errors which were difficult to control due to the movement of the ball during the exposure and to perspective and photographic difficulties. It was found by trial that the departure of the trajectories of balls moving on the membrane from the theoretical trajectories was in fact so great that a timing accuracy of much better than 0.005 second was not significant. In the timing experiments described, the ball traveled in a straight line, and it was found best to use the reliable and standard method of measuring the time intervals by means of a continuously running synchronous motor operating on 60 cycles. The motor was connected to an indicating pointer by energizing a dc clutch during the time of travel of the ball. The absolute lapse of time could then be read to better than the desired 0.005 second.[2] The geometrical quantities, including the angle of inclination, could be read with negligible error. The distance of travel of the ball was measured so as to include the movement of the vane at the receiving point. This movement was about a millimeter and was a small fraction of the total length of the path of the ball. The slowing of the ball in contact with the vane occurs over only a very small interval of time. The slowing down is slight and causes a second order error in the measurement of time which was regarded as negligible.

The over-all absolute error due to all causes was believed not to exceed 1 per cent for all significant measurements. The experiments were found to be repeatable with a much less relative error than this. Therefore comparisons between, for example, the performance of various kinds of steel and aluminum balls (as shown in Table II), were observable to a very much higher accuracy.

The coefficient of friction μ, which, according to the classical theory, should have been constant, was calculated from (7) using observed values of t and x. The results are shown in Table I.

TABLE I

TEST OF CLASSICAL THEORY

Latex sheet stretched over an optically flat surface. Angle of inclination $\alpha = 6.63°$. 0.25 inch diameter stainless steel ball weighing 1.037 grams.

x (cms)	μ
1.365	0.063
7.365	0.038
9.365	0.036
25.365	0.033

Table I shows that μ does not exist as a constant and the classical theory does not, therefore, apply to the rubber membrane.

[2] Model S-1 Timer. The Standard Electric Time Co., Springfield 2, Mass.

No measurement was made to separate the effects of air resistance from friction at the surface because the figures in the right hand column of Table I decrease with the distance traveled and with the increase of the mean velocity of the ball. While air resistance, which increases rapidly with velocity, may be affecting the absolute values of these figures it cannot affect the fact that the coefficient of friction is found not to be a constant.

A corresponding variation of μ was obtained when balls were rolled down an optically flat glass plate instead of over the latex surface. This latter test was performed because it seemed possible that a steel ball rolling on a flat glass surface might approximate to a point contact and so to the classical case, but this was found not to be so. Stainless steel balls of 0.125, 0.25, and 0.375 inch diameter and aluminum balls of 0.125 and 0.25 inch were used on both the glass and latex.

A further requirement of the classic theory is that the distance x traveled in a time t is independent of the mass and diameter of the ball. This was not found to be true of these experiments as will be shown later (Tables II and III).

It is not possible, therefore, to employ the classical theory to predict the trajectories of these balls on either a rubber membrane or on glass, or to give a quantitative measure of the error of the membrane analogy.

3. *The Theory and Region of Validity of the Analogy*

If we assume that energy losses due to the frictional force, including effects due to deformation of the membrane, do not change with the position of the sphere, then because these losses are found by experiment not to be constant, we can assume that they are a function of deformation and the relative velocity S of the surface of the sphere and the surface over which it is traveling. Unfortunately, there does not appear to be any quantitative statement of frictional force on a ball rolling on a rubber membrane, although substantial advances in this direction have been made, for example, by Tabor [15, 16]. Walker [17] has made a measurement of frictional force for balls of various diameters and weights traveling on a rubber sheet. He expresses the frictional force in terms of a certain range of values of translational velocity. He does not measure the rotational velocity of the balls. Therefore, the relationship between frictional force and the relative velocity S between the periphery and surface is not disclosed by his experiments. If the linear relationships he deduces between frictional force and translational velocity are applied without modification to the equations of motion for an inclined plane, the resulting solutions are invalid.

Friction, in fact, is not well understood and the combination of rolling and sliding friction including deformation presumably occurring in the rubber sheet analogy appears at present to be inadequately analyzed in the literature. It is appropriate to quote an interesting discussion on friction [18] which recently took place before the Royal Society in London. Remarks made by the chairman, Dr. F. P. Bowden, and by Dr. D. Tabor are particularly interesting as showing the need for further fundamental work on friction. Quoting Dr. Bowden: "Nowadays, when so many physicists are devoting their time to studying the complexities of nuclear disintegration, it (friction) may seem a humdrum topic, but there are times when it is well to remember that the world in which we live is not entirely made up of disintegrating nuclei and that some other physical properties of matter are important and, as I hope this discussion will show, may be of interest."

The question arises as to whether it is worth while for our purposes to produce a theory of energy loss to become part of a new set of equations which could be used to calculate the case of a rolling ball on a rubber membrane. The whole reason for the use of the rubber membrane analogy is to avoid the use of calculations or experiment to determine a specified two-dimensional electric field and trajectories; therefore the usefulness of a new set of equations would be confined solely to a comparison between the trajectories of an electron and the trajectories of a ball on a rubber membrane as a means of arriving at the theoretical error of the rubber membrane model. Such a comparison would not, of course, yield the practical error, which includes many factors set out later in this paper which are too complicated and indefinite for inclusion in a useful mathematical statement. Moreover, the new equations of motion would plainly be of the general kind exemplified by the classical equations (1), but would be considerably more complicated. It would certainly be found to be impossible to solve these new equations by analytical means, except perhaps for a few trivial cases such as those of the inclined plane. Particular numerical solutions would be all that would be obtainable for those cases to which the rubber membrane model is in fact applied; that is, for those cases where advanced types of vacuum tube are concerned. A convenient general formula for the error would not result.

It so happens that the corresponding electric field, and the trajectories of the electrons in that field, are expressed by governing equations far simpler than the governing equations of rubber membrane analogy. Corresponding trajectory equations of an electron are merely

$$\ddot{x} = \frac{e}{m}\frac{\partial V}{\partial x}$$

$$\ddot{y} = \frac{e}{m}\frac{\partial V}{\partial y}$$

and the corresponding electric potential equation is

$$\nabla^2 V = \frac{\rho}{\epsilon_0}$$

where V is the potential and e/m and ϵ_0 are constants. It would be pointless to use the rubber membrane model and to compute its errors in each particular case by numerical solutions of the new equations of motion; it

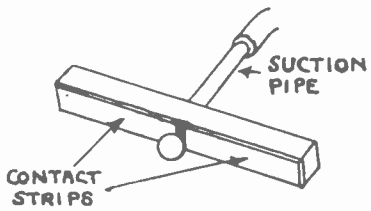

Fig. 5—The device used to hold a ball until it is released and to time the instant of release.

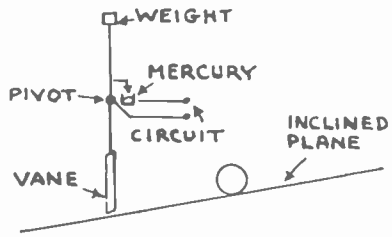

Fig. 6—The contact device used to record the time at which the ball reaches the end of its path.

would be far simpler to abandon the model altogether and to compute numerically[3] the electric field, with or without space charge, and the trajectories, by the solution of the far simpler field and trajectory equations which apply to the vacuum tube itself. Also, a direct calculation of this latter kind would be more accurate than the former because the practical errors of the rubber membrane would not appear.

From the special point of view, therefore, of a radio tube designer, it would appear that there is no point in producing a new set of equations to express accurately the trajectories of balls on a rubber membrane. It follows that the rubber membrane model must be regarded as an analogy in which the errors are not calculable as a practicable matter. It is not practicable to set up a rubber membrane model and to obtain from it a solution in which errors are calculated and known to lie between specified limits.

On the other hand, experience shows that it is sometimes possible to obtain useful information from a rubber membrane model if the results are subjected to a subsequent experimental check, or if they lie in fairly narrow limits between results previously known to be correct so that previously ascertained errors may be interpolated. The rubber membrane model is in fact capable of useful results in the hands of an experienced designer, but it cannot be regarded as a self-sufficient analog for which errors can be assessed without comparison with another method of obtaining the solution.

4. *An Experimental Investigation of the Membrane Model*

The vacuum tube designer requires as much guidance as possible in setting up the rubber membrane model for each case so that when he checks the results later by experiment there will be a reasonable chance that the error will then be found to be no more than is permissible. This prior guidance can largely be obtained from measurements of experimental errors obtained for a number of particular cases. A few such cases which the writer has found useful are set out below.

a) *The Choice of Diameter and Material of the Ball:* The ball which has the minimum of frictional loss will be that which travels the greatest distance down the inclined plane of Figs. 3 to 6 in a given time. In order to choose the most suitable ball type, balls of various diameters and materials were arranged to travel a distance of 15 centimeters between the contacts. Typical results are shown in Table II. The results shown in column five for latex differ from the result for glass shown in column four: on latex the 0.25 inch diameter stainless steel ball was less of an improvement over the 0.125 inch diameter ball than when the glass surface was used, and the 0.375 inch diameter stainless steel ball was slightly worse than the 0.25 inch diameter stainless steel ball. This effect was assumed to be due to the larger and heavier balls indenting into the latex whereas the glass remained flat. An aluminum ball always gave a slightly inferior result as compared to a heavier stainless steel ball of the same diameter.

TABLE II

Relative Values of x/t for Various Balls. Angle of Inclination 7.20°

Ball Diameter (inches)	Ball Material	Weight (grams)	Relative value of x/t	
			Glass Surface	Latex Surface on Glass Support
0.125	Stainless Steel	0.150	0.89	0.91
0.25	Stainless Steel	1.037	1.00	1.00
0.375	Stainless Steel	3.542	1.00	0.98
0.25	Aluminum	0.400	0.99	0.98

No attempt was made to do more than choose between readily available balls. Note that in these experiments the change from stainless steel to aluminum altered both the weight of the ball and the surface condition simultaneously.

Another test was made in which the membrane was not supported by glass, but was stretched over a frame in the usual way. A latex sheet was stretched across a frame approximately 35.5 centimeters square and was depressed by a metal bar along the center so as to form two inclined planes as shown in Fig. 7. An aperture in the metal bar enabled balls to roll down the left hand inclined plane to the right hand inclined plane as shown by the arrow marked "ball path" in Fig. 7. A slight and smooth rise of the membrane in the aperture removed any discontinuity at the junction of the two inclined planes. A photograph of this apparatus is shown in Fig. 8.

Similar precautions as regards leveling were taken as in the case of the previously described apparatus, and the angles of inclination either side of the depression in the middle were both equal to 4.00°. Although the mem-

[3] See note at the end of this paper.

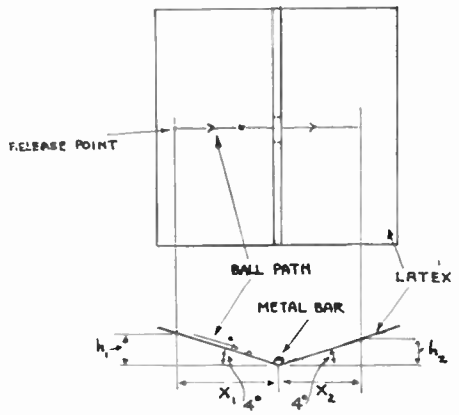

Fig. 7—An arrangement of two inclined latex rubber planes.

brane was bowed up slightly (about one millimeter) in the immediate neighborhood of the aperture a ball released in the center and from a height h_1 on the left hand side of Fig. 7 traveled in a straight line through the center of the aperture and straight up the right hand incline. At a height h_2 on the right hand incline the ball was brought to rest. At this point its kinetic energy is zero. The potential energy at a height h is mgh (where m is the mass of the ball) and the field of force is conservative. If there were no frictional loss h_1 would be equal to h_2. In practice h_2/h_1 will always be less than unity, and h_2/h_1 for a given ball will be a measure of the potential energy remaining at end of trajectory despite frictional losses on the way. Hence energy loss due to friction and air resistance is proportional to $1-h_2/h_1$.

Table III shows the results for various balls and shows that for different ball diameters, materials, and weights, the loss of energy due to friction and air resistance varies not only with the kind of ball but with height h_1 from which it is released. This is contrary to classical theory.

TABLE III

THE LOSS OF ENERGY OF BALLS TRAVELING ON INCLINED AND SUSPENDED LATEX PLANES. THE ANGLE OF INCLINATION 4.0°

Ball Diameter (inches)	Ball Material	Weight (Grams)	h_1 (cms)	h_2/h_1 or X_1/X_2	Loss of Energy $1-h_2/h_1$ per cent
0.125	Stainless Steel	0.150	0.38	0.76	24
			0.74	0.74	26
			1.14	0.73	27
0.25	Stainless Steel	1.037	0.37	0.84	16
			0.73	0.85	15
			1.12	0.83	17
0.125	Aluminum	0.061	0.38	0.71	29
			0.74	0.69	31
			1.14	0.66	34
0.25	Aluminum	0.40	0.37	0.81	19
			0.73	0.84	16
			1.12	0.81	19

The 0.25 inch stainless steel ball gave the least loss. It will be clear that even the minimum loss recorded produces a substantial error when the trajectory reaches its apex on the right hand plane of Fig. 7 because, from

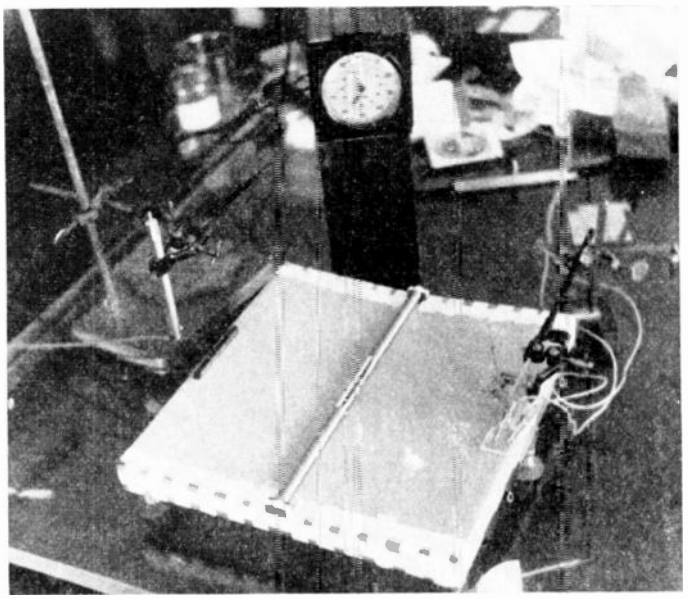

Fig. 8—A photograph of the apparatus illustrated in Fig. 7.

the geometry of Fig. 7, $h_2/h_1=X_2/X_1$ and an electron in the analogous constant electric field would travel a distance X_2 equal to X_1. An 0.25 inch diameter stainless steel ball was used in most subsequent experiments.

b) *The Error of a Ball Traveling Down an Inclined Plane:* In the case of an inclined plane the theoretical expression for pure rolling of a sphere is

$$x = \frac{5}{7} g \sin \alpha \cdot \frac{t^2}{2} \tag{8}$$

and is exactly analogous to the trajectory of an electron in a constant field.

A typical observed trajectory for a 0.25 inch diameter stainless steel ball rolling down the latex sheet in the apparatus of Figs. 3 to 6 is plotted as $x(t)$ in Fig. 9. The angle of inclination was 6.63°. The corresponding plot of (8) is also shown on Fig. 9.

The observed curve did not vary as t^2 as is required in order to provide an exact analogy. At lower values of t the error is substantial; at $t=0.23$ second, for example, the observed value of x is -36 per cent in error. The error varies with the angle of inclination.

We must deduce from this experiment that the rubber model has a substantial error especially at the lower velocities. In a membrane model of a cathode structure, where the ball starts from rest at the cathode, the analogy may have substantial errors of the order of that quoted and, in particular, trajectories which are not straight near the cathode will not have correct form.

c) *Launching Troughs:* A launching trough must be used when the initial velocity is not to be zero.

The launching trough used must guide the ball along at a suitable angle, and should produce a rotational velocity at the point of launching which is as near as possible to that which would have been found had the ball not been guided by the sides of the trough. It follows that only the bottom of the ball must touch the

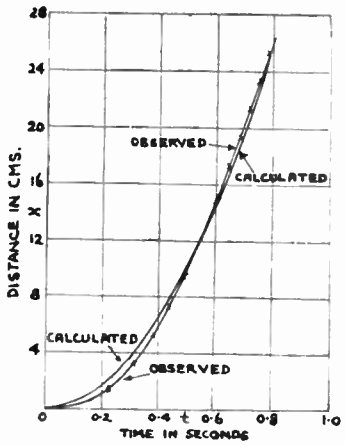

Fig. 9—A comparison of observed and calculated trajectories for the apparatus of Figs. 3 and 4. The angle of inclination was 6.63°. An 0.25 inch diameter stainless steel ball was used. Its weight was 1.037 grams.

trough. Fig. 10a shows a trough of circular cross section of which this is true, but theory shows that the motion down such a trough must involve side to side oscillations unless both trough and ball were infinitely smooth. An acceptable compromise appears to be a narrow guiding groove, as shown in Fig. 10b. The width of the groove can be such that the peripheral speed of the ball is nearly the same as it would be if it were not constrained by the groove. As a check of this, it was found that the use of this trough made no observable difference to the ratio h_2/h_1 when used in the experiments of section 4a instead of the left hand inclined plane shown in Fig. 7.

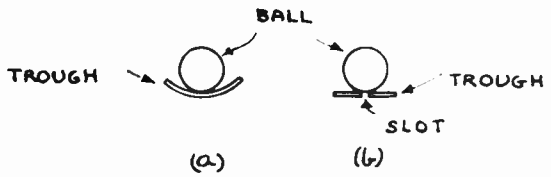

Fig. 10—Designs of launching troughs: (a) is not satisfactory; (b) is the type used by the author.

d) *The Membrane Analogy to a Constant Electric Field*: If an electron is launched into a region between two infinitely extended parallel plane electrodes at respective potentials V_1 and V_2 which are spaced by a distance D, and if the entrance angle is ϕ, then the electron trajectory will be given in terms of the spacing D by

$$y/D = \frac{x}{D}\tan\phi - \frac{x^2}{4D^2}(1+\tan^2\phi) \qquad (9)$$

if $V_1=0$ and V_2 is negative and numerically equal to the entrance energy in volts. The trajectory is a parabola. The maximum distance to which the electron travels in the y direction is

$$\frac{y_{max}}{D} = \sin^2\phi. \qquad (10)$$

The distance in the x direction corresponding to y_{max} is $x_1/D = 2\cos\phi\sin\phi$. The distance in the x direction of which the parabolic trajectory of the electron returns to the $y=0$ axis is $2x_1/D$.

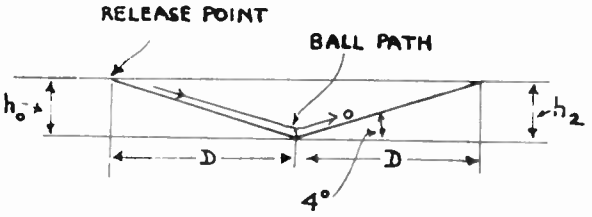

Fig. 11—Two inclined latex rubber planes which were used in applying the analogy to the case of a constant electric field.

The rubber membrane analogy to this case is the apparatus shown in Fig. 11. A launching trough is used on the left-hand plane so that the ball is launched into the right-hand latex plane at an angle ϕ. Here in the analogy the launching height h_0 corresponds to the initial electron potential V_0 and the equal height h_2 spaced from the center by the distance D corresponds to the potential V_2. Fig. 12 compares the parabola de-

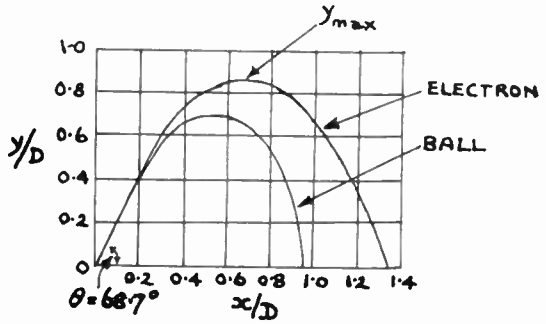

Fig. 12—A comparison between the trajectory of an electron in a constant electric field and the trajectory of an 0.25 inch stainless steel ball in the apparatus shown in Fig. 11. The angle of incidence was 68.7°.

scribed by the electron with the observed path of a 0.25 inch stainless steel ball. The ball path is not a parabola and x_1, x_2 and y_{max} are substantially in error as shown in Table IV. The conclusion from this experiment is that

TABLE IV

COMPARISON BETWEEN THE TRACK OF AN 0.25 INCH DIAMETER STAINLESS STEEL BALL (1.037 GRAMS) LAUNCHED INTO A MEMBRANE MODEL AND THE TRACK OF AN ELECTRON IN A CONSTANT ELECTRIC FIELD. THE ENTRANCE ANGLE WAS 6.87°. THE ANGLE OF INCLINATION WAS 4.00°

Quantity	Observed	Correct	Error
			per cent
y_{max}/D	0.70	0.868	−19.4
x_1/D	0.53	0.678	−21.8
x_2/D	0.97	1.356	−28.5

when this ball has started from rest at a launching height h_0 (analogous to a potential energy V_0) a very large error is produced if it is accelerated and then decelerated by rising to a height h (analogous to V) greater than about, say, 0.4 h_0 (analogous to 0.4 V_0).

In short, the rubber membrane analogy is not satisfactory for electrons which approach a reflecting electrode and produces gross errors if the electron is actually reflected back. This is shown to be so in Table IV, although errors due to "spin" are absent with the inclined

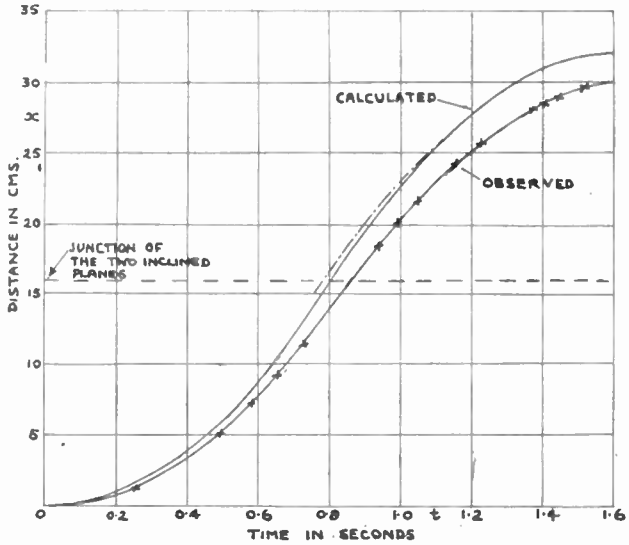

Fig. 13—A comparison between a calculated trajectory and an observed trajectory straight across the two inclined rubber planes of Figs. 7 and 8.

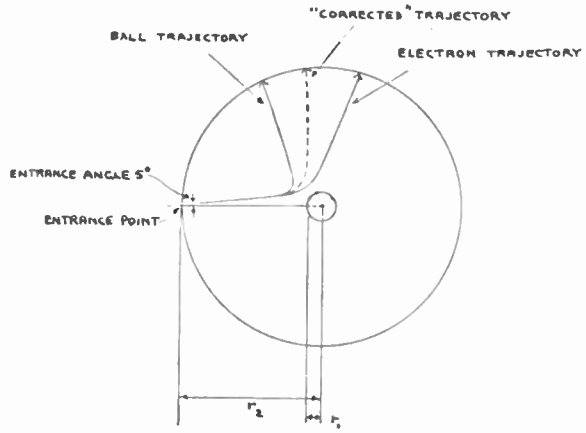

Fig. 14—A comparison between the trajectory of an electron in the field between two concentric cylindrical electrodes of radii r_1 and r_2 respectively at potentials zero and $-V_2$; and the trajectory of an 0.25 inch stainless steel ball in the analogous rubber membrane model. In both cases the initial potential energy was numerically equal to V_2.

plane experiment. The effect is important in conditions when it can be due only to energy loss.

The timing apparatus described with respect to Figs. 3, 4, 5 and 6 was next used with the inclined planes of Figs. 7 and 8 with $\phi = 90°$, that is, with the ball traveling straight across at right angles to the valley along the direction of greatest slope of both inclined planes. Fig. 13 shows the observed trajectory. The return trajectory is not shown. This observed trajectory is compared in Fig. 13 with the theoretical trajectory for perfect rolling. The error in terms of a comparison between the correct and observed distances x is large at the lower velocities at both ends of the trajectory, and the error is also large at the right hand side where the ball is brought to rest by the reverse slope of the membrane.

Only in the middle area of the graph is the error limited to about single figure percentages.

e) *The Analogy Applied to the Field between Concentric Cylinders:* The failure of the rubber membrane analogy when the ball and electron are decelerated more than a small amount (say, $h > 0.4h_0$) was demonstrated by a further experiment for a case where the "spin" terms are not zero and the electric field resembles that around a circular section grid wire at zero potential.

Fig. 14 shows a region between two concentric circular electrodes of radii r_1 and r_2 at potentials respectively of zero and $-V_2$. An electron entering the field on the outer electrode at $r = r_1$ at an entrance angle $\phi = 5°$ has the trajectory shown.

This trajectory was computed from the expression for potential

$$V = \frac{V_2}{\ln \frac{r_2}{r_1}} \ln \frac{r}{r_1} \qquad (11)$$

for concentric cylinders by a numerical solution of the trajectory equations.

An 0.25 inch stainless steel ball was launched from a height h_0 equal to the height h_1 of the central electrode r_1 into a rubber model of the field. In the analogy the radii $r_1 = 1$ cm, $r_2 = 10$ cm and $h_1 = 0.94$ cm. Latex sheet about 0.008 inch thick was used. The error in the trajectory of the ball when it was decelerated appreciably and h became more than about $0.4h_0$ is clear from Fig. 14.

f) *A Suggested Correction:* It has been suggested [3] that one can compensate for frictional error by increasing the height h_0 at which the ball is launched from the launching trough. Such an artifice applied to the right hand inclined plane in the case of the experiment plotted in Fig. 13 might be used to displace the second half of the curve so that it almost coincides with the theoretical curve (see dotted curve). However, because the trajectory of the ball is still not of the same form as that of the electron the "correction" can only be regarded as applicable to this special case. Also, inspection of Fig. 12 shows that there will still be a substantial error in both x_1/D and x_2/D for the ball trajectory because it is not parabolic.

Indefinite errors may exist despite this "correction" in the case of more complicated field shapes. The fact that this is so was demonstrated by applying the "correction" to the experiment of the last section (Fig. 14). The launching height was increased by 1/0.83 because, used at zero angle of incidence in the experiment of Fig. 7, section 4(a), the same ball produced a height ratio h_2/h_1 of 0.83. The result is shown by the dotted curve in Fig. 14. The "correction" is ineffective.

g) *Errors of the Potential Analog:* The differential equation of an infinitely thin rubber membrane is

$$\frac{\partial^2 z}{\partial x^2}\left[1 + \left(\frac{\partial z}{\partial y}\right)^2\right] + \frac{\partial^2 z}{\partial y^2}\left[1 + \left(\frac{\partial z}{\partial x}\right)^2\right] - 2\frac{\partial^2 z}{\partial x \partial y}\cdot\frac{\partial z}{\partial x}\cdot\frac{\partial z}{\partial y} = 0 \qquad (12)$$

where z is the displacement from a level plane. Only when $\partial z/\partial x$ and $\partial z/\partial y$ are very small is this a good ap-

proximation to the Laplacian for the electric field. Walker [15] has pointed out that for the region between two concentric cylinders the exact solution of this equation in radial co-ordinates is

$$z = a(\cosh^{-1} r/a - \cosh^{-1} r_1/a) \qquad (13)$$

where a is an arbitrary constant. This enables a comparison to be made between the trajectory of an electron in the true field given by (11) and the trajectory of an electron supposing that it was subjected to the rubber membrane kind of field given by (13).

This comparison was made for the case set out in section 4(e) and Fig. 14. In this case, the error of the ball compared to the exact electron trajectory was found to be negligible until the trajectory passes the center electrode r_1 in Fig. 14, and then a very slight error gradually appeared until the track according to (13) met the electrode r_2 approximately 0.1 cm out of position around the circumference of this electrode.

This was regarded as a negligible error in comparison with the other errors of the membrane analogy. The error would, of course, have been increased had the height of the electrode r_1 been much increased; but because all relative heights are commonly minimized in a membrane model in order to minimize the effects of "spin," it was concluded that we can disregard the theoretical error of the membrane model due to the non-Laplacian shape predicted by the differential equation (12) in view of the magnitude of the other errors.

The above has ignored oscillatory solutions for the displacement of the rubber membrane. Whether these are serious or not in a given case depends upon the particular membrane model and upon the speed, weight, and diameter of the ball. In practice, a suitable choice of the ball can usually be made to avoid vibration of the membrane.

The finite thickness of a rubber membrane results in a rounding of the contours where it passes over a raised edge representing an electrode. If a rubber membrane is stretched between two parallel electrodes of equal height, it is well known that the weight of the material must cause it to sag in the form of a catenary curve. It was found that an appreciable error is produced by these effects.

A test on a membrane stretched between two parallel electrodes of equal height two inches apart and extending for four inches showed that typical ball trajectories were substantially altered if they came nearer than about 0.5 inch from the electrode. It was found that the ball refused to travel parallel to the electrodes except in the middle of the space between the two electrodes. Notice that to demonstrate this effect the ball must be traveling; if it is initially at rest, the high value of static friction in comparison with rolling friction may prevent any movement of the ball toward the middle.

The principal result of these effects is a limitation upon the minimum slope, that is, upon the minimum analogous electric field which can be effectively represented by the analogy without rounding out the catenary curve causing an appreciable error in the representation by the rubber membrane of the smaller values of the electric field. It has also been pointed out by Allen and Phillips [9] that a limitation also exists to the minimum slope because of the indentation of the ball into the rubber.

It has been stated [17] that to minimize "spin," the inclination of the membrane to the horizontal should be everywhere less than, say, 10°.[4] If, for example, we assume that the maximum allowable inclination is 10°, then we may assume that the analogy may reasonably be required to represent, within say 5 per cent error, an electric field corresponding to, say 2 per cent of this maximum inclination of 10°. This means that the base of the model as a whole, with respect to which the inclination is measured, must be level to about 0.01°. This is a degree of precision which is not attained without special precautions.

The effects of the errors in the shape of the membrane are, therefore, by no means negligible. It does not appear practicable to state these errors in usable quantitative form.

5. *Conclusions about the Rubber Model*

The uses of the rubber sheet model are limited by the considerations set out in section 3. In short, it is dangerous to use such a model in the investigation of new tube designs without a final system of checks. The experiments described above indicate as a very rough rule of thumb that errors will be gross if the trajectory deviates much from a straight line near the start, and if the electron path corresponds to a ball path such that the height h anywhere exceeds about 0.4 of the initial height h_0. The analogy cannot be used to study reflected or sharply diverged electrons.

The errors of "spin" are not calculable for practical rubber models; however, in practice, suitable experimental or numerical checks may avoid serious spin error. But we must assume that any errors we have found in the simpler cases are likely to be less than those we will find in the more complicated cases due to the quantitatively unknown effects of "spin."

The lowest errors indicated by the experiments are not less than single figure percentages. This means that the analogy cannot, in general, be used for electron optics and like purposes. For the evaluation of most lens aberrations, for example, at least six or more significant figures are needed; six significant figures correspond to an error of between 0.001 and 0.00011 per cent.

The errors stated and precautions advocated apply to cases where the model is modified to include the effects of space charge [6]. Any errors due to the space charge modifications are additional. The present author has not assessed them.

[4] Strictly the angle of inclination has nothing to do with "spin" which depends upon the radii of curvature and angles of radii to the normal as set out in section 1.

It is of interest to compare the conclusions of the present paper with certain results described in the literature. As Walker [17] points out, Kleynan [3] is in error in his calculations of the forces on a moving sphere. Kleynan's correction of the height reached by a ball on an inclined plane is not a correction of the error of the ball. His comparison in his Figs. 6 and 7 with calculated trajectories may be somewhat misleading because the calculation uses graphical "arcs of circle" method of electron tracking and this also possesses errors (see Part II). The experiments of sections 4(d) and 4(e) show that the reflected trajectories near negative grid wires shown in Kleynan's Fig. 8 must be very greatly in error. Alma, Diemer and Groendijk [6] show an agreement with a Pierce gun (their Fig. 5) which appears to be consistent with the present analysis, but the reflected trajectories found for the multi-velocity conditions in a triode (their Fig. 12) appear to be greatly in error. Because there is no experimental or mathematical check on this result, we must regard this use of the analogy to be an incorrect one in the light of the argument of section 3 of this paper. Walker [17] states (p. 323) that the error in kinetic energy of a ball can be kept within less than 2 per cent of the difference in potential energy at the boundaries provided that the path length is little more than the shortest distance between the electrodes. This is contradicted here by the experiments of section 4(d) and Figs. 12 and 13. On the other hand, Zworykin and Rajchman [4] used careful experimental checks on the results of a membrane model in much the same way as that advocated in the present paper and the membrane model was therefore of value in the early research on the then new field of electrostatic electron multipliers.

II. The Resistance Paper Analogy

1. *The Equipment*

The flow of electric current through a thin uniform conducting sheet will produce a potential distribution which satisfies the Laplacian and which is, therefore, an analog of a two-dimensional electric field.

Kirchoff [11] over a hundred years ago appears to have been the first to use this method and Liebmann [12] has published a brief account of a practical method using telegraph resistance paper.[5]

The essentials of the apparatus are shown in Fig. 15. The probe and a null reading galvanometer are used with a calibrated potentiometer to indicate the potential anywhere on the resistance paper. The current flow over the paper is between electrodes painted on the surface with conducting paint.

The author has compared the results of this analogy with a number of exact solutions of potential and electron trajectories obtained by numerical methods. It was found that the full performance of the analogy was not obtained unless the following precautions were taken first.

The current flow through the paper should be kept as low as possible or nonlinear resistance effects appear and distort the field. If the current applied to paper sheets of some inches square having minimum path lengths of the order of a centimeter does not exceed about one milliampere, this error appears to be negligible compared to others. A platinum point is used for the probe. The silver paint usually[6] used requires baking at about 150°F after application. This process tends to remove moisture from the paper. The use of an ordinary graphite pencil to draw equipotential lines is found to alter the resistivity of the paper so that the equipotentials move as the lines are drawn. A high resistance marking material is necessary.[7]

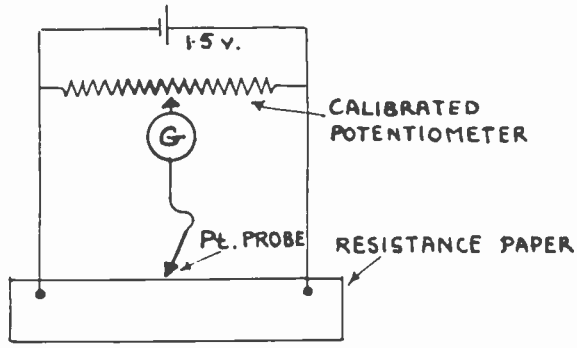

Fig. 15—Apparatus used for operating the resistance paper analogy.

If these precautions are taken, the performance of the paper is such that, in order to make the errors of the measuring equipment (Fig. 15) less than that of the paper itself, a 10,000 ohm potentiometer is used which is adjustable by decade switches to 0.0001 of the total potential across the potentiometer with an accuracy of 0.1 per cent of the fourth figure.[8]

2. *The Use of the Analogy*

The resistance paper gives an approximate potential solution which can be used to yield electron trajectories.

It is usually found by comparison with a numerical solution that the potential thus obtainable from the paper is accurate to about three significant figures (an error of slightly better than 1 per cent. These figures can then be improved by numerical methods to obtain an extra figure or more. This final mathematical solution is then differentiated and the trajectory equations solved by the method of the finite difference calculus. All errors due to the resistance paper are thus removed and the solution can be taken to any desired accuracy. The analogy is not required to provide more than the starting figures for a mathematical and exact solution.

A more usual use of the resistance paper analogy is

[5] "Teledeltos" L39 low resistance paper; International Standard Electric Corp., 50 Church Street, New York 7, N. Y.

[6] E. I. du Pont de Nemours and Co., Inc.; Silver coating material No. 4929.

[7] For example, Eberhard Faber "Mongol" colored pencils No. 865 blue and No. 866 red.

[8] Muirhead type A-201 voltage dividing resistance.

to draw equipotentials on the resistance paper using the apparatus of Fig. 15. A usual graphical method of tracking electrons is used to give the trajectories.

Fig. 16 shows a tracing of part of a solution in the form of equipotentials drawn on resistance paper. The chain dotted line shows a trajectory plotted by graphical means using these equipotentials and a graphical electron tracking method. This trajectory is somewhat in error. The full line with arrow heads is the correct trajectory which was obtained by numerical computation throughout and, therefore, involves neither the error of the resistance paper, nor that of a graphical method of electron tracking. The author believes that he and his associates have tried most if not all of the various published graphical methods of tracking. They have found that the error depends so much upon the skill and patience of the individual operator that mathematical estimates of the error of these step-by-step methods appear to be meaningless.

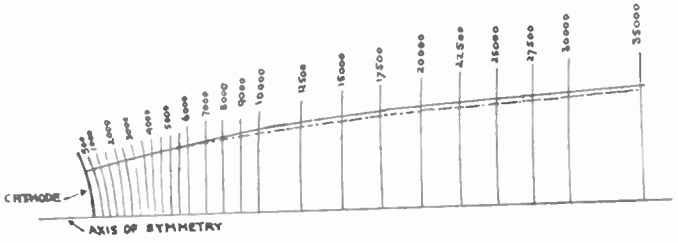

Fig. 16—A tracing of equipotentials obtained from resistance paper. The dotted line is a trajectory obtained by step-by-step graphical methods of electron tracking using the equipotentials. The full line is the correct electron trajectory obtained by numerical solutions of potential and trajectory equations.

Apart from the well known "arcs of circles" method, which is useful in certain cases, the author usually employs a method of joined parabolic segments due in its essentials to Selgin [19]. Selgin used a geometrical construction throughout; the author, however, finds it preferable to calculate the angles on a desk calculator and only to lay out the steps on the paper by graphical means.

3. *The Errors of Graphical Step-by-Step Methods of Electron Tracking*

Fig. 17 illustrates the errors of graphical tracking itself. A tracing is shown of the equipotentials of a portion of a discharge tube near a cylindrical cathode and a zero potential focussing electrode. These equipotentials and the trajectories indicated by full lines with arrow heads were computed by rigorous numerical computation and may be regarded as exact within better than the limits of graphical representation. These exact equipotentials, with the computed trajectories indicated in Fig. 17, were then used by a computer as data for graphical tracking. Selgin's formula was used. To perform this graphical process, extra equipotentials were interpolated as shown, for example, on the trajectory marked *J*. (Other extra equipotentials which were used are not shown in Fig. 17 for the sake of clarity.) The graphical methods of tracking yielded trajectories which, on the scale of Fig. 17, were indistinguishable from the exact trajectories in the case of tracks *D*, *E*, *F* and *H*. In the case of tracks *G*, *I*, *J* and *K* the graphically tracked trajectories diverged from the exact tracts as shown by the chain-dotted lines in Fig. 17.

The errors of the graphical tracking on *G* and *J* are due to mistakes made by the computer. There is no method of graphical step-by-step tracking known to the author for checking graphical errors when the process is in progress, except by the unreliable method of continuous repetition. Hence the errors in tracks *G* and *J* were not detected by the computer until a comparison was made with the exact trajectories. Notice that about a hundred graphical steps were taken correctly; only two were in error, but, as a result, two out of eight trajectories were wrong. (By way of comparison, the numerical methods of the finite difference calculus used to produce the correct trajectories are subject to differencing and other automatic checks which are continuous and automatic during the solution of the trajectory equation.) Unfortunately, in the practical use of the resistance paper analogy, exact trajectories are not available for use as checks; if they were, the use of the analogy would itself be redundant. Repetition and comparisons between different and adjacent graphical tracks are all that can be used to detect errors. This procedure is tedious and dependent for success upon operator's skill.

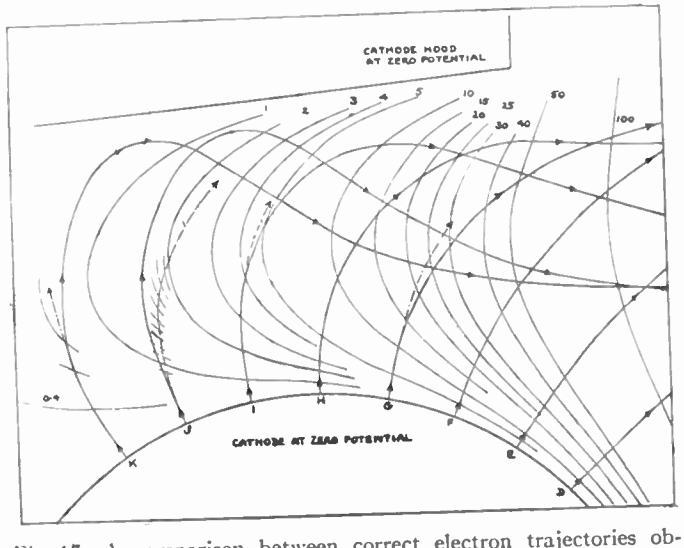

Fig. 17—A comparison between correct electron trajectories obtained by numerical computation and trajectories obtained by step-by-step graphical methods.

The errors exhibited in Fig. 17 on tracks *I* and *K* are inherent to the graphical method. Both of these tracks fail to curve sharply enough. Despite the interpolation of equipotentials at the closest practicable intervals, the usual assumption that the field can be regarded as linear between each pair of equipotentials for the purposes of each step of the graphical step-by-step process must lead to error of this kind. For a finite length of step it can easily be shown that there is a limit to the curvature of the trajectory which can be computed; this

limit is passed by tracks I and K soon after they leave the cathode. In other words, the high order derivatives of the trajectory are neglected. Unfortunately, if the length of each step is shortened to avoid this error, the resulting accumulation of errors from the graphical settings at each of the increased number of steps becomes equally serious. A quantitative statement of this error for all field shapes likely to be used appears impractical.

In the writer's experience of comparisons with exact trajectories, these graphical methods of tracking break down if the curvature of the trajectories is sufficient to describe reflected electrons. Moreover, unless great care is taken, and a number of slightly differing trajectories are graphically computed in the same region, and unless smooth curves of electron track positions are found to exist at all places in the region (in Fig. 17 a test would be to plot the position of each track along a vertical line cutting all the trajectories to the right of the hood) graphical tracking appears to be subject to wild and often undetected cumulative errors.

4. *Conclusions for the Resistance Paper Model*

The two dimensional potential fields obtainable from resistance paper can have an average error which is reasonably low, even less than 1 per cent if all suitable precautions are taken; but, unlike the rubber membrane, the trajectories are then only obtainable directly from the resistance paper by step-by-step graphical tracking and the errors of this lead to the same need for check by numerical calculation or by final experiment as should be applied to the results of the rubber membrane model.

Resistance paper can sometimes be used to supply an initial start for a numerically calculated potential solution which is then subject to the usual computing checks. All errors due to the analogy are eradicated by the calculation.

There appears to be no published way of accurately computing space charge effects by resistance paper. Liebmann [12] states that such effects can be obtained by perforating the paper or painting it with a graphite solution; but this does not appear to be an accurate method.

The resistance paper model has been used to represent in a transistor the flow of minority carriers at zero frequency [20]. The flow of electric current through resistances attached to the edges was used to simulate the loss of current by surface recombination. It has been shown by the present writer [21] that this use of the resistance paper model results in very substantial errors.

General

Provided that the results are always checked by experiment, or by exact computation, the rubber membrane and resistance paper analogies can be used as a guide to the design of some vacuum tubes. If such checks are omitted, serious error may be produced. The accuracies of both analogies are limited and the regions of validity of both cannot be quantitatively defined in practice. An attempt has been made in the present paper to indicate the conditions to be avoided and the precautions which should be taken in the use of both analogies.

A Note on Numerical Methods of Calculation

The static potential function for any arbitrary boundary shape of the electrodes can be found by solving the governing differential equation for numerical values. These values are spaced at the mesh points of a matrix having appropriate boundary shapes and potentials. The method of solution is by relaxation using the resources of the calculus of finite differences. This is a relatively recent development of the numerical solution of ordinary and partial differential equations and is due to Dr. L. Fox [22]. The process is a digital one and is capable of any desired accuracy [23]. The equations of motion of the electrons may also be integrated by this process [24] or by classical methods [25]. Space charge effects can be included by the use of successive iterations which start with an initial estimate of the space charge distribution. This process converges satisfactorily.

Numerical methods could be used in a somewhat similar way to calculate the trajectories of spheres over a rubber membrane; but for the reasons already given this has not been done.

The numerical solutions shown in this paper were calculated straightforwardly by these procedures. Special difficulties do arise however in the application of these methods to some of the broader problems found in the design of vacuum tubes. Special artifices are then required which are not within the scope of the present paper and which do not appear to have been published. The author hopes to describe this relatively new development in a later contribution; meanwhile, a paper on similar problems of computing transistor performance for realistic geometries [21] has been accepted for publication and illustrates the methods in part.

Acknowledgments

The numerical calculations quoted in this paper were carried out by Miss Irene Willis, and the apparatus in its many developmental stages and final form was made by Mr. F. J. Amos, to both of whom the author's thanks are due.

Bibliography

[1] Oliphant, M. L., and Moon, F. B., "Current Distribution Near Edges of a Discharge Tube Cathode." *Proceedings of the Cambridge Philosophical Society*, Vol. 25 (1928–1929), pp. 461–481.

[2] Smyth, P. H. J., Rumbaugh, L. H., and West, S. S., "A High Intensity Mass Spectrometer." *Physics Review*, Vol. 45 (May 15, 1934), pp. 724–726.

[3] Kleynan, P. H. J. A., "The Motion of an Electron in Two-Dimensional Electrostatic Fields." *Philips Technical Review*, Vol. 2, No. 11 (1937), pp. 338–345.

[4] Zworykin, V. K., and Rajchman, J. A., "The Electrostatic Electron Multiplier." PROCEEDINGS OF THE IRE, Vol. 27 (1939), pp. 558–566.
[5] Zworykin, V. K., Morton, G. A., Ramberg, E. G., Hillier, J., and Vance, A. W., *Electron Optics and the Electron Microscope*. New York, John Wiley & Sons, Incorporated (1945).
[6] Alma, G. A., Diemer, G., and Groendjik, H., "A Rubber Membrane Model for Tracing Electron Paths in Space Charge Fields." *Philips Technical Review*, Vol. 14, No. 11 (1953), pp. 336–343.
[7] Clark, J. W., and Neuber, R. D., "A Dynamic Electron Trajectory Tracer." PROCEEDINGS OF THE IRE, Vol. 38 (May, 1950), pp. 521–524.
[8] Hollman, H. E., "Theoretical and Experimental Investigations of Electron Motions in Alternating Fields with the Aid of Ballistic Models." PROCEEDINGS OF THE IRE, Vol. 29 (February, 1941), pp. 70–79.
[9] Allen, K. R., and Phillips, K., "Use of a Rubber Sheet Model." *Electronic Engineering*, Vol. 27, No. 324 (February, 1955), pp. 82–85.
[10] Sander, K. F., Oatley, C. W., and Yates, J. G., "Factors Affecting the Design of an Automatic Electron-Trajectory Tracer." *Journal of the Institution of Electrical Engineers*, Part III (July, 1952), pp. 169–180.
[11] Kirchoff, G., "Ueber ven Durchgang Eines Elektrischen Stromes Durch Eine Ebene, Insbesondere Durch Eine Kreisförmige." *Annallen der Physik* (Leipzig), Vol. 64 (1845), p. 497. "Collected Papers," (Leipzig) (1882), p. 56.
[12] Liebmann, G., "Electrical Analogues." *British Journal of Applied Physics*, Vol. 4 (July, 1953), pp 193–200.
[13] Loney, S. L., "Dynamics of a Particle." Cambridge, The Cambridge University Press (1950).
[14] Routh, E. J., "Dynamics of a System of Rigid Bodies." 6th Ed. Dover Press (1905).
[15] Tabor, D., "Elastic Work Involved in Rolling a Sphere on Another Surface." *British Journal of Applied Physics*, Vol. 6 (March, 1933), pp. 21–23.
[16] Tabor, D., "The Mechanism of Rolling Friction." *Philosophical Magazine*, Vol. 43 (1952), pp. 1055–1059.
[17] Walker, G. B., "Factors Influencing the Design of a Rubber Model." *Journal of the Institution of Electrical Engineers*, Part II, Vol. 96, pp. 319–324.
[18] A Discussion on Friction Led by F. P. Bowden. *Proceedings of the Royal Society A*, Vol. 212, pp. 439–519.
[19] Selgin, P. J., "Plotting Electron Paths." *Electronics*, Vol. 21 (September, 1948), pp. 124–126, 162–166.
[20] Moore, A. R., and Pankove, J. I., "The Effect of Junction Shape and Surface Recombination on Transistor Current Gain." PROCEEDINGS OF THE IRE, Vol. 42 (1954), pp. 907–913.
[21] Harries, J. H. O., "An Analysis of Transistor Performance as a Function of Frequency and for Realistic Geometries." *Quarterly Journal of Mechanics and Applied Mathematics*. Forthcoming paper accepted for publication.
[22] Fox, L., "Some Improvements in the Use of Relaxation Methods for the Solution of Ordinary and Partial Differential Equations." *Proceedings of the Royal Society A*, Vol. 190 (1947), pp. 31–59; "The Numerical Solution of Elliptic Differential Equations When the Boundary Conditions Involve a Derivative." *Philosophical Transactions of the Royal Society A*, Vol. 242, No. 849 (1950), pp. 345–378.
[23] Fox, L., "Some New Methods for the Numerical Integration of Ordinary Differential Equations." *Proceedings of the Cambridge Philosophical Society*, Vol. 45, Part I, pp. 50–68.
[24] Burfoot, J. C., "Numerical Ray Tracing in Electron Lenses." *British Journal of Applied Physics*, Vol. 2 (January, 1952), pp. 22–24.
[25] Scarborough, J. B., "Numerical Mathematical Analysis." Johns Hopkins Press, 1950.

Radar Polarization Power Scattering Matrix*

C. D. GRAVES†

Summary—**Because the polarization sense of an electromagnetic wave is changed when the direction of propagation is reversed, a new type of polarization vector which is directionally dependent is introduced. The scattering matrix formulation is then introduced in terms of directional vectors and directional transformation matrices, and the transformation of the scattering matrix under a unitary change of polarization basis transformation is shown to be a congruent transformation. The congruent sub-group of unitary transformations of the polarization basis is then discussed, and it is shown that the scattering matrix can be reduced to diagonal form by this sub-group of transformations. A new matrix, called the polarization power scattering matrix, is then introduced and its relation to the scattering matrix is discussed. The power matrix gives the total power back-scattered from the target for any transmitted polarization. It specifies the scattering matrix up to two phase angles (one of which is of no importance), and is more easily measured. The total power scattering matrix can be determined for any target by measuring only the total power in the backscattered return; no phase measurement is necessary and only plane polarizations need be transmitted.**

* Original manuscript received by the IRE, June 6, 1955; revised manuscript received, September 6, 1955. Work supported by the Signal Corps.
† University of Michigan, Willow Run Labs., Ann Arbor, Mich.

Polarization Vectors

THE electric field vector of an electromagnetic wave transmitted from a radar and propagating in the z direction referred to a Cartesian x and y coordinate system or basis has components E_x and E_y:

$$\vec{E} = \mathrm{Re}\,(E_x\vec{e}_x + E_y\vec{e}_y) \tag{1}$$

where

$$E_x = A_x e^{j\phi_x} e^{j(\omega t-\beta_z)}$$
$$E_y = A_y e^{j\phi_y} e^{j(\omega t-\beta_z)} \tag{2}$$

and $\vec{e}_x$ and $\vec{e}_y$ are unit vectors and the other symbols have their usual meaning. In the x-y plane the locus of the tip of the electric field vector will in general form an ellipse and will, for example, describe the ellipse in time in a clockwise fashion (right-hand sense) looking in the direction of propagation if E_x leads E_y in phase. The figure described by the field vector is called the polarization of the wave. Since the polarization is

completely specified by the ratio of the x and y components,[1] we can suppress the dependence on t and z, and write the electric field vector as 2×1 matrix with complex components; e.g., in a Cartesian x, y basis

$$\vec{E} = \begin{pmatrix} E_x \\ E_y \end{pmatrix} = \begin{pmatrix} A_x e^{j\phi_x} \\ A_y e^{j\phi_y} \end{pmatrix}. \tag{3}$$

A scalar product of any two complex vectors may then be defined using conventional matrix multiplication:

$$\vec{V}\cdot\vec{U} = \tilde{V}^*U = v_1^*u_1 + v_2^*u_2 = (\vec{U}\cdot\vec{V})^* \tag{4}$$

where V^* is the complex conjugate of V and $\tilde{V}$ is the transpose (rows and columns interchanged) of V. The scalar product of the electric field vector with itself is simply the power contained in the electromagnetic wave. Two non-vanishing vectors are said to be orthogonal if their scalar product is zero:

$$\vec{V}\cdot\vec{U} = 0. \tag{5}$$

Change of Basis

We have so far discussed elliptically polarized electromagnetic waves with respect to a Cartesian x, y basis. It is often convenient to refer elliptically polarized waves to some other orthogonal basis. Once the components of a vector are known wtih respect to one basis, they can be found with respect to any other. If the vectors e_1 and e_2 and the vectors e_1' and e_2' are any two sets of basis complex vectors for the two-dimensional space (for example a plane polarized x, y basis and a circularly polarized right and left-hand sense basis), then we may always write one basis as a linear combination of the other:[2]

$$\begin{aligned} \vec{e_1}' &= \vec{q_{11}e_1} + \vec{q_{12}e_2} \\ \vec{e_2}' &= \vec{q_{21}e_1} + \vec{q_{22}e_2} \end{aligned} \tag{6}$$

or

$$\begin{pmatrix} e_1' \\ e_2' \end{pmatrix} = \begin{pmatrix} q_{11} & q_{12} \\ q_{21} & q_{22} \end{pmatrix} \begin{pmatrix} e_1 \\ e_2 \end{pmatrix}. \tag{7}$$

The complex square matrix $Q=q_{ij}$ is called the change of basis matrix. In changing the reference basis of a polarized electromagnetic wave to another basis, the power in the wave must be conserved; i.e., the magnitude of E must be invariant under the change-of-basis transformation. Thus we are only interested in unitary change-of-basis transformations, because under these transformations the magnitude of a vector invariant.

The type of transformation of interest for polarized waves is then

$$E' = QE, \tag{8}$$

where Q is the unitary matrix which transforms the basis complex vectors to a new basis and E' is then the polarized wave referred to the new basis. Imposing the further restriction that the determinant of the transformation matrix Q is $+1$, yields an interesting insight into the transformation. The unitary condition on Q yields four real equations. The additional condition on the determinant yields a fifth equation. Thus only three of the eight quantities (the 4 complex q_{ij}'s) in the transformation are independent; hence, to specify this type of change-of-basis transformation, we need only specify three independent quantities. However, for the transformation to be useful, three independent quantities should be chosen so as to have some easily interpretable physical meaning in the electromagnetic wave. This problem has been considered in some detail by workers in the field, and it has been shown that a very convenient choice for the three transformation quantities are the phase, ellipticity and the orientation of the elliptical vectors.[3]

Direction Complex Vectors

In the above sections we discussed elliptically polarized basis vectors and unitary transformations of these vectors. We defined the polarization of these vectors looking in the direction of propagation of the wave, say in a positive z direction, and using a right-handed coordinate system. In discussing radar scattering it is convenient to use the same coordinate system for both the transmitted and back-scattered field; i.e., to use the same complex basis vectors to resolve both the transmitted and back-scattered fields into components. However, to do this, it must be possible to distinguish the direction of propagation of the polarized wave, since two waves with the same components but traveling in opposite directions will have opposite senses of polarization. Therefore subscript plus (+) and minus (−) signs are used to indicate the direction of propagation and the vectors are called direction vectors. Thus a wave propagating in the positive z direction has components

$$E_+ = \begin{pmatrix} E_1 \\ E_2 \end{pmatrix}_+. \tag{9}$$

A wave traveling in the $-z$ direction has components

$$E_- = \begin{pmatrix} E_1 \\ E_2 \end{pmatrix}_-, \tag{10}$$

where E_1 and E_2 are the components of the wave referred

[1] V. Rumsey, G. Deschamps, M. Kales, and J. I. Bonnert, "Techniques for handling elliptically polarized waves with special reference to antennas," Proc. IRE, vol. 39, pp. 533–534; May, 1951.

[2] G. Birkhoff, and S. MacLane, "A survey of Modern Algebra," The Macmillan Co., New York, N. Y., pp. 192–193; 1948.

[3] A general discussion of change of polarization basis transformations is given in J. Huynen, and W. Thormahlen, "Interim Engineering Rep. No. 2; On Effect of Polarization on the Radar Return from Ground Targets and Rain," (Confidential Classification) Dalmo Victor Co., San Carlos, Calif.; 1953. A very limited discussion is given in reference 1.

to some fixed reference basis; e.g., right and left circular polarizations.

We must now define the operations on direction vectors which will be useful for polarization analysis. The scalar product of a positive and a negative direction vector with components v_i and u_i defined by

$$V_+ \cdot U_- \equiv \tilde{V}U = v_1u_1 + v_2u_2 = U_- \cdot V_+ \tag{11}$$

and is different from the usual scalar product given by (4). The unitary change-of-basis transformation matrix Q operating on a positive direction vector

$$E_+' = Q_{++}E_+ \tag{12}$$

would have a corresponding change-of-basis transformation Q^* operating on a negative direction vector:

$$E_-' = Q_{--}{}^*E_-. \tag{13}$$

Thus we may say that $Q_{++}=Q_{--}{}^*$, where the equality is meant to imply that, when viewed from the same coordinate system, a positive direction transformation Q_{++} on the positive direction vector E_+ has the same effect as a negative direction transformation, $Q_{--}{}^*$, on the negative direction vector E_-. We can also define a direction matrix M_{+-} or M_{-+} as an arbitrary transformation with matrix M operating on a direction vector which not only transforms the components but reverses the direction of propagation. Thus,

$$\begin{aligned} E_-' &= M_{-+}E_+ \\ E_+' &= M_{+-}E_-. \end{aligned} \tag{14}$$

Note that the second subscript on a matrix indicates the type of vector it operates on and first subscript indicates the type of vector resulting from the transformation. Thus, $Q_{++}E_-$ or $M_{+-}E_+$ are not defined.

The Scattering Matrix

The field back-scattered from a target for an arbitrarily polarized transmitted wave can be specified using a complex scattering matrix formulation.[4] The scattering matrix referred to a complex x and y basis and omitting the range dependence is defined by:

$$\begin{pmatrix} E_x{}^S \\ E_y{}^S \end{pmatrix} = \begin{pmatrix} a_{11} & a_{12} \\ a_{21} & a_{22} \end{pmatrix} \begin{pmatrix} E_x{}^T \\ E_y{}^T \end{pmatrix} \tag{15}$$

or

$$E^S = AE^T, \tag{16}$$

where the superscripts S and T refer to the back-scattered and transmitted (incident) fields, respectively, and where $a_{12}=a_{21}$ by reciprocity. Thus, we see that the back-scattered field at either polarization is due in part to the transmitted field at that polarization and in part to the transmitted field of the orthogonal polarization which has been "cross polarized" by the target.

A noteworthy aspect of the scattering matrix formulation is the fact that the transmitted wave and the back-scattered wave are traveling in opposite directions. Thus a three-dimensional problem is being characterized with only two dimensions. This procedure is permissible providing the distinction between the two waves is kept in mind at all times. This distinction is directly evident by writing the scattering matrix formulation in terms of direction vectors and matrices as:

$$E_-{}^S = A_{-+}E_+{}^T. \tag{17}$$

We see that in the scattering matrix formulation the transmitted and back-scattered fields are given by the elliptically polarized direction vectors

$$E_+{}^T = \begin{pmatrix} E_1{}^T \\ E_2{}^T \end{pmatrix}_+, \qquad E_-{}^S = \begin{pmatrix} E_1{}^S \\ E_2{}^S \end{pmatrix}. \tag{18}$$

The component of the back-scattered field that would be received by the transmitting antenna is then given by the direction scalar product (11):

$$E_+{}^T \cdot E_-{}^S \tag{19}$$

where $E_+{}^T$ is normalized to unit magnitude. Similarly the component of the back-scattered field that would be received by another antenna with a different polarization $E_+{}^R$ would be given by the direction scalar product:

$$E_+{}^R \cdot E_-{}^S, \tag{20}$$

where $E_+{}^R$ is normalized to unit magnitude.

Transformation of the Scattering Matrix

We are now in a position to examine the transformation properties of the scattering matrix. If the basis undergoes a unitary transformation Q^{-1}, (where Q^{-1} is the inverse transformation of Q), then the transmitted and back-scattered field will be transformed as indicated in (12) and (13):

$$\begin{aligned} E_+{}^T &= Q_{++}E_+{}^{T'} \\ E_-{}^S &= Q_{--}{}^*E_-{}^{S'} \end{aligned} \tag{21}$$

where the primed complex vectors are complex vectors referred to the transformed basis.[5] Since the inverse of a unitary transformation is given by $Q^{-1}=\tilde{Q}^*$, the scattering matrix formulation in terms of the transformed basis is

$$Q_{--}{}^*E_-{}^{S'} = A_{-+}Q_{++}E_+{}^{T'} \tag{22}$$

or

$$E_-{}^{S'} = \tilde{Q}_{--}A_{-+}Q_{++}E_+{}^{T'}. \tag{23}$$

Therefore we have the general transformation property

[4] G. Deschamps, "Geometrical representation of the polarization of a plane electromagnetic wave," Proc. IRE, vol. 39, p. 543; May, 1951.

[5] The transformation Q^{-1} is used here to transform from the original basis to the new basis so as to bring out explicitly the transformation properties of the scattering matrix (24).

of the scattering matrix; under a unitary change-of-basis transformation the scattering matrix undergoes a congruent transformation,

$$S = \tilde{Q}AQ, \tag{24}$$

where the matrix S is now the scattering matrix referred to some arbitrary transformed elliptical polarization basis. Note that the congruent transformation preserves the symmetry of the scattering matrix; i.e.,

$$\tilde{S} = (\widetilde{\tilde{Q}AQ}) = \tilde{Q}\tilde{A}Q = \tilde{Q}AQ = S \tag{25}$$

since $\tilde{A} = A$.

Equivalent Scattering Matrices and the Polarization Power Scattering Matrix

In the previous section we gave the general transformation property of the scattering matrix. We will now introduce a new matrix, called the polarization power scattering matrix, which is useful for polarization analysis and, using the transformation properties above, show its relation to the scattering matrix. To show this relationship it is helpful to reduce the scattering matrix to diagonal form; i.e., to find within the congruent group of unitary transformations of the polarization basis a particular polarization basis (that is, a transformation Q) for which the scattering matrix can be made diagonal. The reduction of matrices to their diagonal form has been much discussed in the literature. In Appendix I it is shown that it is always possible to reduce the scattering matrix to diagonal form, D_S, by a congruent unitary transformation of the polarization basis; i.e.,

$$D_S = \begin{pmatrix} K_1 & 0 \\ 0 & K_2 \end{pmatrix} = \tilde{Q}_S S Q_S \tag{26}$$

where Q_S is a unitary transformation of the polarization basis and K_1 and K_2 are generally complex.

Let us now consider the diagonalized scattering matrix by introducing the polar form of the scattering matrix. Any matrix S can be represented by the product of a non-negative matrix $P = \sqrt{\tilde{S}^*S}$ and unitary matrix U:[6]

$$S = UP. \tag{27}$$

This is called the polar decomposition of a matrix and is analogous to the polar form of a complex number. U can be thought of as the phase of the matrix and P as the magnitude. The matrix P has a simple interpretation, *viz.* P^2 specifies the total power back scattered from the target *for any transmitted polarization;* hence, we shall call it the polarization power scattering matrix. The total power back scattered [using (4) and (17)] is

$$\vec{E}^S \cdot \vec{E}^S = \tilde{E}_-{}^{S*}E_-{}^S = \tilde{E}^{T*}\tilde{S}^*SE^T = \tilde{E}^{T*}P^2E^T. \tag{28}$$

The polar components of the scattering matrix are transformed by a unitary change of basis transformation as follows:

$$S' = \tilde{Q}SQ = \tilde{Q}UPQ = \tilde{Q}UQQ^{-1}PQ = U'P' \tag{29}$$

where

$$U' = \tilde{Q}UQ \quad \text{and} \quad P' = Q^{-1}PQ. \tag{30}$$

The phase matrix U undergoes a congruent transformation and the magnitude matrix P undergoes a similarity transformation.

Since P^2 is a Hermitian matrix, it can always be diagonalized by a similarity transformation

$$Q^{-1}P^2Q = \tilde{Q}^*P^2Q = D_P \tag{31}$$

where the transformation matrix Q is unitary, the eigenvalues of P^2 are real, the eigenvectors are orthogonal, and D_P is a diagonal matrix with real diagonal elements. It is shown in Appendix II that *the same unitary matrix Q, which diagonalizes P^2 by a similarity transformation, diagonalizes the scattering matrix S by a congruent transformation. Furthermore the eigenvalues of the power matrix are simply the magnitudes squared of the respective eigenvalues of the scattering matrix.* If the diagonal scattering matrix is given by

$$D_S = \begin{pmatrix} K_1 & 0 \\ 0 & K_2 \end{pmatrix} = \begin{pmatrix} k_1e^{j\phi_1} & 0 \\ 0 & k_2e^{j\phi_2} \end{pmatrix}, \tag{32}$$

then the diagonal polarization power scattering matrix is given by

$$D_P = \begin{pmatrix} k_1k_1^* & 0 \\ 0 & k_2k_2^* \end{pmatrix} = \tilde{D}_S{}^*D_S. \tag{33}$$

The actual diagonalization of the scattering matrix S or the polarization power scattering matrix P^2 is done by solving the eigenvalue problem

$$E_-{}^S = S_{-+}E_+{}^T = KE_+{}^{T*} \tag{34}$$

or

$$(\tilde{S}^*S - KK^*I)E^T = 0 \tag{35}$$

where I is the unit matrix and K is a complex constant (the eigenvalue). It is interesting to note that the polarization coordinate system (the eigenvectors), which diagonalizes the scattering matrix or the polarization power scattering matrix, also specifies the transmitted polarization to be used for the maximum power return; i.e., maximizes the Hermitian form for the power.[7] Knowledge of the polarization power scattering matrix is sufficient to specify the polarization to be used for

[6] P. Halmos, "Finite Dimensional Vector Spaces," Princeton University Press, Princeton, N. J., 1948.

[7] Specification of polarization of maximum power return and diagonalized scattering matrix have been discussed in a series of excellent reports by Ohio State University and are in the reference cited in footnote 3. The Ohio State report of particular interest is, "Fourth Quarterly Progress Report on the Effects of Type of Polarization on Echo Characteristics," The Antenna Laboratory, The Ohio State University Research Foundation Rep. No. 389-4, June, 1950.

maximum power return. Note also that the diagonal form of the scattering matrix also uniquely determines the scattering matrix; i.e., all S's with the same diagonal form are related by unitary change-of-basis transformation. The polarization power scattering matrix is related to the scattering matrix by (27), has the same "eigenvectors" as the scattering matrix, and has eigenvalues equal to the square of the magnitude of the eigenvalues of the scattering matrix.

Once the scattering matrix is in its diagonal form its polar components simplify to:

$$U_D = \begin{pmatrix} e^{j\phi_1} & 0 \\ 0 & e^{j\phi_2} \end{pmatrix}; \qquad P_D = \begin{pmatrix} k_1 & 0 \\ 0 & k_2 \end{pmatrix}. \tag{36}$$

The polar components of the scattering matrix S can then be found for any other polarization basis very simply. If T is a unitary change-of-basis transformation from the diagonal basis to some arbitrary basis, then the scattering matrix referred to the T basis is given by (31).

$$S = \tilde{T}DT = \tilde{T}U_D P_D T = UP, \tag{37}$$

where

$$U = \tilde{T}U_D T \quad \text{and} \quad P = T^{-1}P_D T. \tag{38}$$

It is important to note that the polarization power scattering matrix completely specifies the scattering matrix up to the two phase angles ϕ_1 and ϕ_2; i.e., up to the phase matrix U. Furthermore, since one phase angle is of no practical interest, the scattering matrix is actually specified up to one phase angle if the power matrix is known. Thus the polarization power scattering matrix specifies the total back-scattered power for each transmitted polarization and specifies the polarization of the back-scattered wave up to a great circle on the Poincaré polarization sphere.[8] Furthermore, the polarization power scattering matrix can be found by measuring only the total power in the back-scattered return; no phase measurement is necessary. It is therefore simpler to measure and gives almost as much information as the scattering matrix. The form of the polarization power scattering matrix is

$$P^2 = \tilde{S}^*S = \begin{pmatrix} S_{11}^*S_{11} + S_{12}^*S_{12} & S_{11}^*S_{12} + S_{12}^*S_{22} \\ S_{12}^*S_{11} + S_{22}^*S_{12} & S_{12}^*S_{12} + S_{22}^*S_{22} \end{pmatrix} = \begin{pmatrix} a & b \\ b^* & c \end{pmatrix}, \tag{39}$$

where a and c are real. If, for example, P^2 is referred to a plane-polarized x, y basis, then P^2 can be completely specified by transmitting at horizontal, vertical, and the $\pm\pi/4$ plane polarization, and measuring the total power back-scattered; no elliptically polarized transmissions or phase measurements are required.

I would like to thank Mr. James Wolf for many helpful discussions on radar polarization analysis.

Appendix I

Any square matrix S can be transformed to diagonal form D by unitary matrices M and Q:[9]

$$MSQ = D. \tag{40}$$

We can now easily show that if S is also symmetric then $M = \tilde{Q}$. Taking the transpose of this equation, we have

$$\tilde{Q}\tilde{S}\tilde{M} = \tilde{Q}S\tilde{M} = \tilde{D} = D \tag{41}$$

since $\tilde{S} = S$ if S is symmetric and $\tilde{D} = D$ if D is diagonal.

Comparing these equations we see $M = \tilde{Q}$. Thus, the scattering matrix can always be diagonalized with a congruent transformation by a unitary matrix Q.

Appendix II

Multiplying (40) by its complex conjugate after substituting Q for M gives

$$\tilde{Q}^*S^*Q^*\tilde{Q}SQ = \tilde{Q}^*\tilde{S}^*SQ = Q^{-1}\tilde{S}^*SQ = D^*D, \tag{42}$$

since $Q^{-1} = \tilde{Q}^*$ and $\tilde{S} = S$. But $\tilde{S}^*S = P^2$, the power scattering matrix, and D^*D is diagonal since D is diagonal. Hence, the power matrix is reduced to diagonal form by a similarity transformation using the same unitary matrix Q which diagonalized the scattering matrix, and the eigenvalues of the power matrix are just the magnitude squared of eigenvalues of scattering matrix.

[8] For an introduction to the use of the Poincaré sphere see Deschamps, op. cit., p. 541.

[9] H. Turnbull, A. Aitken, "An Introduction to the Theory of Canonical Matrices," Blackie and Son, Ltd., London, Eng., p. 181; 1932.

Statistical Design and Evaluation of Filters for the Restoration of Sampled Data*

R. M. STEWART†

Summary—A new analysis of the problem of continuously recovering periodically sampled data is given which starts with the assumption that the waveform being sampled is a stationary random function of time. The popular idealization of a band-limited frequency spectrum is not made; results obtained apply to all types of spectra and for any sampling frequency. In addition to such things as telemetering, radar, and data storage systems, for which the solution of this problem is of direct interest, the analytic techniques used may also be applied in the design and analysis of closed-loop control systems which utilize some digital elements.

I. Introduction

THE PROBLEM to be treated[1] can be represented by the block diagram in Fig. 1. According to the well-known sampling theorem, if $m(t)$ has no frequency components higher than f_0, all of $m(t)$ can be perfectly reconstructed from samples taken periodically at any frequency greater than $2f_0$. Since this is an idealization of the usual true situation, it is of interest to examine the relationship between sampling frequency and minimum attainable errors in the output for messages having arbitrary spectra.

Using mean-square error as a measure of fidelity, the following major results are obtained for the case of noise-free sample pulses: (a) A straightforward procedure is developed for determining the optimum physically realizable time-invariant linear smoothing filter. (b) There is no time-varying linear filter (whose characteristics vary periodically in synchronism with the sampling frequency) which is better than the optimum time-invariant linear filter. (c) The weighing function $y(\tau)$ of such an optimum filter should always be equal to unity for $\tau = D$, where D is the desired delay in recovery of the message, and should equal zero for $\tau = D + n\Delta$, where n is any integer other than zero, and Δ is the sampling interval. For physical realizability, $y(\tau) \equiv 0$ for $\tau < 0$. (d) If the spectral density of the original data or message is of the form $K/(f_0^2 + f^2)$ and if these optimum recovery filters are used, the sampling frequency must be of the order of $10^4 f_0$ in order to obtain 1 per cent error in the reproduction.[2] (e) If the spectral density of the original message at frequencies near half the sampling frequency and above is approximately of the form K/f^{2n} the rms error σ_ϵ varies with sampling frequency f_s approximately as $f_s^{-(n-1/2)}$.

II. Optimum Time-Invariant Linear Filter

The train of sample pulses $h(t)$ can be represented by

$$h(t) = m(t) \sum_{n=-\infty}^{+\infty} \delta\left(t - \frac{n}{f_s}\right) \tag{1}$$

where δ is the unit-impulse, or Dirac-δ, function.[3] The infinite train of δ functions in this expression may be represented by a complex Fourier series in which all coefficients are equal. Then

$$h(t) = m(t) f_s \sum_{n=-\infty}^{+\infty} e^{jn2\pi f_s t}. \tag{2}$$

If, in the usual way, finite sections of $m(t)$ and $h(t)$ extending from $-T$ to $+T$ are considered, both sides of (2) are Fourier-transformable. The result of the transformation is

$$H_T(f) = f_s \sum_{n=-\infty}^{+\infty} M_T(f - nf_s). \tag{3}$$

Hence

$$G_T(f) = YH_T(f) = f_s Y \left\{ M_T(f) + \sum_{n=1}^{\infty} [M_T(f - nf_s) + M_T(f + nf_s)] \right\} \tag{4}$$

and the transform of the error in recovered message is[4]

$$E_T = G_T - M_T = (f_s Y - 1) M_T(f) + f_s Y \sum_{n=1}^{\infty} [M_T(f - nf_s) + M_T(f + nf_s)]. \tag{5}$$

* Original manuscript received by the IRE, June 20, 1955; revised mansucript received October 10, 1955. This paper presents the results of one phase of research carried out at Jet Propulsion Lab., Calif. Inst. Tech., under Contract No. DA-04-495-Ord 18, sponsored by the Dept. of the Army, Ordnance Corps; part of this work was done under contract with the Air Force Flight Test Center while the author was employed by the Ralph M. Parsons Co., Research and Development Department, Pasadena.

† Research Specialist, Jet Propulsion Laboratory, Calif. Inst. Tech., Pasadena, Calif.

[1] The editors have brought to the author's attention two independent contributions to this subject which have appeared since this paper was written: Gene Franklin, "Linear Filtering of Sampled Data," 1955 IRE Convention Record, Part 4, and S. P. Lloyd and B. McMillan, "Linear Least Squares Filtering and Prediction of Sampled Signals," presented at 1955 Symposium on Network Theory sponsored by the Polytech. Inst. of Brooklyn. However, the methods used and results obtained appear to differ sufficiently to warrant publication of this work.

[2] This result confirms quantitatively the feeling expressed to the author by Dr. A. J. Mallinckrodt of the Ralph M. Parsons Co. that, in many cases, current practices in applying the sampling theorem to the design of data-transmission systems have resulted in errors far in excess of those expected.

[3] Cf., e.g., W. K. Linvill, "Sampled-data control systems studied through comparison of sampling with amplitude modulation," *Trans. AIEE*, vol. 70, pp. 1–10; 1951.

[4] Eq. (4) is not strictly correct. However, the error is only a transient effect just following $-T$ and $+T$ which becomes less and less important when, as in the following work, T is allowed to increase without bound. Hence, for the sake of simplicity, it is disregarded from the beginning.

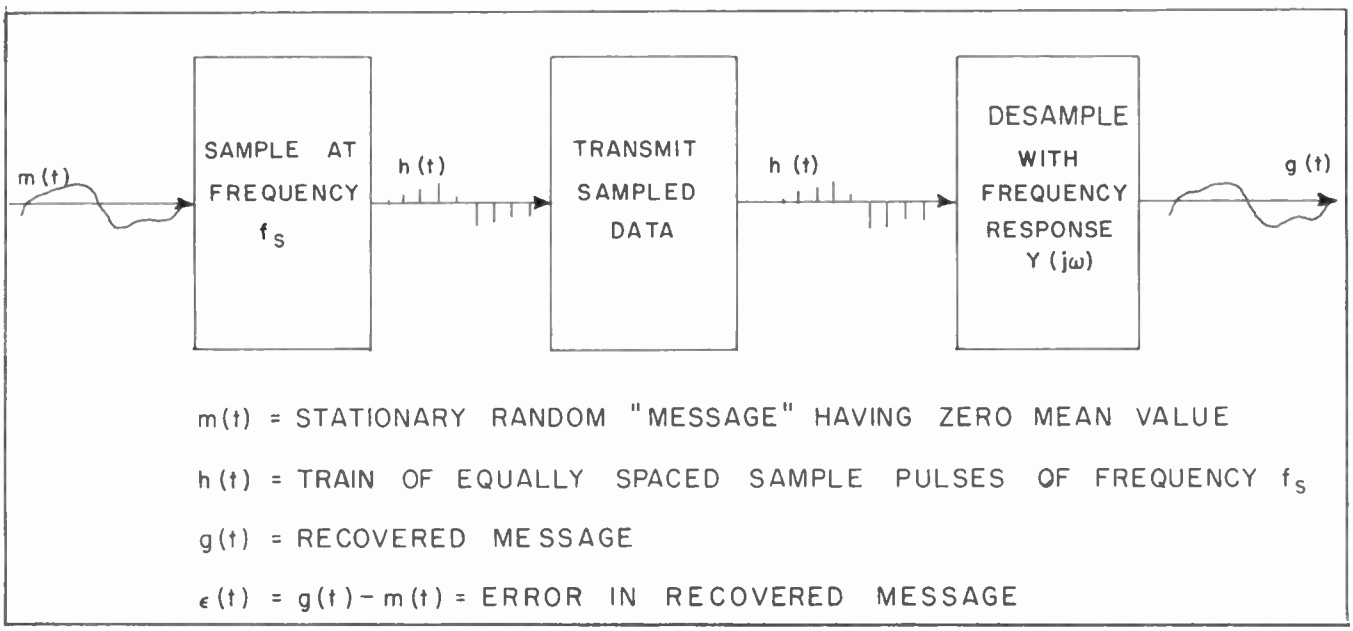

Fig. 1—Sequence of operations.

The spectral density of the error,

$$\Phi_\epsilon(f) = \lim_{T\to\infty} \frac{1}{T} \mid E_T \mid^2 = \lim_{T\to\infty} \frac{1}{T} E_T E_T^* \tag{6}$$

may be computed using (5) and (6). The result is

$$\Phi_\epsilon(f) = \mid (f_s Y) - 1 \mid^2 \Phi_m(f) + \mid (f_s Y) \mid^2 \cdot \sum_{n=1}^{\infty} [\Phi_m(f - nf_s) + \Phi_m(j + nf_s)] + [\text{cross spectral density terms}]. \tag{7}$$

A typical cross-spectral-density term is

$$\Phi_c(f) = \lim_{T\to\infty} \frac{1}{T} [M_T(f - nf_s) + M_T(f + nf_s)] \cdot [M_T(f - mf_s) + M_T(f + mf_s)]^*. \tag{8}$$

By transforming each of the terms in brackets in (8), it may be seen that this expression represents the cross-spectral density between the two real functions

$$2m(t) \cos 2\pi nf_s t \tag{9}$$

and

$$2m(t) \cos 2\pi mf_s t$$

and must be equal to the Fourier transform of the cross-correlation function of these two functions; that is,

$$\Phi_c(f) = 2 \int_{-\infty}^{+\infty} \phi_c(\tau) e^{-j2\pi f\tau} d\tau \tag{10}$$

where

$$\phi_c(\tau) = \overline{[2m(t) \cos 2\pi nf_s t][2m(t+\tau) \cos 2\pi mf_s(t+\tau)]} = \overline{4[m(t)m(t+\tau)][\cos 2\pi nf_s t \cos 2\pi mf_s(t+\tau)]}, \tag{11}$$

the bar denoting time average.

If the original message and the phase of the sampling device are independent, then the average value of the product of the two bracketed terms is equal to the product of the average values, and hence

$$\phi_c(\tau) = 4\overline{[m(t)m(t+\tau)]}\,\overline{[\cos 2\pi nf_s t \cos 2\pi mf_s(t+\tau)]} = 4\phi_m(\tau)\overline{[\cos 2\pi nf_s t \cos 2\pi mf_s(t+\tau)]}. \tag{12}$$

For $m \neq n$, average value of term in brackets is zero. Hence $\phi_c(\tau) = 0$ for $m \neq n$, and, from (10), $\Phi_c(f) = 0$. Thus all cross-spectral-density terms are zero. For $m = n$, (12) gives

$$\phi_n(\tau) = 2\phi_m(\tau) \cos 2\pi nf_s\tau \tag{13}$$

and hence, by direct transformation,

$$\Phi_n(f) = [\Phi_m(f - nf_s) + \Phi_m(f + nf_s)]. \tag{14}$$

Thus (7) may be written

$$\Phi_\epsilon(f) = \mid Y' - 1 \mid^2 \Phi_m(f) + \mid Y' \mid^2 \Phi_s(f) \tag{15}$$

where

$$Y' = f_s Y \tag{16}$$

and the side-band spectrum Φ_s is

$$\Phi_s(f) = \sum_{n=1}^{\infty} [\Phi_m(f - nf_s) + \Phi_m(f + nf_s)]. \tag{17}$$

This spectrum is illustrated in Fig. 2. It may be noted that (15) is identical in form with the well-known expression for error spectral density for continuous smoothing of message plus noise if the noise were independent of the message and had a spectral density equal to the side-band spectrum (17).

Hence Wiener's method[5] may be applied directly to give the optimum (in the sense of minimum rms error)

[5] N. Wiener, "Extrapolation, Interpolation, and Smoothing of Stationary Time Series," John Wiley and Sons, New York, N. Y., 1949.

linear filter function Y' (and $Y = Y'/f_s$) for any given sampling rate f_s. Eq. (15) can be easily modified to allow for delay in recovering the message if such delay is desirable for greater accuracy.

If the sampling rate is fairly high compared with the effective bandwidth of $m(t)$, then in computing the mean-square error given by

$$\sigma_\epsilon^2 = \int_0^\infty \Phi_\epsilon(f)df \tag{18}$$

all but the first side band to the right may be neglected, giving

$$\Phi_s(f) \cong \Phi_m(f - f_s). \tag{19}$$

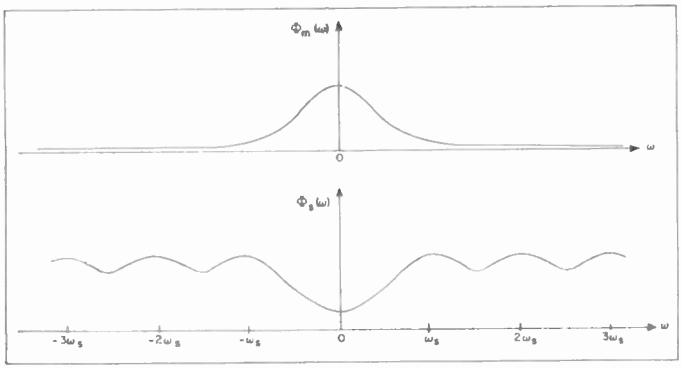

Fig. 2—Spectra of typical original message and of side bands of effective noise.

III. Synchronous Time-Varying Linear Filters

Because of the periodically time-varying (and hence nonstationary) statistical nature of the sampled-data pulse train, it is to be expected, perhaps, that some improvement over linear time-invariant filtering might be gained by using time-varying linear filters whose characteristics vary periodically in synchronism with the sampling frequency.

If one considers the possibility of replacing $Y(j\omega)$ in Fig. 1 by such a time-varying filter, one is led, however, to the conclusion that no improvement is possible; the optimum filter of the class of all linear filters (both time-varying and time-invariant) is actually the time-invariant filter discussed in the previous section. This fact may be explained as follows: Suppose that an attempt is made to determine the weighting function $y(\tau, t)$ for an optimum time-varying filter; $y(\tau, t)$ is the response at time t to an impulse at the input τ seconds previously.[6] If one considers just the ensemble of errors which occurs at the sample times (*e.g.*, $t=0$), each error of this type can be affected only by the value of $y(\tau, 0)$ at $\tau = 0, \Delta, 2\Delta, 3\Delta, \cdots$ where Δ is the time between samples since, for other values of τ, the input is always zero. The value of $y(\tau, 0)$ for other values of τ is thus immaterial with regard to minimizing errors just at the sample times. Similarly an optimum choice of $y(\tau, \alpha\Delta)$ for $0 < \alpha < 1$ can be made only for

$$\tau = \alpha\Delta, \qquad (1+\alpha)\Delta, \qquad (2+\alpha)\Delta, \cdots$$

and is determined at these points entirely by consideration of the ensemble error at $t = \alpha\Delta$. Thus a single time-invariant weighting function $y(\tau)$ can be determined which minimizes the ensemble mean-square error for every point in the sampling interval. Obviously this function must correspond to the filter function obtained by applying Wiener's method to (15) of the previous section.

Since the error at each point can be minimized separately, it is also apparent that the error just at the sampling times can be made equal to zero without jeopardizing the error at other points. Hence, for all optimum zero-delay recovery filters,

$$y(0) = 1$$
$$y(N\Delta) = 0, \qquad N = 1, 2, 3, \cdots.$$

When delay D is allowed,

$$y(D) = 1$$
$$y(D \pm N\Delta) = 0, \qquad N = 1, 2, 3, \cdots.$$

This requirement is illustrated by the weighting function shown in Fig. 3. That these conditions must apply can be confirmed by direct calculation in a number of

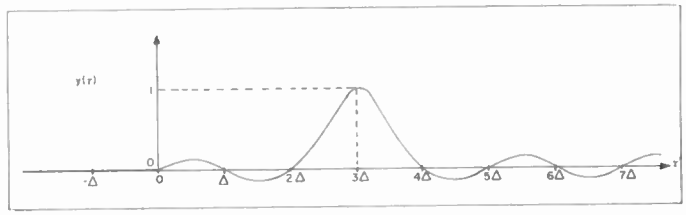

Fig. 3—Typical optimum weighting function for delay $= 3\Delta$.

ways. As an example, consider the optimum "unrealizable" filter function,

$$Y(\omega) = \frac{1}{f_s} \frac{\Phi_m(\omega)}{\sum_{n=-\infty}^{+\infty} \Phi_m(\omega - n\omega_s)} \tag{20}$$

which is real and even in ω. The cosine transform of $Y(\omega)$ should give the weighting function

$$y(N\Delta) = \frac{1}{\omega_s} \int_{-\infty}^{+\infty} \cos 2\pi N \left(\frac{\omega}{\omega_s}\right) \left[\frac{\Phi_m(\omega)}{\sum_{n=-\infty}^{+\infty} \Phi_m(\omega - n\omega_s)}\right] d\omega. \tag{21}$$

When N is an integer not equal to zero, this integral has the value zero. This fact may be shown as follows:

$$I_0 = y(N\Delta)$$

$$I_m = \int_{-\infty}^{+\infty} \cos 2\pi N \left(\frac{\omega}{\omega_s}\right) \left[\frac{\Phi_m(\omega - m\omega_s)}{\sum_{n=-\infty}^{+\infty} \Phi_m(\omega - n\omega_s)}\right] d\omega. \tag{22}$$

For realizable filters, $y(\tau, t) = 0$ for $\tau < 0$.

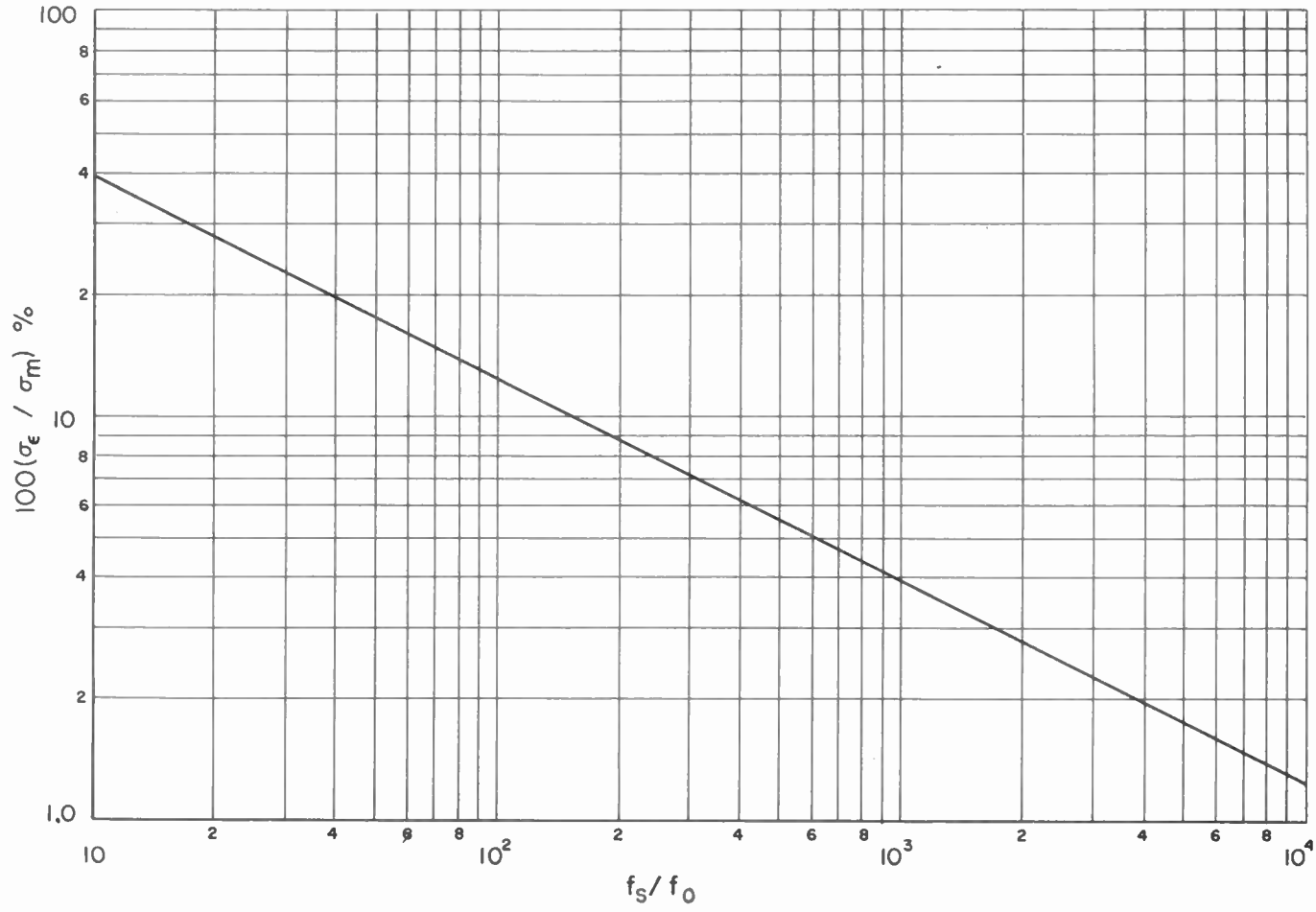

Fig. 4—Minimum error vs sampling frequency at high frequencies for message spectrum of the form $1/(f_0^2+f^2)$.

Then, by a simple linear transformation of variable,

$$I_m = I_0 \tag{23}$$

for all integral values of m. But

$$\sum_{m=-\infty}^{+\infty} I_m = \int_{-\infty}^{+\infty} \cos 2\pi N \left(\frac{\omega}{\omega_s}\right) d\omega. \tag{24}$$

Then, since the integral of the cosine is bounded, $I_0 = 0$. Similarly it may be shown from (21) that $y(0) = 1$.

IV. Applications in Some Special Cases

The following results on minimum error vs sampling frequency apply when a long delay relative to the reciprocal of the bandwidth of $m(t)$ is allowed. The minimum mean-square error is given by

$$\sigma_\epsilon^2 = \int_0^\infty \frac{\Phi_m \Phi_s}{\Phi_m + \Phi_s}\, df. \tag{25}$$

When

$$\Phi_m(\omega) = \frac{4\sigma_m^2 \omega_0}{\omega_0^2 + \omega^2}, \tag{26}$$

the integration gives approximately

$$\left(\frac{\sigma_\epsilon}{\sigma_m}\right)^2 = \frac{1}{2\sqrt{1+\left(\frac{f_s}{2f_0}\right)^2}} \cdot \left\{1 + \frac{2}{\pi}\tan^{-1}\left[\frac{\frac{f_s}{2f_0}}{\sqrt{1+\left(\frac{f_s}{2f_0}\right)^2}}\right]\right\} \tag{27}$$

where f_0 is the half-power bandwidth. For high sampling frequencies, (27) gives

$$\frac{\sigma_\epsilon}{\sigma_m} = \sqrt{\frac{3}{2}\,\frac{f_0}{f_s}}. \tag{28}$$

Fig. 4 shows a curve of relative error vs (f_s/f_0) computed using this equation. It may be noted that, for 1 per cent accuracy, the sampling frequency must be about 10^4 times the half-power bandwidth.

It is often true that, at frequencies near to and higher than half the sampling frequency, the message spectrum can be approximated by

$$\Phi_m(f) = \frac{K}{f^{2n}} \tag{29}$$

where n is an integer. Instead of using K, one may define

$$\beta = \frac{\Phi(f_1)f_1}{\sigma_m^2} \tag{30}$$

and then

$$\Phi_m(f) = \frac{\beta\sigma_m^2}{f_1}\left(\frac{f_1}{f}\right)^{2n}. \tag{31}$$

Here f_1 is some relatively high reference frequency, and β may be interpreted then as the ratio of spectral density at the reference frequency to average spectral density over the band from 0 to f_1. Then, again considering infinite delay,

$$\left(\frac{\sigma_\epsilon}{\sigma_m}\right)^2 = \beta\left(\frac{f_1}{f_s}\right)^{2n-1}\int_0^\infty \frac{dx}{(x-1)^{2n}+x^{2n}}. \tag{32}$$

For $n>1$, the lower limit of integration can be changed to $-\infty$ without serious error, and the integral can be easily evaluated using the theory of residues. Then

$$\left(\frac{\sigma_\epsilon}{\sigma_m}\right)^2 = I_n\beta\left(\frac{2f_1}{f_s}\right)^{2n-1} \tag{33}$$

where I_n has the following values for $n=2$ and 3:

n	I_n
2	0.554
3	0.168

Fig. 5 shows the relative accuracy vs sampling frequency computed by (33). In every case, it has been assumed that f_1 is chosen so that $\beta=1/10$.

Other special cases and extensions of the theory are currently being studied; further results will be reported as they become available. These studies include consideration of the following additional factors:

A. Noise

Noise can enter the system in either of two ways, before or after sampling. The optimum time-invariant filter in either case can be determined by the same techniques as those used in Section II.

B. Finite Pulse Width

There are two types of finite-width pulses, those which are essentially finite-time samples of the message and those for which the amplitude of an entire pulse of known and constant shape is proportional to the amplitude of the message at just one point. The optimum

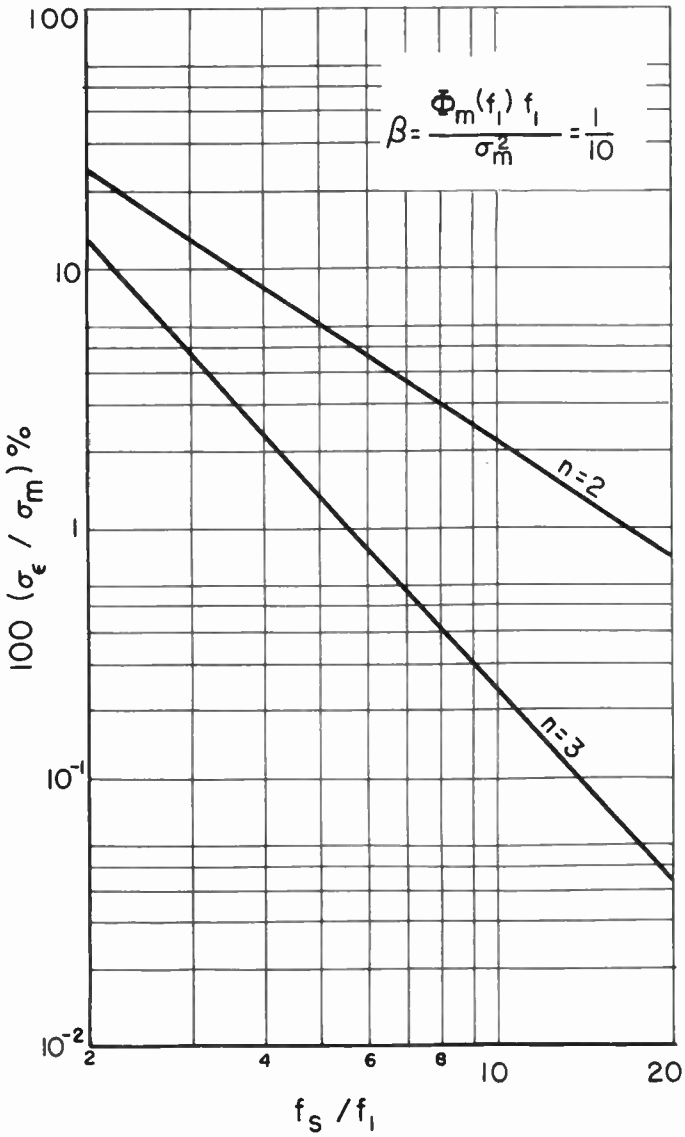

Fig. 5—Minimum error vs sampling frequency for message spectra of the form $1/f^{2n}$ for $f \geq f_1$.

time-invariant filter in either case can again be determined by the means of the techniques which are used in Section II.

C. Time-Varying Filters

In most of the situations just described, the best periodically time-varying filter may be expected to give improvement over the best time-invariant linear filter.

However, when the actual circumstances are close to those analyzed in Section II, the time-variation required for optimum smoothing should be small since, as was shown in Section III, the optimum filter among all linear filters in the limiting case is time-invariant.

Correspondence

Comment on "Echo Distortion in the FM Transmission of Frequency-Division Multiplex,"* W. J. Albersheim and J. P. Schafer[1]

In view of the considerable engineering interest of Albersheim and Schafer's paper, it seems worthwhile, even at this late date, to call attention to an error which found its way into their expression (4), for the distortion due to an in-phase echo of short delay and small amplitude. There is a missing factor $\frac{1}{2}$ [in fact the $\frac{1}{2}$ to be found in equation (3) of Appendix B of the paper by W. R. Bennett[2]], so that the expression should be

$$\frac{D_3}{s} = 0.028 r_p \tau^3 s^2 p \sqrt{1 - 0.333k^2}. \quad (1)$$

In Albersheim and Schafer's Fig. 4, it would appear that the measured points are in good agreement with the incorrect theoretical expression. Inserting the missing factor, one might expect to produce a discrepancy between theory and measurement of $3\frac{1}{2}$ db. Actually, there was an error in plotting the theoretical curve as computed by Albersheim and Schafer from their original formula. The final result is that the measured distortion levels are about 9 db lower than those predicted from the corrected theoretical expression.

In a paper[3] submitted for publication to the *Proceedings of the Institute of Electrical Engineers*, it is hoped that most of this discrepancy can be accounted for by giving more careful consideration to the effect of the echo amplitude. Expression (4) of Albersheim and Schafer's paper suggests that the distortion should be accurately proportional to the echo amplitude. In fact, this only holds when the echo amplitude is sufficiently small. A more exact formula is (writing r for r_p):

$$\frac{D_3}{s} = 0.028 \frac{r(1-r)}{(1+r)^3} \tau^3 s^2 p \sqrt{1 - 0.333k^2} \quad (2)$$

which differs from the "small echo" formula only in the term involving r. It turns out that Albersheim and Schafer's experimental echo amplitude, -15 db, is not sufficiently small for expression (1) above to be satisfactory. Use of expression (2) recovers 6 db of the discrepancy between measurement and theory. The residual 3 db is probably within experimental error.

I am indebted to Mr. W. J. Albersheim for correspondence which has helped to clarify this matter.

R. G. Medhurst
Research Laboratories
General Electric Co., Ltd.
Wembley, Middlesex, England

* Received by the IRE, September 15, 1955.
[1] Proc. IRE, vol. 40, pp. 316–328; March, 1952.
[2] W. R. Bennett, "Cross modulation requirements on multichannel amplifiers below overload," *Bell Sys. Tech. Jour.*, vol. 19, pp. 587–610; October, 1940.
[3] R. G. Medhurst and G. F. Small, "An extended analysis of echo distortion in the F.M. Transmission of frequency-division multiplex" (Submitted to *Proc. I.E.E.*, July, 1955).

Rebuttal[4]

We are grateful to Mr. Medhurst for pointing out the missing factor 1.5 in (4) of our 1952 paper and the plotting error in our Fig. 4.

The additional factor $1-r/(1+r)^3$ is negligible for the limit of very small echoes but does amount to -6 db for the experimental echo amplitude.

The residual discrepancy of 3 db between our experiments and Mr. Medhurst's (2) can be explained as follows:

Medhurst's equation as well as ours is based on the "short delay range" approximations which according to our paper are valid only for: $\tau P_m < 1$ [our equation (1)]. The experimental conditions correspond to

$$\tau P_m = 0.8\pi = 2.54.$$

Hence, a more rigorous theory should be applied. This rigorous analysis has been supplied by Bennett, Curtis and Rice.[5] The authors of this paper kindly informed us that our test results agree to within 1 db with their exact equations—a fortunate accident indeed.

Since the exact formulas are cumbersome and hard to evaluate, the approximations given in our equations and in Medhurst's correction remain useful in their validity range.

W. J. Albersheim and J. P. Schafer
Bell Telephone Laboratories, Inc.
Whippany, N. J.

[4] Received by the IRE, September 28, 1955.
[5] W. R. Bennett, H. E. Curtis, and S. O. Rice, "Interchannel interference in fm and pm systems under noise loading conditions," *Bell Syst. Tech. Jour.*, vol. 34, pp. 601–636; May, 1955.

On Network Determinants*

The problem of invariance of electrical network determinants under changes of reference frame has been dealt with in a number of papers. The determinant of the admittance matrix taken with respect to some reference node has been repeatedly recognized as invariant for a change of the reference node.[1–3] Also the determinants of the impedance matrices for any two independent loop systems have been found to be in a constant real ratio.[4] In a paper of the author, recently published,[5] this problem has been discussed for a general loop or cut-set[6] representation. Since by comparison of the two last papers[3,4] an impression might be gained that there exists a distinct difference in the invariant properties of the network determinants for the admittance and impedance representations respectively it seems worthwhile to present, for the readers of the Proceedings, the main results of the above work. They are given here without proofs. Readers who are interested in details are referred to the original paper.

(1-i) The determinant of the impedance matrix corresponding to a system of link currents is invariant under transformations from one such system to another.

(1-a) The determinant of the admittance matrix corresponding to a system of voltages of tree-branches is invariant under transformations from one tree to another.

Let us call the values of the determinants associated with a system of link currents or tree-branch voltages—the basic values and any system which shares with those basic systems the property of having the basic value of the associated network determinant—a simple one.

(2-i, a) The determinant of the impedance (admittance) matrix is always equal to the basic value multiplied by the square of an integer. The basic value is the minimum value possible for the network determinant.

(3-i) The necessary and sufficient condition for a system i of independent loop currents to be simple is that the matrix M transforming any system of independent link currents j into i (*i.e.*, $i = Mj$) be a matrix of integer entries.

(3-a) The necessary and sufficient condition for a system of independent cut-set voltages v to be simple is that the matrix N transforming any system of tree-branch voltages u into v (*i.e.*, $v = Nu$) be a matrix of integer entries.

(4-i) To ascertain whether a loop system is simple we are allowed to remove any loop current which appears alone in some branch. If, by a successive application of this procedure, all loop currents may be removed, the loop system is simple.

(4-a) To ascertain whether a cut-set system is simple we are allowed to remove any cut line which alone cuts some branch. If, by a successive application of this procedure, all cut lines may be removed, the cut-set system is simple.

From (3-a) follows:

(5-a) The system of independent node-pair voltages is always simple (the determinant of its admittance matrix being thus invariant under transformations from one such system to another).

* Received by the IRE, June 23, 1955.
[1] Sir J. Jeans, "The Mathematical Theory of Electricity and Magnetism," Cambridge University Press, Cambridge, Eng., p. 328; 1948.
[2] W. S. Percival, "Improved matrix and determinant methods for solving networks," *Proc. IEE*, part IV, vol. 101, pp. 258–265; 1954.
[3] J. Shekel, "Two network theorems concerning change of voltage reference terminal," Proc. IRE, vol. 42, p. 1125; July, 1954.
[4] S. Seshu, "The mesh counterpart of Shekel's theorem," Proc. IRE, vol. 43, p. 342; March, 1955.
[5] I. Cederbaum, "Invariance and Mutual Relations of Electrical Network Determinants," *Jour. Math. Phys.*, vol. 35, scheduled for February, 1956.
[6] Cf. "Standards on circuits: definitions of terms in network topology, 1950," Proc. IRE, vol. 39, pp. 27–29; January, 1951.
[7] For the notion "link," cf. E. A. Guillemin, "Introductory Circuit Theory," John Wiley and Sons, Inc., New York, N. Y., p. 8; 1953.

As a further specialization we have:

(6-a) The system of node voltages with respect to some reference node is always simple [the determinant of its admittance matrix being thus invariant under changes of the reference node, or in general with respect to transformations to other simple systems, as specified; *e.g.*, under (5-a)].

Using (4-i) we have:

(6-i) The system of independent mesh[8] currents for a planar network is always simple [the determinant of its impedance matrix being thus invariant under transformations from one such system to another, or to other simple systems, as specified; *e.g.*, under (1-i)].

Having in this manner defined the basic values of the determinants of the impedance and admittance matrices we may be interested in a relation between them. Such a relation is given in the following theorem:

(7) The ratio of the basic values of the determinants of the impedance and admittance matrices is equal to the determinant of the branch impedance matrix.

In the special case when there are no mutual inductances or unilateral transmittances we have:

(8) For a network with independent branches the ratio of the basic values of the determinants of the impedance and admittance matrices is equal to the product of all the branch impedances.[9]

I. Cederbaum
11, Birchington Road
London, N.8, England

[8] In this paper a distinction is made between a general loop and a mesh, following Guillemin, *op. cit.*, p. 24. The notion "mesh" is applied only to the simplest loops in a planar network.

[9] Cf. N. F. Tsang, "On electrical network determinants," *Jour. Math. Phys.*, vol. 33, pp. 185–193; 1954.

Nonlinearity of Propagation in Ferrite Media*

The experiments of Sakiotis, Chait, and Kales on ferrite nonlinearity[1] were read with considerable interest on my part, since I have also made similar measurements. My measurements were concerned with phase shift in rectangular waveguide using transverse magnetic fields of a value small compared to that required at resonance. These measurements were made at both *X* band and *C* band. The material used was General Ceramics R-1 ferrite.

At power levels of 250 kw the insertion loss of a 90-degree phase-shift section was increased by 1.2 db over the low level loss. The phase shift, however, did remain constant as reported by Sakiotis, Chait, and Kales. At constant power and variable temperature both loss and phase shift changed. The loss seemed to decrease with increasing temperature while the loss increased with increasing power, the latter being the dominant factor.

Our solution to this problem was to use a nickel zinc ferrite with a high Curie temperature. The low power insertion loss with this ferrite is higher than with R-1; however, it is less sensitive to heat and high power rf fields. At high power the insertion loss is little different from that at low power, and therefore considerably superior to the R-1 ferrite. At *X* band a circulator can be built having less than 0.5 db insertion loss at 250-kw peak power. At *C* band the use of a nickel zinc ferrite does not look as promising for a near side of resonance circulator design, since at that frequency the low power insertion loss is quite high. A *C*-band R-1 ferrite circulator having only a few tenths of a db loss at low power had over 2.0 db loss at 250 kw peak. It is felt that a low loss circulator for high power, low-frequency (less than 5 kmc), will have to be a far-side-of-resonance design employing nickel zinc ferrite and resulting in large and bulky magnets.

Alvin Clavin
Canoga Corporation
Van Nuys, Calif.

* Received by the IRE, August 19, 1955.

[1] Proc. IRE, vol. 43, p. 1011; August, 1955.

A Note on the Small Amplitude Transient Response of *P-N* Junctions*

As a result of investigating the small amplitude transient response of *p-n* junctions,[1,2] relations have come to light which concern both (a) the interpretation of, and (b) the improvement in response time. For example, it was noted that the transient behavior could be described without explicit dependence on the individual lifetimes, τ_n and τ_p, by using average lifetimes of the form

$$\overline{\tau^r} = \frac{I_{ps}\tau_p{}^r + I_{ns}\tau_n{}^r}{I_{ps} + I_{ns}} \qquad r = \tfrac{1}{2},\ 1,\ \text{and}\ 2, \qquad (1)$$

in which I_{ps} and I_{ns} are the saturation currents for holes and electrons respectively. A further generalization

$$\overline{W(\tau)} = \frac{I_{ps}W(\tau_p) + I_{ns}W(\tau_n)}{I_{ps} + I_{ns}} \qquad (2)$$

was found to remove the explicit dependence on τ_n and τ_p with the two most general results at hand, the first by Shockley,[3] and the second by Lehman.[4]

The small amplitude ac admittance of a junction[5] may be written in terms of (2) as follows

$$Y(j\omega) = G_b\overline{(1 + j\omega\tau)^{1/2}} + j\omega C_b \qquad (3)$$

in which the conductance G_b is the slope of the dc characteristic curve, C_b is the capacitance of the barrier, ω is the circular frequency of ac and $j = \sqrt{-1}$.

Lehman has treated the transient response of the *p-n* junction, restricting the barrier voltage $V(t)$ to the range over which the current I obeys the Wagner[6] dc relation $(e^{qV/kT} - 1)$.[6] Lehman's transient solution for the current may be written

$$I(t) = I_s(e^{qV/kT} - 1) + I_s\overline{F(\tau)} + \frac{d}{dt}C_bV(t) \qquad (4)$$

in which

$$F(\tau_n) = \int_0^t dt_1 \left(\frac{d}{dt_1}e^{qV(t_1)/kT}\right) \cdot \left(\sqrt{\frac{\tau_n}{\pi(t - t_1)}}e^{-(t-t_1)/\tau_n} - \operatorname{erfc}\sqrt{\frac{t - t_1}{\tau_n}}\right) \qquad (5)$$

and $F(\tau_p)$ is the same as (5) except that τ_p replaces τ_n. The first term on the right of (4) is the steady state solution, the second term is the transient conduction current, and the third term is the displacement current.

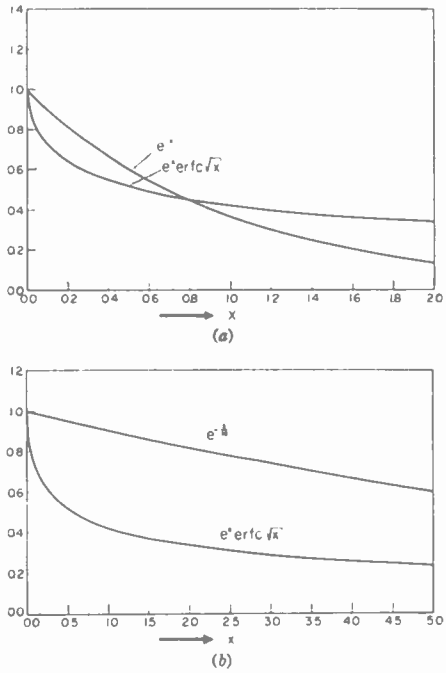

Fig. 1—A comparison of the function e^x erfc $\sqrt{x}$ with (a) e^{-x} and (b) $e^{-x/10}$.

It was also found that with the extreme cases of low and high bias, the performance may be concisely summarized as follows: The response of the barrier voltage to an impulse current takes the form e^{-x} with low bias, in which x is measured in units of time $C_b/G_b + \bar{\tau}/2$. The corresponding function with high bias is e^x erfc $\sqrt{x}$, in which x is measured in units of time $(C_b/G_b\bar{\tau}^{1/2})^2$. The two functions e^{-x} and e^x erfc $\sqrt{x}$ are plotted in Fig. 1 (a). In practice the units in which x is measured are at least 10 times greater when the voltage decay is exponential, and therefore the two functions $e^{-x/10}$ and e^x erfc $\sqrt{x}$, plotted in Fig. 1 (b) provide a more appropriate comparison of the two types of transient response. These functions represent typical cases with low and high bias, the plot of e^x erfc $\sqrt{x}$ representing the case of high bias in which $C_b/G_b \ll \bar{\tau}$. Thus, it may be seen by Fig. 1(b) that when there is sufficient forward bias to make the barrier RC time constant small compared with the average recombination time $(C_b/G_b \ll \bar{\tau})$, the response is very fast.

B. R. Gossick
Purdue University
Lafayette, Ind.

* Received by the IRE, September 28, 1955. This investigation was supported by the U. S. Signal Corps.

[1] B. R. Gossick, "The transient response of *p-n* junction rectifiers," *Phys. Rev.*, vol. 94, p. 1427; June, 1954.

[2] B. R. Gossick, "Small amplitude transient response of *p-n* junction," *Proc. N.E.C.*, Vol. 11; October, 1955.

[3] W. Shockley, "The theory of *p-n* junctions in semiconductors and *p-n* junction transistors," *Bell Syst. Tech. Jour.*, vol. 28, pp. 435–489; July, 1949.

[4] G. Lehman, private communication.

[5] C. Wagner, "Theory of current rectifiers," *Physick Z.*, vol. 32, p. 641; August, 1931.

[6] Symbols k, T and q have their familiar significance, denoting respectively Boltzmann's constant, temperature in °K, and the electronic charge.

Some Thoughts on Technical Meetings*

As a result of my recent experiences as Chairman of the Organizing Committee of the 1954 Symposium on Information Theory, I have given some thought to the general problem of technical meetings with particular regard to the relative functions of Professional Group Symposia and the technical sessions at the National Convention. I am jotting down my thoughts on this matter as I understand that the organization of technical meetings is a subject of current interest to many IRE members.

I shall begin with a brief report on the 1954 Symposium on Information Theory. The organization of the Symposium departed from current practice in two major respects. In the first place, all papers presented at the Symposium were published in a special issue of the TRANSACTIONS OF THE PROFESSIONAL GROUP ON INFORMATION THEORY and distributed to all participants two weeks before the date of the Symposium. In the second place, ample time was allotted to discussion; it averaged about ½ hour per paper, while the formal presentation of the papers averaged about 20 minutes. Furthermore, a Discussion Leader was formally appointed ahead of time for each of the 6 sessions of the Symposium; the function of the Discussion Leader was to start off the discussion on the right track by making carefully prepared comments about each paper.

The total number of registrants was 300. Although I did not make detailed checks, I would say the attendance at all sessions averaged between 80 and 90 per cent of registration. The discussion was quite lively most of the time and had to be stopped by the Chairman to keep the meeting on schedule. I noticed with particular pleasure that most of the Discussion Leaders, Chairmen, and authors attended all 6 sessions and seemed to enjoy the meeting. All in all, the consensus seemed to be that the unconventional features of the Symposium represented a step in the right direction. It was obvious, however, that a technical meeting such as that could not be attended by any appreciably larger audience.

The 1954 Symposium on Information Theory met fairly well, in my opinion, the needs of the relatively small group of IRE members who are doing active research in the field of information theory. I felt that the discussion was fruitful in stressing the present state of development and in suggesting avenues of approach to unsolved problems. On the other hand, I doubt that a person interested primarily in specific practical applications or a person interested in keeping up to date in general terms with the over-all progress in information theory, could have gotten much out of attending the Symposium. The realization of this brought to my mind the problem of how to meet the different technical needs represented in the IRE membership.

Broadly speaking, I would say that the IRE members interested in each specialized field represented by a particular Professional Group may be divided into three main groups:

A. The people who are doing active advanced research in the field and who, therefore, badly need opportunities for thorough discussion among themselves,
B. the people who are interested in specific practical developments and who, therefore, need to keep abreast of results obtained by the people in group A as well as by people doing similar developmental work, and
C. the people who, for various reasons, wish to keep themselves informed of the broad lines of progress in the field but are not interested in the detailed developments.

Two points should be noted in this regard. First of all, the size of group A is relatively small in each specialized field while groups B and C are rather large. In the second place a person who fits in group A for one particular field will, in general, fit into group B or into group C in other fields. In other words, the three groups represent divisions of interests and not divisions of people, so that the same IRE members may be grouped in different ways for different fields.

My feeling is that for groups A and C live technical meetings are at least as necessary and as effective as printed articles. However, while technical meetings for group A should emphasize advanced research and allow ample time for discussion, the meetings for group C should consist primarily of up-to-date review and tutorial papers presented by appropriate experts. Professional Group symposia are eminently suited to meet the needs of group A. In this respect I believe that the organization of the 1954 Symposium on Information Theory was a step in the right direction and that the effectiveness of similar meetings in the future will increase, once the audience becomes accustomed to reading carefully the printed papers ahead of time. On the other hand, the sessions at the National Convention should be devoted primarily to meet the needs of group C through the presentation of review and tutorial papers, and of original papers of broad significance. This suggestion appears to be in line with the present editorial policy of devoting the PROCEEDINGS OF THE IRE to contributions of interest to a broad audience and to invited tutorial papers. Some of the review papers could well be reports on the latest developments that have emerged at Professional Group symposia or other important technical meetings. It should be noted in this connection that the National Convention is just the occasion at which IRE members have the opportunity to keep themselves informed about a number of fields without any undue expenditure of time. Personally, I feel that in addition to the pleasure of meeting old friends, a broad up-to-date education is what I would like to obtain from the National Convention.

The needs of groups A and C can thus be met without much difficulty. On the contrary, the organization of technical meetings designed to meet the special needs of group B presents serious problems. Any meeting dealing with developmental work is bound to be attended by such a large number of people that worthwhile discussion from the audience is precluded for all practical purposes. Even the formal presentation of original technical papers constitutes a very serious problem because very often the importance of developmental papers resides in details, the significance of which can hardly be conveyed in a short time to an audience unfamiliar with the background of the specific problem. Perhaps review papers covering systematically recent work in each problem of interest are still a reasonably good answer to the needs of group B. In any case, it seems to me that the needs of group B can be met more realistically by the quick distribution of printed literature than by live technical meetings.

The fact of the matter seems to be that the needs of groups A and C are still fairly similar to those felt long ago by members of learned societies and therefore can still be fulfilled by meetings and publications of the traditional form. The existence of very large groups of the B type, on the contrary, is a new phenomenon resulting from the tremendous expansion of the electronics industry in the last decade. The needs of these groups present new problems on which little experience is yet available and which are often made more difficult by failure to recognize their nature.

The problem of how the IRE can best keep serving the technical needs of its fast growing membership deserves careful thought on the part of all concerned. Perhaps the classification of interests used above is not quite appropriate. Yet, I feel that full recognition must be given to the wide range of interests—research, development, management, etc.—required in the modern electronic industry, and to the obligation of serving all such interests with equal professional and intellectual standards, within the framework of the Institute of Radio Engineers.

R. M. FANO
Associate Professor of
Electrical Communications
M.I.T., Cambridge, Mass.

* Received by the IRE, August 25, 1955.

The Unit for Frequency*

The contribution by P. W. Crist[1] deals with a subject which is of particular interest at the present moment, because the matter is not one of terminology only. It may indeed help to resolve part of the present difficulty relating to the exact definition of the unit of time.

It seems likely that the recent development of a frequency standard (or, according to some, a clock) employing caesium has given us the means of defining an interval of time more accurately than can be done by referring it to the motion of the earth, our present standard.[2] It has therefore been sug-

* Received by the IRE, November 15, 1955.
[1] PROC. IRE, vol. 43, p. 880, July, 1955.
[2] L. Essen and J. V. L. Parry, "An atomic standard of frequency and time interval," *Nature*, vol. 176, pp. 280–282; August 13, 1955.

gested by Bullard,[3] as has been done on several occasions in the past, that the earth should no longer be used for this purpose, and that the standard unit of time, *i.e.*, the second, should now be redefined in terms of the resonant frequency of caesium.

However, there are serious objections to this proposal as far as the standard of time is concerned. Time cannot, like other standards, be kept in a box and taken out for comparison when needed. It is forever moving forward, and it follows that a definition of the standard of time has no significance at all apart from the standard clock which is used for keeping it. Man-made clocks can never be used for this purpose because, no matter how well constructed, they will all stop after a longer or shorter period. While the earth may be a somewhat inaccurate timekeeper, it has the overriding advantage that it will carry on for as long as human beings are likely to be interested. Moreover, its errors can be determined. A quartz crystal or caesium "clock" may be more accurate over short periods, but, compared to the earth, it is more in the nature of stop watch.

However, a considerable length of time is required to determine the errors of the earth's rotation, and hence the exact time as well as the length of one second, as indicated on our quartz or caesium "stop watch," is in some doubt until many months later. This is not generally of great importance to astronomers and surveyors, who are interested in the instant of time rather than in the length of time intervals, but it is of great inconvenience to radio engineers and all those who deal with frequency standards. Frequency has until now been expressed as so many cycles per second, but there seems to be no particular reason why this should be so, and the relation between frequency and the mean solar second exists for historical reasons only.

It is therefore suggested that the practical standard of frequency should be divorced from the standard of time, and this can be done quite easily because a term which does not involve the word "second" is already in use, namely the "hertz." Frequency could from now on be expressed, as before, as so many hertz, but this unit should be redefined as 9,192,632th part of the frequency of caesium. The adoption of a more precise value for this ratio would be a matter for international agreement, and the chosen value should be such that one hertz should equal one cycle per second at some convenient date. The difference between the two units at other times would, of course, be negligible for all but the most precise measurements. Observatories would continue to measure the relationship between the two units for other dates, but in the meantime it would be possible to express the corrections to the frequencies transmitted from standard frequency stations immediately in hertz, without waiting for astronomical data.

J. Hers
Union Observatory
Johannesburg
South Africa

[3] E. C. Bullard, "Definition of the second of time," *Nature*, vol. 176, p. 282; August 13, 1955.

E and C Type Traveling-Wave Devices*

In a letter Heffner and Watkins[1] have defined the E tubes in which the electrons travel on a circular path, the only forces acting upon them being a radial electrostatic force and the centrifugal force. This model was first proposed by Huber[2] and studied by Versnel and Jonker.[3]

Besides the E, M, and O type devices another type of focusing for traveling wave tubes was treated by Mourier[4] and for which the name C type (cyclotron) is proposed. It consists in the same structure as an E device, the electric field being replaced by an axial magnetic field. The cyclotron is the most important device of this type. E-type devices should have a higher efficiency than C types because, as Watkins and Heffner pointed out, in E types potential energy is transformed into rf energy. But the gain/cm of the E types is $\sqrt{\frac{7}{3}}$ smaller than for the C type.

However in the C and E devices as Heffner and Watkins pointed out, the "stiffness" of focusing is insufficient and therefore the limiting current is small. For the E type in the case of a thin beam injected tangentially the limiting current per unit height is

$$I_e \leqq 4\epsilon_0 \sqrt{\frac{2e}{m}} \frac{r_b - r_a}{r_b^2} V_0^{3/2}$$

$$= 2.2 \cdot 10^{-5} \frac{r_b - r_a}{r_b^2} V_0^{3/2}. \qquad (1)$$

r_b = average radius of the beam (cm)
r_a = inner radius of the structure (cm)
V_0 = average voltage of the beam.

In the C type the limiting current is given by a similar formula and is $I_c = \frac{1}{2} I_e$.

In M type devices for a magnetic field equal to the cutoff field the limiting current per unit height is given by

$$I = 0.5 \cdot 10^{-5} \frac{V^{3/2}}{d}. \qquad (2)$$

d = distance line-sole (cm)

d must be of the same order as $r_b - r_a$ and is given by the condition that $\Gamma d = 1 \cdots 3$ (Γ = propagation constant).

r_b in (1) is proportional to the length of the delay line. Therefore in E and C types the limiting current is a function of the length of the delay line; in the O and M type the limiting current is independent of the length of the delay line.

This limits seriously the possibilities of application of C and E types.

P. Guenard and O. Doehler
Compagnie Générale de T.S.F.
Paris, France

* Received by the IRE, November 11, 1955.

[1] H. Heffner and D. A. Watkins, The practicality of E type traveling-wave devices," Proc. IRE, vol. 43, p. 1007; August, 1955.

[2] H. Huber, "Tube à ondes progressives avec focalisation purement électrostatique," French Patent no. 993.492; April 21, 1949.

[3] A Versnel and J. L. H. Jonker, "A Magnetless Magnetron," *Philips Res. Rep.*, p. 458; December, 1954.

[4] G. Mourier, "L'anticyclotron, un nouveau type de tube à propagation d'ondes à champ magnétique," *Ann. Radioélect.*, vol. 5, p. 21; July, 1950.

Transistor Power Converter Capable of 250 Watts DC Output*

The Signal Corps Engineering Laboratories at Fort Monmouth, New Jersey have developed a transistor power converter capable of delivering 250 watts dc output from a nominal 24-volt dc input supply. The type of circuitry employed is that of the "Self-Excited Square-Wave Transistor Power Oscillator"[1] reported on previously.

The complete circuit diagram is shown in Fig. 1 and consists of a pair of high power germanium power transistors[2] connected in a push-pull common base arrangement, in connection with a transformer consisting of a center-tapped primary, center-tapped feedback, and output winding working into a starting reactor, full-wave germanium bridge rectifier and filter condenser, and a single dc source.

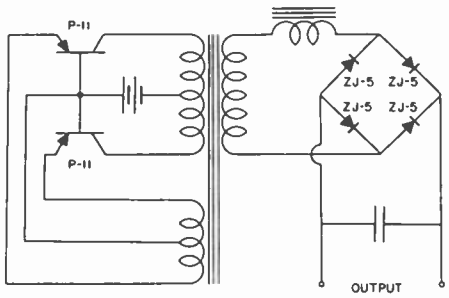

Fig. 1—Circuit diagram of transistor power converter.

Operation at this high power level is made possible by the excellent switching characteristic afforded by selected transistors. Stabilized short circuit collector characteristics, common base connection, obtained for the particular power transistors used in the power converter are shown in Fig. 2. This diagram depicts the emitter to base voltage drive, emitter current, temperature of mounting stud, and collector-to-base voltage drop vs collector current.

As shown in Fig. 2, and dictated by the manufacturer's specifications, utility of characteristics is had up to a collector current of approximately 13.5 amperes when the transistor is mounted directly upon three aluminum heat sink plates with dimensions of 6×6×3/32 inches and standing in an upright position. It is possible to extend this range of utility up to higher collector currents by employing larger heat sinks or by the use of artificial cooling. Similar characteristics were run on the transistors as they will be employed in an actual circuit whereby each transistor is electrically insulated from the metal chassis by a mica washer as suggested by the transistor manufacturer. For this particular test, the same heat sink arrangement is used and results are indicated by dashed curves on Fig. 2. The range of utility, as shown in Fig. 2, indicates the operating points one can design for.

* Received by the IRE, November 11, 1955.

[1] G. C. Uchrin and W. O. Taylor, Proc. IRE, vol. 43, p. 99; January, 1955.

[2] Selected P-11 transistors, manufactured by the Minneapolis-Honeywell Regulator Co.

A check of transistor driving power necessary for a 12.0 ampere collector current gives a value of 29.2 watts. The mounting stud temperature at this current was 136°F. From maximum transistor dissipation curves as a function of mounting stud temperature, as given in the manufacturer's literature concerning these transistors, it is shown that for a mounting stud temperature of 136°F, 37 watts of peak power dissipation is a maximum limit and 21 watts of peak power dissipation is a recommended limit. The actual net transistor dissipation when the transistor is conducting as a closed switch is the difference between the emitter driving power and the power which is additive to the supply source by reason of the forward voltage drop across the collector-to-base diode. The net dissipation is then $V_BI_B+V_CI_C=29.2-6.6=22.6$ watts, which is reasonably close to the recommended dissipation.

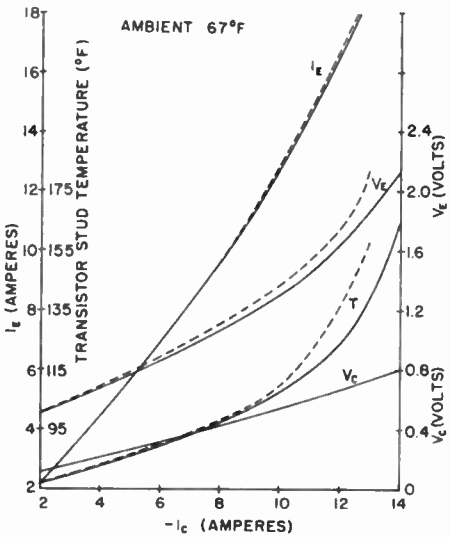

Fig. 2—P-11 type transistor, short circuit collector-to-base characteristic.

In the absence of complete information concerning the emitter and collector dissipations which are had during the switching and off periods of the transistor, particularly the switching-off period when the transistor goes through rather high V_CI_C instantaneous powers in the collector, but also considering that the duty cycle for each transistor is 50 per cent, therefore giving an average dissipation of one-half the dissipation encountered during the whole cycle if the cut-off period of dissipation is neglected, it is considered feasible to design for operation at this particular collector current.

With emitter driving voltage given by the transistor short circuit collector characteristic, and a maximum collector-to-base reverse voltage given as a normal transistor rating, it then becomes a matter of transformer design to arrive at a particular output for a certain size and efficiency.

Due to the principle of operation being dictated by a combination of saturation in the transformer and current limitation in the circuit, frequency of operation was chosen to be in the neighborhood of 100 cycles so as not to encounter high core losses and also to allow for good switching conditions. In the design of the transformer, it is necessary to obtain good switching operation because during the period when the transistor is switching off, it goes through high peak instantaneous powers and therefore the period of transition must be kept short. A transformer with core material having a rectangular hysteresis loop with no air gap (toroidal tape-wound core) gives optimum operation. However, such a type of transformer is rather costly due to the higher core material cost and to the fact that machine winding is not possible when the available window area is to be used to its utmost. Practical considerations may dictate the use of transformers employing Hipersil split "C" cores or laminated cores of various materials. Use of these materials leads to less efficient designs because of the poorer transition characteristics obtained.

TABLE I
(Measured values of voltages and currents are in dc)

V_{in} (volts)	I_{in} (amps)	I_{r1} (amps)	V_{r1} (volts)	Frequency (cps)	Power Input (watts)	Power Output (watts)	Efficiency (per cent)
			Circuit Using Deltamax Transformer				
24.0	11.5	1.82	122.5	107	276	223	80.8
25.0	12.0	1.90	127.0	112	300	241	80.4
26.0	12.5	1.98	131.5	117	325	*260*	80.1
26.5	13.0	2.03	137	120	345	*278*	80.6
			Circuit Using Hipersil Transformer				
24.0	11.0	1.72	117.5	100	264	204	76.6
25.0	11.5	1.81	123	105	288	223	77.4
26.0	12.1	1.90	128	110	315	243	77.4
26.5	12.2	1.93	130	113	323	251	77.6

Some experimental results for the 250-watt dc output supplies working into a resistive load of 70 ohms, with nominal filtering, and operating in an ambient of 25°C are listed in Table I.

The results show that the circuit employing the Deltamax transformer is superior both from the standpoint of power output obtainable and overall efficiency. Operational wave shapes are very rectangular in the Deltamax transformer circuit whereas rounding off is observed for Hipersil transformer circuit at maximum loads.

Operation with the recommended maximum input voltage of 28 volts for these transistors and slight redesign of transformer can lead to power outputs of approximately 300 watts at optimum load.

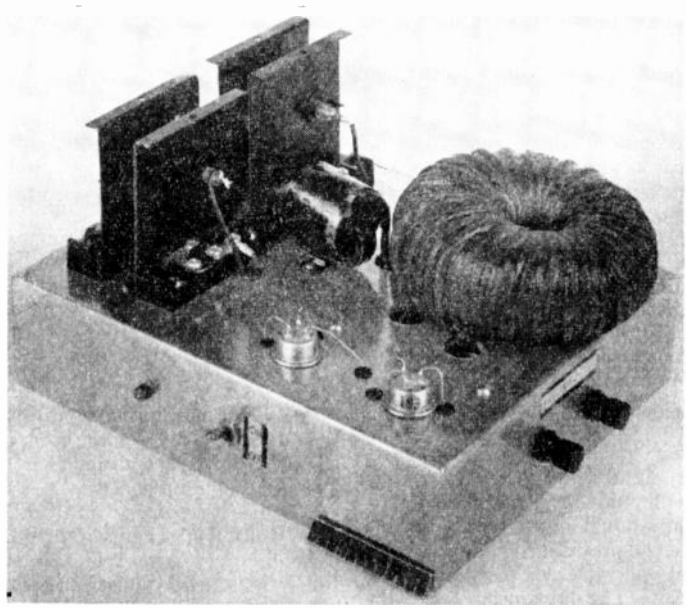

Fig. 3—250-watt, dc power transistor supply.

Two transformer designs were made for use in this circuit. A Deltamax 2-mil tape wound core (6379-D2) transformer was made which weighs 8 pounds, 10 ounces. This transformer was wound with circular cross-section wire with the secondary winding located next to the core so that it could be applied by machine. The second transformer design employs a Hipersil 5-mil "C" core, G-337, whose weight is 9 pounds, 2 ounces, including a mounting bracket. Rectangular wire of equivalent copper cross section was used for the windings for better copper space factor, and the primary winding was located next to the core.

Fig. 3 pictures a demonstration model of the 250 watt power supply employing the Deltamax transformer.

Power conversion measurements were made at an ambient temperature of 25°C. In the case of military ground equipments which are required to operate in ambient temperatures of up to 70°C, derating will be necessary. Preliminary investigations show that for a similar type arrangement 175 watts of dc power output will be possible when operating in an ambient of 70°C.

George C. Uchrin
Power Sources Branch
Signal Corps Engineering Labs.
Fort Monmouth, N. J.

Correspondence

Optimum Gain of Amplifiers*

H. F. Mathis[1,2] has recently presented a graphical method for determining the input and terminating impedances that give maximum efficiency of power transfer through a passive reciprocal two-terminal-pair network. H. M. Altschuler[3] has added an elegant graphical construction that yields the value of the maximum efficiency of power transfer. The present note gives an extension of Mathis' and Altschuler's work to active, nonreciprocal networks. As a result, we can quickly find the input and terminating impedances that yield maximum power gain of an amplifier.

The maximum power gain obtainable from an amplifier that is only conditionally stable with regard to endloading is infinite. Thus, in the search for optimization of the power gain of amplifiers we have to limit ourselves to amplifiers unconditionally stable with regard to endloading.

It has been shown[4] that a nonreciprocal *passive* network can be split into a cascade connection of a reciprocal passive network and an "ideal amplifier-phase shifter" (IAPS). The latter contains the nonreciprocal character of the network. The "matrix of the generalized circuit parameters" (the ABCD matrix) of the IAPS is $ke^{j\phi}I$, where k is a real constant and I is the identity matrix. The resulting equivalent circuit is shown in Fig. 1. The matrix of the IAPS commutes with the matrix of any part of the equivalent circuit. Thus, the IAPS can be inserted anywhere within the equivalent circuit without affecting it. The passivity of the network represented by Fig. 1 imposes the condition

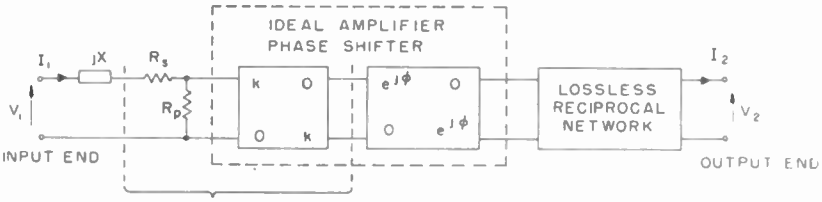

Fig. 1—Equivalent circuit.

$$\tfrac{1}{2}(k + 1/k) \leqq [(R_s + R_p)/R_p]^{1/2}. \quad (1)$$

The equivalent circuit for the passive nonreciprocal network in Fig. 1 can be generalized to represent an arbitrary amplifier by removing restriction (1) (above) and by allowing R_s and R_p to assume negative as well as positive values.

The amplifier is unconditionally stable if and only if the part of its equivalent circuit singled out by brackets in Fig. 1 is unconditionally stable. The latter is unconditionally stable if, and only if, R_s and R_p are restricted to positive values only.

Since the IAPS can be inserted anywhere within the equivalent circuit we can place it at the right end of the equivalent circuit in cascade with the reciprocal part of the amplifier. Thus, every unconditionally stable amplifier can be split up into a cascade connection of a reciprocal passive network and an IAPS. The power gain of the amplifier is optimized when the power loss in the reciprocal passive part of the amplifier equivalent circuit is minimized; in other words, when the efficiency of the reciprocal part is optimized.

The IAPS does not affect impedance transformations. Thus, any impedance transformation of the amplifier can be studied by disregarding the IAPS entirely. The optimization of the efficiency of the passive reciprocal part can be thus carried out directly by following the method of Mathis. Employing reflection coefficient notation we repeat Mathis' and Altschuler's constructions in Fig. 2. The Γ' circle is obtained as the locus of the input reflection coefficient corresponding to all reactive terminations of the amplifier. The reflection coefficient of the input impedance for optimum gain is the point Γ_a. The length $|ON|$ gives the maximum efficiency, η_{max}, of the power transfer through the reciprocal part of the amplifier equivalent circuit. Since the nonreciprocal part of the amplifier yields a power gain $1/|k|^2$, and since

$$\frac{1}{|k|^2} = \left|\frac{Z_{21}}{Z_{12}}\right|^2 \quad (2)$$

where Z_{12} and Z_{21} are the transfer impedances of the over-all amplifier, we find for the optimum power gain, G_{max},

$$G_{max} = \eta_{max}\left|\frac{Z_{21}}{Z_{12}}\right|^2 = |ON|\left|\frac{Z_{21}}{Z_{12}}\right|^2. \quad (3)$$

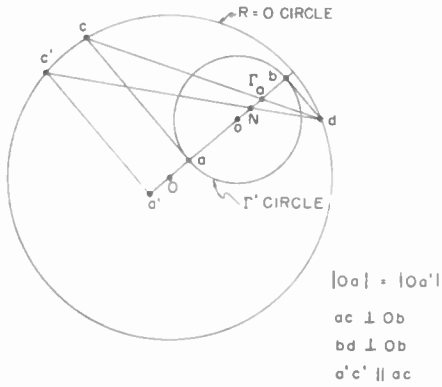

Fig. 2—The graphical construction in the Smith chart (Γ plane).

The writer is indebted to Mr. Folke Bolinder, of the Research Laboratory of Electronics, M.I.T., for drawing his attention to references 1, 2, and 3.

H. A. Haus
Res. Lab. of Electronics and
Dept. of Elect. Engrg.
Mass. Inst. Tech.
Cambridge, Mass.

* Received by the IRE, October 27, 1955. This work was supported in part by the Signal Corps· the Office of Scientific Research, Air Research and Development Command; and the Office of Naval Research.

[1] H. F. Mathis, "Maximum efficiency of four-terminal networks," PROC. IRE, vol. 43, pp. 229–230; February, 1955.

[2] H. F. Mathis, "Experimental procedures for determining the efficiency of four-terminal networks," *Jour. Appl. Phys.*, vol. 25, pp. 982–986; August, 1954.

[3] H. M. Altschuler, "Maximum efficiency of four-terminal networks," PROC. IRE, vol. 43, p. 1016; August, 1955.

[4] H. A. Haus, "Equivalent circuit for a passive nonreciprocal network," *Jour. Appl. Phys.*, vol. 25, pp. 1500–1503; December, 1954.

Contributors

R. S. Berkowitz (S'47–A'48–M'55) was born in Philadelphia, Pa., on February 21, 1923. He received the B.S. degree in electrical engineering from the University of Pennsylvania in October, 1943, and joined the Television Terminal Equipment section of the Radio Corporation of America in Camden, N. J. after graduation.

R. S. Berkowitz

From 1944 to 1946, he was an electronic technician in in the Navy. He then attended the Moore School of Electrical Engineering of the University of Pennsylvania, receiving the M.S. degree in February, 1948.

Since July, 1947, he has been on the research and teaching staffs of the Moore School. He received the Ph.D. degree in June, 1951. At present, as assistant professor in electrical engineering, he is teaching courses in circuit theory and communications theory. He is also a project supervisor for the Institute of Cooperative Research.

Dr. Berkowitz is a member of Sigma Xi, AIEE, SIAM, and AAUP.

❖

D. M. Bowie was born in Tulsa, Okla., on March 12, 1923. He entered the College of Engineering of the University of Tulsa in 1940. During World War II, he served eighteen months in master layout work with Douglas Aircraft Co., and two years as electrical technician with the Army Air Force. He received the B.S. degree in geophysical engineering from the University of Tulsa in 1948.

D. M. Bowie

From 1949 to 1951 he worked as seismic computer with Geophysical Service, Inc. of Dallas, Texas. He entered the University of Utah in 1951 as a teaching fellow and conducted research in nuclear physical measurements. He received the M.S. degree in physics in 1954. Later that year, he joined the staff of Melpar, Inc., Falls Church, Va. where he has worked principally on techniques of microwave measurement.

Mr. Bowie is a member of Sigma Pi Sigma and Sigma Xi.

❖

C. C. Cheng (S'50–A'53) received the B.S. degree in electrical engineering in 1943 from the National Central University of China, and the M.S. degree in communication engineering in 1946 from Harvard University. He has done further graduate study at the Polytechnic Institute of Brooklyn.

C. C. Cheng

He was associated with the National Resources Commission of China from 1943 to 1944. From 1946 to 1949, he worked with the Central Electric Co. of China, and received special training at the Westinghouse Electric Co. In 1952, he joined the RCA Victor Division in Camden, N. J., where he was engaged in advanced development work on transistor circuitry and network theory. Since his transfer to RCA Tube Division in Harrison, N. J. in 1954, he has been working on transistor network and noise study.

Mr. Cheng is the co-author of a book on transistor electronics.

❖

Jess Epstein (A'42–SM'46) received the E.E. degree and the M.S. degree in physics from the University of Cincinnati in 1932 and 1934. From 1934 to 1935, he was an instructor in physics at the Cincinnati College of Pharmacy. In 1935, he joined the research division of RCA Manufacturing Co. at Camden, N. J. He was transferred to RCA Laboratories Division at Princeton, N. J., in 1942, where he is now engaged in work on antennas, transmission lines and propagation.

Jess Epstein

Mr. Epstein is a member of Sigma Xi.

❖

C. D. Graves was born on June 15, 1928 in Detroit, Mich. He received his A.B. degree in physics from the University of Michigan in 1950, and his M.A. degree in physics from Wayne University in 1951. He is now completing work on his Ph.D. degree in physics at the University of Michigan.

C. D. Graves

Since, 1951, Mr. Graves has been doing research work at the University of Michigan Engineering Research Institute, primarily at the Willow Run Research Center. For the past two years this work has been in the field of radar polarization. Previously he has worked on high speed data processing systems and air defense problems.

❖

W. M. Hall (A'33–M'44–SM'45) was born in Burlington, Vt., on July 10, 1906. He attended the University of Vermont and received the B.S. degree in electrical communications from the Massachusetts Institute of Technology in 1928.

W. M. Hall

He was on the staff of the electrical engineering department of M.I.T. until the beginning of World War II, specializing in acoustics and radio communication. In 1934, he received the Sc.D. degree from that institution. During 1940 and 1941, Dr. Hall was on the staff of the M.I.T. Radiation Laboratory.

Since 1941, he has been associated with the Raytheon Manufacturing Co., where he was the project engineer on various radar and countermeasures systems during the war and where he now holds the position of staff engineer on the staff of the manager of the Wayland Laboratory.

Dr. Hall is a member of Sigma Xi and a fellow of the Acoustical Society of America.

❖

J. H. O. Harries (A'28–SM'44) was born on October 13, 1906, at Warley, Essex, England.

J. H. O. Harries

From 1927 to 1934 he worked in his own laboratory near London, and for a time in New York, on television devices, and developed beamed critical distance power tubes. In 1928, he published a computation of the bandwidth likely to be needed by a television service. He became technical head and managing director of Harries Thermionics Ltd. of London in 1934. Between 1934 and 1937 his work included the design of ten types of beamed power output tetrodes, the first tubes of this kind to be manufactured commercially. He also worked on high fidelity amplifiers and the effects of intermodulation distortion.

In 1937 he designed a series of broadcast receivers. One of these designs consisted of a set of replaceable units and used a single

"all stage" tube type for ease of servicing. This unitized receiver was manufactured in South Africa for use in remote districts. Between 1939 and 1941 he designed beam deflection microwave transmitting tubes for the British Government as part of the wartime radar research program. In 1942, he advised the Ministry of Supply on the introduction of radio frequency heating to British industry. During the remainder of the war he worked in London on research on microwave tubes and cavities for Rediffusion Ltd.

He now heads a consulting and research laboratory in Bermuda.

Mr. Harries is a member of the Institution of Electrical Engineers (London) and a Fellow of the Television Society of London.

❖

For a biography and photograph of R. W. Klopfenstein, see page 113 of the January, 1956 issue of PROCEEDINGS OF THE IRE.

❖

D. Loev was born on May 1, 1926, in Philadelphia, Pa. After serving in the Navy as an electronic technician from 1944 to 1946, he received the A.B. degree in mathematics in 1951, and the B.S. degree in electrical engineering in 1952, both from the University of Pennsylvania.

D. LOEV

In 1952, he joined the research staff of the Burroughs Corp. in Paoli, Pa. where he did logical design development of core systems. In 1954, he joined the staff of the Weizmann Institute of Science where an IAS computer is being constructed.

Mr. Loev is a member of the Mathematical Association of America and Pi Mu Epsilon, and an associate member of the American Institute of Electrical Engineers, and RESA.

❖

R. G. Medhurst was born in London, England, on April 29, 1920. He received the B.Sc. degree in mathematics from Queen Mary College, University of London in 1941.

R. G. MEDHURST

In 1942 he joined the Research Laboratories of the General Electric Co., Ltd., in Wembley where he is now on the senior scientific staff. His work has included investigation of antenna design and vhf measurement problems.

At present, he is studying distortion problems in connection with uhf trunk radio systems.

J. L. Melchor was born on July 6, 1925 in Mooresville, N. C. He received the B.S. degree and the M.S. degree in physics from the University of North Carolina. His undergraduate studies were interrupted by military service in the U. S. Navy. In 1949 he worked as a civilian physicist with the U. S. Navy Mine Countermeasures Station. Attending the University of Notre Dame in 1950 he was a U. S. Rubber Co. Fellow in High Polymer Physics. In 1952 and 1953 he worked with Missile Division of Bendix Aviation Corp. and received the Ph.D. from Notre Dame in 1953.

J. L. MELCHOR

Since 1953 he has been with the Electronic Defense Laboratory of Sylvania Electric Products Inc. and is currently engaged in ferrite research at microwave frequencies. He is a member of Sigma Xi.

❖

W. Miehle (A'42–M'47) was born in Ulm, Germany in 1915. He received the B.S. degree in physics from M.I.T. in 1938 and studied at the Princeton Graduate School in 1938 and 1939.

W. MIEHLE

From 1940 to 1946 he was with RCA Victor in Camden, N. J. and was a member of the research department of Philco Corp. in Philadelphia, Pa. from 1946 to 1949. His work included design of test equipment and Schmidt optical systems, and numerical analysis of circuits and noise in radar systems. He also taught mathematics for engineers at RCA.

Since 1949, Mr. Miehle has been with the Burroughs Research Center, in Paoli, Pa. He has done systems, logical design and applications studies for computers, and is now in charge of a programming project.

Mr. Miehle is a member of the American Physical Society, the Association for Computing Machinery, the Society for Industrial and Applied Mathematics, and the Scientific Research Society of America.

❖

John Paivinen (S'47–A'51) was born in Chicago, Ill. on May 19, 1924. He received the B.S. in electrical engineering and the B.S. in engineering mathematics in 1949, and in 1951, the M.S. from University of Michigan. Since then he has been with Burroughs Corp. with assignments in circuit design of digital computers using tube, magnetic, and transistor techniques.

J. PAIVINEN

J. I. Pankove (A'45–S'47–A'49–SM'55) was born in Russia on November 23, 1922. He completed his secondary education in France, and attended the University of California in Berkeley, Calif. from 1942 to 1944. He received the B.S. degree in 1944.

J. I. PANKOVE

After serving with the Army for two years, he returned to the University of California and received the M.S. degree in 1948. Since then he has been engaged in semiconductor research at the RCA Laboratories in Princeton, N. J.

Mr. Pankove is a member of Sigma Xi.

❖

W. O. Puro (S'49–A'50) was born in Bessemer, Mich., on June 6, 1926. In 1949, he received the B.S. degree in electrical engineering from the University of Michigan.

W. O. PURO

He joined the Bell Aircraft Corp. immediately afterward, where he worked on antenna design for guided missile applications. In 1952 he joined Melpar, Inc., where he has worked on antenna systems for aircraft use. He is currently employed at Melpar, Inc., as a project engineer.

❖

J. E. Rowe (A'51) was born in Highland Park, Mich., in 1927. He received the B.S. degree in electrical engineering and in mathematics in 1951, the M.S. degree in electrical engineering in 1952, and the Ph.D degree in 1955, all from the University of Michigan.

J. E. ROWE

Since 1951, he has been associated with the Engineering Research Institute of the University of Michigan, engaged in research on microwave systems and tubes. Formerly a lecturer in electrical engineering. Dr. Rowe is now an assistant professor of electrical engineering at the University of Michigan.

He is a member of American Institute of Electrical Engineers, Sigma Xi, Phi Kappa Phi, Tau Beta Pi, and Eta Kappa Nu.

❖

J. Shmoys (S'44–A'46–M'52) was born on October 6, 1923, in Warsaw, Poland. He received the B.E.E. degree from the Cooper

Union in 1945 and the Ph.D. degree in physics from New York University in 1952.

In 1945 and 1946 he was with the Marine Division of the Bendix Aviation Corp. and Sperry Gyroscope Co. Research Laboratories working on servomechanism development. From 1946 to 1949, Dr. Shmoys was a research assistant at N.Y.U., engaged in millimeter wave research. Since 1949, he has been doing theoretical research in propagation at the Electromagnetics Division of the Institute of Mathematical Sciences at N.Y.U. He is now in the electrical engineering department of the Polytechnic Institute of Brooklyn.

J. SHMOYS

Dr. Shmoys is a member of the American Physical Society, Sigma Pi Sigma, Pi Mu Epsilon, and Tau Beta Pi.

❖

R. M. Stewart was born October 17, 1925, in Washington, D. C. He attended the California Institute of Technology where he received the B.S. degree in physics in 1947. During 1948 and 1949, he was a student and instructor in physics at George Washington University and received the M.S. in physics.

R. M. STEWART

He then worked for the Ryan Aeronautical Co. as an analyst on problems of aircraft aerodynamics, automatic control and performance. From 1950 to 1954, Mr. Stewart worked at the California Institute of Technology, Jet Propulsion Laboratory, where he held the position of senior research engineer in charge of the guidance and control system analysis group. During this time, he also organized and taught a course at the Institute on advanced communication theory. In the latter half of 1954, he was employed by the Ralph M. Parsons Co. to work on theoretical problems and the planning of communication and instrumentation systems. Since then, he has returned to the Jet Propulsion Laboratory where he now holds the position of staff engineer.

Mr. Stewart is a member of Sigma Xi and the American Rocket Society.

L. B. Valdes (A'46–M'52) was born in Marianao, Havana, Cuba, on June 12, 1928. He received the B.E. in E.E. degree from Tulane University in 1946 and the M.S. and Ph.D. degrees in electrical engineering from Northwestern University in 1947 and 1954.

L. B. VALDES

From June, 1949, to September, 1954, Dr. Valdes was a member of the Technical staff at Bell Telephone Laboratories in Murray Hill, N. J. There he worked on transistor problems in the Transistor Development Department and later in the Transistor Physics Research Department. For one year afterward he directed the development of intrinsic-barrier transistors at Pacific Semiconductors, Inc., Culver City, Calif. Since October, 1955, Dr. Valdes has been a member of the group which Dr. Shockley has organized at Beckman Instruments, Inc., Fullerton, Calif. to do research and development and to manufacture semiconductor devices.

Dr. Valdes is a member of the American Physical Society, Eta Kappa Nu, and Sigma Xi.

❖

P. H. Vartanian was born in Rochester, N. Y. on June 14, 1931. He received the B.S. degree in electrical engineering in 1953 from the California Institute of Technology and the M.S. degree from Stanford University in 1954. At Stanford he was a Tau Beta Pi Fellow and later a research assistant at the Electronics Research Laboratory. In 1951 and 1952 he worked part time at the U. S. Naval Radiological Defense Laboratory on radiation detectors.

P. H. VARTANIAN

In 1954 he joined the Electronic Defense Laboratory of Sylvania Electric Products Inc. and is engaged in research in microwave applications of ferrites. He is also doing work at Stanford University under the Honors Cooperative Program leading to the Ph.D. degree in electrical engineering.

He is a member of Tau Beta Pi.

❖

H. T. Ward, Jr., (A'51) was born in Granite Falls, N. C., on June 16, 1926. He received the B.S. degree in physics from the University of North Carolina in 1948 and the M.S. degree in electrical engineering from North Carolina State College in 1950.

H. T. WARD, JR.

From 1950 to 1953 he worked on dielectric measurements at the U. S. Naval Ordnance Laboratory, Silver Spring, Md. Subsequently he spent a year with the Washington Institute of Technology, College Park, Md. working on radiosondes. Since 1954, he has been with Melpar, Inc., in Falls Church, Va., where his research studies are primarily concerned with the development of microwave antennas.

Mr. Ward is a member of Sigma Xi and Eta Kappa Nu.

❖

J. Wylen (S'48–A'51) was born on May 11, 1924, in Philadelphia, Pa. He received the B.S. degree in electrical engineering from the University of Pennsylvania in 1949, and the M.S. degree in electrical engineering from M.I.T. in 1950. Since that time he has been employed by the Burroughs Corporation at the Research Center in Paoli, Pennsylvania. He has worked on magnetic memory systems, ferroresonant circuits, high frequency magnetic amplifiers, and application of magnetic cores to digital circuits. At present he is working on a large scale electronic digital computer.

J. WYLEN

Mr. Wylen is a member of the American Institute of Electrical Engineers, RESA and Sigma Xi.

IRE News and Radio Notes

Seventh Regional Conference Set for April 11–13, 1956

The Seventh Regional Technical Conference and Trade Show will be held at Hotel Utah, Salt Lake City, April 11–13.

Technical sessions will feature the following topics: transistors and transists circuitry, antennas and propagation, nuclear science and instrumentation, military electronics and communications, audio systems, and circuit theory. The Atomic Energy Commission testing station at Arco, Idaho, will make facilities and personnel available for the nuclear and instrumentation sessions. A student technical session will be held on Wednesday evening, April 11.

The first day of the conference will be highlighted by a luncheon at which R. L. Evans, announcer and narrator of the Sunday morning broadcasts from Salt Lake City, will be the speaker. The following day will feature a Mormon Tabernacle organ recital after which the organ may be inspected. In the evening the speaker at the dinner meeting will be Simon Ramo, executive vice-president of the Ramo-Wooldridge Corporation. A technical inspection trip will be arranged for the last day of the conference to the Kennecott Open Pit Mine at Bingham, Utah.

Women's activities will consist of two luncheons and a scenic tour of Salt Lake City, and they are also invited to join the men for the dinner meeting and organ recital. Skiing facilities will also be available to conference visitors.

Conference registration will begin April 10 and continue throughout the conference. No advance registrations through the mail will be accepted. Hotel reservations may be made directly with any hotel in Salt Lake City or through the registration committee chairman, Clay Westlund, Engineering Hall, University of Utah, Salt Lake City, Utah.

S. Ramo will speak at Conference dinner meeting.

World's largest open pit copper mine at Bingham.

Stanford Announces 1956–57 Fellowships in Electronics

Stanford University has announced its program of fellowships and assistantships for graduate study in electrical engineering during the term 1956–57. Fellowship holders registering for a full program of study may participate in the research program and receive academic credit for this work. Holders of research assistantships will be assigned to organized projects on transistors, microwaves, electron tubes, radio propagation, computers, network theory, high voltage, and illumination. A few part-time research assistants will also be assigned to the Stanford Research Institute to work in fields of special interest such as antennas, acoustics, and computers. Teaching assistantships will include assisting in electronics and machinery laboratory instruction.

Letters of inquiry should be addressed to the Assistantship Committee, Electrical Engineering Department, Stanford University, Stanford, California, from whom application forms and bulletins will be available upon request. To receive full consideration applications should be submitted by March 15, 1956, except for the University Graduate Fellowship which closes February 15.

IRE Section Formed in Japan

At its December meeting the IRE Executive Committee approved the establishment of an IRE Section in Japan, the fifth Section to be formed outside North America and the fifteenth outside the continental United States. In addition to Japan, IRE Sections are now operating in Egypt, Israel, Buenos Aires, Hawaii, and in ten Canadian cities. Sixty-six Sections are also operating within the United States.

Calendar of Coming Events

IRE-AIEE-U. of P. Conference on Transistor Circuits, U. of Pennsylvania, Philadelphia, Pa., Feb. 16–17

IRE-AIEE Scintillation Counter Symposium, Shoreham Hotel, Washington, D. C., Feb. 28–29

Conference on Radio Interference Reduction by Armour Research Foundation, Chicago, Ill., Mar. 6–7

IRE National Convention and Radio Engineering Show, Waldorf-Astoria Hotel and Kingsbridge Armory, New York City, Mar. 19–22

Symposium on the Application of Ferrite Devices to Microwaves, Harvard Univ., Cambridge, Mass., Apr. 2–4

PGIE-AIEE-ISA Conference on Magnetic Amplifiers, Syracuse, N. Y., Apr. 5–6

Seventh Regional Technical Conference and Trade Show, Hotel Utah, Salt Lake City, Utah, Apr. 11–13

Tenth Annual Spring Television Conference of the Cincinnati Section, Engineering Society of Cincinnati Building, Cincinnati, Ohio, Apr. 13–14

National Industrial Research Conference, Hotel Sherman, Chicago, Ill., Apr. 18–19

New England Radio Engineering Meeting, Sheraton Plaza Hotel, Boston, Mass., Apr. 23–24

PGCT-PIB Symposium on Nonlinear Network Theory, Engineering Society Building, New York City, Apr. 25–27

URSI Spring Meeting, National Bureau of Standards, Washington, D. C., Apr. 30–May 3

IRE-RETMA-AIEE-WCEMA Electronic Components Symposium, U. S. Department of Interior, Washington, D. C., May 1–3

National Aeronautical and Navigational Conference, Hotel Biltmore, Dayton, Ohio, May 14–16

Symposium on Reliable Applications of Electron Tubes, University of Pennsylvania, Philadelphia, Pa., May 22–23

Over 400 Attend November National Aeronautical Symposium in Utica, New York

Left—Shown at the symposium, which was sponsored by the Professional Group on Communications Systems, are (*left to right*): P. J. Schenk, Advisory Staff; L. N. Ridenour, editor-in-chief of the M.I.T. Radiation Laboratory Series of technical books and banquet speaker; R. C. Benoit, Jr., Publicity Chairman; and W. J. Kuehl, Symposium Chairman. *Below*—(*Front row*): L. N. Ridenour; P. J. Schenk; W. R. Krafft, Vice-Chairman, Technical Program; R. C. Benoit, Jr.; W. J. Kuehl; H. Davis, A. A. Kunze, and R. L. Marks, Advisory Staff; J. T. Pyle, Special Aide to Assistant Secretary of Navy for Air; E. V. Hogan, Chairman of the Guest Speakers Committee. (*Rear*): H. J. Crowley, Arrangements Chairman; Major S. J. Wisniewski, Arrangements Committee; H. A. Carlson, Technical Program Assistant; C. Willard, Registration Committee, and R. McMillan.

The IRE Presents Plaque to Employees of the George Banta Company, Inc.

. plaque to commemorate twenty-eight years of mutually satisfying association was ecently given to the employees of the George Banta Company, Inc. The inscription eads "for more than one-quarter of a century, the major advances in radio and lectronics have appeared in the publications of the Institute of Radio Engineers. 'heir printing and distribution have been effectively handled in a cooperative spirit y the George Banta Company, Inc. Thus the Banta personnel have substantially contributed to the advancement of radio and electronics. In grateful appreciation, the Institute of Radio Engineers, by action of its Board of Directors, presents this plaque." Shown making the presentation at a dinner are (*left to right*): G. W. Bailey, Executive Secretary of the IRE; George Banta, Jr., President of the George Banta Company, Inc.; J. D. Ryder, 1955 IRE President; C. A. Peerenboom, Vice-President of the printing firm; and E. K. Gannett, Managing Editor of the IRE.

IRE ACTIVITIES

Along the Eastern Seaboard

The IRE Instrumentation Conference at Atlanta, Georgia, jointly sponsored by the Professional Group on Instrumentation and the Atlanta Section, was held November 28–30. Thirty-two papers were presented in six technical sessions. Tours of the Lockheed Aircraft Corporation plant at Marietta and the Electronic Computer Center at Georgia Institute of Technology, and a speech at the banquet by 1955 IRE President J. D. Ryder were highlights of the conference.

A sightseeing tour, a visit to an art museum and a tea featured the women's program. B. J. Dasher was general chairman of the conference. Other session chairmen were: E. K. Ritter, *Recording and Data Utilization;* T. L. Greenwood, *Data Handling Systems;* G. B. Hoadley, *Processing Techniques;* R. L. Sink, *Analogue to Digital Conversion;* R. D. Hurlbert, *Transducers*. Committee chairmen for the conference were: R. E. Eskew, *Arrangements;* W. B. Wrigley, *Exhibits;* D. L. Finn, *Program;* and W. K. Bugg, *Publicity*. F. G. Marble was chairman of the Professional Group on Instrumentation and D. L. Finn was chairman of the Atlanta Section.

The 1955 IRE President also visited the Northwest Florida Section at its November meeting which was presided over by Fred Howard, Vice-Chairman of the Section. Dr. Ryder gave a short talk on printed circuitry. He also visited the air-borne radar laboratories of the Air Force Armament Center.

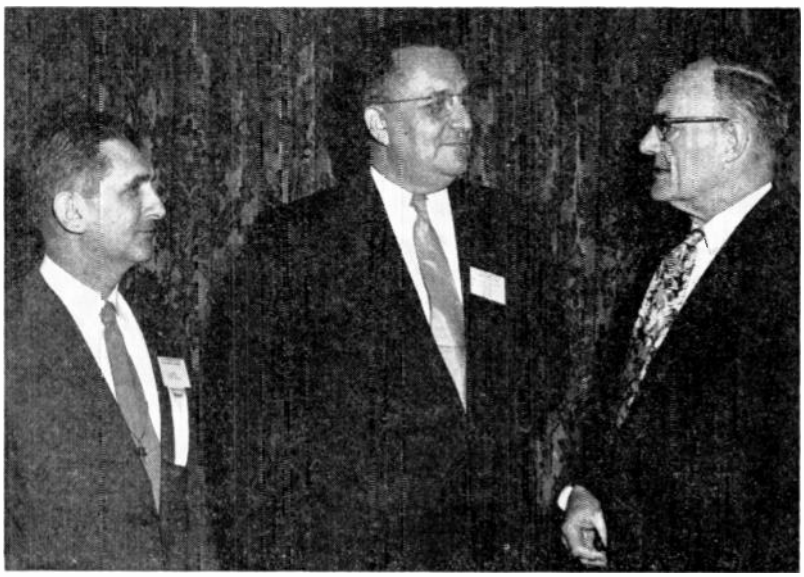

Above: Col. B. R. Van Leer, President of the Georgia Institute of Technology, chats with Dr Ryder (*center*) while B. J. Dasher (*left*), General Chairman of the conference looks on.

Above: On a visit to the Northwest Florida Section, 1955 IRE President J. D. Ryder (*left*) tours the Air Force Armament Center at Eglin Air Force Base with Maj. Gen. E. P. Mechling. They are shown inspecting a M-39 aircraft gun. *Left:* Dr. Ryder toured also the Bombing Systems Branch and Test Equipment Laboratory of the Center where he was shown the ERA 1103 Computer, which is used for armament test data reduction. Then following a dinner meeting of the Section, Dr. Ryder visited the Naval Mines Defense Laboratory at Panama City, Florida.

Further north along the Atlantic seaboard, the Boston Section and the Professional Group on Audio held a joint meeting at Kresge Auditorium on the campus of Massachusetts Institute of Technology. The meeting, presided over by Weiant Wathen-Dunn, Acting Chairman of the Professional Group on Audio, featured a discussion of the acoustical design of Kresge Auditorium. R. H. Bolt spoke on the structural features of the building that were necessary to take care of its heavy schedule of planned cultural and religious activities. R. B. Newman discussed its architectural design and acoustical facilities. Gabriel Farrell, Jr. described the audio facilities of the auditorium.

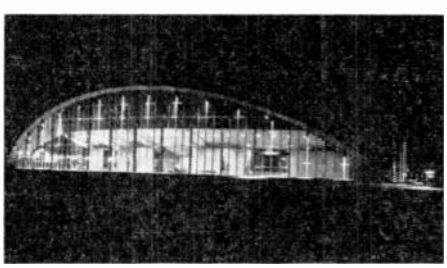

Kresge Auditorium, M.I.T.'s cultural and religious center, contains a 1200-seat auditorium, a 200-seat theater, two rehearsal rooms, and storage space.

L. to R.: R. H. Bolt, L. L. Beranek, acoustical consultants; Weiant Wathen-Dunn; R. B. Newman, acoustical consultant; G. Farrell, Jr., audio designer.

C. R. Kraus, Section Chairman, introduces speaker.

H. F. Olson explains the principles upon which his music synthesizer is based to an audience in Philadelphia, which numbered over a hundred people.

Music Synthesizer Shown to Philadelphia Section

The Philadelphia Section of the IRE held a joint meeting with the Professional Group on Audio recently at the Engineers' Club, Philadelphia. Over a hundred attended.

C. R. Kraus, Section Chairman, introduced H. F. Olson, who spoke on the electronic music synthesizer, the work of Dr. Olson and Herbert Belar of RCA Laboratories, Princeton, New Jersey. The synthesizer is a device that produces music from a coded record. The record is produced by a musician, musical engineer, or composer. The synthesizer provides means for recording and reproducing a tone of any frequency, intensity, growth, duration, decay, portamento, timbre, vibrato, or variation. In addition to explaining the audile and engineering principles upon which the synthesizer operated, Dr. Olson played a demonstration record to show the fidelity of synthesized reproduction.

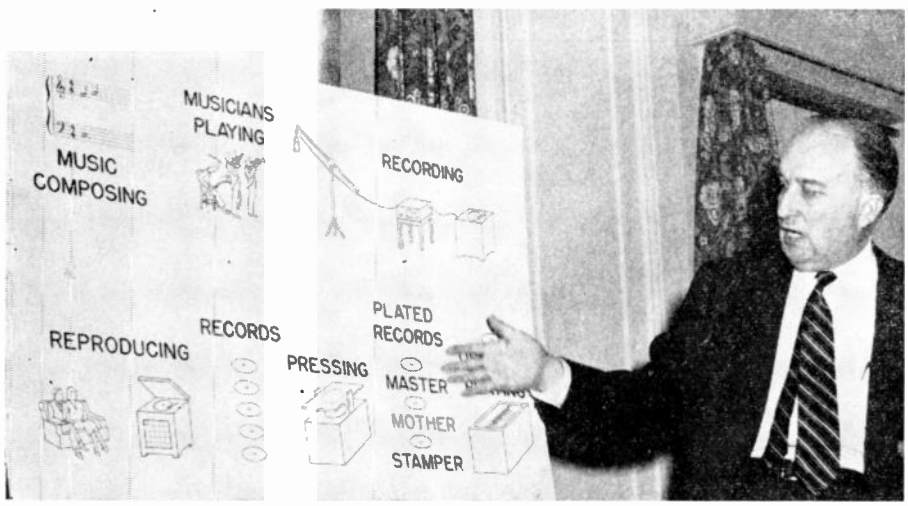

Complete Standards Available

It is now possible to purchase a complete set of all available IRE Standards published through December, 1955 from IRE Headquarters, 1 East 79 Street, New York 21, N. Y. The cost of one set is $32.50.

A sturdy three-ring binder for holding a set of Standards, with "IRE Standards" imprinted in gold on the cover and spine, may be purchased for an additional $5.50.

During the calendar year 1955, the IRE has published the following Standards: Standards on Television: Definitions of Television Signal Measurement Terms, 1955; Standards on Television: Definitions of Color Terms, 1955; Standards on Antennas and Waveguides: Definitions for Waveguide Components, 1955; Standards on Industrial Electronics: Definitions of Industrial Electronics Terms, 1955; Standards on Radio Receivers: Methods of Testing Receivers Employing Ferrite Core Loop Antennas, 1955; Standards on Graphical and Letter Symbols for Feedback Control Systems, 1955; and Standards on Pulses: Methods of Measurement of Pulse Quantities.

Swedish Honor Goes to Kelly

Mervin J. Kelly, President of Bell Telephone Laboratories, and a Fellow of the IRE, has been elected a Foreign Member of the Swedish Royal Academy of Sciences for his research in the fields of electronics and electrotechnics.

The Swedish Royal Academy of Sciences was founded in 1739 by Carl Linnaeus and others for the encouragement of the natural sciences and mathematics. It awards the prizes in chemistry and physics of the Nobel Foundation. The academy, which is associated with a number of Swedish museums, carries out its work mostly through scientific institutions, publication of scientific pamphlets, and in providing funds to outstanding scientists and authors.

Automation Symposium Held by Cedar Rapids Section

Approximately one hundred and eighty-five engineers recently attended a one-day Symposium on Automation for Electronics, sponsored by the Cedar Rapids Section of the IRE. Papers presented included *Automation Is Coming of Age* by L. K. Lee of General Mills, *Design and Plant Engineering Considerations in Automatized Television Receiver Production* by John Landeck of Admiral, and *Automatic Testing* by G. F. Baldwin of General Electric. At the luncheon immediately preceding the symposium John Diebold of John Diebold & Associates delivered an address entitled "Why We Have Automation," and at the banquet following the symposium R. C. Sprague of Sprague Electric spoke on "The Future of Electronics through Automation."

Committee chairmen for the symposium were J. Briggs, General Chairman; R. Weeks, Program; D. Hodgin, Properties; R. Olson, Luncheon and Banquet; V. Perry, Publicity; G. March, Publications; F. Dill, Registration; R. Vander Hamm, Specialties; J. McElroy, Hospitality; and C. Tinch, Treasurer.

Magnetic Amplifiers Subject of Conference at Syracuse

A Special Technical Conference on Magnetic Amplifiers, co-sponsored by the AIEE Committee on Magnetic Amplifiers, the IRE Professional Group on Industrial Electronics and the ISA, Central New York Section, will be held in Syracuse, New York at the Syracuse Hotel on April 5 and 6, 1956. Technical sessions, a manufacturers' exhibit of magnetic amplifiers, components and associated products, and a banquet on Thursday evening, April 5, are planned.

The first technical session will be tutorial in nature and will consist of four papers by guest speakers. Papers and speakers for this session are as follows: *A General Introduction to the Theory of Magnetic Amplifiers* by W. C. Johnson of Princeton University; *Recent Advances in the Theory of Magnetic Amplifiers* by R. Barker of Yale University; *Fundamentals of the Magnetization Process* by Charles Bean of the General Electric Co.; and *Present Methods of Core Evaluation, Matching and Grading* by R. W. Roberts of Westinghouse Electric Corp.

The remaining three technical sessions will each consist of four or five papers chosen from those submitted to the Technical Program Committee and will cover the subjects of materials, components, theory and application.

Committee chairmen for the conference are as follows: *Steering Committee*, H. W. Lord and A. B. Haines; *Technical Program*, P. L. Schmidt; *Publications*, David Feldman; *Hotel Arrangements*, John Becker; *Registration*, August Haedecke; *Finance*, J. W. Munnis; *Publicity*, F. J. Lingel; *Coordination*, C. F. Spitzer; *Exhibits*, Samuel Seely.

The registration fee for the conference will be $3.00 and the cost of the banquet Thursday evening will be $5.00 per plate. Papers presented at the conference will be published subsequent to the conference in the report of the Special Technical Conference and will be available at $4.00 each if ordered in advance at the conference.

Exhibit space can be obtained at a cost of $2.50 per square foot. The usual booth size is 6′×8′ or 6′×10′. This charge includes the booth, background curtains, a table, and chairs. Manufacturers desiring exhibit space are invited to contact S. Seely, Dept. of Electrical Engineering, Syracuse University, Syracuse, New York.

OBITUARY

Robert E. Shelby (A'29–M'36–SM'43–F'48), vice-president and chief engineer of the National Broadcasting Company, died recently.

R. E. SHELBY

A pioneer in the development of black-and-white and color television, Mr. Shelby had been with NBC since 1929. He was promoted to vice-president and chief engineer in July, 1954.

Mr. Shelby, who entered television twenty-four years ago and became one of the leading figures in the industry, had a long list of technical achievements to his credit.

When NBC first established its television development laboratory in the Empire State Building in 1931, he was placed in charge of the project, supervising the earliest experimental work in TV operation techniques.

From 1935 to 1937, Mr. Shelby assisted in the organization of RCA-NBC field tests of all-electronic television and in the design of equipment and facilities for those tests.

During World War II, Mr. Shelby directed NBC's wartime research and development activities, including the development of an air-borne television reconnaissance system for the Navy. He also served during this period as technical consultant to the National Defense Research Committee.

Mr. Shelby participated actively for a number of years in the television standardization work of various industry committees, including the National Television System Committee, the Radio Technical Planning Board and the Radio-Electronics-Television Manufacturers Association.

Before his promotion to vice-president and chief engineer he was director of color television systems development for NBC, and in this post played an important role in the introduction of RCA-pioneered compatible color television.

Among the other executive positions Mr. Shelby held in the NBC engineering department were director of technical development and director of technical operations for the television network.

Born in Austin, Tex., on July 20, 1906, Mr. Shelby was graduated from the University of Texas, where he received the degrees of Bachelor of Science in electrical engineering, Bachelor of Arts and Master of Arts. He went to work for NBC shortly after he graduated.

❖

Carleton H. Schlesman (SM'45), deputy chief of the Underwater Ordnance Department at the Naval Ordnance Laboratory, White Oaks, Maryland, died recently. Dr. Schlesman was graduated from Lehigh University with a bachelor's degree in engineering in 1922. He got his Ph.D. from Johns Hopkins in 1925 and afterward joined the Socony-Vacuum Oil Company in Brooklyn as chief automotive engineer. In 1945 he became associate laboratory manager of the oil company in New Jersey, the position he held until he came to this area in 1949 as a technical consultant and chief of the torpedo division at the Naval Ordnance Laboratory.

Dr. Schlesman held over twenty-three patents in petroleum and instrumentation.

He held membership in the American Chemical Society, the American Physical Society, Society of Automotive Engineers, American Association for the Advancement of Science, and American Petroleum Institute.

PROFESSIONAL GROUP NEWS

EIGHT NEW CHAPTERS ANNOUNCED

The Executive Committee, at its meeting on December 5, approved the following chapters: Washington, D. C. Section, PG on Medical Electronics; San Francisco Section, PG on Microwave Theory and Techniques; Baltimore Section, PG on Automatic Control; Houston Section, PG on Electronic Computers; Pittsburgh Section, PG on Broadcast Transmission Systems.

The Executive Committee, at its meeting on January 4, approved the following chapters: China Lake Section, PG on Circuit Theory; Montreal Section, PG on Electronic Computers; Washington, D. C. Section, PG on Military Electronics.

BUSY PROGRAM PLANNED BY VEHICULAR COMMUNICATIONS PG

The Professional Group on Vehicular Communications is planning a symposium entitled "New Horizons for Vehicular Communications" for the 1956 National Convention. J. C. Neubauer is in charge of details. The next issue of *Transactions*, to be published in early 1956, will include the papers presented at the 1955 National Convention which was held in Portland, Oregon, September 26–27.

K. G. Worthen has been appointed chairman of the committee representing the Group at the 1956 WESCON Meeting in Los Angeles.

Two new chapters are being organized in Portland, Oregon, and San Francisco. The establishment of the Portland Chapter has already been approved by the IRE Executive Committee, and the San Francisco Chapter will be headed by I. M. Ellis when plans for its establishment are completed.

TECHNICAL COMMITTEE NOTES

The **Antennas and Waveguides** Committee met at IRE Headquarters on November 9 with Chairman H. Jasik presiding. A large portion of the meeting was devoted to the discussion of the Proposed Standards on Waveguide and Component Measurements. The committee discussed the Antenna and Propagation Section of the coming National IRE Convention. In response to an inquiry from the International Electrotechnical Commission requesting comments regarding international standardization of waveguide sizes, Dr. Jasik pointed out that the IRE does not attempt to standardize components, only definitions and measurements.

Chairman W. R. Bennett presided at a meeting of the **Circuits** Committee held at IRE Headquarters on November 29. The entire meeting was devoted to the discussion of the Proposed Standard on Definitions that is being prepared by the committee.

The **Facsimile** Committee met at the Times Building on November 18 with Chairman K. R. McConnell presiding. The Committee reviewed the Proposed Standards on Facsimile: Definitions of Terms that is presently under consideration in the Standards Committee. The Proposed IRE Facsimile Test Chart was reviewed and corrections were made in the explanatory text that will accompany the Test Chart.

Chairman H. R. Mimno presided at a meeting of the **Navigation Aids** Committee held at IRE Headquarters on November 18. The committee continued its discussion of the Proposed Standard on VHF Omni-range. As usual, the discussion was directed primarily toward clarification of the purpose of each measurement and toward a thorough understanding of the recommended procedure.

The **Radio Frequency Interference** Committee met at the RCA Plant, Cherry Hill, New Jersey, on December 5 with Chairman R. M. Showers presiding. The business meeting held at IRE Headquarters on September 11 by the RETMA Radiation Committee, which was also attended by members of the Federal Communications Commission and this committee, was reviewed. The manual of good engineering practice, being prepared by a task group under E. O. Johnson, is being actively developed. A draft of this document should be available in two months. J. A. Hansen reported that he had contacted W. O. Swinyard, chairman of the subcommittee that is preparing the Proposed Standards for TV Receivers, and discussed with him the section on interference measurements. He reported that the proposed standard is now undergoing extensive revision.

Chairman E. Weber presided at a meeting of the **Standards** Committee held at IRE Headquarters on November 10. The Proposed Standards on Electron Devices: Definitions of Terms Related to Microwave Tubes (Klystrons, Magnetrons, and Traveling Wave Tubes) was unanimously approved as an IRE Standard. The following Proposed Standards were given consideration: Proposed Standards on Electron Devices: Definitions of Terms Related to Storage Tubes; Proposed IRE Facsimile Test Chart; Proposed Standards on Facsimile: Definitions of Terms.

The **Solid State Devices** Committee met at IRE Headquarters on November 30 with Chairman H. L. Owens presiding. The following subcommittees have been organized: Subcommittee 28.4 on Semiconductor Devices, Subcommittee 28.5 on Dielectric Devices, and Subcommittee 28.6 on Magnetic Devices. Mr. Owens announced that R. R. Law has been appointed vice-chairman of the committee. Mr. Owens reported that the following Proposed Standards have been approved by the committee and are awaiting the approval of the Standards Committee: Proposed Methods of Testing Transistors, and the Proposed Letter Symbol Standard for Semiconductor Devices.

Books

Static and Dynamic Electron Optics by P. A. Sturrock

Published (1955) by Cambridge University Press, 32 East 57th St., N. Y. 22, N. Y., 236 pages+4 page index+x pages. Illus. 8¼×5½. $5.50.

This monograph is the latest addition to the relatively large number of books on electron optics which have appeared in Europe during the last ten years. The interest in this specialized discipline of electron physics is as great in the United States as it is in Europe but European publishers appear to be in a better position to publish books on this subject than their American counterparts.

In view of the large amount of material which exists in this field, few authors have even attempted to give a comprehensive account of the subject. It implies therefore no criticism if the omissions in Sturrock's book are pointed out.

First of all it should be pointed out that the monograph is a theoretical book. Material on devices, experimental methods for determining electron optical parameters, and comparisons between theory and experimental results are not included. The theory is developed very systematically starting from first principles; the optical or Hamiltonian method rather than the electron ballistical method is used, and as far as this reviewer is aware, the book gives the most lucid account of this method, which was first applied to the field of electron optics by W. Glaser. Furthermore, this book is the first to develop these methods to make them applicable to time-varying fields as employed in particle accelerators.

The theory presented in the book deals only with problems of motion of electrons in fields and does not give methods—even mathematical ones—for determining the fields from electrode geometries. Furthermore, it is limited to geometrical electron optics and hence phenomena due to the wave nature of electrons and due to space charge effects in electron streams are not presented. Also, radiation reactions occurring in particle accelerators are neglected.

All these omissions are deliberate and actually increase the value of the book, permitting the author a thoroughness, otherwise impossible, which make the book very readable.

The book is divided in two parts. The first part deals with static problems which occur in cathode ray tubes, electron microscopes, mass spectrometers, etc., and in it, general methods are developed. The second part contains an account of the "strong focussing" method, or perhaps better called "periodic focussing" method, but only as it is applicable to beams of small space charge densities.

In conclusion, it should be stated that this book is a most worthwhile addition to the bookshelf of anyone concerned with the field of electron optics, especially in view of the clear outline of the Hamiltonian method.

R. G. E. Hutter
Sylvania Elec. Prods., Inc.
Bayside, L. I., N. Y.

Electronic Transformers and Circuits, second edition, by Reuben Lee

Published (1955) by John Wiley and Sons, Inc., 440 4th Avenue, N. Y. 11, N. Y. 345 pages+xvi pages +9 index pages+3 pages bibliography. 263 figures. 9¼×6. $7.50.

The second edition of this useful book is little changed from the first one. Certain sections have been strengthened and revised to include current practice. Conversely some of the relatively weak sections have been deleted and the reader referred to "more thorough treatments." Chapters on magnetic amplifiers and on pulse circuits have been added. All this is to the good.

As discussed in the review of the first edition[1] the book is a detailed exposition of the design of transformers for electronic circuits. Even the type of paper to be used between layers receives full treatment.

The approach is largely empirical, with many useful charts and graphs scattered through the book.

The second edition is again "a valuable addition to the literature on transformers."

Knox McIlwain
Hazeltine Electronics Corporation
Little Neck, L. I., N. Y.

[1] Knox McIlwain, Proc. IRE, vol. 36, p. 383; March, 1948.

1956 TRANSISTOR CIRCUITS CONFERENCE

University of Pennsylvania
Philadelphia, Penna.

February 16–17, 1956

Sponsored by

IRE, AIEE, and the

University of Pennsylvania

Thursday, February 16

8:00 a.m.
Irvine Auditorium

Registration opens

Special Circuits

9:30 a.m.–12:00
Irvine Auditorium

Chairman: P. L. Bargellini, University of Penna.

Audio Automatic Volume Control Circuit, B. D. Griffith and J. Tom (U. S. Army), Radio Corp. of America.

Linear Amplifier Employing Nonlinear Amplification, R. F. Grantges and J. Holzer, Signal Corps Engineering Laboratory.

Voltage-Tuned Networks Using Junction Diodes, C. R. Hurtig, Massachusetts Institute of Technology.

Multi-Terminal Semiconductors Operated as Two-Terminal Source-Free Switching-Devices, Abraham Har'l, University of Penna.

Session A—Tutorial

9:30 a.m.–12:00
University Museum

Analysis and Equivalent Circuits, R. B. Adler, Massachusetts Institute of Technology.

Switching Circuits, R. H. Baker, Lincoln Laboratory, M.I.T.

12:00 Noon–2:00 p.m.
Houston Hall
Lunch

2:00 p.m.–2:30 p.m.
Irvine Auditorium

Formal opening of conference by George L. Haller, Chairman of Conference; Donald G. Fink, Past Chairman of Conference; and J. Grist Brainerd, University of Penna.

Switching Circuits

2:30 p.m.–5:30 p.m.
Irvine Auditorium

Chairman: H. E. Tompkins, Burroughs Corporation.

Direct-Coupled Transistor Logic Circuitry in Digital Computers, J. R. Harris, Bell Telephone Laboratories.

Transistor Requirements for Direct-Coupled Transistor Logic Circuits, J. W. Easley, Bell Telephone Laboratories.

Junction Transistor Switching Circuits for High Speed Digital Computer Applications, G. J. Prom and R. L. Crosby, Sylvania Electric Products, Inc.

Circuit Properties of the Conjugate-Emitter (Hook-Collector) Transistor, J. J. Suran, General Electric Company.

High Speed Transistor Computer Circuits, S. Y. Wong and A. K. Rapp, Philco Corp.

SESSION B—TUTORIAL

2:45 p.m.–5:30 p.m.

University Museum

Low Frequency Circuits, F. D. Waldhauer, Radio Corp. of America.

High Frequency Circuits, J. B. Angell, Philco Corporation.

6:00 p.m.

Penn Sherwood Hotel

Cocktail—Buffet

7:00 p.m.

Penn Sherwood Hotel

Informal group discussions

FRIDAY, FEBRUARY 17

8:30 a.m.

Registration opens

SMALL SIGNAL AMPLIFIERS

9:00 a.m.–12:00

Irvine Auditorium

Chairman: R. H. Mattson, Bell Telephone Laboratories.

Transistor D-C Amplifiers, J. W. Stanton, G. E. Advanced Electronics Center at Cornell University.

Transistor Amplifier Performance, J. F. Gibbons, Stanford University.

Behavior of Noise Figure in Junction Transistors Over Their Useful Frequency Spectrum, E. G. Nielsen, Bell Telephone Laboratories.

A Carrier-Frequency Transistor Feedback Amplifier, D. A. DeGraaf and F. H. Blecher, Bell Telephone Laboratories.

The Design of Bridge-Derived Circuits for Precision Control of Transistorized Amplifiers, W. S. Chaskin, V. Babin and I. Gottlieb, Lenkurt Electric Company, Inc.

12:00 Noon–2:00 p.m.

Houston Hall

Lunch

POWER AMPLIFIERS AND POWER SUPPLIES

2:00 p.m.–4:30 p.m.

Irvine Auditorium

Chairman: G. H. Royer, Westinghouse Electric Corp.

Temperature Effects in Circuits Using Junction Transistors, H. C. Lin and A. A. Barco, R.C.A. Laboratories.

Design Considerations for Semi-Conductor Regulated Power Supplies, S. Sherr and P. Levy, General Precision Laboratory.

The Design of Transistor DC to DC Transformers for a High Degree of Reliability and Stability, P. M. Thompson, Canadian Defence Research Establishment.

Single Power Transistor DC-DC Converter, D. A. Paynter, General Electric Company.

Characteristics and Circuit Applications for a New Type Power Transistor, J. F. Marshall, Minneapolis-Honeywell Regulator Company.

Abstracts of IRE Transactions

The following issues of *Transactions* are now available from the Institute of Radio Engineers, Inc., 1 East 79 Street, New York 21, N. Y. at the following prices.

Sponsoring Group	Publication	Group Members	IRE Members	Non-Members*
Audio	Vol. AU-3, No. 6	$0.95	$1.40	$2.85
Circuit Theory	Vol. CT-2, No. 3	1.40	2.10	4.20
Component Parts	Vol. PGCP-4	2.00	3.00	6.00
Electron Devices	Vol. ED-2, No. 4	1.50	2.25	4.50
Medical Electronics	PGME—3	1.10	1.65	3.30
Microwave Theory & Techniques	Vol. MTT-3, No. 5	1.70	2.55	5.10
Reliability & Quality Control	Vol. PGRQC-6	1.50	2.25	4.50

*** Public libraries and colleges may purchase copies at IRE Member rates.**

Circuit Theory

VOL. CT-2, NO. 3, SEPTEMBER, 1955

What Is Circuit Theory?—W. H. Huggins

Preface to the Fourier-Integral Papers—J. G. Brainerd

The Fourier Integral—A Basic Introduction—E. A. Guillemin

The object of this introduction is to give the reader an idea of the various kinds of problems in which the Fourier series or integral is useful, and to discuss not only the essential properties which make it useful, but also to point out the limitations and restrictions imposed by these properties. Collaterally it is significant to recognize the flexibility that is inherent in the Fourier representation, if we consider its mathematical form from a nonconventional point of view. Thus it is a common belief, that only the integral representation applies to aperiodic functions, and that the Fourier series is restricted to the representation of periodic time functions. If we are interested in sampled time functions, this attitude turns out to be incorrect, and we find that the series rather than the integral is at once the pertinent tool.

Inherent properties of the partial sums, such as the Gibbs phenomenon and the mean-square-error criterion are discussed, as well as the fact that in dealing with stable systems for which the response must be zero before the advent of the excitation, it turns out that the real or imaginary parts of the system function are separately sufficient to characterize the response: and one may dispense with the need of having to deal with complex system functions, or to distinguish between such things as minimum-phase and nonminimum-phase transfer functions.

Applications of the Fourier Integral in Physical Science—Chester H. Page

"Physical" philosophy of Fourier Transform approach is presented, and formalism discussed in 1-, 2-, and 3-dimensional problems.

Application is made to the dissipative wave equation in three dimensions, and the responses are found for (1) distributed driving force, (2) relaxation from initial conditions, and (3) time-varying boundary conditions.

One-dimensional heat-flow problems are also discussed.

Application of the Fourier Integral in Circuit Theory and Circuit Problems—W. R. Bennett

The straightforward application of the Fourier integral to determine the response of a linear invariable circuit to an arbitrary impressed force is reviewed. When a Fourier integral representation of the impressed force exists and the system starts from rest, the problem is routine. Extensions to cases such as impulses, step functions, and ramp functions, for which the Fourier integral along the real axis does not converge, may be made by suitable changes in the path of integration. Boundary conditions other than zero stored energy can be included by introducing equivalent driving forces to produce the same effect as the initial voltages and currents.

Noise voltages and currents in general can not be represented as Fourier integrals over all time. Representation over a finite time with a subsequent limiting process can be used to define a spectral density or mean-square amplitude in an elementary frequency interval. Spectral densities of network responses to a specified noise source are then calculable by multiplying the squared absolute value of the appropriate transfer function versus frequency by the spectral density function of the source. Knowledge of spectral densities can be used to design optimum circuits for separation of signal and noise.

Evaluation of Fourier Transforms—W. K. Linvill, R. E. Scott, and E. A. Guillemin

This paper deals with numerical methods as well as with the use of digital and analog computer methods for the evaluation of Fourier integrals. Graphical methods of integration are

escribed which enable one to obtain arbitrarily ood accuracy with a minimum amount of com- utational effort through the use of the Fourier ntegral property that permits a representation n terms of an appropriate higher derivative of ne real part of the transform. This method, hich makes use of impulse trains, can be ap- lied in such a way as to take proper account f the pertinent asymptotic behavior of the ansform, even though the integration for ractical purposes is extended over only finite equency intervals. A simple error criterion given for estimating the accuracy of a con- emplated calculation. Computational economy achieved through letting the nonuniform pacing of impulses, in the impulse train epresentation, be dictated by the nature of the nction dealt with, rather than choosing an rbitrary uniform interval as is done in many onventional methods of graphical procedure.

If digital computers are used in this kind of umerical evaluation, then economy of im- ulses is of no consequence, and one achieves a mplification of the programming through using n arbitrary uniform spacing. Other than this, ne digital computer process is fundamentally ke the numerical method already discussed.

Analog methods belong in a different cate- ory. Here circuit analyzers, as well as the otential analog provided by the electrolytic ank methods, are presented and fields of use- lness discussed.

Applications of the Fourier Integral in the nalysis of Color Television Systems—T. furakami and Murlan S. Corrington

It is shown that a linear-phase network has better transient response than one having a inimum net phase shift, since it will have a ymmetrical transient response to a unit- npulse or unit-step driving force. In the case f RC low-pass filter characteristic, one having near phase shift will have faster rise time than ne having minimum net phase shift.

For best response there should be regions of ontrolled gain, with linear phase shift well eyond the cutoff frequency of the filter. The rst region beyond cutoff should be carefully esigned for the best transient rise time. In the ase of a video amplifier in a color television re- eiver with a trap at 3.58 megahertz and high ttenuation beyond 4.5 megahertz, the gain f the system halfway between these two fre- uencies should be approximately 6 db less han the gain at low frequencies to best utilize ne available bandwidth.

The response of an idealized bandpass filter ith a linear phase shift to a ramp change of the arrier-wave phase is worked out. Such a net- ork can follow the ramp phase change quite ell over most of the range, but it has a phase vershoot and some coincidental amplitude odulation.

Generalized Fourier Integrals—K. S. Miller nd L. A. Zadeh

Classical Fourier analysis is based on the ecomposition of time functions into pure sine aves or exponentials. In this paper, a more eneral method of decomposition involving eriodic elementary time functions is de- eloped. Explicit inversion formulas are ob- ained and a general expression for the inverse ernel is derived. In the special case of ele- ientary signals having the form of square aves, it is found that the coefficients entering nto the expression for the inverse kernel are iven by a function which is closely related to ne Mobius function. As an application, the npulsive response of an ideal filter which asses all square waves whose fundamental fre- uency is less than ω_0 and stops all those whose ndamental frequency is greater than ω_0, is etermined.

Evaluation of Oscillator Quality—Giuseppe rancini

A general type of oscillator is considered, hich results from the combination of an active ement with a selective network. Amplitude and frequency are deduced by a simple method, valid for quasi-sinusoidal oscillation. If the oscillator is perturbed, relative amplitude and frequency variations can be calculated. Their product depends only upon the perturbation itself and a coefficient which is a function of the selective network. It seems apt to choose this coefficient as the figure of merit of the oscillator. For ordinary LC oscillators it is approximately equal to the Q. Values are calculated for certain RC oscillators. Some experiments confirm the results.

Energy Relations in Multiterminal Transducers—Jacob Shekel

A multiterminal transducer is a network with a set of n input terminals and a set of n output terminals. The representation of multiterminal transducers and their properties is a generalization of four-pole theory. In this paper the energy relations in multiterminal transducers are expressed in matrix notation, and the special properties of passive transducers and lossless transducers are investigated.

Analysis of Nonlinear Circuits Using Impedance Concepts—J. S. Thomsen and S. P. Schlesinger

An LRC series circuit containing a nonlinear inductor and a nonlinear capacitor is analyzed in terms of equivalent impedances which are functions of current; the range of validity is discussed. The circuit equations are also put into dimensionless form, and a set of curves is presented in terms of these variables. A method for extending the results to more general circuits by use of Thévenin's theorem is outlined. Experimental results are given and shown to be in fair agreement with theory.

Component Parts

Vol. PGCP-4, November, 1955

A system consisting of an input driving amplifier and resolver with shielded output cables used for transmitting the rotor voltages an appreciable distance to a resistive load is considered. This "R-C" loading is shown to affect the resolver function error and to change the time phase shift of output voltage.

Voltage fluctuations due to direct current flowing in composition resistors have been measured with a National Bureau of Standards experimental test set. A second group of measurements were made as prescribed in the JAN-R-11 Specification. The two measuring systems are described and test results compared.

Several groups of commercial resistors of different manufacture have been measured and the results analyzed and compared.

Background theory is included.

A description of the noise generated in composition resistors due to direct-current flow is given, based on measurements of mean-square values of voltage fluctuations.

Various commercial resistors including some film types have been measured in a study of the relationships between "current-noise" and several parameters such as dc current and voltage, dc power, resistance, duration of current flow, power rating, etc.

A description of the measuring equipment and details of experiments and data analyses are also included.

Electron Devices

Vol. ED-2, No. 4, October, 1955

In the Post-Deflection-Focus Color Kinescope, there is an array of parallel wires next to the phosphor screen for the purpose of focusing the electron beam and for deflecting it up and down in order to change colors. Expressions are derived for the deflection sensitivity and focusing properties of such a system which are applicable for all points within the picture area. The theoretical results are compared with experimental measurements; good agreement is obtained. Contour maps showing the variation over the grid plane of deflection sensitivity and the voltage ratio for optimum focus are included.

Silicon-aluminum alloy junction diodes have been made that have rectifying properties up to frequencies of 500 megacycles per second. Recovery times from storage effects are of the order of 0.1 microsecond.

In this paper some characteristics of switch circuits using junction transistors are analyzed. The switch properties result from the large changes in small-signal admittance of one junction of a transistor when the bias polarity of the other junction is reversed. The characteristics analyzed include the small-signal, low-frequency conductance and the associated potentials. The circuits are suitable for low level modulators and commutators.

Using both an analog computer and an approximate analytical method, the equation describing the beam shapes which result from a uniform pencil beam of electrons entering a periodic magnetic field has been studied. The investigation has been primarily directed toward beams emergent from ideal cathodes only partially shielded from the magnetic field. Cases of both small and large scalloping have been considered.

Curves relating the magnetic field coefficient α and the space-charge coefficient β are presented. A previously proposed relationship between α and β for small scalloping is shown to be inaccurate for large scalloping. Stable solutions for the motion of an electron beam having no thermal velocities are obtained for values of α less than 0.66 and in addition they are also found for some values of α greater than 0.66.

An electronic theory of the operation of tape-helix traveling-wave structures is given. This includes the case of traveling-wave amplifiers and backward-wave oscillators operating on any space harmonic. The method of solution is based upon an integral equation for the longitudinal electric field which is solved approximately for the case of small beam currents. This method is equally applicable to thin beams, thick beams, and annular beams with or without a transverse variation of dc density or velocity. Explicit expressions are obtained for the impedance and space-charge parameter of each space harmonic.

A method is given for computing the efficiency of traveling-wave amplifiers with high gain and low C, including the effects of space charge and attenuation. The ballistics of the electrons is governed by the Boltzmann transport equation which, together with the circuit equation, is solved in a power series expansion of the input voltage. Only the first two terms of this series are computed and various nonlinear results are given in the form of curves. It appears that for small C and small convergence parameters, overtaking affects the nonlinear operation slightly.

Study of a Plane Short on a Shielded Helix—W. H. Watson and J. R. Whinnery

The results of probe measurements along a shielded helix terminated in a plane conducting "short" are given. These results seem to indicate that the higher-order fields at the short are reactive and that the minimums are shifted out from the normal 180-degree position. The amount of this shift seemed to be relatively constant at approximately 38 degrees from 500 to 2,000 megacycles for a particular helix. A very approximate analysis of the helix short is made where the helix and its image wire are considered as a tapered two-wire transmission line. The position of the first minimum is determined by a numerical integration using the transmission line equations. This analysis predicts the correct direction of the shift of the minimum and also gives a rough idea as to the amount of this shift over the given band of frequencies.

A Coupled Mode Description of the Backward-Wave Oscillator and the Kompfner Dip Condition—R. W. Gould

The start oscillation condition for the backward-wave oscillator and the operation of the traveling-wave tube amplifier at the Kompfner dip point are described from the point of view of the coupling of two modes of propagation. Growing waves are not involved. Two waves are sufficient when the tube is more than a half plasma wavelength long. Operation in this "large space charge" domain is inherently simpler than in the "low space charge" domain. The start oscillation condition and the Kompfner dip condition are simply expressed in terms of the coupling constant between modes, $\mathfrak{C}L=(2n+1)\pi/2$, where n is an integer. In addition, the uncoupled modes must have the same velocity. The result is also expressed in terms of the more familiar parameters CN and hL. The effect of loss in the circuit mode is calculated.

When the two waves carry energy in opposite directions, growing waves result. This case is discussed briefly.

Medical Electronics

PGME—3, November, 1955

(Conference on Plethysmography, Buffalo, N. Y., December 10–11, 1953)

Foreword

Introduction

Electronic Plethysmography—Jan Nyboer

Electronic Flowmeter System—H. P. Kalmus

Electrical Properties of Body Tissues and Impedance Plethysmography—H. P. Schwan

Resistance and capacitance of body tissues and blood are reported over a wide frequency range. It is shown that it cannot be assumed in impedance plethysmography that tissue and blood have comparative resistance values and that the capacitance is of negligible influence, if presently used 200 kc frequency is considered. In order to obtain a stable ratio of blood and tissue impedance, frequency must be below 10 kc; and in order to exclude capacitive currents, frequency should be near 1 kc. Electrode polarization phenomena and their effect on impedance measuring devices are discussed briefly. It is concluded that not only in two terminal impedance measuring devices, but also in four terminal devices, as currently used in impedance plethysmography, polarization is disturbing if the frequency is substantially below 1 kc. Therefore, in this article, the conclusion is made that impedance plethysmography should be carried out with frequencies near 1 kc, instead of the currently used 200 kc. A mathematical analysis which relates quantitatively observed relative resistance change and relative blood volume change concludes this article. This ratio is found near 3.5. It is substantially higher than assumed previously and suggested for experimental verification in order to elevate impedance plethysmography from a qualitative to a valuable quantitative tool for blood-volume research.

Variation of impedance of body segments due to variation in blood volume (impedance plethysmography) has been introduced as a technique for studying blood-volume changes. While the qualitative dependence between blood volume and impedance change has been well established, little work has been done so far to ascertain a quantitative relationship between blood volume and impedance change. The only analytical approach to date assumes comparable data for specific tissue and blood impedance and predicts under this condition equal relative change of impedance and blood volume. It is intended to present in this paper experimentally determined tissue and blood-data and to discuss quantitatively the significance of this material with regard to plethysmography. The material will be presented in several sections, as follows: (1) electrical properties of body tissues and blood; (2) electrical phase shift in body tissues and its significance in impedance plethysmography; (2) electrode polarization and impedance plethysmography; and (4) quantitative relationship between impedance and blood volume change.

The Design of Finger-Tip Plethysmographs with Photoelectric and Strain-Gage Transducers—(Abstract)—S. Feitelberg

Why are we interested in the volume pulsations of the finger tip? Vascular physiology states that the principal control of the rate of blood flow is in the small, peripheral blood vessels. The peripheral resistance is continually changing under various stimuli. Observation of this peripheral vascular system is rather conveniently accomplished on the fingers and toes. The general specifications of a finger-tip and toe plethysmograph should be: (1) volume sensitivity of about 10 cubic millimeters full scale with provision for frequent calibration; (2) response from DC to five cycles per second; (3) no reaction of physiological significance due to the measurement; and (4) response to large slow shifts in base line without loss of sensitivity.

A plethysmograph whose sensing element is an air chamber with a photoelectric transducer is described in detail. It incorporates periodic volume calibration, automatic centering of the recorder pen after full scale deflection, and a photomultiplier tube bridge with a 1 mw output into a 1,000 ohm load. The disadvantages of this instrument are nonlinearity and a fragile optical system.

Because of these disadvantages, the author recommends, and has used for the last three years, a sensing element with a relatively standard strain gage transducer having high compliance and giving 2 mv signal on a typical finger pulse. It is reported that satisfactory clinical service has been obtained from such an instrument.

In comparing impedance and volume plethysmographs it is noted that one measures fractional volume change and the other fractional resistance change. Little difference in their ultimate utility is expected if the fractional volume is not vastly different from the fractional resistance change.

Clinical Applications of Plethysmography—(Abstract)—R. Megibow

A paper is presented on the clinical aspects of finger and toe plethysmography using Dr. Feitelberg's electromechanical strain gauge plethysmograph.

Impedance Plethysmography in Experimental Psychology—Ulric Moore

A paper concerning the use of the impedance plethysmograph in sensing the physiological response of animals to psychological stimuli in the extension of Pavlov's work at the Behavior Farm, as carried on under the guidance of Dr. Liddell, is presented.

Changes in peripheral circulation were often noticed which appeared to be far more sensitive indicators of physiological activity than many of the standard physiological parameters (such as heart rate, respiration rate or blood pressure). In some instances complete cessation of pulsatile indications were experienced when heart action and respiration were definitely near normal. In general, a relaxed condition or a lowered blood pressure contributed to larger pulsatile indication. Blood pressures as low as 40% of normal (drug induced) did not cause any appreciable fall in pulsatile indication.

In one specific instance of recording, following electroshock therapy, some of the animals tested showed a periodic cessation of pulsatile indication lasting as long as a minute at periods of three to five minutes for an hour or more after shock. Such cessation was not accompanied by cessation of heart activity but rather appeared to be due to some sort of vasomotor activity.

It is also pointed out that the amplitude of pulsatile indication is a strong function of ambient temperature. On a cold day, a human can show a difference of 3:1 between left and right forefingers if one hand is first held under the armpit for a few minutes. Animals such as dogs, sheep and goats show from one-fifth to one-half the pulsatile indications of man and, in general, the younger the subject, the greater the pulsatile indication.

Microwave Theory & Techniques

Vol. MTT-3, No. 5, October, 1955

Message from the Editor

Microwaves—Science and Art—Ernst Weber

Shunt Impedance of Klystron Cavities—E. L. Ginzton and E. J. Nalos

Values of R/Qf or re-entrant resonators are given for configurations for which neither the coaxial-field nor the radial-field approximations are valid. The values are calculated by net point methods, and agree well with experimental values obtained by perturbation methods. Some errors arising from the finite dimensions of perturbing plungers are also discussed.

Planar Transmission Lines—II—David Park

An expression is found for the characteristic impedance of a transmission line consisting of two parallel strips of foil placed between, and perpendicular to, two wide plates.

A High-Speed Broadband Microwave Waveguide Switch—W. L. Teeter

A switch which switches microwave energy to any of several separate waveguide loads is described. The switch has the bandwidth and power-carrying capability which is essentially that of the input and output waveguides. Data are given for a switch which operates over the frequency range of 8,600 to 10,000 mc with a vswr of less than 1.15 during transmission and less than 1.5 during switching. The switching speed is limited only by the practical limit for rotating the metal shorting vane. A typical example is given of a 5-output switch with a switching rate of 1,800 per second (vane rotation of 3,600 rpm) and a dead time during

switching of 94 per cent of total time. Dead time is a function of switch diameter and vane rotation rate and could be reduced by increasing the vane diameter or rotation rate.

Effect of Ellipticity on Dominant-Mode Axial Ratio in Nominally Circular Waveguides—P. I. Sandsmark

An investigation is made of the effect of ellipticity on the dominant-mode axial ratio (AR) in nominally circular waveguides. Equations for calculating the AR are derived for the case where the difference between the major and minor axes of the guide cross section is small and the waveguide is not too long. Values of AR obtained by calculations are compared with measured values, and a method for improving the AR performance of a waveguide run is demonstrated.

The Design of Ridged Waveguides—Samuel Hopfer

Shielded Coupled-Strip Transmission Line—S. B. Cohn

An analysis is made of the odd and even TEM modes on a pair of parallel co-planar strips midway between ground planes. Rigorous formulas are presented for the case of zero-thickness strips, while approximate formulas are given for strips of finite thickness and for strips printed on opposite sides of a thin dielectric sheet supported in air between ground planes (AIL construction). The characteristic impedances and the phase velocities of the two modes are necessary and sufficient information for the design of directional couplers, coupled-line filters, and other components utilizing the coupling between parallel-strip lines. In order to facilitate design work, nomograms are included in the paper which give the dimensions of the coupled-strip cross section in terms of the odd- and even-mode characteristic impedances. The characteristic-impedance scales of these nomograms may be read to an accuracy of better than one per cent over a wide range of values that is sufficient for most purposes.

High-Power Ferrite Load Isolators—Alvin Clavin

The principles of ferromagnetic resonance have been well described in literature. It is the purpose of this paper to point out the application of these principles to the design of practical microwave components, especially for high power. The various types of ferrite microwave circuits that can be used in the design of a load isolator are presented. The advantages and disadvantages of each of these circuits are discussed in regard to the electrical, mechanical, thermal, and magnetic field requirements. Experimental data are given for the optimum design of nonreciprocal ferrite absorbers for rectangular guide. Finally, practical design information for a power circulator in rectangular waveguide is presented which has been modified for use as a load isolator. This device has extremely high isolations (50 db) and low insertion loss (.5 db), and has maintained an isolation in excess of 30 db over a 25 per cent bandwidth with a permanent magnet field. Power handling ability of 250 kw peak with a .001 duty cycle is easily accomplished without external cooling. This isolator requires quite small magnetic fields for proper operations and hence packaged isolator is quite lightweight. Use of this power circulator for high-power modulators and duplexers is discussed.

Step-Twist Waveguide Components—H. A. Wheeler and Henry Schwiebert

The step twist is a number of adjoining sections of straight rectangular waveguide, twisted about their common axis at their junction faces. The technique of designing the step twist resides in the proportioning of the section dimensions and the angles at the twist faces. The resulting design is much shorter than the usual twisted waveguide; it offers further advantages in ease of specifying shape and dimensions, and in their reproducibility in construction.

A series of fixed 90-degree step twists has been designed for the rated 40 per cent frequency bandwidths in the standard waveguide sizes for 1 to 40 kmc. The total angle is divided equally among seven faces spaced about $\frac{1}{8}$ wavelength in the guide. Each step twist is matched within 0.3 db swr with plain flanges or 0.5 db swr with choke flanges at both ends.

Rotary step twists for operation at all angles out to ± 90 degrees have been designed for the same bandwidths. The total angle is divided unequally among four faces (choke flanges) spaced about $\frac{1}{4}$ wavelength in the guide. The entire unit at maximum rotation is matched within 1.2 db swr with choke flanges at both ends; the matching is closer at lesser rotation.

A Double-Ground-Plane Strip-Line System for Microwaves—B. A. Dahlman

The double-ground-plane strip line consists of two parallel conducting planes with a conducting strip imbedded in a homogeneous dielectric between them. Transmission characteristics for this system are calculated, and design formulas are given. Practical viewpoints on design and application of strip lines are discussed. System can be used as an inexpensive base for microwave circuits and is well adapted to laboratory experiments and mass production.

Correspondence

Contributors

Reliability & Quality Control

Vol. PGRQC-6, December, 1955

RACER: A Proposed Rating System For Electronic Components and Devices—J. J. Lamb

Choice of an electronic component or electron device for a particular application is more likely than not to be based on a personal estimate of one or two obvious attributes such as first cost, assumed reliability or, simply, availability. The author proposes a set of five basic criteria, with quantitative evaluation, to comprehend all attributes of any candidate device or component. These criteria are stated and defined as Reliability, Availability, Compatibility, Economy and Reproducibility, the initial letters of which are combined to form the acronym, "RACER." A method of assigning numerical values to each criterion of the RACER system is proposed so that a summary evaluation figure of merit may be derived for unbiased engineering and managerial comparison and decision among individual devices and components for particular applications. A practical example is given.

Surface Resistivity of Non-Porous Ceramic and Organic Insulating Materials at High Humidity with Observations of Associated Silver Migration—J. C. Williams and D. B. Herrmann

An investigation was made of the behavior of the surface resistivity of a number of ceramic and organic materials during exposure to high relative humidity. Particular emphasis was given to glazed high alumina ceramics from commercial sources. The effects of variables such as contamination, standing direct current potentials, firing atmosphere, surface finish and electrodes of different metals were investigated.

The uncontaminated specimens of the materials examined can be listed in the order of diminishing surface resistivity as follows: high molecular weight polymers, glazed high alumina ceramics, glasses and glazed ceramics, unglazed ceramics and glass bonded mica. All of the materials are very sensitive to contamination, which tends to reduce them to a nearly common level of surface resistivity. Severe and rapid migration of silver from silver electrodes under the test conditions were observed. Electrodes of solder, tin, copper and platinum showed no discernible migration.

The necessity for the development of better means for avoiding contamination and its effects, maintaining high surface resistivity and eliminating silver migration is emphasized by the results of this work.

Engineering and Testing for Reliability—H. G. Romig

Current definitions of reliability are considered and evaluated. That meaning best suited for the treatment of electronic components and systems built therefrom is selected and discussed. The establishment of engineering and quality standards is shown to be essential in appraising reliability and performance. Means for controlling the quality of components with respect to their most critical requirements are presented. This is tied in closely with final systems performance requirements, attention being paid to the final operations in production and test required to unite components and subassemblies into a functioning system.

Various sources of error are presented covering all phases of procurement, research, development, design, production, test and operation. Steps for minimizing these errors are covered, particular attention being given to the nature of the electrical tests required to evaluate not only electrical troubles, but also mechanical deficiencies. Those failures or extreme departures from normal that appear unexpectedly, often termed "mavericks," are analyzed and ways and means for detecting them are proposed. These unusual cases are shown to be valuable aids to engineering and production.

Statistical and empirical methods for obtaining over-all tolerances from component tolerances are presented. Confidence bands are obtained that are associated with such sets of tolerances. Tests are proposed for the determination of conformance to such tolerances, and ways for reducing their impact on design and production are given. Concrete proposals for programming for reliability are listed. Emphasis is placed on the necessity for teamwork between all groups in order to obtain the maximum reliability for electronic components and related systems.

Parts vs. Systems: The Reliability Dilemma—D. A. Hill, H. D. Voegtlen and J. H. Yueh

The high cost of spares and maintenance support together with a shortage of trained maintenance technicians have caused the services to put a premium on inherent reliability for electronic system. A basic inconsistency exists between the reliability goals for systems and the component parts reliability implicit in military standard specifications. Comparisons are made between parts failure rates derived from the specifications and operating experience. The effect of these failure rates on system reliability is shown for systems of various complexities, both in theory and in practice. An estimate is made of the reliability required for various classes of parts in order to achieve a reasonable reliability goal for a complex system. If the indicated improvements are to be achieved, the traditional approaches to setting specifications and test values are inadequate. Several relations between the distribution of environmental stress and the distribution of parts strength are reviewed and some proposals made on designing an adequate and economic reliability testing program.

An Effective Reliability Program Based Upon a "Triad for Design Reliability"—F. E. Dreste

A successful electronics reliability program followed on a recent R and D missile project is reviewed. A "triad" of requirements for carrying out the premise that reliability must be designed into equipment from the beginning to achieve the highest order of result is presented. The requirements are:

1. Reliable parts (including tubes) at the start.
2. Realistic operational parts tolerances statistical approach to circuit design.
3. Thorough testing of models.

Experience with the "triad" is related, and developed methods are explained. Sample data of several kinds are furnished and the major conclusion that each part of the "triad" must receive strong emphasis is reached.

A Basic Study of the Effects of Operating and Environmental Factors on Electron Tube Reliability—W. S. Bowie

Lots of fifty (50) tubes each have been operated under thirty-nine (39) different conditions for five thousand (5000) hours. These include variations (both above and below rated) in heater voltage, heater cycling, plate voltage, plate current, plate wattage, pulse operation, ambient temperature and shock and vibration. The effects of these variations in conditions on tube characteristics and tube survival rate have been calculated. The equipment designer should find these results of value to determine what things to avoid in designing for stable life and reliability in equipment.

Surface Contamination of Dielectric Materials—S. W. Chaikin

A research program was undertaken to investigate the effects of surface contaminants on the performance of dielectric materials. The approach to the problem was fundamental in that suitably clean materials were contaminated under controlled conditions in the laboratory and the effect on an electrical property (surface resistance) studied as a function of relative humidity. Concurrently, analytical chemical techniques were developed for detection of the contaminants so that application to field problems could be made.

The contaminants studied thus far include fingerprints, solder flux, aerosols of sodium chloride and of sulfuric acid, residual iron from ferric chloride etching of printed circuits, and silver from silver migration. The dielectrics studied include the paper base phenolic XXXP, nylon base phenolic (N-1), epoxy-glass, Teflon, Teflon-glass, melamine-glass (G-5), silicone-glass (G-6), diallyl phthalate-glass, Kel-F, neoprene, nylon, Plexiglas, polyethylene, polystyrene, polyester-glass, steatite (L-54), and Pyrex glass.

While the scope of the research program was broad, the applications of greatest immediate interest seemed to be in the fields of printed circuits and silver migration. Accordingly, field studies were concentrated in those particular areas.

Audio

Vol. AU-3, No. 6, November–December, 1955

Two Grams in 1956?—B. B. Bauer

PGA Chapter News

Tape Recording Applications—Marvin Camras

Standard designs are flexible enough for most uses of tape recorders. Special machines have been devised for unusual applications such as pronouncing dictionaries, length measuring devices, time compressors, dc and square wave recorders, memory devices, and automatic machine control. The construction and operation of typical devices are reviewed.

Design Principles for Junction Transistor Audio Power Amplifiers—D. R. Fewer

Junction transistors may be employed as audio frequency power amplifiers which will supply up to several watts of output power. The fact that there are two basic types of transistor (*n-p-n* and *p-n-p*) allows a freedom of circuit design which is impossible with electron tubes.

In power amplifier design the usual small signal assumptions cannot always be considered valid. Hence, large signal techniques must be applied in order to describe the behavior of the device. The non-linear distortion associated with large signal operation is discussed in terms of the transistor characteristics and methods of reducing this distortion are outlined. Operation in several circuit connections is considered with particular emphasis on the common emitter configuration.

Contributors

IRE Professional Group on Audio Combined Index for 1955

Abstracts and References

Compiled by the Radio Research Organization of the Department of Scientific and Industrial Research, London, England, and Published by Arrangement with that Department and the *Wireless Engineer*, London, England

NOTE: The Institute of Radio Engineers does not have available copies of the publications mentioned in these pages, nor does it have reprints of the articles abstracted. Correspondence regarding these articles and requests for their procurement should be addressed to the individual publications, not to the IRE.

The number in heavy type at the upper left of each Abstract is its Universal Decimal Classification number and is not to be confused with the Decimal Classification used by the United States National Bureau of Standards. The number in heavy type at the top right is the serial number of the Abstract. DC numbers marked with a dagger (†) must be regarded as provisional.

An annual index to Abstracts and References is published each Spring as a supplement to PROC. IRE. It is also published by *Wireless Engineer* and included in the March issue of that journal. Included with the Index is a selected list of journals scanned for abstracting with publishers' addresses.

ACOUSTICS AND AUDIO FREQUENCIES

534.13:534.845 1

Wedge-Shaped Cavity Resonators—E. Kohlsdorf. (*Hochfrequenztech. u. Elektroakust.*, vol. 64, pp. 33–34; July, 1955.) A calculation is made of the characteristics of acoustic resonators formed in a hall by the steps and the sloping floor supporting them. The height of the resonator considered is 0.4 m, the depth 0.8 m and the width 1 to 2 m; the front wall is slotted. Maximum absorption occurs near 158 and 365 c; this is shown graphically.

534.213.4 2

On Webster's Horn Equation—E. S. Weibel. (*J. acoust. Soc. Amer.*, vol. 27, pp. 726–727; July, 1955.) "A wave equation for the sound propagation through tubes is derived by means of Hamilton's variational principle. It is assumed that the wave fronts can be approximated by surfaces of constant stream potential; this is the only assumption made. The variational principle ensures that the best equation that is compatible with this assumption will be obtained. The equation has the form of Webster's horn equation; however, its coefficients are defined differently."

534.232 3

On the Radiation Impedance of an Array of Finite Cylinders—D. H. Robey. (*J. acoust. Soc. Amer.*, vol. 27, pp. 706–710; July, 1955.) Analysis is presented for an array of sound sources in the form of collinear cylinders.

534.232:546.431.824–31 4

On the Radiation Impedance of the Liquid-Filled Squirting Cylinder—D. H. Robey. (*J. acoust. Soc. Amer.*, vol. 27, pp. 711–714; July, 1955.) Analysis is presented for the underwater transducer discussed previously (1847 of 1955).

534.24 5

Nonspecular Reflection of Sound from a Sinusoidal Surface—H. S. Heaps. (*J. acoust. Soc. Amer.*, vol. 27, pp. 698–705; July, 1955.) The reflected field is obtained as the sum of an infinite number of terms whose coefficients may be found from a recurrence relation. The three central terms in the series correspond to the first-order approximation. The results are used to determine the average intensity and fluctuations of the sound reflected from a traveling sinusoidal boundary. The degree of roughness required to destroy the effect of Lloyd's mirror fringes is discussed in terms of the size of the surface corrugations relative to λ.

534.614–8 6

Variation of Acoustic Velocity with Temperature in Some Low-Velocity Liquids and Solutions—G. W. Marks. (*J. acoust. Soc. Amer.*, vol. 27, pp. 680–688; July, 1955.) Measurements on various organic liquids are reported, using an ultrasonic interferometer and a frequency of 500 kc.

534.75 7

Some Parameters influencing the Pitch of Amplitude-Modulated Signals—A. M. Small, Jr. (*J. acoust. Soc. Amer.*, vol. 27, pp. 751–760; July, 1955.)

534.78 8

Effect of Duration on the Perception of Voicing—P. Denes. (*J. acoust. Soc. Amer.*, vol. 27, pp. 761–764; July, 1955.) An investigation of factors affecting the recognition of phonemes is described based on the observed differences in the relative durations of the vowels and consonants according as the latter are voiced or unvoiced.

534.78 9

Acoustic Loci and Transitional Cues for Consonants—P. C. Delattre, A. M. Liberman, and F. S. Cooper. (*J. acoust. Soc. Amer.*, vol. 27, pp. 769–773; July, 1955.) Experiments on the synthesis of speech are described.

534.844.5 10

Optimum Reverberation Time of Studios—W. Reichardt, E. Kohlsdorf, and H. Mutscher. (*Hochfrequenztech. u. Elektroakust.*, vol. 64, pp. 18–25; July, 1955.) The reported tests, involving 85 listeners, lead to results similar to those obtained by Kuhl (620 of 1955). While the mean reverberation characteristic adjudged optimum agreed with the accepted characteristic, the preferred reverberation times varied with the type of music.

534.846 11

Comparison of Objective and Subjective Observations on Music Rooms—J. Blankenship, R. B. Fitzgerald, and R. N. Lane. (*J. acoust. Soc. Amer.*, vol. 27, pp. 774–780; July, 1955.) Experiments made at the University of Texas are reported; an attempt is made to relate the terminology and viewpoints of architects, physicists, and musicians.

621.395.623.7 12

The Twin-Cone Moving-Coil Loudspeaker—J. J. Schurink. (*Philips tech. Rev.*, vol. 16, pp. 241–249; March, 1955.) A description is given of a loudspeaker with a small cone arranged inside and attached to a larger cone; satisfactory response is obtained at frequencies up to about 18 kc. Advantages of this arrangement over the use of separate loudspeakers for the upper and lower af ranges are indicated.

621.395.625:621.317.76 13

Measurement of "Wow" and "Flutter"—O. E. Dzierzynski. (*Wireless World*, vol. 61, pp. 547–552; November, 1955.) The subject is discussed generally and a detailed description of a flutter meter is given.

ANTENNAS AND TRANSMISSION LINES

621.315.2:621.396.97 14

Transmission Properties of Low-Frequency Programme Lines used in German Carrier-Frequency Trunk Cables—E. A. Pavel. (*Fernmeldetech. Z.*, vol. 8, pp. 455–461; August, 1955.) Report of tests on a 2212-km af line superimposed on carrier-frequency cable. Lines of this type more than satisfy CCIR transmission-quality requirements for distances up to at least 4000 km. See also 1578 of 1953 (Pavel and v. Schau).

621.315.212 (083.74) 15

Present Position on Standardization of High-Frequency Coaxial Transmission Cables—H. Peters. (*Fernmeldetech. Z.*, vol. 8, pp. 443–444; August, 1955.) Reasons are given for the retention in Germany of 60Ω as the standard value of characteristic impedance for hf coaxial cables, in spite of international standardization of 50Ω and 75Ω. See also 2299 of 1954 (Gutzmann).

621.372.2 16

Propagation of Microwaves on a Single Wire: Part 1—S. K. Chatterjee and P. Madhavan. (*J. Indian Inst. Sci.*, Section B, vol. 37, pp. 200–223; July, 1955.) "Some quantitative measurements on cylindrical surface waves excited on a cylindrical bare copper conductor have been made at 3.2-cm wavelength. The results on radial field measurements indicate fair agreement with results predicted by theory. The decay coefficient for the radial field is 14.0 m^{-1}. It is suggested that the surface conductivity of metals in the form of wire can be found at microwave frequencies by using this method. Field distributions near the launching horn have been found to be considerably distorted due probably to the presence of complementary waves. The design and constructional details of the launching system, probe, etc. used in the experiment are presented."

621.372.8+621.372.413 17

A Step-by-Step Method for designing Waveguides and Oscillatory Systems—M. S.

Neyman. (*Radiotekhnika, Moscow*, vol. 10, pp. 12–22; January, 1955.) A method is proposed which permits calculation of the parameters of distributed electromagnetic systems such as waveguides and cavity resonators without recourse to electrodynamic wave equations. Rectangular and cylindrical waveguides and resonators are considered as examples.

621.372.8 18

Calculation of the Angular Momentum of the Electromagnetic Field in a Waveguide—L. Ronchi and G. Toraldo di Francia. (*Alta Frequenza*, vol. 24, pp. 204–218; June, 1955.) General formulas for the flux of the angular momentum of the em field are applied to the case of a circular waveguide in which only the TE_{11} mode is propagated; an investigation is made of the types of polarization possible. For the case of a guide containing a polarization converter calculations are made of the angular momentum delivered to the converter per unit of time when the polarization is converted from elliptical to linear; two different methods are used.

621.372.8 19

Theory of Circularly Symmetric Standing TM Waves in Terminated Iris-Loaded Guides—C. C. Grosjean. (*Nuovo Cim.*, vol. 2, pp. 11–26; July 1, 1955. In English.) An exact treatment is developed based on matching the field components at the diaphragm apertures, and on similar lines to that described previously (2832 of 1955) in relation to infinite guides.

621.372.8:538.22 20

Electromagnetic Waves in a Magnetized Ferrite in the Presence of Conducting Planes—A. L. Mikaelyan and A. A. Pistol'kors. (*Radiotekhnika, Moscow*, vol. 10, pp. 14–24; March, 1955.) Theory is presented for the propagation of electromagnetic waves in an infinite space between ideally conducting planes, the space being totally or partially filled with ferrite and a constant magnetic field oriented in various directions being applied.

621.372.8:621.315.6 21

Propagation Coefficients of Waves on Dielectric Tubes—H. G. Unger. (*Fernmeldetech. Z.*, vol. 8, pp. 438–443; August, 1955.) See 3458 of 1954.

621.372.8:621.396.11.029.4/.51:551.510.535 22

The Radial Propagation of Electromagnetic Waves between Two [parallel] Conducting Planes (Radial Waveguide)—H. Kaden. (*Frequenz*, vol. 9, pp. 241–249; July, 1955.) In the radial waveguide E and H modes propagate as in a linear guide, the orientation of the modes being with respect to the normal to the conducting planes. The theory is used to calculate the "internal" and "external" dynamic capacitance of a parallel-plate capacitor. The radiation from electric and magnetic dipoles situated between the planes is also calculated; the result represents to a close approximation the conditions for propagation of long waves ($\lambda > 3$ km) in the guide formed between the earth and the ionosphere. The number of modes propagated varies inversely as λ and the field-strength /distance curve at the earth's surface is of the nature of a statistical function, since many incommensurable waves interfere mutually. Resonance effects occur when the height of the ionosphere is an integral multiple of $\lambda/2$, both the distant field strength and the retroaction of the radiation on the dipole becoming very great.

621.396.677:523.16 23

Chord Construction for Correcting Aerial Smoothing—Bracewell. (See 98.)

AUTOMATIC COMPUTERS

681.142 24

The Design and Construction of a High-Speed Electronic Differential Analyzer—N. N. Biswas, V. N. Chiplunkar, and V. C. Rideout. (*J. Indian Inst. Sci.*, Section B, vol. 37, pp. 186–199; July, 1955.)

681.142 25

Improvement of an Iteration Process suitable for Automatic Division—C. Böhm. (*Ricerca sci.*, vol. 25, pp. 2077–2080; July, 1955.) Electronic computers having no organ of division are provided with a subroutine for the computation of reciprocals. An improvement of this subroutine is proposed which permits a reduction of about 30 per cent in the number of operations without affecting the accuracy.

681.142:413 26

Use of a Computing Machine as a Mechanical Dictionary—A. D. Booth. (*Nature, Lond.*, vol. 176, p. 565; September 17, 1955.) The time required to locate a stored word is reduced by applying binary-division principles in the searching process.

681.142:621.3.078/.079 27

Industrial Uses of Special-Purpose Computers—A. II. Kuhnel. (*Instrum. & Automation*, vol. 28, pp. 1108–1113; July, 1955.) An account is presented of the analysis of a simple machine-control problem and the design of a suitable special-purpose computer to perform the task. Economic factors are also briefly considered.

681.142:621.318.5 28

A Method for Synthesizing Sequential Circuits—G. H. Mealy. (*Bell Syst. tech. J.*, vol. 34, pp. 1045–1079; September, 1955.) A theory is developed from design procedures suggested by Huffman (*J. Franklin Inst.*, vol. 257, pp. 161–190, 275–303; March/April, 1954.) and Moore (to be published in Automata Studies, Princeton Univ. Press) enabling intricate relay systems to be built up from an initial diagrammatic statement of the essential requirements. By successive application of simplifying reductions a unique circuit is finally obtained.

681.142:621.372.45 29

A Nonlinear Resistance-Capacitance Circuit—F. A. Key and W. G. P. Lamb. (*Electronic Engng.*, vol. 27, pp. 446–448; October, 1955.) An amplifier in a negative-feedback loop is used to provide the nonlinear resistance in an analog equipment representing air-pressure variations.

681.142:621.383 30

A Photoelectric Analogue Computer for investigating the Dynamic Behaviour of Linear Systems—S. Kitsopoulos. (*Bull. schweiz. elektrotech. Ver.*, vol. 46, pp. 690–693; July 23, 1955.) Apparatus is described for determining the output function of a linear system such as an amplifier or servomechanism when the input and transfer functions are known. The two known functions are represented by appropriately shaped apertures in diaphragms interposed between light source and photocell; the mechanical system used to produce the required continuous variation of the input function is described in detail.

681.142:621.395.625.3 31

High-Density Tape Recording for Digital Computers—(*Tech. News Bull. nat. Bur. Stand.*, vol. 39, pp. 121–124; September, 1955.)

CIRCUITS AND CIRCUIT ELEMENTS

621.3(083.7) 32

Standardization of Electronic Components—H. W. Ghijsen. (*Tijdschr. ned. Radiogenoot.*, vol. 20, pp. 227–242; July, 1955. In English.) A survey with particular reference to the activities of the International Electrotechnical Commission.

621.316.8+621.318.42+621.319.4].011.2 33

The Impedance of Chokes, Resistors and Capacitors at High Frequency—A. Weis. (*Frequenz*, vol. 9, pp. 221–227; July, 1955.) Analysis indicates that in order to represent the impedance variation of cylindrical inductors, resistors and capacitors at frequencies above the first resonance point, equivalent circuits are needed combining a ladder network with simple parallel or series networks; nonuniform field distribution along the component can then be taken into account. The validity of the theory is confirmed by reference to measurement results, shown graphically. The effect of an earthing lead on a lead-through capacitor is demonstrated.

621.316.86:621.396.822 34

Contact Noise—B. S. Gal'perin. (*Zh. tekh. Fiz.*, vol. 25, pp. 410–413; March, 1955.) A composition resistor is considered as consisting of a number of parallel circuits each containing an equal number of particles and the same number of contacts of equal resistance. It is shown that the noise energy of such a homogeneous system is equal to that of a single contact and that for a given gradient of the applied direct voltage it is determined by the degree of dispersion and the specific resistance of the conductor material. Expressions are also derived for heterogeneous systems and imperfect contacts.

621.316.86.049.75 35

Printed Resistors—R. S. Marty, E. M. Davies, and P. J. Franklin. (*Elect. Mfg.*, vol. 55, pp. 56–63; January, 1955.) Preparation of resistors by injection molding is described. The effect of ink composition and the printing and curing processes on the resistor characteristics are described.

621.318.435:621.373.43 36

Magnetic Pulse Modulators—K. J. Busch, A. D. Hasley, and C. Neitzert. (*Bell Syst. tech. J.*, vol. 34, pp. 943–993; September, 1955.) Mathematical analyses are given of ac- and dc-charged series-type saturable reactors for generating pulses in radar systems. Automatic core resetting is achieved. The production of pulses of duration <0.1 μs and the prevention of parasitics in the output are discussed and a circuit is described enabling the thyratron cathode in a dc-charged modulator to be operated at ground potential.

621.318.57:621.374.32:621.314.7 37

A Multistable Transistor Circuit—R. A. Henle. (*Elect. Engng., N.Y.*, vol. 74, pp. 570–572; July, 1955.)

621.372.4 38

Proof of a Theorem on the Equivalence of Two-Pole Networks with only Two Types of Impedance Element—S. Spiess. (*Hochfrequenztech. u. Elektroakust.*, vol. 64, pp. 25–32; July, 1955.) Note on 961 of 1955 (Weber and Schlegel).

621.372.41 39

Theorem on the Reactive Energy in an Electric Dipole in a State of Variation—L. Lunelli. (*Alta Frequenza*, vol. 24, pp. 246–267; June, 1955.) Analysis is based on differentiation of the operational impedance. A simple formula is derived giving the instantaneous difference between the stored magnetic and electric energy.

621.372.413+621.372.8 40

A Step-by-Step Method for designing Waveguides and Oscillatory Systems—Neyman. (See 17.)

621.372.5 41

Some Fundamental Properties of Networks without Mutual Inductance—A. Talbot. (*Proc. I.E.E.*, Part C, vol. 102, pp. 168–175; September, 1955. Digest, *ibid.*, Part B, vol. 102, pp. 554–555; July, 1955.) Elementary methods not involving determinants are used to prove theorems on the voltage and current gains obtainable from a resistance network. The results are used to determine properties of general

networks without mutual inductance; RC networks are investigated by a method simpler than that of Fialkow and Gerst (3369 of 1952). Attention is drawn to a neglected paper by Kirchhoff (*Ann. Phys. Chem.*, vol. 72, p. 497; 1847.) giving the foundations of the topology of networks.

621.372.5 42

Synthesis of Ladder Networks to give Butterworth or Chebyshev Response in the Pass Band—E. Green. (*Proc. I.E.E.*, Part C, vol. 102, p. 290; September, 1955.) Addendum to 370 of 1955.

621.372.5 43

Ladder Networks with Similar Quadripole Sections—U. Ruelle. (*Alta Frequenza*, vol. 24, pp. 268–283; June, 1955.) Formulas for the section input and output currents and voltages and input impedances are derived directly from Kirchhoff's laws, using determinants.

621.372.5:512.83 44

On Node and Mesh Determinants—S. Okada. (PROC. IRE, vol. 43, p. 1527; October, 1955.) An extension of the analysis presented by Seshu (1581 of 1955).

621.372.512.3.015.3 45

Initial Transients in some Special Passive Networks with Amplitude and Frequency Modulation—E. Henze. (*Arch. elekt. Übertragung*, vol. 9, pp. 326–338; July, 1955.) It is shown that for multistage selective circuits there is an optimum coupling for which the output corresponding to unit-step input is aperiodic and free from overshoot. The performance of two frequency-shift circuits is studied, and the existence of an optimum ratio of shift to keying frequency is demonstrated. A formula is derived for calculating distortion factor for two-circuit band-pass filters with fm.

621.372.54 46

New Filter Theory of Periodic Structures—W. K. R. Lippert. (*Wireless Engr.*, vol. 32, pp. 260–266, 305–310; October/November, 1955.) Theory for linear passive quadripoles is developed in terms of characteristic reflection and transmission factors which can be specified by reference to the standing-wave pattern on lines connected to the input and output. The relations between these factors and the usual circuit constants, particularly the image function of symmetrical circuits, are studied. The method is illustrated by examining multisection structures combining quadripoles and loss-free lines. The use of these characteristic factors leads to major simplifications in dealing with loss-free structures, where most of the work can be done graphically.

621.372.542.2:621.396.61 47

A Ten-Kilowatt Low-Pass Filter—E. R. Broad and E. J. P. May. (*P.O. elect. Engrs' J.*, vol. 48, pp. 94–96; July, 1955.) The filter is designed for use in the antenna feed lines of transmitters working in the frequency range 4–28 mc and discriminates by about 60 db against any frequencies in the television band 40–70 mc which may be present as harmonics. In measuring the effectiveness of the filter account must be taken of radiation from sources other than the antenna.

621.372.542.32:621.372.412 48

A Piezoelectric High-Pass Filter—Ya. I. Velikin, Z. Ya. Gel'mont, and E. V. Zelyakh. (*Radiotekhnika, Moscow*, vol. 10, pp. 41–49; March, 1955.) A lattice filter is considered (Fig. 1) whose special feature is the use of transformers in its arms, with crystals included in the secondary circuits. The main parameters of the filter are determined, and formulas are derived for calculating the resonance and antiresonance frequencies of the arms. A method is proposed for designing the filter elements and for calculating its basic loss. The experimental curve of a filter designed in this manner (Fig. 7) shows a sharp cut-off.

621.372.543.2.029.4 49

A High-Q RC Feedback Filter—M. J. Tucker and L. Draper. (*Electronic Engng.*, vol. 27, pp. 451–453; October, 1955.) Description of the design and construction of a 175-c acceptor filter which will maintain a Q of 1,000 stable to within 2 per cent over one hour and a Q of 500 to within 2 per cent over considerable periods. The circuit uses a twin-T rejector filter in the negative-feedback path of an amplifier.

621.372.56:621.314.632 50

A Voltage-Controlled Attenuator—G. M. Ettinger. (*Electronic Engng.*, vol. 27, pp. 458–459; October, 1955.) "A three-stage voltage controlled germanium diode attenuator is described. Transmission may be varied over a range exceeding 35 decibels by a 12 v control signal. Push-pull operation is discussed and various applications are suggested."

621.372.56.029.6:621.372.8 51

An S-Band Variable Attenuator for High-Power Working—B. E. Kingdon. (*J. Brit. Instn. Radio Engrs*, vol. 15, pp. 471–478; September, 1955.) "The description is given of a waveguide insertion attenuator in which the loss in rf power is produced by the action of a column of water flowing in a glass tube mounted in the waveguide, continuous variation of attenuation being obtained by adjustment of the water column height. Resonance effects in the water column are exploited by choosing the cross-sectional dimensions of the glass such that an optimum attenuation per unit length of tube is obtained. Experimental results are given for a model covering the range 0 to 30 db, the input vswr at $\lambda_0 = 10.00$ cm being ≤ 0.87 at any setting and ≥ 0.97 over the greater part of the range. Satisfactory operation has been achieved in an evacuated test-system fed by a magnetron delivering 2mw peak power (200 w mean) at a wavelength of 10 cm. Various modifications in design are suggested for use with higher mean powers."

621.372.6 52

The Graphs of Active Networks—W. S. Percival. (*Proc. I.E.E.*, Part C, vol. 102, pp. 270–278; September, 1955. Digest, *ibid.*, Part B, vol. 102, pp. 727–729; September, 1955.) Results obtained previously (2587 of 1953 and 379 of 1955) are used to develop the properties of the graphs of linear networks including tubes and transformers.

621.373.4+621.376.32 53

Linear and Nonlinear Effects in Reactance and Oscillator Circuits—T. Zagajewski. (*Hochfrequenztech. u. Elektroakust.*, vol. 64, pp. 8–18; July, 1955.) The analysis presented of the behavior of a reactance tube in various circuits is based on an expression for the anode current containing terms up to the third degree in the grid and anode voltages. Two nonlinear effects are considered: (*a*) the primary effect of the curvature in the tube characteristic, and (*b*) the secondary effect due to the presence of harmonic components in the applied signal. These were also investigated experimentally and the results are presented graphically. A circuit for reducing the effect of nonlinearity was also investigated.

621.373.4 54

Stability of Oscillation in Valve Generators—A. S. Gladwin. (*Wireless Engr*, vol. 32, pp. 206–214, 246–253, 272–279, 297–304; August /November, 1955.) "A comprehensive theory of stability is developed which is applicable to a large class of harmonic oscillators. The paper is concerned mainly with the 4-terminal regenerative type of oscillator with grid-leak bias but the analysis applies also to circuits with fixed grid-bias and to 2-terminal oscillators. All known forms of instability appear as special cases of the general theory and some new forms are predicted. Stability is determined by the nature of the roots of a characteristic equation and stability criteria are obtained in the form of inequalities between the parameters of the amplifier and feedback network. A modified form of Nyquist locus-diagram can also be used. When the feedback network is symmetrical with respect to the oscillation frequency the characteristic equation can be factorized to give independent criteria for frequency and amplitude stability. Hysteresis effects and periodic instability are analysed in detail. In addition to the general treatment, specific forms of the various parameters which appear in the stability criteria are worked out for a three-halves-law amplifier with a semi-linear or exponential grid-current characteristic. Quantitative experimental confirmation is provided."

621.373.4:621.396.822 55

Effect of Electrical Fluctuations on a Valve Oscillator—P. I. Kuznetsov, R. L. Stratonovich, and V. I. Tikhonov. (*Zh. eksp. teor. Fiz.*, vol. 28, pp. 509–523; May, 1955.) The effect of "slow" normal fluctuations is considered. Expressions are derived for the one-dimensional probability density functions for amplitude and phase. An approximate method is shown for calculating the correlation functions for amplitude and phase variations.

621.373.421:621–526 56

The Frequency-Response Analysis of Nonlinear Systems—P. E. W. Grensted. (*Proc. I.E.E.*, Part C, vol. 102, pp. 244–253; September, 1955. Digest, *ibid.*, Part B, vol. 102, pp. 721–723; September, 1955.) If the waveform at the input to the nonlinear elements in the system is approximately sinusoidal, the analysis may be carried out on the assumption that all harmonics generated by the nonlinear elements can be ignored. Analysis of on-off control systems on this basis gives results within about 10 per cent of the exact solutions for both transient and steady oscillations.

621.373.421.13 57

Synthesizing Crystal Stability—W. A. Hayes. (*Radio-Electronic Engng.*, vol. 24, pp. 20, 30; May, 1955.) The output from two crystal oscillators, combined to give a 10-kc beat frequency, is squared and triggers a blocking oscillator, producing a 10-kc pulse which is used to quench a tunable oscillator. The tunable oscillator locks to harmonics of the 10-kc signal.

621.373.423:621.316.726 58

An Electromechanical Stabilizer of the Frequency of a Klystron—A. I. Barchukov, G. A. Vasil'ev, M. E. Zhabotinski, and B. D. Osipov. (*Radiotekhnika, Moscow*, vol. 10, pp. 29–32; March, 1955.) In the method proposed a portion of the klystron output is applied to a cavity resonator, the natural frequency of which is modulated by a separately excited vibrating diaphragm. The output of the resonator is detected, amplified and, through a phase detector, applied to the klystron reflector. The theory of the method is discussed and its accuracy is determined. A comparison with the resonance frequency of the absorption line of ammonia has shown that the relative frequency error of the method is of the order of 5×10^{-6}.

621.373.424.029.42 59

Subaudio Oscillator Tunes 0 to 50 cycles—L. Fleming and W. W. Follin. (*Electronics*, vol. 28, pp. 144–145; October, 1955.) A beat-frequency oscillator using carrier frequencies of about 2 kc provides an output of up to 3 v constant within 2 per cent over the frequency range, with <0.2 c per hour drift and <1 per cent distortion. The need for low-frequency amplification is avoided by the use of a high-level mixer circuit consisting of two Se rectifiers with balancing adjustment to eliminate the dc component.

621.374.3:621.315.212 60
Some Transmission Line Devices for Use with Millimicrosecond Pulses—I. A. D. Lewis. (*Electronic Engng.*, vol. 27, pp. 448–450; October, 1955.) A phase inverter, impedance transformers, and a tube heater isolating transformer are described, all comprising coaxial-cable sections.

621.374.4:621.385.832 61
Generation of Harmonics of a Given Fundamental—H. Katz and K. L. Rau. (*Frequenz*, vol. 9, pp. 234–240; July, 1955.) Theory and experimental results are given for a frequency multiplier based on use of a cr tube in which a ribbon beam is deflected across a metal target with an appropriate profile. Suitable beam-forming structures are described.

621.375.1.029.63:621.396.822 62
Noise in U.H.F. Amplifiers—E. P. Dement'ev. (*Radiotekhnika, Moscow*, vol. 10, pp. 45–52; January, 1955.) General noise effects in uhf amplifiers of any type are considered. Relations between the noise parameters are established using the method of the transfer of the current generators proposed previously (*ibid.*, 1954, No. 4). General expressions for the noise factors are derived, and the minimum number of noise parameters required to characterize a circuit is determined. A concept of "partial" noise parameters is introduced.

621.375.232:623.011.21 63
A Negative Impedance Converter for Use as a Two-Terminal Amplifier—J. R. Tillman. (*P.O. elect. Engrs' J.*, vol. 48, Part 2, pp. 97–101; July, 1955.) A specified stable negative impedance may be generated by connecting a positive impedance between the output and input of an amplifier possessing a high degree of negative feedback. An amplifier suitable for use in transmission-line systems is described.

621.375.3.049.75 64
Etched Wiring simplifies Magnetic Amplifier Design—K. H. Sueker. (*Elekt. Mfg.* vol. 55, pp. 106–107; January, 1955.)

621.373/.376 65
Active Networks. [Book Review]—V. C. Rideout. Publishers: Prentice-Hall, New York, and Constable, London, 1954, 485 pp., 42s. (*Sci. Progr.*, vol. 43, pp. 534–535; July, 1955.) Deals with circuits including tubes, transistors, and other devices. There are sections on the basic principles of analog computers, servo systems, and wave-shaping circuits as well as on general aspects of amplifiers and oscillators.

GENERAL PHYSICS

53.087/.088 66
The Correction of Observational Data for Instrumental Bandwidth—F. D. Kahn. (*Proc. Camb. phil. Soc.*, vol. 51, Part 3, pp. 519–525; July, 1955.) The formula relating the readings, $\phi(x)$, of an instrument having the apparatus function $g(x)$ to the true values $f(x)$ of an observed function is stated. A three-point interpolation operator can be chosen to simulate the spreading action of a class of functions $g(x)$. Under certain conditions the interpolation operator has an exact inverse which, when applied to $\phi(x)$, gives a function which is a better approximation to $f(x)$. The accuracy obtained is discussed, and the effect of the method on the standard errors in the measurement is found.

531+537].001.362 67
Electromechanical Analogies—G. Meyer. (*Frequenz*, vol. 9, pp. 227–232; July, 1955.) A discussion of the physical significance of various analogies and of circuit concepts and terminal representation in mechanics.

535.215 68
State of Research on Photoelectricity—W. Kluge. (*Z. angew. Phys.*, vol. 7, pp. 302–311; June, 1955.) A survey is presented of research since 1949. 122 references.

535.22 69
Velocity of Light from the Molecular Constants of Carbon Monoxide—E. K. Plyler, L. R. Blaine, and W. S. Connor. (*J. opt. Soc. Amer.*, vol. 45, pp. 102–106; February, 1955.) From infrared spectroscopy measurements the value of 299792 km is deduced for the velocity of light, with a standard deviation of 6 km. A short account of the work is given in *Tech. News Bull. nat. Bur. Stand.*, vol. 39, pp. 1–3; January, 1955.

535.642.08 70
Simple Color Computer Gives Tristimulus Values—R. P. Burr and J. R. White. (*Electronics*, vol. 28, pp. 166–169; October, 1955.) Trichromatic coefficients for the CIE color-specification system are automatically computed on a simple analog machine.

537.223/.224 71
An Interesting Phenomenon observed on some Dielectrics—I. Sumoto. (*J. phys. Soc. Japan*, vol. 10, p. 494; June, 1955.) A glass tube, either empty or containing a polar liquid or a metal rod, rotates continuously when placed in an inhomogeneous electric field of sufficient strength if the electrodes and part of the tube are immersed in carnauba wax or a higher alcohol, stearic acid, palmitic acid, or xylol.

537.29:621.315.61 72
Field-Dependent Conductivity in Nonuniform Fields and its Relation to Electrical Breakdown—P. T. G. Flynn. (*Proc. I.E.E.*, Part C, vol. 102, pp. 264–269; September, 1955. Digest, *ibid.*, Part B, vol. 102, pp. 723–725.) "A method is given for calculating the resulting field distribution when the conductivity is a function of the field strength. This is applied to a point-plane electrode system in an amorphous solid, with the assumption that the conductivity at low field-strengths is electronic and that the conductivity at high field-strengths is described by a relation due to Fröhlich. The results show that for polymethylmethacrylate with average fields of the order of 10^6 volt/cm, the reduction in maximum field-strength from that calculated for constant conductivity can be a factor of five or more, the magnitude of the reduction depending on the degree of nonuniformity of the field." Various other insulating materials are also discussed.

537.5:538.561 73
Study of Gyromagnetic Resonance in the Penning Gauge—G. Dumas. (*Rev. gén. Élect.*, vol. 64, pp. 331–350; July, 1955.) Conditions in the Penning gauge are particularly favorable for studying rf radiation resulting from gyromagnetic resonance of electrons [see 1139 of 1951 (Laffineur and Pecker)]. Both longitudinal oscillations and thermal agitation of the electrons are involved, resulting in an accumulation in the anode plane. The presence of plasma has an important effect on the potential distribution, introducing a radial electric field. The equations of electron motion are established; some particular solutions indicate the possibility of a circular path in the anode plane, with an angular frequency about half the gyrofrequency. With values of magnetic induction between 100 and 1,000 G radiation at decimeter wavelengths was produced. Measurements of the radiation are described. Investigation of the complete spectrum emitted indicates that coherent oscillations may occur. The results are compared with those of other workers.

537.52:535.215.9 74
Influence of Light on the Mechanism of Gas Discharges (Joshi Effect)—S. R. Mohanty. (*Z. Phys.*, vol. 140, pp. 370–375; April 20, 1955.) Results of previous experimental work are reviewed. The variation of the discharge current with the intensity and frequency of the incident light and in particular the reversal of this current variation in a certain voltage range are interpreted in terms of space-charge effects.

537.533 75
The Mechanism of High-Field Electron Emission from Tarnished Metal Surfaces—T. J. Lewis. (*Proc. phys. Soc.*, vol. 68, pp. 504–512; August 1, 1955.) A theory of field-dependent thermal emission is proposed which takes into account the existence of patch fields due to variation in work function over the surface.

537.533 76
Numerical Ray Tracing in Electron Lenses—J. C. E. Jennings and R. G. Pratt. (*Proc. phys. Soc.*, vol. 68, pp. 526–536; August 1, 1955.) Corrections are suggested to Liebmann's formulas for tracing paraxial rays (966 of 1950); a more accurate method is developed, applicable also to marginal rays, and is compared with methods suggested by other workers. The use of the constancy of the Wronskian determinant as a criterion of accuracy of paraxial ray tracing is discussed.

537.533 77
Effect of Space Charge on the Propagation of Intense Beams of Charged Particles—M. D. Gabovich. (*Uspekhi fiz. Nauk*, vol. 56, pp. 215–256; June, 1955.) A review. About a third of the 81 references given are to Russian work.

537.533:538.691 78
A Method of finding a Large Class of Electrostatic and Magnetic Fields for which the Solutions of the Fundamental Equation of Electron Optics may be expressed in Terms of Known Functions—B. E. Bonshtedt. (*Zh. tekh. Fiz.*, vol. 25, pp. 541–543; March, 1955.) Exact solutions of equation (1) are of great interest for various types of es and magnetic fields. Until recently such solutions were known only for a very limited number of cases. Grinberg in particular indicated a class of fields for which the trajectories of electrons are expressed in terms of cylindrical functions (*Zh. tekh. Fiz.*, vol. 23, p. 1904; 1953.) Solutions are now found for a much larger class of fields.

537.533.1 79
Velocity Distribution of Electrons in Presence of an Alternating Electric Field and Constant Magnetic Field—V. M. Fain. (*Zh. eksp. teor. Fiz.*, vol. 28, pp. 422–430; April, 1955.) Two cases are considered theoretically: (*a*) the electric field varies sinusoidally, and (*b*) the variation is amplitude modulated. Case (*b*) is of interest in the investigation of ionospheric cross-modulation. The effect of collisions between electrons is taken into account.

537.562:621.317.335.3:621.372.413 80
Resonant-Cavity Measurements of the Relative Permittivity of a D.C. Discharge—K. W. H. Foulds. (*Proc. Instn. elect. Engrs.*, Part C, vol. 102, pp. 203–216; September, 1955. Digest, *ibid.*, Part B, vol. 102, pp. 564–567; July, 1955.) Measurements at 2.1, 2.5, and 3 kmc on low-pressure dc discharges in (*a*) a mixture of Hg vapor and Ar, and (*b*) Hg vapor alone. Decrease of permittivity with increase of discharge current was noted in all cases. In case (*b*) the cavity Q-factor exhibited a minimum at a value of discharge current depending on the resonance frequency; this is attributed to electron resonance. Theory of the method is given.

538.1 81
General Theory of Magnetic Masses at Rest and in Movement—É. Durand. (*Rev. gén. Élect.*, vol. 64, pp. 350–356; July, 1955.) Theory is presented based on the analogy with electric charge.

538.1 82
A New Vectorial Transformation of a Curved-Line Integral into a Surface Integral, and its Application to Magnetostatics—É.

Durand. (*C. R. Acad. Sci., Paris*, vol. 241, pp. 594–596; August 17, 1955.)

538.1:538.221 83

Magnetostatics with Ferromagnetic Materials—V. I. Skobelkin and R. N. Solomko. (*Zh. eksp. teor. Fiz.*, vol. 28, pp. 385–393; April, 1955. Correction *ibid.* vol. 28, p. 766; June, 1955.) A variational principle is formulated and proved in the theory of ferromagnetic materials in the field of electric currents. A direct method is developed for investigating magnetic fields in the general case of a nonlinear dependence of permeability on magnetic field strength.

538.3 84

Comments on the Nonlinear Electrodynamics—K. Bechert. (*Ann. Phys., Lpz.*, vol. 16, pp. 97–110; July 15, 1955.) Some solutions of the equations presented earlier (1969 of 1953) are examined.

538.3:512.831 85

Description of the Electromagnetic Field by Means of Matrices—G. A. Zaitsev. (*Zh. eksp. teor. Fiz.*, vol. 28, pp. 524–529; May, 1955.) The properties of "matrix-tensors" are briefly considered and the quantities characterizing an em field are then expressed in matrix form.

538.56:537.5 86

Note on Plasma-Electron Oscillations—L. G. Emeleus and T. K. Allen. (*Aust. J. Phys.*, vol. 8, pp. 305–306; June, 1955.) Brief report of the results of experiments on hot-cathode discharges in Hg vapor or Ar at pressures of the order of 10^{-3} mm Hg, and discussion of their relation to the work of Wild et al. (704 of 1955).

538.566 87

The Perturbation of an Electromagnetic Field by Small Deformations of a Metal Surface—B. Z. Katsenelenbaum. (*Zh. tekh. Fiz.*, vol. 25, pp. 546–557; March, 1955.) A general expression is derived for the perturbation due to the deformation. If the deformation is slight this perturbation can be found by the usual method of quadratures. The method is applied to the problem of the diffraction of a plane wave at a step, the height of which is small compared with λ. From this the well known formulas of Rayleigh for reflection from small and smooth irregularities are easily derived.

538.566 88

Study of the Local Electromagnetic Field at the Junction of Three Dielectric Media—G. Veill. (*C.R. Acad. Sci., Paris*, vol. 241, pp. 554–556; August 8, 1955.) Analysis is given for the case of three media with a common edge.

538.566:535.42 89

A Diffraction Problem—P. Poincelot. (*C.R. Acad. Sci., Paris*, vol. 241, pp. 625–627; August 22, 1955.) Analysis is presented for the case of a plane em wave incident normally on a infinitely long perfectly conducting strip.

538.566:537.31 90

Scattering of Electromagnetic Waves from "Lossy" Strip on a Conducting Plane—J. R. Wait. (*Canad. J. Phys.*, vol. 33, pp. 383–390; July, 1955.) An examination is made of the error introduced in the analysis of radiation and propagation problems by assuming perfect conductivity in media, such as the ground, which are in fact imperfectly conducting. The result of the approximate calculation is compared with that of an exact calculation involving elliptic wave functions. For the approximation to be permissible, the surface impedance of the lossy regions should not exceed 0.1 times the impedance of free space.

538.566:537.56 91

Hydromagnetic Waves in Ionized Gas—H. Piddington. (*Nature, Lond.*, vol. 176, 508; September 10, 1955.) The equation representing the em field in a moving isotropically conducting medium is discussed and expressions are derived for the velocities of the ordinary, extraordinary and *S* (sound-type) waves, for gas pressures (*a*) much less than and (*b*) much greater than the "magnetic pressure." See also 3579 of 1955.

538.569.4:535.33 92

New Technique for High-Resolution Microwave Spectroscopy—R. H. Romer and R. H. Dicke. (*Phys. Rev.*, vol. 99, pp. 532–536; July 15, 1955.) Spectral lines of width substantially less than the Doppler width are produced by containing the gas in a pillbox-shaped cavity of height about $\lambda/2$ and diameter large compared to λ.

538.615:538.569.4.029.6:546.171.1 93

The Zeeman Effect in Ammonia Microwave Spectra—Y. Torizuka, Y. Kojima, T. Okamura, and K. Kamiryo. (*J. phys. Soc. Japan*, vol. 10, pp. 417–420; June, 1955. *Sci. Rep. Res. Tohoku Univ., Ser. A*, vol. 7, pp. 316–320; June, 1955.) The Zeeman effect was investigated experimentally using magnetic fields up to 15,000 oersted. Results indicate that the $J=1$, $K=1$ line shows a change from the Zeeman effect to the Paschen-Back effect at field strengths near 10,000 oersted.

538.63:538.221 94

Theory of the Nernst Effect in Ferromagnetic Metals—K. Meyer. (*Z. Naturf.*, vol. 10a, p. 166; February, 1955.) On the basis of a two-band model with one band nearly empty and the other nearly fully occupied, theory for the Nernst effect can be derived simply from that for the Hall effect.

538.632 95

The Hall Effect and Related Phenomena—F. A. Vick. (*Sci. Progr.*, vol. 43, pp. 454–461; July, 1955.) A brief review is presented of recent work on the theory of the Hall effect in ferromagnetic, in strongly paramagnetic, and in semiconducting materials. Practical applications of the effect, such as in the InSb power amplifier [2576 of September (Ross and Thompson)] are also mentioned.

539.155 96

Reliability of Atomic Masses in the Chromium-Germanium Region—J. T. Kerr, J. G. V. Taylor, and H. E. Duckworth. (*Nature Lond.*, vol. 176, pp. 458–459; September 3, 1955.) Discrepancies between atomic mass values obtained from transmission data and those obtained by mass-spectrometer methods are discussed. The mass-spectrometer values for Ni may be in error, but those for the other elements from Cr to Ge are considered to be accurate.

GEOPHYSICAL AND EXTRATERRESTRIAL PHENOMENA

523.16:523.3 97

Lunar Occultation of a Radio Star and the Derivation of an Upper Limit for the Density of the Lunar Atmosphere—B. Elsmore and G. R. Whitfield. (*Nature, Lond.*, vol. 176, pp. 457–458; September 3, 1955.) Brief report of observations made at Cambridge, England, of the passage of the moon across the large-diameter radio source in Gemini. Wavelengths of 7.9 and 3.7 m were used.

523.16:621.396.677 98

Chord Construction for Correcting Aerial Smoothing—R. N. Bracewell. (*Aust. J. Phys.*, vol. 8, pp. 200–205; June, 1955.) A graphical method of correcting for antenna smoothing in radio astronomy, simpler and no less accurate than methods described previously.

523.5:621.396.96 99

The Influence of Noise on Radar Meteor Observations—C. D. Ellyett and G. J. Fraser. (*Aust. J. Phys.*, vol. 8, pp. 273–278; June, 1955.) An experimental investigation has been made of the minimum detectable echo power from meteor trails using 69-mc radar equipment with incoherent detection. For optimum signal/noise ratio the pulse width must exceed the width of the cr-tube spot. Extraterrestrial noise is predominant, receiver noise figure being of second-order importance. Variations in the effective antenna temperature introduce corresponding variations in the observed meteor rate. Using artificial echoes, a minimum signal/noise ratio of 8 db is found to be necessary for detection; the most important parameter is the total received signal energy. It is not likely that meteors of smaller size can be made observable by improving receivers.

523.5:621.396.96 100

Diffusion Coefficients from the Rate of Decay of Meteor Trails—A. A. Weiss. (*Aust. J. Phys.*, vol. 8, pp. 279–288; June, 1955.) An estimate of the diffusion coefficient in the meteor zone is obtained by an extension of Huxley's theory of ambipolar diffusion (*Aust. J. Sci. Res., Ser. A*, vol. 5, p. 10; 1952.). The absolute value of the diffusion coefficient thus calculated, and its gradient with height, are confirmed by comparison with results of measurements made at Adelaide, using cw radar technique at a wavelength of 11.2 m [1424 of 1954 (Robertson et al.)]. The theory appears adequate to account for the observed variation of diffusion coefficient with height.

523.7 101

The Identification of Sunspots by means of Chromospheric Faculae—M. d'Azambuja. (*C.R. Acad. Sci., Paris*, vol. 241, pp. 592–594; August 17, 1955.)

550.372:621.396.11 102

Influence of Temperature and Humidity on the Electrical Constants of the Ground—M. Argirovic. (*Ann. Télécommun.*, vol. 10, pp. 113–116; May, 1955.)

550.38:551.510.535 103

Comparison of Records of the Horizontal Component of the Terrestrial Magnetic Field (*K* index) at Kerguelen and at Heard Island—A. Luchet. (*C.R. Acad. Sci., Paris*, vol. 241, pp. 569–571; August 8, 1955.) The records confirm that magnetic activity is particularly strong during the equinoxes. The correlation coefficient for the two stations is about 0.7. Ionograms obtained during the strong magnetic variations are characteristic of a highly disturbed ionosphere.

550.380.8 104

NOL Vector Airborne Magnetometer Type 2A—E. O. Schonstedt and H. R. Irons. (*Trans. Amer. geophys. Union*, vol. 36, pp. 25–41; February, 1955.) The instrument previously described (719 of 1954) has been modified so as to be suitable for use in all latitudes and to simplify the reduction of results.

550.380.87 105

A Recording Magnetic Variometer—J. H. Meek and F. S. Hector. (*Canad. J. Phys.*, vol. 33, pp. 364–368; July, 1955.) Description of an electronic magnetometer designed for continuous measurement of changes in the earth's magnetic field at one place; variations as small as 10^{-4} oersted can be recorded.

550.385 106

Notes on the Distribution of *SC in High Latitudes**—T. Nagata and S. Abe. (*Rep. Ionosphere Res. Japan*, vol. 9, pp. 39–44; March, 1955.) An examination of experimental data shows that the equivalent overhead currents for the preliminary reverse impulse in this type of magnetic storm in the northern hemisphere are represented by current flows across the polar cap from the longitude corresponding to 10 h to that corresponding to 22 h and by the resulting two vortices extending to lower latitudes, a clockwise vortex in the afternoon hemisphere and a weaker counter-clockwise vortex in the forenoon hemisphere.

550.385:523.78 107
The Effect on Geomagnetism of the Solar Eclipse of 30 June 1954—J. Egedal and N. Ambolt. (*J. atmos. terr. Phys.*, vol. 7, pp. 40–48; August, 1955.) An examination of records of magnetic declination from 11 observatories near the path of totality shows that a maximum magnetic effect occurs at the time of totality, appearing as a diminution of normal daytime departures from the night-time value of the declination. Quantitative agreement with theory is shown.

551.510.52:535.325 108
Survey of Airborne Microwave Refractometer Measurements—C. M. Crain. (Proc. IRE, vol. 43, pp. 1405–1411; October, 1955.) Results of measurements made at various places in the U.S.A., over land and off the east and west coasts, are summarized. Variations of the vertical distribution of refractive index are studied in relation to time and place. Particular attention is paid to the fine detail of the refractive-index structure. See also *e.g.*, 2662 of 1954 (Crain et al.).

551.510.52:535.325 109
Amplitude, Scale and Spectrum of Refractive-Index Inhomogeneities in the First 125 Meters of the Atmosphere—G. Birnbaum and H. E. Bussey. (Proc. IRE, vol. 43, pp. 1412–1418; October, 1955.) Report of an extensive series of observations made using two refractometers at various levels on a 128-m tower. The correlation between the refractive-index variations and variations of meteorological conditions is studied.

551.510.534 110
Seasonal and Latitudinal Temperature Changes in the Ozonosphere—J. Pressman. (*J. Met.*, vol. 12, pp. 87–89; February, 1955.) Computations are presented relevant to the elucidation of the temperature structure in the middle atmosphere. See also 1028 of 1955.

551.510.535 111
Hydromagnetic Resonance in Ionospheric Waves—C. O. Hines. (*J. atmos. terr. Phys.*, vol. 7, pp. 14–30; August, 1955.) The large-scale traveling ionospheric disturbances detected by various workers in the F_2 layer may be partially explained as an electron resonance effect, produced when an initial atmospheric disturbance generates natural modes of electromagnetic oscillation, as a result of hydromagnetic coupling.

551.510.535 112
Some Features of the E_2 Layer observed at the Ionosphere Field Station, Haringhata, Calcutta—A. K. Saha and S. Ray. (*J. atmos. terr. Phys.*, vol. 7, pp. 107–108; August, 1955.) Photographic records are reproduced showing how the E_2 ionization originates at F_1-layer level, moves downwards and forms a sporadic E layer.

551.510.535 113
Recombination and Ion Production from the Total Electron Content—N. J. Skinner and R. W. Wright. (*J. atmos. terr. Phys.*, vol. 7, pp. 105–107; August, 1955.) Revised values are given for the figures suggested previously (1338 of 1955) for the mean recombination coefficient and the mean rate of ion production in the F layer. Results of observations at Ibadan for magnetically quiet and disturbed days are plotted and discussed.

551.510.535 114
A Consideration of the Mechanism of Electron Removal in the F_2 Layer of the Ionosphere—T. Yonezawa. (*Rep. Ionosphere Res. Japan*, vol. 9, pp. 17–37; March, 1955.) Possible mechanisms of electron removal are discussed in the light of observations. No satisfactory theory of the phenomenon exists. See also 1036 of 1955.

551.510.535:523.78 115
Variation of fE_s during Solar Eclipses—W. Stoffregen. (*Nature, Lond.*, vol. 176, p. 610; September 24, 1955.) Records obtained by Minnis at Khartoum in 1952 (2298 of 1955) and by Stoffregen in the north of Sweden in 1945 (1778 of 1947) are discussed and compared with observations from various stations in 1954. A decrease of fE_s during the eclipse is found only at places where the eclipse is total or nearly so. The typical eclipse configuration of sun-moon-earth is thought to be in some way responsible for the associated preliminary increase of fE_s.

551.510.535:525.624 116
The Lunar Semidiurnal Oscillation in the Ionospheric Absorption of 150-kc/s Radio Waves—A. P. Mitra. (*J. atmos. terr. Phys.*, vol. 7, pp. 99–100; August, 1955.) Vertical-incidence absorption measurements made at Pennsylvania State University during 1949–1953 appear to confirm earlier work by Appleton and Beynon (3133 of 1949).

551.510.535:550.385 117
Geomagnetic Activity and Average Deviations of Daytime F_2-Layer Critical Frequencies in Different Geomagnetic Latitudes—G. Lange-Hesse. (*J. atmos. terr. Phys.*, vol. 7, pp. 49–60; August, 1955. In German.) Analysis of data from six ionospheric sounding stations and one geomagnetic observatory shows a distinct dependence of the average daytime deviations from median values on the geomagnetic latitude, the seasons, and the sunspot cycle. The effect on the prediction of ionospheric disturbances is discussed and the reliability of predictions is assessed. See also 2942 of 1954.

551.510.535:551.55 118
Sporadic-E Movements—N. C. Gerson. (*J. Met.*, vol. 12, pp. 74–80; February, 1955.) Reports of radio amateurs on vhf reception in N. America are consistent with atmospheric movements at a height of 110 km with speeds averaging about 300 km/h. Data on winds at heights up to 120 km, determined by various methods, indicate that at all heights the winds are predominantly from the east during summer and from the west during winter.

551.510.535:551.594.5 119
The Auroral E-Layer Ionization and the Auroral Luminosity—A. Omholt. (*J. atmos. terr. Phys.*, vol. 7, pp. 73–79; August, 1955.) An empirical relation is established between the photon emission within the negative nitrogen bands of auroras in zenith and the maximum electron density in the E layer. The recombination coefficient in the layer during auroras is $>10^{-7}$ cm^3. In medium to strong auroras the mean electron density, deduced from critical frequencies, is between 2.10^5 and 10.10^5 electrons/cm^3. VHF echoes observed during auroras may be explained as backscatter from the ground reflected at low incidence from the auroral E layer.

551.510.535:621.396.11 120
The Effects of Anisometric Amplitude Patterns in the Measurement of Ionospheric Drifts—G. J. Phillips and M. Spencer. (*Proc. phys. Soc.*, vol. 68, pp. 481–492; August 1, 1955.) Measurement of ionospheric drift by determination of time shifts between fading curves of ionospherically reflected waves received at three spaced points is discussed and the errors involved in assuming that the amplitude pattern on the ground is statistically isometric are evaluated. From 15 recordings of fading curves on 2.4 mc a mean error of 15° in the direction of drift was found, the greatest error being 53°. The errors are not generally systematic.

551.510.535:621.396.11 121
The Shape of Irregularities in the Upper Ionosphere—M. Spencer. (*Proc. phys. Soc.*, vol. 68, pp. 493–503; August 1, 1955.) Observations of radio stellar scintillations made with three spaced receivers on a frequency of 38 mc show that irregularities in the amplitude pattern on the ground are, regarded statistically, elliptically shaped, the ratio of major to minor axis being at least 5:1. The direction of the major axis of the corresponding ellipsoidal ionospheric irregularities appears to be along the lines of force of the earth's magnetic field. Estimates of the drift velocity of ionospheric irregularities based on the assumption that the ionospheric pattern has spherical symmetry are hence subject to error.

551.594.6 122
Some Waveforms of Atmospherics and their Use in the Location of Thunderstorms—F. Horner and C. Clarke. (*J. atmos. terr. Phys.*, vol. 7, pp. 1–13; August, 1955.) The main types of atmospherics waveforms recorded in southern England are illustrated and their use in estimating range is discussed. In an analysis of recordings made during one year, 3 per cent of the waveforms recorded by day and 5 per cent of those by night were suitable for this purpose. Most night-time storms within a distance of 2,000 km produce some waveforms from which range may be determined with an accuracy within ±30 per cent; by day the corresponding distance is 500 km in summer and 1,000 km in winter.

LOCATION AND AIDS TO NAVIGATION

621.396.9 123
International Conference on Lighthouses [and other aids to navigation] at Scheveningen [31st May-9th June 1955]—C. B. Broersma. (*Tijdschr. ned. Radiogenoot*, vol. 20, pp. 257–264; July, 1955.) A report is given of the papers and discussion. Navigation aids discussed included radar, loran, consol, radar beacons, radio-range beacons, radiocommunication.

621.396.93 124
Microwave Harbour Beacon—A. L. P. Milwright. (*Wireless World*, vol. 61, pp. 569–570; November, 1955.) A 3-cm-λ pulse transmitter feeds alternately two vertical resonant-slot antennas erected at the harbor entrance and arranged on either side of a separator plate, so that the radiated beams overlap, defining the safe course for entry along a sector 1° wide within which a continuous signal is received. Reception is by a pre-tuned transistor receiver, coupled to a horn antenna having a horizontal beam width of 16°. On trial the equipment, which is intended for small craft, operated satisfactorily at ranges up to 7 miles.

621.396.933 125
TACAN Navigation System shows Bearing and Distance—(*Electronics*, vol. 28, pp. 174, 176; October, 1955.) Information is automatically transmitted by a ground installation to an aircraft on interrogation by means of correctly spaced pulses. Bearing accuracy is within ±1° and range is within 600 ft+0.15 per cent of the distance measured. Operating frequency is around 1 kmc. An outline is given of the principles involved.

621.396.96 126
Portable Precision Approach Radar—J. B. Levin. (*Electronics*, vol. 28, pp. 154–159; October, 1955.) The system described uses two corner reflectors to determine the touch-down point, the runway center-line, and the elevation reference. The equipment takes six hours to set up and provides touch-down accuracy within ± 20 feet.

621.396.96:551.577 127
Radar Observations of Rain at Poona—B. K. Gupta, A. M. Mani, and S. P. Venkiteshwaran. (*Indian J. Met. Geophys.*, vol. 6, pp. 31–40; January, 1955.) Observations made with a search radar Type SCR 717 C operating

at 9.1 cm λ are reported and illustrated by photographs.

621.396.96:621-526 128
The Stability and Time Response of Fast-Operating Closed-Loop Pulsed Radar Circuits.—McDonnell and Perkins. (See 269.)

621.396.963.3:621.396.822 129
Detection of Pulse Signals in Noise—D. G. Tucker and J. W. R. Griffiths. (*Wireless Engr.*, vol. 32, pp. 290–297; November, 1955.) Visual detection of pulse signals against a noise background on an intensity-modulated display is considered; an examination is made of the relation between the probability of detection at any given signal/noise ratio and the measured qualities of the cr tube and its phosphor, or of the chemical recorder and its iodized paper. Theory is presented in terms of just-noticeable differences (j.n.ds.), defined as the increase of voltage or current which can with certainty cause a just-noticeable increase in visible intensity; the size and number of j.n.ds. constitute a subjective measure of the display characteristics. Numerical examples illustrating the theory are presented.

MATERIALS AND SUBSIDIARY TECHNIQUES

535.215:546.482.21 130
Influence of Infrared Rays on the Photoconductivity of the Polycrystalline CdS—S. Yoshimatsu, C. Kanzaki, S. Ibuki, and N. Murai. (*J. phys. Soc. Japan*, vol. 10, p. 493; June, 1955.) In the specimens investigated, the photocurrent under irradiation by visible light decreased when infrared illumination was added. The dependence of this effect on the wavelength of the infrared radiation is shown graphically for temperatures of 18°, 110°, and 150°C.

535.37+535.215 131
Infrared Stimulation and Quenching of Photoconductivity in Luminescent Powders—H. Kallmann, B. Kramer, and A. Perlmutter. (*Phys. Rev.*, vol. 99, pp. 391–400; July 15, 1955.) Continuing previous work (2021 of 1953), measurements are reported on a range of (ZnCd)S phosphors, indicating that photoconductivity excited by ultraviolet or gamma rays may be stored for days and revealed by infrared stimulation, whereas application of the infrared radiation at the same time as the excitation produces quenching of both fluorescence and photoconductivity. An explanation of the observations is given in terms of the action of the infrared radiation on trapped and valence-band electrons.

535.37:537.311.33 132
Present-Day Problems in Crystal Luminescence—M. Curie and D. Curie. (*Cah Phys.*, nos. 55–58, pp. 1–36, 29–48, 52–80; March/June, 1955.) A comprehensive survey. The structure of inorganic crystal phosphors, as typified by ZnS, is studied by the methods used for investigating semiconductors generally as well as by specialized luminescence methods. Numerous electrons at the bottom of the conduction band contribute to the luminescence but are not sufficiently displaced to contribute effectively to photoconduction. Radiationless transitions are discussed and a synthesis of various theories is presented. Experimental work, to be effective, should be conducted with transparent films.

535.37+537.226.2]:546.472.21 133
Change of the Dielectric Constant of Phosphors under the Influence of Infrared Radiation—E. E. Bukke. (*Zh. eksp. teor. Fiz.*, vol. 28, pp. 507–508; April, 1955.) In all cases when luminescence was increased by illumination with radiation of wavelength 0.8 μ or 1.3 μ, the dielectric constant also increased; in cases when the luminescence decreased the dielectric constant remained unchanged. Results for ZnS-Cu, Tm and Zns·Cds-Cu, Ni are presented graphically, results for other phosphors are tabulated.

535.37:546.472.21 134
State of Cu Activator in Zinc-Sulphide Phosphors—A. A. Cherepnev. (*Zh. eksp. teor. Fiz.*, vol. 28, pp. 458–462; April, 1955.) Experimental results on ZnS-Cu phosphors prepared by several different methods and excited by ultraviolet radiation indicate that the Cu is in a dispersed state in the phosphor.

535.37:546.482.21 135
An Experimental Contribution on the Problem of Field Breakdown of CdS Single Crystals—K. W. Böer and U. Kümmel. (*Ann. Phys., Lpz.*, vol. 16, pp. 181–191; July 15, 1955.)

535.372 136
A Comparison of the Luminescence of Calcium Silicate (Mn, Pb) and Zinc-Beryllium Silicate (Mn)—H. Dziergwa and H. Lange. (*Z. Phys.*, vol. 140, pp. 359–369; April 20, 1955.) Fundamental differences between the emission spectra of the two materials at temperatures between −180° and +400°C and between their decay characteristics are discussed.

535.376 137
Brightness Waves in the Luminescence of Phosphors excited by Alternating Electric Fields—H. Gobrecht, D. Hahn, and F. W. Seemann. (*Z. Phys.*, vol. 140, pp. 432–439; April 20, 1955.) CRO traces are shown of the brightness variations of electroluminescent phosphors. These exhibit characteristic differences for different phosphors but are not greatly influenced by the frequency, field strength, or binding dielectric. The variations are more advanced in phase with respect to the voltage waveform than those of a glow discharge. The asymmetry of the waveforms with increased layer thickness indicates an additional surface effect at the anode.

535.376:539.23 138
Field-Enhanced Cathodo-luminescence in Magnesium Oxide—J. Woods and D. A. Wright. (*Proc. phys. Soc.*, vol. 68, pp. 566–569; August 1, 1955.

537.226/.227 139
On Interactions among Ions of a $BaTiO_3$ Crystal and on its 180° and 90° Type Domain Boundaries—W. Kinase. (*Progr. theor. Phys.*, vol. 13, pp. 529–539; May, 1955.)

537.226:621.3.029.6 140
Methods for calculating the Dielectric and Magnetic Permeabilities of Artificial Media—A. L. Mikaelyan. (*Radiotekhnika, Moscow*, vol. 10, pp. 23–36; January, 1955.) Artificial dielectrics are considered in which the size of the included particles and the distance between them are much smaller than the operating wavelength, so that the properties of the medium are independent of frequency. Several methods are proposed for calculating the dipole moments of conducting and nonconducting particles; the results are tabulated for different shapes of particle. Media can be produced having a refractive index smaller than that of free space.

537.226.2/.3:621.317.335.029.6 141
Determination of Dielectric Properties from the Brewster Angle of Incidence and the Restored Azimuth at Wavelengths below 3 cm—Rabenhorst. (See 208.)

537.226.8:621.315.616.9 142
Creep-Path Formation in Synthetic Materials—K. Schumacher. (*Elektrotech. Z., Edn A*, vol. 76, pp. 369–376; June 1, 1955.) An experimental investigation is reported. Local heating was produced by means of an electrically heated filament stretched near the specimen, across which a potential was applied. The changes in the specimens up to the time of breakdown were recorded.

537.227:547.476.3 143
Some Peculiarities of the Polarization of Rochelle Salt exposed to Radioactive Irradiation—I. S. Zheludev, M. A. Proskurnin, V. A. Yurin, and A. S. Boberkin. (*C.R. Acad. Sci. U.R.S.S.*, vol. 103, pp. 207–208; July 11, 1955. In Russian.) The effect of irradiation at an intensity of 10^{19} ev.$h^{-1}\cdot g^{-1}$ is shown by a series of hysteresis oscillograms recorded (*a*) at the beginning of the experiment, (*b*) after 30 minutes of irradiation, (*c*) after 1 h, (*d*) after 2 h, and (*e*) after 13 h 30 minutes. The polarizing field applied was 1340 v/cm. As the period of irradiation increases, the loop becomes more and more constricted in the middle, the constriction changes into a straight line the length of which increases until the whole characteristic is linear.

537.228.1:534.2-8 144
Ultrasonic Velocities in Polarized Barium Titanate Ceramics—H. B. Huntington and R. D. Southwick. (*J. acoust. Soc. Amer.*, vol. 27, pp. 677–679; July, 1955.) "Measurements have been made of the ultrasonic velocities in polarized barium titanate ceramic blocks for both compressional and transverse waves, parallel and perpendicular to the axis of polarization. Some variation in compressional velocity with the degree of binding was evident. The largest variation between the velocities for transverse waves causing shear amounted to nearly 12 per cent and proved to be accounted for by electromechanical coupling. The compressional velocity parallel to the axis of polarization ran some four per cent higher than that at right angles. Here again it appeared that the effect was caused principally by differences in electrical boundary conditions and that the constant field elastic constants varied only slightly with polarization."

537.311.33 145
Semiconductors—(*J. Electronics*, vol. 1, pp. 103–230; September, 1955.) This issue is devoted to a series of papers presented at a symposium noted previously [3634 of 1955 (Ross)]. The titles are as follows:

Speculations on the Energy-Band Structure of Zinc-Blende-Type Crystals—F. Herman. (pp. 103–114.)

Bond Relationships in Diamond-Type Semiconductors—C. H. L. Goodman. (pp. 115–121.)

The Validity of the Hydrogen-Like Approximation for Impurity Levels—G. Rickayzen. (pp. 122–125.)

Photovoltaic and Photoconductive Theory applied to InSb—T. S. Moss. (pp. 126–133.)

The Photoelectromagnetic Effect in Indium Antimonide—C. Hilsum, D. J. Oliver, and G. Rickayzen. (pp. 134–137.)

Some Implications of the Small Energy Gap and Small Effective Electron Mass in InSb—J. W. Allen and I. M. Mackintosh. (pp. 138–144.)

Measurements of Diffusion Length in Indium Antimonide—D. G. Avery and D. P. Jenkins. (pp. 145–151.)

Accurate Measurements of Absorption in Indium Antimonide and Gallium Antimonide—V. Roberts and J. E. Quarrington. (pp. 152–160.)

A Study of the Conduction Band of InSb—R. Barrie and J. T. Edmond. (pp. 161–170.)

The Electrical Properties of Indium Antimonide at Low Temperatures—B. V. Rollin and A. D. Petford. (pp. 171–174.)

The Magneto-resistance Effect in Indium Antimonide—R. Mansfield. (pp. 175–177.)

A Simple Method to visualize Degeneracy of an Intrinsic Semiconductor—G. Busch. (pp. 178–180.)

Optical and Electrical Properties of GaAs, InP and GaP—H. Welker. (pp. 181–185.)

On the Degeneracy Effect in InAs—R. Talley and F. Stern. (pp. 186–189.)

Preparation and Electrical Properties of CdTe Single Crystals—F. A. Kröger and D. de Nobel. (pp. 190–202.)

The Preparation, Electrical, and Optical Properties of Mg_2Sn—W. D. Lawson, S. Nielsen, E. H. Putley, and V. Roberts. (pp. 203–211.)

Zone Melting of Decomposing Solids—J. van den Boomgaard, F. A. Kröger, and H. J. Vink. (pp. 212–217.)

Thermoelectric Applications of Semiconductors—H. J. Goldsmid. (pp. 218–222.)

Applications of Indium Antimonide—I. M. Ross and E. W. Saker. (pp. 223–230.)

537.311.33 146

Physical Theory of Semiconductor Surfaces—C. G. B. Garrett and W. H. Brattain. (*Phys. Rev.*, vol. 99, pp. 376–387; July 15, 1955.) Properties associated with the space-charge region and with surface states are discussed in the light of experimental evidence. The theory of the space-charge region is fairly precisely established, but knowledge about the exact structure of the surface states under given chemical conditions is still incomplete. Measurements of surface photoeffect are not alone sufficient to fill the gaps; field-effect experiments with controlled chemical environment would probably give useful results.

537.311.33 147

Measurement of Minority Carrier Lifetimes in Semiconductors—N. F. Durrant. (*Proc. phys. Soc.*, vol. 68, pp. 562–563; August 1, 1955.) A modification of a method proposed by Haynes and Westphal (2233 of 1952) is used in which a short pulse of minority carriers is injected into the specimen and made to drift towards the collector by a sweeping field triggered with variable delay by the emitter pulse. The collected pulse is proportional to the number of carriers surviving. The method permits the detection and elimination of errors due to trapping effects and conductivity modulation and gives results consistent within 5 per cent.

537.311.33 148

On Lattice Scattering in Homopolar Semiconductors—J. M. Radcliffe. (*Proc. phys. Soc.*, vol. 68, pp. 675–680; August 1, 1955.) A particular solution of the Boltzmann equation for the stationary states of a system subject to electric and magnetic fields is obtained, assuming a non-degenerate conduction band of arbitrary shape. The theory is applied in a discussion of the temperature variation of the mobility of holes in Ge and Si.

537.311.33 149

Scattering of Electrons and Holes by Charged Donors and Acceptors in Semiconductors—R. B. Dingle. (*Phil. Mag.*, vol. 46, pp. 831–840; August, 1955.) The problem of determining the time of relaxation due to scattering of electrons and holes by charged impurity donors and acceptors in semiconductors is reconsidered and new formulas are derived using an approach which is basically the same as that used by Mott (*Proc. Camb. phil. Soc.*, vol. 32, p. 281; 1936.) Results obtained by these formulas are compared with those derived by other workers.

537.311.33:546.28 150

Optical Properties of Indium-Doped Silicon—R. Newman. (*Phys. Rev.*, vol. 99, pp. 465–467; July 15, 1955.) Absorption and photoconduction measurements at low temperatures (<77°K) indicate that the ionization energy of In as an impurity in Si is 0.16 ev. Sharp absorption lines observed at 20°K broaden as the temperature rises and practically disappear at 77°K.

537.311.33:546.28 151

Spin Resonance of Impurity Atoms in Silicon—C. P. Slichter. (*Phys. Rev.*, vol. 99, pp. 479–480; July 15, 1955.) "An explanation is proposed for the weak satellite lines observed in the microwave electron spin resonance of Group V impurity atoms in silicon. The satellites occur halfway between the main hyperfine lines. It is proposed that the satellites represent the resonance of pairs of impurities close enough together for their exchange interaction to be very large compared to the hyperfine coupling. Mathematical details are worked out."

537.311.33:546.28:539.32 152

The Determination of the Elastic Constants of Silicon by Diffuse X-Ray Reflexions—S. C. Prasad and W. A. Wooster. (*Acta Cryst.*, vol. 8, Part 6, p. 361; June 10, 1955.)

537.311.33:546.289 153

Electrical Properties of Germanium Semiconductors at Low Temperatures—H. Fritzsche. (*Phys. Rev.*, vol. 99, pp. 406–419; July 15, 1955.) The low-temperature maximum of Hall coefficient and the saturation of resistivity observed by Hung and Gliessman (1696 of 1955) have been confirmed by measurements over the temperature range 1.5°–300°K, using n and p type crystals with various impurity concentrations. Field effects were excluded, and the anomalous observations were shown not to be due to surface conduction or crystal anisotropy. To explain the results, conduction in at least two energy bands must be assumed, one of which is characterized by very low carrier mobility.

537.311.33:546.289 154

Optical Properties of Plastically Deformed Germanium—H. G. Lipson, E. Burstein, and P. L. Smith. (*Phys. Rev.*, vol. 99, pp. 444–445; July 15, 1955.) Samples of $1-\Omega\cdot$cm n type Ge were deformed to various degrees by compression at about 700°C. Resistivity and thermoelectric-power measurements indicated that the larger deformations were accompanied by conversion to p type. Transmission measurements over the wavelength range 1–15 μ indicated that in all cases the deformation gave rise to a shift of the intrinsic absorption edge towards longer wavelengths, together with an extended tail. A theoretical explanation of the changes is indicated briefly.

537.311.33:546.289 155

Hall Theory in n-Type Germanium—L. Gold. (*Phys. Rev.*, vol. 99, p. 596; July 15, 1955.) Brief interim report of a study of the galvanomagnetic properties of n type Ge based on the value of the scattering time.

537.311.33:546.289 156

Some Observations on Growth and Etching of Crystals with the Diamond or Zincblende Structure—E. Billig and P. J. Holmes. (*Acta Cryst.*, vol. 8, Part 6, pp. 353–354; June 10, 1955.) Characteristic features are described of dendritic plates of Ge and other crystals which have been prepared in the form of long thin lamellas.

537.311.33:546.289:621.314.632 157

Rectification Properties of Metal/Semiconductor Contacts—E. H. Borneman, R. F. Schwarz, and J. J. Stickler. (*J. appl. Phys.*, vol. 26, pp. 1021–1028; August, 1955.) Experiments were made using n and p type Ge specimens with various metals plated on. No correlation was found between the reverse saturation current densities and the work function of the metal. For the Ge-metal combinations giving the lowest saturation-current densities, calculations indicate that most of the current is carried by holes, the magnitude of this hole current depending primarily on the diode geometry. This is confirmed by the observed variation of the I/V characteristic with Ge resistivity in the case of Ge-In contacts, and by the temperature variation of the zero-voltage conductance. It is inferred that while it is easy to establish a high barrier to electrons flowing on Ge surfaces, no barrier to hole flow was established with any of the metals used. For a given metal there is an upper limit to the electron current, corresponding to the lowest Ge resistivity.

537.311.33:546.46-31 158

Electrical Conductivity induced in MgO Crystals by 1.3-MeV Electron Bombardment—M. A. Pomerantz, R. A. Shatas, and J. F. Marshall. (*Phys. Rev.*, vol. 99, pp. 489–490; July 15, 1955.)

537.311.33:546.561 159

Effect of Temperature of Oxidation on the Electrical Conductivity of the Cuprous/Oxide Copper System—M. Moldovanova. (*C.R. Acad. Sci. U.R.S.S.*, vol. 103, pp. 223–225; July 11, 1955. In Russian.) The effect of oxidation at temperatures between 980° and 1,040°C was investigated experimentally. Specimens oxidized at 1,000°C were found to have a minimum dissociation energy u, and a minimum value of constant A in the expression for specific conductivity $\sigma = A \exp(-u/kT)$. The conductivity passed through a minimum for oxidation temperatures between 1,000° and 1,020°C.

537.311.33:546.682.86 160

Electrical Properties of p-Type Indium Antimonide at Low Temperatures—H. Fritzsche and K. Lark-Horovitz. (*Phys. Rev.*, vol. 99, pp. 400–405; July 15, 1955.) Measurements over the temperature range 1.5°–370°K indicate anomalies similar to those observed in Ge by Hung and Gliessman (1696 of 1955) for the temperature variation of resistivity and Hall coefficient. The magnetoresistance changes sign from positive to negative as the crystals are cooled through a temperature somewhat lower than that of maximum Hall coefficient; no theory capable of explaining this negative magnetoresistance has yet been advanced.

537.311.33:546.682.86 161

Effect of Pressure on the Electrical Properties of Indium Antimonide—D. Long. (*Phys. Rev.*, vol. 99, pp. 388–390; July 15, 1955.) Resistivity and Hall-coefficient measurements were made at pressures up to 2,000 atm and temperatures of 0°, 24.3°, and 54.3°C, on a sample which was i type down to about 220°K and p type at lower temperatures. The results indicate that the energy gap increases by 14.2×10^{-6} ev/atm and the electron mobility decreases by 14 per cent for a pressure increase of 2,000 atm at room temperature.

537.311.33:546.682.86 162

Effect of Pressure on the Electrical Conductivity of InSb—R. W. Keyes. (*Phys. Rev.*, vol. 99, pp. 490–495; July 15, 1955.) Measurements have been made over the temperature range -78° to $+300$°C at pressures up to 12,000 kg/cm². The activation energy increases with pressure at a rate 15.5×10^{-6} ev/(kg/cm²). The electron mobility is approximately inversely proportional to the activation energy, and the hole mobility is independent of pressure. Conclusions are drawn regarding the energy-band structure.

537.311.33:546.682.86 163

Magnetic Susceptibility of Indium Antimonide—D. K. Stevens and J. H. Crawford, Jr. (*Phys. Rev.*, vol. 99, pp. 487–488; July, 1955.) Measurements of the susceptibility of n and p type samples over the temperature range 65°–650°K are reported. The value deduced for the energy gap at 0°K is 0.262 ev, with an effective electron mass of 0.028 m_0.

537.311.33:549.351.12 164

Electrical Characteristics of Chalcopyrite. The Effect of Surface Treatment on the Rectifying Properties of Crystals—B. I. Boltaks and N. N. Tarnovski. (*Zh. tekh. Fiz.*, vol. 25, pp. 402–409; March, 1955.) Experiments were con-

ducted over a wide range of temperatures to determine the electric and thermoelectric properties of natural and synthetic $CuFeS_2$. The temperature dependence of the electrical conductivity of these materials is of a more complex character than in ordinary impurity semiconductors. By etching the surface it is possible considerably to improve the rectifying properties of the crystals and in a number of cases to obtain static characteristics not inferior to those of Ge and Si detectors.

537.311.33:621.314.634 165

The Effectiveness of Cadmium Selenide Layers in Selenium Rectifiers—H. Strosche. (*Z. Phys.*, vol. 140, pp. 409–413; April 20, 1955.) To determine the lowest useful thickness for the intermediate CdSe layer formed in a Se rectifier with a counter electrode containing Cd, measurements were made of the voltage /current characteristics of samples with CdSe or Cd layers evaporated on to a Se-coated plate and with a Bi counter electrode. No deleterious effects were noticed until the layer thickness dropped below about 10^{-7} cm. If the coating is dense, a monomolecular thickness is sufficient to maintain the rectifying properties.

537.323 166

Thermoelectric Properties of Alloys of the Bismuth-Tellurium System—F. I. Vasenin. (*Zh. tekh. Fiz.*, vol. 25, pp. 397–401; March, 1955.) Application of powder-metallurgy pressing and sintering technique enabled much higher values of thermo-emf to be obtained than hitherto. It was established experimentally that the inversion of the sign of the thermo-emf in pressed and sintered alloys of the system occurs for compositions in close proximity (within 0.2 per cent to the compound Bi_2Te_3. It is shown that the theory of Telkes (*J. appl. Phys.*, vol. 18, pp. 1116–1127; 1947) that there exists a second compound in the system with negative thermo-emf, is erroneous.

537.533 167

Photoelectric Work Functions of the Borides of Lanthanum, Praseodymium, and Neodymium—R. W. Decker and D. W. Stebbins. (*J. appl. Phys.*, vol. 26, pp. 1004–1006; August, 1955.) Using the DuBridge method of determining the photoelectric threshold, the values 2.74 ev, 3.12 ev, and 4.57 ev were found for the work function of LaB_6, PrB_6, and NdB_6 respectively.

538.22:546.3-1-711-621-26 168

The Structure and Magnetic Properties of the Alloy Mn_3AlC—R. G. Butters and H. P. Myers. (*Phil. Mag.*, vol. 46, pp. 895–902; August, 1955.) In the as-cast state an alloy of composition close to Mn_3AlC is feebly magnetic at room temperature and the magnetic property is retained after homogenization at 1,000°C. The ordered structure is similar to that of Mn_3ZnC (2333 of 1955). The alloy Mn_3AlC is strongly magnetic at low temperatures; the variation of the paramagnetic susceptibility over the range 65°–800°C is different from that of a normal ferromagnetic material.

538.221 169

Domain Configurations and Crystallographic Orientation in Grain-Oriented Silicon Steel—W. S. Paxton and T. G. Nilan. (*J. appl. Phys.*, vol. 26, pp. 994–1000; August, 1955.) The domain structure was investigated by powder-pattern technique and the orientation of the individual domains was determined by the etch-pit optical-goniometer technique. The relations between the two sets of observations are discussed and some conclusions are drawn regarding the three-dimensional domain configuration.

538.221 170

Dependence of the Coercive Force on the Density of Some Iron Oxide Powders—A. H. Morrish and S. P. Yu. (*J. appl. Phys.*, vol. 26, pp. 1049–1055; August, 1955.) Fe_3O_4 and γ-Fe_2O_3 are investigated. Calculations are made of the critical size below which the particle comprises a single domain; the value is about 3μ for the major axis of a prolate spheroid of Fe_3O_4 with ratio of major to minor axis 10:1, and slightly greater for γ-Fe_2O_3. The observed variation of coercive force with size and shape of particles is consistent with the calculated value of critical size, but the absolute value of the coercive force of the single-domain particles is much smaller than predicted by theory.

538.221 171

Magnetic Transformation in MnBi—R. R. Heikes. (*Phys. Rev.*, vol. 99, pp. 446–447; July 15, 1955.) "Manganese bismuth loses its spontaneous magnetization very sharply at 633°K. At the same temperature drastic changes occur in the lattice constants. Previous workers have interpreted both these phenomena as arising from a ferromagnetic-antiferromagnetic transition. The present work indicates that the phase existing above 633°K is actually a ferromagnetic one with a Curie temperature of about 470°K."

538.221 172

Multiple Resonances in Cobalt Ferrite—P. E. Tannenwald. (*Phys. Rev.*, vol. 99, pp. 463–464; July 15, 1955.) "Double microwave resonances have been observed in cobalt ferrite when a magnetic field was applied in crystal directions near the hard axis. One resonance occurs before the magnetization vector is lined up with the external magnetic field and another occurs in the aligned state. The experimental results exhibit characteristic features expected before complete line-up and yield, at 90°C, $K_1/M = 2200 \pm 200$ and $g = 2.7 \pm 0.3$."

538.221 173

Electrical Conductivity and Seebeck Effect in $Ni_{0.80}Fe_{2.20}O_4$—F. J. Morin and T. H. Geballe. (*Phys. Rev.*, vol. 99, pp. 467–468; July 15, 1955.) Measurements over a temperature range from about 100° to 350°K indicate thermal hysteresis in the conductivity but not in the Seebeck-effect variation. This suggests that the hysteresis involves the charge-carrier transfer process but not the production of carriers. The activation energy associated with the transfer process is estimated to be 0.10 ev in the high-temperature state and 0.06 ev in the low-temperature state.

538.221 174

Electronic Energy Bands in Iron—J. Callaway. (*Phys. Rev.*, vol. 99, pp. 500–509; July 15, 1955.)

538.221 175

Ferromagnetism in Noble-Metal Alloys containing Manganese—F. A. Otter, Jr., P. J. Flanders, and E. Klokholm. (*Phys. Rev.*, vol. 99, pp. 599–600; July 15, 1955.)

538.221 176

A Study of Domain Structures in Alnico—L. F. Bates and D. H. Martin. (*Proc. phys. Soc.*, vol. 68, pp. 537–540; August 1, 1955.)

538.221 177

A Theory of the Uniaxial Ferromagnetic Anisotropy induced by Magnetic Annealing in Cubic Solid Solutions—S. Taniguchi. (*Sci. Rep. Res. Inst. Tohoku Univ., Ser. A*, vol. 7, pp. 269–281; June, 1955.) A theory is developed on the basis of van Vleck's model. The results obtained are similar to those of Néel (2983 of 1954).

538.221 178

Magnetic Behavior of Fe-Ni Compacts under Sintering Process—H. Kojima. (*Sci. Rep. Res. Inst. Tohoku Univ., Ser. A*, vol. 7, pp. 321–328; June, 1955.) The magnetic properties and density variations of specimens containing between 45 per cent and 85 per cent Ni were investigated as functions of the sintering temperature between 600° and 1100°C. Results are presented graphically.

538.221 179

Demonstration of Magnetization-Reversal Starting Centres in Iron-Nickel Wires under Tension, using the Bitter-Pattern Method—C. Greiner. (*Ann. Phys., Lpz.*, vol. 16, pp. 176–180; July 15, 1955.)

538.221:539.23 180

Energy of the Bloch Walls in Thin [spontaneously magnetized] Layers—L. Néel. (*C.R. Acad. Sci., Paris*, vol. 241, pp. 533–536; August 8, 1955.) It is shown that as the thickness of the layer is reduced the energy of the Bloch walls first increases, then passes through a maximum and regains its usual value when the layer becomes extremely thin.

538.221:539.234 181

Preparation of Thin Magnetic Films and their Properties—M. S. Blois, Jr. (*J. appl. Phys.*, vol. 26, pp. 975–980; August, 1955.) Evaporation technique is described for producing films of ferromagnetic material, particularly Ni-Fe alloys, with thicknesses from 1,000 Å to 100,000 Å and coercivities of 0.1–40 oersted. Magnetic orientation is used to produce a rectangular hysteresis loop. Questions of suitable substrate materials, evaporable dielectrics for use in insulating multilayer films, and control of alloy composition are discussed.

538.221:621.3.042.14 182

Compressional Stress on Magnetic Laminations—R. E. Fischell. (*Elect. Engng., N. Y.*, vol. 74, p. 585; July, 1955.) Digest of paper to be published in *Trans. Amer. Inst. elect. Engrs, Communication and Electronics*, 1955. Report of an experimental investigation of the effect of stress, such as that produced by clamping, on the magnetic properties of laminations of various materials.

538.221:621.318.134 183

Ferromagnetic Resonance of Gadolinium Ferrites as a Function of Temperature at 9,000 Mc/s—J. Paulevé. (*C.R. Acad. Sci., Paris*, vol. 241, pp. 548–550; August 8, 1955.) The value of the field strength H corresponding to resonance becomes very low in the neighborhood of 306°K, the compensation temperature. The results of measurements are consistent with the two-sublattice theory of rare-earth ferrites developed by Néel (3275 of 1954); the discontinuity in the value of H is due to reversal of the magnetization of one of the sublattices near the compensation point.

538.221:621.318.134 184

Dilatometer Thermal Analysis of Samarium Ferrite and Magnetic Transitions of Rare-Earth Ferrites—G. Guiot-Guillain and X. Waché. (*C.R. Acad. Sci., Paris*, vol. 241, pp. 550–552; August 8, 1955.)

538.221:621.318.134 185

Resonance Field Strength for a System of Magnetic Sublattices (Ferrimagnetic Resonance)—B. Dreyfus. (*C.R. Acad. Sci., Paris*, vol. 241, pp. 552–554; August 8, 1955.) Formulas are presented facilitating calculation of the resonance field strength for ferrites.

538.222/.224 186

Some Remarks on S. G. Salikhov's Work—N. N. Neprimerov. (*Zh. eksp. teor. Fiz.*, vol. 28, pp. 719–724; June, 1955.) Detailed critical discussion of recently published papers by Salikhov (*e.g.*, 1833 of 1954) on paramagnetic microwave resonance absorption in metals.

546.3-1-681 187

Composition of Binary and Multiple Compounds of [sub-group] B Metals: Part 1—System comprising Gallium with [sub-group]

B Metals—H. Spengler. (*Z. Metallkde*, vol. 46, pp. 464–467; June, 1955.)

546.3–1–682 188

Indium Alloys—S. Valentiner. (*Z. Metallkde*, vol. 46, pp. 442–449; June, 1955.) A comprehensive review of research on In alloys, having regard to the position of In in the periodic system. Over 86 references.

621.315.61 189

Breakdown of Solid Dielectrics in Divergent Fields—J. H. Mason. (*Proc. I.E.E.*, Part C, vol. 102, pp. 254–263; September, 1955. Digest, *ibid.*, Part B, vol. 102, pp. 725–727; September, 1955.) Experiments with electrode systems in which one electrode is a needle point embedded in polythene or polyisobutylene are reported. Dependence of breakdown stress on the polarity of the point is discussed in relation to the stress-enhanced conductivity and space-charge accumulation. The electric strength of various insulators under industrial conditions is discussed in relation to test data.

621.315.612 190

Structure in Vitreous Silicates as shown by Low-Angle Scattering of X-Rays—L. C. Hoffman and W. O. Statton. (*Nature, Lond.*, vol. 176, pp. 561–562; September 17, 1955.)

621.315.612.4 191

Solid-State Reactions and Dielectric Properties in the System Magnesia/Lime/Tin-Oxide/Titania—L. W. Coughanour, R. S. Roth, S. Marzullo, and F. E. Sennett. (*J. Res. nat. Bur. Stand.*, vol. 54, pp. 149–162; March, 1955.) A detailed study is reported of the solid-state reactions occurring among the oxide components in this system and of the effects of composition and temperature on the dielectric properties; the results are presented in numerous tables and graphs.

621.318.134.002.2 192

Magnetic Ceramics: Part 1—General Methods of Magnetic Ferrite Preparation—G. Economos. (*J. Amer. ceram. Soc.*, vol. 38, pp. 241–244; July 1, 1955.) Various methods with commercial possibilities are discussed.

666:621.791.3 193

Review of High-Temperature Metal-Ceramic Seals—H. Palmour, III. (*J. electrochem. Soc.*, vol. 102, pp. 160C–164C; July, 1955.) Emphasis is on electronic applications. Practical designs are illustrated and properties of several ceramics and glasses are listed.

MATHEMATICS

512.3 194

The Solution of the Cubic Equation—E. Astuni. (*Ricerca sci.*, vol. 25, pp. 2048–2068; July, 1955.) A method derived from the analysis for coupled circuits under transient conditions (3189 of 1955). Numerical examples are given.

517.512.2 195

Convergence and Summation of a Fourier Series corresponding to an Analytical Function—R. Cazenave. (*Ann. Télécommun.*, vol. 10, pp. 102–108; May, 1955.)

519.2 196

The Analysis of Non-Markovian Stochastic Processes by the Inclusion of Supplementary Variables—D. R. Cox. (*Proc. Camb. phil. Soc.*, vol., 51, Part 3, pp. 433–441; July, 1955.)

519.2 197

The Probability Distribution of the Amplitude of a Constant Vector plus a Rayleigh-Distributed Vector—K. A. Norton, L. E. Vogler, W. V. Mansfield, and P. J. Short. (PROC. IRE, vol. 43, pp. 1354–1361; October, 1955.) It is emphasized that both amplitude distribution and phase distribution are required to describe a Rayleigh-distributed vector. A summary is presented of physical conditions which must be satisfied for a given phenomenon to exhibit statistical properties of a Rayleigh-distributed vector. The application of the theory to various aspects of radio propagation is indicated.

517 198

Reihenentwicklungen in der mathematischen Physik [Book Review]—J. Lense. Publishers: de Gruyter, Berlin, 1953, 216 pp., D.M. 26. (*Proc. phys. Soc.*, vol. 68, pp. 764–765; August 1, 1955.) An account of the use of expansions in terms of orthogonal functions, and of related techniques.

517.564.3:518.2 199

Bessel Functions of Integer Orders and Large Arguments [Book Review]—L. Fox. Publishers: University Press, Cambridge, 1954, 28 pp., 6s.6d. (*Sci. Progr.*, vol. 43, p. 526; July, 1955.) Royal Society Shorter Mathematical Tables, No. 3. Auxiliary functions are given permitting computation of $J_n(x)$, $Y_n(x)$, $I_n(x)$, $K_n(x)$ for integral values of n from 0 to 20 and $x \geqq 20$, using in addition merely tables of trigonometric or exponential functions.

MEASUREMENTS AND TEST GEAR

531.761 200

New Definition of the Unit of Time and Frequency—L. Essen. (*Wireless Engr.*, vol. 32, p. 312; November, 1955.) At the 9th General Assembly of the International Astronomical Union, 1955, the second was defined as 1/31556925.975 of the tropical year for 1900. Some implications of this decision are briefly indicated.

621.317.3:537.311.33 201

Apparatus for measuring Resistivity and Hall Coefficient of Semiconductors—T. M. Dauphinee and E. Mooser. (*Rev. sci. Instrum.*, vol. 26, pp. 660–664; July, 1955.) Use of the isolating potential-comparator circuit [3064 of 1953 (Dauphinee)] secures the elimination of errors due to thermal emfs while permitting the use of dc measuring apparatus. Contact and lead resistances do not affect the results.

621.317.3:621.372.412 202

Spectrum Analyzer for Quartz Crystals—T. E. McDuffie. (*Electronics*, vol. 28, pp. 160–162; October, 1955.) The output from a frequency-sweep oscillator having a sweep range variable up to ±300 kc from a 20 mc mean frequency is mixed with a selected signal from a 20.5–40-mc oscillator. The crystal under test is included in an amplifier circuit fed by the difference-frequency signal, and the detected output is displayed on a cro.

621.317.32:621.314.63 203

Measurement of [voltage] Ratios using Dry Rectifiers as Voltage-Dependent Resistors—H. Matusche. (*Frequenz*, vol. 9, pp. 232–234; July, 1955.) Theory and experimental results are given for circuits based on a voltage divider comprising a linear resistor in series with the rectifier.

621.317.32:621.385.832 204

Method of measuring the Screen Potential of Cathode-Ray Tubes—J. R. Young. (*Rev. sci. Instrum.*, vol. 26, pp. 647–648; July, 1955.) The Kelvin vibrating-capacitor method is described. A small Al disk arranged parallel to the screen and earthed through a resistor is made to vibrate at mains frequency. When the screen and the disk are at different potentials ac flows in the resistor. In typical experiments the screen potential could be determined to within about 5v.

621.317.331 205

Residual Effects in the Campbell Bridge Method for the Absolute Measurement of Resistance, and a Note on a New Bridge—N. F. Astbury. (*Proc. I.E.E.*, Part C, vol. 102, pp. 279–283; September, 1955. Digest, *ibid.*, Part B, vol. 102, pp. 729–730; September, 1955.) Systematic errors associated with coil reversals are shown to be due to uncompensated eddy-current coupling between supply and detector meshes. In the proposed modified bridge this effect can be eliminated without external compensation if three mutual impedances, two of which are nearly equal, are determined instead of two.

621.317.332 206

Corrections for Line Losses in [microwave] Impedance Measurements—F. Mayer. (*Ann. Télécommun.*, vol. 10, pp. 109–111; May, 1955.) A formula is derived giving the true swr as a function of the measured swr and the attenuation constant of the line. A nomogram is hence developed, and its use is illustrated by examples.

621.317.335.029.6 207

Microwave Measurements on Low-Loss Dielectrics—D. Missio. (*Alta Frequenza*, vol. 24, pp. 219–237; June, 1955.) Report of measurements made on various dielectrics, at a frequency of about 3 kmc and normal temperature, using the method of standing-wave measurements in a short-circuited coaxial line. Various corrections are included in order to improve the accuracy of determination of losses. Results are tabulated and discussed.

621.317.335.029.6:537.226.2/.3 208

Determination of Dielectric Properties from the Brewster Angle of Incidence and the Restored Azimuth at Wavelengths below 3 cm—H. Rabenhorst. (*Ann. Phys., Lpz.*, vol. 16, pp. 163–175; July 15, 1955.) The refractive index and the absorption coefficient are determined from (*a*) the Brewster angle and (*b*) the ratio of intensities of the reflected-wave components parallel and perpendicular to the plane of incidence. The incident wave is plane polarized at 45° to the plane of incidence. From (*a*) and (*b*) the dielectric characteristics can be calculated using the Fresnel relations. Measurements were made at 2.52 cm λ on trolitul, glass, phenol, and calcium sulphate. The apparatus is described.

621.317.335.3:621.372.413:537.562 209

Resonant-Cavity Measurements of the Relative Permittivity of a D.C. Discharge—Foulds. (See 80.)

621.317.335.3.029.6 210

A Method for the Determination of the Dielectric Constant of Loss-Free Solid Bodies in Uniform Transmission Lines—H. Lueg and F. Gemmel. (*Arch. elekt. Übertragung*, vol. 9, pp., 307–310; July, 1955.) Measurements at dm λ and cm λ are considered. The test specimen is shaped so as accurately to fill the cross-section of a coaxial line or waveguide, the system then constituting a line-type transformer. The dielectric constant of the specimen is found from the ratio of the characteristic impedances of the line with and without the specimen, and this ratio is determined from the transformer characteristic without requiring precise knowledge of the position of the line short-circuit or of the specimen.

621.317.382:621.373.43 211

A Method for determining the Power of a Pulse Generator—G. F. Novozhenov. (*Radiotekhnika, Moscow*, vol. 10, pp. 33–40; March, 1955.) The peak power of a pulse generator can be calculated from the mean power measured by a wattmeter and the "energy coefficient" of pulses, which is the ratio of the actual pulse energy to the product of pulse period and peak power. This coefficient can be determined from observations of pulses on the screen of a cro. Since these are voltage rather than power pulses, it is necessary to introduce correction factors, and these are calculated for sinusoidal, bell-shaped, trapezoidal, and exponential-rise pulses. Curves of the correction factors are also given.

621.317.4 212
Measurement of the D.C. Magnetization Curve and of the Hysteresis Loop—H. Neumann. (*Arch. tech. Messen*, No. 232, pp. 105–108; May, 1955.) A brief survey of practical methods.

621.317.4 213
A New Astatic Magnetometer for Measurements on Ferromagnetic Sheet in Direct and Alternating Fields—K. Mellentin and H. Lange. (*Z. Metallkde*, vol. 46, pp. 450–456; June, 1955.) The main features of the instrument described are (*a*) use of only one magnetizing coil, and (*b*) the particular arrangement of the system in relation to the specimen. The shape of the latter is such that it becomes uniformly magnetized in a uniform field. Loss measurements can be made very rapidly.

621.317.733:621.372.542.2 214
A General-Purpose 50-c/s Null Indicator, particularly Suitable for Use with High-Voltage Bridges—W. P. Baker. (*J. sci. Instrum.*, vol. 32, pp. 268–269; July, 1955.) A tapered low-pass RC filter, in which every third passive resistance element is replaced by the anode impedance of an amplifying tube, forms the basis of an indicator having a sensitivity of 10–20 μv and a dynamic range of 80 db, with third-harmonic attenuation 130:1.

621.317.742:621.372.8 215
A Direct-Reading Waveguide Standing-Wave Detector for Use at Low Power Levels—H. V. Shurmer. (*Proc. I.E.E.*, Part C, vol. 102, pp. 176–180; September, 1955. Digest, *ibid.*, Part B, vol. 102, p. 563; July, 1955.) A directional coupler is used to measure reflected power from the load, which is a function of its vswr. Errors introduced by the coupler are compensated. The main application is to measurements on crystal rectifiers at 3.2 cm. λ, at power levels from 5 to 650 μw.

621.317.755 216
Electronically Controlled Electromagnetic Scanning System for High-Voltage Cathode-Ray Oscillograph—J. Lagasse and J. Clot. (*C.R. Acad. Sci., Paris.*, vol. 241, pp. 598–600; August 17, 1955.) The scanning system for a multibeam cro [1624 of 1954 (Fert et al.)] is discussed. The scanning current is obtained by discharging a capacitance through the scanning coil via a vacuum triode controlled by pulses applied to the grid. Synchronization of blanking and scanning is performed by means of an auxiliary thyratron which operates a delaying circuit on receipt of the primary triggering pulse. Photographic records can be obtained corresponding to a trace speed of 70 mm/μs.

621.317.755:621.396.41.029.62 217
An Instrument for the Measurement and Display of V.H.F. Network Characteristics—J. S. Whyte. (*P.O. elect. Engrs' J.*, vol. 48, Part 2, pp. 81–83; July, 1955.) Group-delay /frequency and gain/frequency characteristics are displayed on a cro. A discrimination of 10^{-9} sec is obtainable over a bandwidth of 20 mc centered on 60 mc. Gain/frequency characteristics can be measured with a discrimination of about 0.1 db.

621.317.76:621.395.625 218
Measurement of "Wow" and "Flutter"—Dzierzynski. (See 13.)

621.317.761.029.6 219
High-Precision [cavity-] Resonator Frequency Meter for Decimetre Wavelengths—H. Groll and G. Pusch. (*Fernmeldetech. Z.*, vol. 8, pp. 462–466; August, 1955.)

621.317.791 220
A Quasistatic Multipurpose Meter for Direct and Alternating Voltages—K. Müller-Lübeck. (*Arch. tech. Messen*, no. 232, pp. 113–116; May, 1955.) The universal instrument described, which also includes a facility for capacitance measurements between 50 pf and 20 μf, is based on a modified cathode-follower stage. Some of the characteristics of the instrument are presented graphically.

621.317.794:621.396.822 221
The Sensitivity of Radiometers—F. V. Bunkin and N. V. Karlov. (*Zh. tekh. Fiz.*, vol. 25, pp. 430–435; 733–741; March/April, 1955.) A precise definition of the sensitivity of a radiometer is given and the value is calculated for a compensation-type radiometer, taking into account the fluctuation of the amplification factor at high frequency. Similar calculations are carried out for a radiometer of the modulation type. In both cases particular attention is given to the effect of the width of the band received.

621.317.794:621.396.822 222
Null Method of Measuring Weak Electrical Fluctuations—V. S. Troitski. (*Zh. tekh. Fiz.*, vol. 25, pp. 478–496; March, 1955.) In this method the amplifier is used only as a null indicator, hence errors due to variations of the amplification factor are completely eliminated. The theory of the method is discussed in application to long and medium waves, and conditions of balance are established for both linear and quadratic detectors. The errors due to various characteristics of the circuit used, as well as to noise in the apparatus itself are discussed in detail.

621.373.1.029.42 223
A Sine-Wave Generator for Very Low Frequencies—W. A. Penton (*J. sci. Instrum.*, vol. 32, pp. 282–283; July, 1955.) Two probes rotating continuously in an electrolyte cell, across which there is a potential difference, generate a sinusoidal voltage with frequency range 0.1–2.0 c, and output level variable between 2.5 and 60 v peak to peak. The generator has been used in measurements on high-pass filters to cut off below 0.5 c.

OTHER APPLICATIONS OF RADIO AND ELECTRONICS

413:681.142 224
Use of a Computing Machine as a Mechanical Dictionary—Booth. (See 26.)

531.768:546.431.823–31 225
Some Developments in Vibration Measurement—S. Edelman, E. Jones, and E. R. Smith. (*J. acoust. Soc. Amer.*, vol. 27, pp. 728–734; July, 1955.) Two types of $BaTiO_3$ accelerometer and associated equipment and technique developed at the National Bureau of Standards are described.

534.6–8 226
Microacoustic Interferometer using 30-Mc/s Pulses—R. A. McConnell and W. F. Mruk. (*J. acoust. Soc. Amer.*, vol. 27, pp. 672–676; July, 1955.) An instrument for determining ultrasonic velocity and absorption in liquids uses ultrasonic pulses of duration about 10 μs and frequency 30 mc and detects the reflection from a layer of the test material whose thickness is varied to pass through a resonance condition.

621.3.078/.079:681.142 227
Industrial Uses of Special-Purpose Computers—Kuhnel. (See 27.)

621.317.39:531.71 228
Single-Tube Capacitance Transducer Circuit—L. Fleming. (*Electronics*, vol. 28, pp. 182, 190; October, 1955.) A capacitance probe with a resistor in series is connected across the tuned circuit of a rf oscillator to give a simple and stable transducer for measurement of mechanical displacements.

621.384.611 229
A Variable-Energy Cyclotron—D. E. Caro, L. H. Martin, and J. L. Rouse. (*Aust. J. Phys.*, vol. 8, pp. 306–309; June, 1955.) Brief description of a cyclotron designed to accelerate protons in the range 2–12.5 mev, deuterons in the range 4–6.3 mev, and α particles in the range 8–12.5 mev.

621.384.622.2 230
The Theory of Electron Beam Loading in Linear Accelerators—G. Saxon. (*Metrop. Vick. Gaz.*, vol. 26, pp. 219–225; July, 1955.) "An analysis is made of the waveguide circuit of a linear accelerator of electrons employing radio-frequency power feedback to show how the power flowing into such an accelerator varies with the beam loading."

PROPAGATION OF WAVES

538.566:551.510.535 231
Notes on the Propagation of Long-Wave Lightning Atmospherics around the Earth—H. G. Stäblein. (*Z. angew. Phys.*, vol. 7, pp. 290–291; June, 1955.) The discussion presented by Schumann (528 of 1955) is supplemented by an analysis of the propagation of a signal represented by exponential time functions.

538.566.029.43 232
The Influence of the Earth's Magnetic Field on the Propagation of Very Long Electrical Waves—W. O. Schumann. (*Z. angew. Phys.*, vol. 7, pp. 284–290; June, 1955.) Analysis is presented in which the ionosphere is regarded as an anisotropic poor conductor. Ordinary and extraordinary wave components penetrate the ionosphere traveling normal to the boundary, with resulting attenuation of and interference with the components traveling in the waveguide formed by the earth and the ionosphere. To satisfy the boundary conditions, both an E mode and an H mode must be propagated in the guide; an original E mode gives rise to an auxiliary H mode, and vice versa. The ratio of the horizontal components at the earth's surface of magnetic field strength perpendicular to and parallel to the propagation direction is a measure of the relative intensities of the E and H modes. A short account of the work is given in *Naturwissenschaften*, vol. 42, pp. 91–92; February, 1955.)

621.396.11 233
Radio Communication by Wave Scattering—R. L. Smith-Rose. (*Wireless Engr.*, vol. 32, pp. 287–290; November, 1955.) A brief survey of investigations carried out in America and in Europe; both tropospheric and ionospheric scattering are discussed. Experimental results indicate that over the frequency range from about 25 to 60 mc a signal steady enough for communication with a bandwidth of ≥ 3 kc, over distances up to about 1,200 miles, is propagated by scattering from the E layer.

621.396.11 234
Scatter Propagation—(PROC. IRE, vol. 43, pp. 1173–1526; October, 1955.) The main part of this issue is devoted to a group of papers together providing a comprehensive survey of the state of knowledge on scatter propagation, including both extended-range ionospheric and beyond-horizon tropospheric propagation. The ionospheric mode is of interest for frequencies from about 25 to 60 mc and path lengths of 600 to 1,200 miles; the tropospheric mode is of interest for frequencies from about 100 mc to at least 10 kmc and path lengths of 100 miles upwards. Abstracts of several of the papers are given individually; titles of the others are as follows:—

Characteristics of Beyond-the-Horizon Radio Transmission—K. Bullington. (pp. 1175–1180.)

Aerodynamical Mechanisms producing

Electronic-Density Fluctuations in Turbulent Ionized Layers—R. M. Gallet. (pp. 1240–1252.)

Some Remarks on Scattering from Eddies—R. A. Silverman. (pp. 1253–1254.)

Factors affecting Spacing of Radio Terminals in a U.H.F. Link—I. H. Gerks. (pp. 1290–1297.)

Demonstration of Bandwidth Capabilities of Beyond-Horizon Tropospheric Radio Propagation—W. H. Tidd. (pp. 1297–1299.)

Results of Propagation Test at 505 Mc/s and 4090 Mc/s on Beyond-Horizon Paths—K. Bullington, W. J. Inkster, and A. L. Durkee. (pp. 1306–1316.)

Some Tropospheric Scatter-Propagation Measurements near the Radio Horizon—H. B. Janes and P. I. Wells. (pp. 1336–1340.)

The Probability Distribution of the Amplitude of a Constant Vector plus a Rayleigh-Distributed Vector—K. A. Norton, L. E. Vogler, W. V. Mansfield, and P. J. Short. (pp. 1354–1361.) (See 194.)

Trans-horizon Microwave Propagation over Hilly Terrain—Y. Kurihara. (pp. 1362–1368.)

Tropospheric Overwater Measurements far beyond the Radio Horizon—L. A. Ames, P. Newman, and T. F. Rogers. (pp. 1369–1373.)

Note on Scatter Propagation with a Modified Exponential Correlation—A. D. Wheelon. (pp. 1381–1383.)

Measurements of the Phase of Radio Waves received over Transmission Paths with Paths with Electrical Lengths varying as a result of Atmospheric Turbulence—J.W. Herbstreit and M. C. Thompson. (pp. 1391–1401.)

Phase-Difference Variations in 9350-Mc/s Radio Signals arriving at Spaced Antennas—A. P. Deam and B. M. Fannin. (pp. 1402–1404.)

Some Fading Characteristics of Regular V.H.F. Ionospheric Propagation—G. R. Sugar. (pp. 1432–1436.)

Line-of-Sight Propagation Phenomena: Part 1—Ray Treatment—R. B. Muchmore and A. D. Wheelon. (pp. 1437–1449.)

Line-of-Sight Propagation Phenomena: Part 2—Scattered Components—A. D. Wheelon and R. B. Muchmore. (pp. 1450–1458.)

Near-Field Corrections to Line-of-Sight Propagation—A. D. Wheelon. (pp. 1459–1466.)

Certain Mode Solutions of Forward Scattering by Meteor Trails—G. H. Keitel. (pp. 1481–1487.)

621.396.11 235

Radio Propagation Prediction considering Scattering Wave on the Earth's Surface—K. Miya and S. Kanaya. (*Rep. Ionosphere Res. Japan*, vol. 9, No. 1, pp. 1–15; March, 1955.) MUF predictions for multi hop communication circuits can take into account scattered reflections at the earth's surface by use of a new "control-line" method, in which the distance of the control points of the older method is taken as the radius of arcs round transmitter and receiver forming the control lines, the mufs being then determined in the normal way. By including propagation paths other than great circles mufs may be increased. A comparison of predictions with experience on several commercial circuits confirms the greater efficiency of the new method and shows that land scatter is of chief importance at frequencies below 20 mc, while sea scatter should also be considered in the range 20–30 mc.

621.396.11:523.5 236

The Role of Meteors in Extended-Range V.H.F. Propagation—O. G. Villard, Jr., V. R. Eshleman, L. A. Manning, and A. M. Peterson. (Proc. IRE, vol. 43, pp. 1473–1481; October, 1955.) The main factors influencing the propagation of continuous radio signals by reflection from meteor ionization trails are reviewed. A method is indicated for calculating the required values of system parameters to maintain the received field strength above the background-noise level for 95 per cent of the time. Measurement results indicate that in some cases forward-scatter propagation in the ionosphere is predominantly governed by meteor ionization; in these cases the performance of existing communication circuits could be improved by appropriate redesign of antennas.

621.396.11:551.510.52 237

Characteristics of Tropospheric Scattered Fields—L. G. Trolese. (Proc. IRE, vol. 43, pp. 1300–1305; October, 1955. Trans. IRE, vol. AP-3, pp. 117–122; July, 1955.) Measurements made on cm-λ signals transmitted over a 46.3-mile path are compared with values calculated from the theory of Booker and Gordon (1757 of 1950). Tests with a narrow-beam antenna indicate that the scattered field on reception is spread over an angle five to seven times as large as indicated by the theory, assuming that the scale of tropospheric turbulence is large compared to λ. Fading observations support the view that the phenomenon is due to beating between scattered components whose frequencies differ owing to motion of the scatterers.

621.396.11:551.510.52 238

Investigations of Angular Scattering and Multipath Properties of Tropospheric Propagation of Short Radio Waves beyond the Horizon—J. H. Chisholm, P. A. Portmann, J. T. deBettencourt, and J. F. Roche. (Proc. IRE, vol. 43, pp. 1317–1335; October, 1955.) Report of experiments carried out in the N.E. coastal region of the U.S.A., over paths of lengths 161–188 miles, to determine the possibilities of establishing communication circuits at uhf and microwave frequencies. The results indicate that reliable communication with bandwidths of the order of thousands of mc can be established if power of the order of several kilowatts is used together with highly directional antennas; the tropospheric scattering mechanism is directive and multipath delays are less serious than indicated by previous investigations.

621.396.11:551.510.52 239

Forward Scattering of Radio Waves by Anisotropic Turbulence—H. Staras. (Proc. IRE, vol. 43, pp. 1374–1380; October, 1955.) Theory of tropospheric scattering is extended to derive propagation formulas for the case where the scale of turbulence is different in the horizontal and vertical directions. The frequency dependence of the scattered radiation is the same for anisotropic large-scale turbulence as for isotropic. Those radio-system parameters which depend only on the rate of decrease of scattered energy with elevation angle (*e.g.*, vertical correlation function and height gain) are not affected by the anisotropy, while those which depend on the departure from the great-circle plane (*e.g.*, horizontal correlation function) may be substantially affected. The effect on longitudinal correlation function, bandwidth, and effective aerial gain is also discussed.

621.396.11:551.510.52 240

Propagation of Short Radio Waves in a Normally Stratified Troposphere—T. J. Carroll and R. M. Ring. (Proc. IRE, vol. 43, pp. 1384–1390; October, 1955.) An explanation of the main features of beyond-horizon propagation is presented on the basis of careful calculations assuming absence of turbulence in the troposphere. Internal reflection effects associated with coherent molecular scattering in the atmosphere must be taken into account.

621.396.11:551.510.52 241

Some Applications of the Monthly Median Refractivity Gradient in Tropospheric Propagation—B. R. Bean and F. M. Meaney. (Proc. IRE, vol. 43, pp. 1419–1431; October, 1955.) Results of an extensive program of transmission-loss measurements at 100 mc in the U.S.A. are found to indicate consistent correlation with ΔN, the difference between the atmospheric refractive index at the earth's surface and that at a height of 1 km at the midpoint of the propagation path. Six-year average values of ΔN are presented as an aid in predicting annual transmission-loss variations. The observed dependence of transmission loss on ΔN is much greater than indicated by standard propagation theory.

621.396.11:551.510.52 242

The Use of Angular Distance in estimating Transmission Loss and Fading Range for Propagation through a Turbulent Atmosphere over Irregular Terrain—K. A. Norton, P. L. Rice, and L. E. Vogler. (Proc. IRE, vol. 43, pp. 1488–1526; October, 1955.) A comprehensive investigation of beyond-horizon tropospheric propagation; theoretical formulas are developed on the assumption that the energy may be propagated by diffraction or by forward scattering. The formulas involve the "angular distance," defined as the angle in the great-circle plane between the radio-horizon rays from transmitting and receiving aerials. For fixed linear and angular distances the nature of the terrain has a much larger influence on the diffracted-mode intensity than on the scattered-mode intensity. Comparison of calculated and observed values of transmission loss over 122 paths at frequencies between 66 mc and 1.046 kmc provides strong evidence in favor of the Weisskopf-Villars theory of tropospheric forward scatter. Theoretical curves of the average value of the path antenna gain to be expected in tropospheric forward-scatter propagation are presented as a function of the angular distance, the asymmetry factor and the free-space gains of the transmitting and receiving antennas.

621.396.11:551.510.535 243

Radio Transmission at V.H.F. by Scattering and Other Processes in the Lower Ionosphere—D. K. Bailey, R. Bateman, and R. C. Kirby. (Proc. IRE, vol. 43, pp. 1181–1231; October, 1955.) The results of a comprehensive investigation extending over four and a half years are presented; the transmissions used were mainly cw Solar wave radiation, corpuscular radiation of presumably solar origin, and meteors are recognized as ionizing agents producing different effects on propagation. The dependence of the received signal strength on time of day, season, solar activity, path details, frequency, and scatter angle was studied. The height at which the scattering occurred was determined by a pulse method. The results do not fit existing propagation theories entirely satisfactorily. The significance of the antenna patterns for the results is examined. The possibilities of this type of propagation for communication over distances from about 1,000 to 2,300 km are discussed. Notes are appended by two of the authors and by the editor regretting that certain material has been eliminated from the paper on government instructions.

621.396.11:551.510.535 244

On the Scattering of Radio Waves by Turbulent Fluctuations of the Atmosphere—F. Villars and V. F. Weisskopf. (Proc. IRE, vol. 43, pp. 1232–1239; October, 1955.) A theoretical analysis is presented of the mechanism by which vhf signals are transmitted over distances of the order of 10^3 km. It is found that turbulent mixing at the lower edge of the E layer produces fluctuations of electron density large enough to account for the observed signals. The basic assumptions are the existence of an electron-density gradient $>10^3/\text{cm}^3$ per km and a reasonable level of turbulent activity. Errors in previous work (2747 of 1954) are indicated.

621.396.11:551.510.535 245

Investigations of Scattering and Multipath Properties of Ionospheric Propagation at Radio Frequencies Exceeding the M.U.F.—W. G. Abel, J. T. deBettencourt, J. H. Chisholm, and J. F. Roche. (PROC. IRE, vol. 43, pp. 1255–1268; October, 1955.) Data obtained from measurements covering about 13,000 *h* are analyzed. Paths used were mostly about 1,000 miles long and situated in medium latitudes. The main frequency used was 49.6 mc, but some measurements were also made on 27.8, 22.9, and 21.6 mc. Short-period fading on 49.6 mc exhibited Rayleigh distribution, long-period fading was essentially Gaussian. The median received signal levels were of the order of 100 db below free-space values and were higher in winter and summer than in spring and autumn; there was some indication of correlation with sunspot activity and of dependence on direction of polarization. Effective scattering heights of 84–94 km were found in December, 1954, using a pulse method. Comparison of 49.6 mc and 27.8 mc signals indicates that received power probably varies as the inverse third or fourth power of frequency.

621.396.11.029.4/.51:551.510.535:621.372.8 246

The Radial Propagation of Electromagnetic Waves between Two [parallel] Conducting Planes (Radial Waveguide)—Kaden. (See 22.)

621.396.11.029.62 247

Abnormal Radio Propagation December 3, 1954—R. F. Jones. (*Met. Mag., Lond.*, vol. 84, pp. 225–226; July, 1955.) Abnormally strong signals on 180.4 mc were received at Beddingham, near Lewes, from the B.B.C. station at Sutton Coldfield, distance 147 miles, on the evening of December 3, 1955. Meteorological records for this period indicate the presence of extraordinarily dry air at levels as low as 2,200 feet, together with a temperature inversion.

621.396.11.029.63 248

Transmission Tests at 530 Mc/s to Distances beyond Optical Range—E. Prokott. (*Fernmeldetech. Z.*, vol. 8, pp. 430–437; August, 1955.) Tests were carried out over two transmission paths of nearly 200 km in order to determine the practical requirements for satisfactory communication. A 50 w transmitter was used with an antenna system comprising dipole array and reflectors. The effect of meteorological conditions at the horizon point is noted. The value of radio-path attenuation corresponding to the value of receiver input voltage attained or exceeded during 50 per cent of the test time is estimated as 162 db. This value is compared with previous results based partly on theory and partly on observations. The results show that optical visibility and freedom from obstructions in the first Fresnel zone are not absolutely essential though reliable operation would be difficult at grazing incidence.

621.396.81 249

Long-Period Fading in Medium-Wave Radio Signals—M. S. Rao and B. R. Rao. (*Nature, Lond.*, vol. 176, pp. 459–460; September, 3, 1955.) Fading of 1.42 mc signals observed over the 600 km path between Madras and Waltair during May, 1954, between 0700 and 0800 hours I.S.T., is illustrated by a typical record. The average period of the variations is about 7 minutes; calculations give a value in good agreement with this.

621.396.812.3:551.510.52 250

The Rate of Fading in Propagation through a Turbulent Atmosphere—K. A. Norton, P. L. Rice, H. B. James, and A. P. Barsis. (PROC. IRE, vol. 43, pp. 1341–1353; October, 1955.) Fading rate is defined as the number of times per minute that the envelope of the received field strength crosses its median level with a positive slope. The value thus obtained is numerically related to the relevant parameters of the propagation medium under conditions generally satisfied in ionospheric and tropospheric propagation; for beyond-horizon propagation these parameters are the location and shape of the scattering volume and the turbulent and drift velocities of the scatterers. Fading-rate data obtained with 92 mc and 1.046 kmc signals over transmission paths of lengths 70 to 394 miles are analyzed. Fading over within-sight paths is also discussed. See also 2399 of 1955 (Barsis et al.).

RECEPTION

621.376.23:621.396.822 251

Signal/Noise Performance of Multiplier (or Correlation) and Addition (or Integrating) Types of Detector—D. G. Tucker. (*Proc. I.E.E.*, Part C, vol. 102, pp. 181–190; September, 1955. Digest, *ibid.*, Part B, vol. 102, pp. 558–563; July, 1955.) Discussion is mainly directed to narrow-band pulse systems in which post-detection integration plays little part. The analysis indicates that pulse-to-pulse multiplication is not in general more effective than adding; the slight advantage afforded by the square-law response can be obtained more simply by using square-law rectifiers. When the multiplication is performed before rectification the output contains no direct component in the absence of correlated signals; this is an important advantage when the noise background is varying. Numerical results obtained by various alternative addition and multiplication techniques are tabulated for values of input signal/noise ratio from 0.1 to 4.

621.376.333:621.396.62 252

The Ratio Detector—K. R. Sturley. (*Wireless World*, vol. 61, pp. 532–537; November, 1955.) The working of the ratio detector in fm receivers is simply explained.

621.396.62:621.396.3:621.376.3 253

Automatic Frequency Control in Frequency-Shift Radiotelegraphy—G. Bronzi. (*Alta Frequenza*, vol. 24, pp. 284–287; June, 1955.) A theoretical discussion indicates that receivers for frequency-shift radiotelegraphy should be provided with afc of the second local oscillator, in order to keep the required bandwidth low.

621.396.62:621.396.812.3 254

Diversity Reception in U.H.F. Long-Range Communications—C. L. Mack. (PROC. IRE, vol. 43, pp. 1281–1289; October, 1955.) "Several diversity techniques employed in uhf beyond-the-horizon systems are discussed. Field experience is evaluated in terms of equipment reliability, flexibility, and performance. A nonswitching parallel combiner has become the standard military diversity circuit for uhf long-range receivers. The circuit is described and analyzed."

621.396.822:621.317.794 255

The Sensitivity of Radiometers—Bunkin and Karlov. (See 2211.)

621.396.822:621.317.794 256

Null Method of measuring Weak Electrical Fluctuations—Troitski. (See 222.)

STATIONS AND COMMUNICATION SYSTEMS

621.376.2+621.376.4 257

Quadrature Amplitude-Phase Modulation—E. M. Vereshchagin. (*Radiotekhnika, Moscow*, vol. 10, pp. 72–77; March, 1955.) The energy of sidebands can be increased and the width of the radiated spectrum halved by using the proposed method, in which the carrier is simultaneously subjected to am and phm. To do this it is necessary to displace the sidebands so obtained by 90°. Two circuits satisfying the required conditions are considered and the theory of the method is discussed under the following headings: (*a*) frequency spectrum of modulation; (*b*) estimated distortion; (*c*) energy relations; and (*d*) effects of interference. Experiments with both circuits gave satisfactory results and confirmed the validity of the theory.

621.376.56:621.39 258

Methods of reducing the Effects of Noise and increasing Channel Capacity with Pulse-Code Modulation—F. Benz. (*Arch. elekt. Übertragung*, vol. 9, pp. 299–306, 381–387; July/August, 1955.) Noise entering the rf part of the system is considered, its effect is reduced in a pulse system because the pulses occupy only a fraction of the total time. The ratio of theoretical channel capacity C_{th} to actual capacity C is a measure of the noise reduction attained. This ratio can be improved by using the bandwidth-economy system previously described (3415 of 1953) in which am is combined with a type of phase modulation termed "transverse" modulation. Theory based on that of Shannon (1649 of 1949) is used to determine the probability of confusion between the partial signals and hence to determine that arrangement of individual signals which makes C as nearly as possible equal to C_{th}. Practical circuits for this purpose are described briefly.

621.39.001.11 259

On the Limiting Transmission Capacity of a Communication System—A. A. Kharevkich and E. L. Blokh. (*Radiotekhnika, Moscow*, vol. 10, pp. 14–20; February, 1955.) Shannon's geometrical proof of his well known expression (1) determining the transmission capacity of a communication system (1649 of 1949) is criticized, and a more rigorous proof is developed. The results obtained indicate that expression (1) is valid only at the limit when signal/noise ratio becomes infinite.

621.39.001.11:061.3 260

Information Theory—(*Wireless World*, vol. 61, pp. 545–546; November, 1955.) A review of papers presented at the conference held at the Royal Institution, London, in 1955.

621.39.001.11:621.376.5 261

Electrical Pulse Communication Systems: Part 1—Information Theory and Pulse System—R. Filipowsky. (*J. Brit. I.R.E.*, vol. 15, pp. 451–467; September, 1955.) A survey including an account of the historical development of pulse systems and information theory. The four main classes of system distinguished are communication, data transmission, location, and computers. The main features of a system are source, message encoding, signal formation, multiplexing (train formation), wave formation (carrier modulation), transmission over the medium, reception, decoding, destination; individual steps may be omitted in particular systems. The various steps are described.

621.395.44+621.397.242+621.315.212 262

The Position of the Italian Coaxial Network at 31st December 1953—L. Niccolai. (*Elettrotecnica*, vol. 41, pp. 242–250; May, 1954.) The network provides 960 telephone channels in a 4 mc band, together with a television channel a little over 6 mc wide. The average spacing of repeaters is 9.3 km. The cables and repeater characteristics are described.

621.396.41:551.510.52 263

U.H.F. Long-Range Communication Systems—G. L. Mellen, W. E. Morrow, A. J. Poté, W. H. Radford, and J. B. Wiesner. (PROC. IRE, vol. 43, pp. 1269–1281; October, 1955.) Aspects of scatter propagation relevant to the design of multichannel systems operating over distances of 200 miles or more beyond the horizon are considered. Details of antenna systems, modulation techniques, and fm transmitting and receiving equipment are dis-

cussed. Space-diversity reception is used to overcome fading. System reliability is defined and its value is calculated for a particular system.

621.396.41:621.376.3 264
Multiplexing F.M. Broadcast Transmitters—J. H. Bose. (*Electronics*, vol. 28, pp. 146–150; October, 1955.) The problems of background noise in auxiliary fm subcarrier channels and cross modulation in the multiplier stages of the transmitter have been solved by narrowing the bandwidth of the early multiplication stages of the main channel and by introducing the auxiliary modulation at a late stage. Field tests have proved that the main fm carrier can be modulated to a depth of ±20 kc with a 30-kc fm subcarrier without affecting quality. See also 849 of 1954 (Armstrong and Bose).

621.396.41:621.396.65 265
Beyond-Horizon Signals Extend Communications—J. R. Day. (*Electronics*, vol. 28, pp. 122–127; October, 1955.) Klystrons giving a power output of 10 kw and antenna systems giving gains of 40 db over a single dipole, together with diversity reception, make possible uhf multiplex communication circuits with repeater spacings of 175 miles; propagation is by tropospheric forward scatter.

621.396.97:621.315.2:621.396.8 266
The Influence of Delay Distortion and Frequency-Band Limitation on the Quality of Broadcast Transmissions—E. Belger, E. A. Pavel, and H. Rindfleisch. (*Fernmeldetech. Z.*, vol. 8, pp. 445–455; August, 1955.) Report of tests carried out in 1950 and 1951 on the Federal German broadcasting line network. Subjective tests indicate that the tolerable delay in the transmission lines is about 8 ms at the top of the af band, 24 ms at 100 c and 120 ms at 50 c. The transmission band should go up to at least 10 kc, and about 12 kc for high-quality transmissions. See also 3709 of 1954 (Belger).

SUBSIDIARY APPARATUS

621–526:621.3.015.7 267
The Pulse Transfer Function and its Application to Sampling Servo Systems—R. H. Barker. (*Proc. I.E.E.*, Part C, vol. 102, pp. 291–292; September, 1955.) Addendum to 1131 of 1953.

621–526:621.373.421 268
The Frequency-Response Analysis of Non-linear Systems—Grensted. (See 56.)

621–526:621.396.96 269
The Stability and Time Response of Fast-Operating Closed-Loop Pulsed Radar Circuits—D. McDonnell and W. R. Perkins. (*Proc. I.E.E.*, Part C, vol. 102, pp. 191–202; September, 1955. Digest, *ibid.*, Part B, vol. 102, pp. 567–568; July, 1955.) "The paper deals with the stability and time responses of a sampling servo-system typical of agc, afc, range-measuring and overall-feedback circuits used in pulsed radar equipments in which the loop-response time is not many times greater than the pulse-repetition time. The case of a high-speed radar-controlled missile may be such a system. Conditions under which Nyquist plots can be made are given. Expressions for the output both at and between the sampling times are obtained in terms of the input functions of the system. The operation of the systems in the presence of noise is considered in the Appendix. A short list of transformations suitable for analysis is included."

621.314.632.1 270
The Temperature Dependence of the Capacity of the Copper-Oxide Rectifier—T. Niimi. (*J. phys. Soc. Japan*, vol. 10, pp. 444–453; June, 1955.) The variation of the capacitance at the metal/semiconductor boundary is calculated on the assumption that it is caused by the temperature variation of the free-charge-carrier concentration in the semiconductor. The calculated results are compared with experimental results for the temperature range from −160°C to +60°C.

621.314.634 271
Properties of Selenium Rectifiers with Various Impurities—F. Eckart and A. Schmidt. (*Ann. Phys., Lpz.*, vol. 16, pp. 134–152; July 15, 1955.) Se rectifiers were prepared with halogen and halogen-compound impurities and their characteristics were investigated. The effect of fluorine and fluorine compounds on the conductivity was nil, that of alkali halides small and that of bromine pronounced. Thallium bromide, copper bromide, tellurium, and arsenic have a deleterious effect on the rectifier properties. Results also show that useful rectifiers can be made using very pure Se.

621.314.653:537.311.33 272
Semiconducting Ignitors for Ignitron Rectifiers—V. V. Pasynkov. (*Zh. tekh. Fiz.*, vol. 25, pp. 377–396; March, 1955.) A detailed report on an experimental investigation is presented, as a result of which methods are proposed for the design and manufacture of ignitors based on silicon carbide.

621.316.722.1 273
On the Design of Rectifiers with Electron Stabilization—G. I. Levitan. (*Radiotekhnika, Moscow*, vol. 10, pp. 40–49; February, 1955.) The design of a stabilized rectifier should be divided into two stages: (*a*) calculation of the limits of stability, *i.e.*, of the limiting values of the mains voltage and load current for normal operation of the rectifier, and (*b*) determination of the coefficient of stability. Suitable methods for dealing with stage (*a*) are proposed. Details of the calculation are set out, and the case of the regulating tube with a shunt is discussed separately.

TELEVISION AND PHOTOTELEGRAPHY

621.397.2:621.397.8 274
The European Television Transmission Network and "Eurovision 1954"—F. Kirschstein and H. Bodeker. (*Fernmeldetech. Z.*, vol. 8, pp. 419–425; August, 1955.) Details are given of the network and its operation. The observed transmission faults are described and illustrated by means of oscillograms and photographs. An indication is given of improvement work in hand.

621.397.24:621.372.552:621.375.2 275
A Balanced Equalizer-Amplifier for transmitting Video Signals over Telephone Lines—J. B. Sewter and D. Wray. (*Electronic Engng.*, vol. 27, pp. 422–429; October, 1955.) The response of ordinary balanced telephone lines is equalized by controlling the common cathode feedback network of balanced tube pairs. One equalizer unit gives up to 70 db lift at 3 mc. Five corrected telephone links have been connected in tandem to give a video-signal line about 8 miles long.

621.397.242+621.395.44+621.315.212 276
The Poisition of the Italian Coaxial Network at 31st December 1953—Niccolai. (See 262.)

621.397.5 277
Scientific and Technical Conference on Television Broadcasting—(*Radiotekhnika, Moscow*, vol. 10, pp. 75–77; February, 1955.) Brief report on a conference held in Leningrad in December, 1954. Twenty-six papers were read dealing with the operation of television centers of the country, color television, transmitting and receiving tubes, commercial applications of television, long-range reception, etc.

621.397.5 278
2½ Years of German Television—W. Nestel. (*Fernmeldetech. Z.*, vol. 8, pp. 414–418; August, 1955.) An illustrated review.

621.397.61:621.372.55 279
Differentiating Equalizer for Television Studio Equipment—A. Krolzig. (*Fernmeldetech. Z.*, vol. 8, pp. 426–429; August, 1955.) Advantages and limitations of equipment based on principles described by Gouriet (1936 of 1953) are discussed. Cases of successful use in film transmissions are instanced.

621.397.611.2 280
Basic Problems in Film Pickup for TV Broadcasting—E. M. Gore. (*Elect. Engng., N. Y.*, vol. 74, pp. 600–604; July, 1955.) Includes a description of a commercially available system for color films using three vidicon tubes.

621.397.62 281
New Vision A.G.C. System—S. E. Gent and D. J. S. Westwood. (*Wireless World*, vol. 61, pp. 542–544; November, 1955.) A gated agc system for television receivers is described in which the gating pulse is obtained by differentiating the line synchronizing pulse and using the positive half of the resultant waveform.

621.397.62:621.373.43 282
A Self-Oscillating Line Timebase Circuit—A. Boekhorst. (*Philips tech. Commun., Aust.*, No. 2, pp. 12–18; 1955. *Electronic Applic. Bull.*, vol. 15, pp. 69–75; June, 1954.) A simple circuit for television receivers uses a single Type-PL81 pentode, with a feedback coil in its control-grid circuit, operating simultaneously as saw-tooth generator and output tube. The synchronization is highly insensitive to noise on the synchronizing signal.

621.397.7 283
The Synchronization and Delay Correction of Scattered Television Picture Sources—A. B. Shone. (*Electronic Engng.*, vol. 27, pp. 454–457; October, 1955.) The system used in B.B.C. outside broadcasts is described. All synchronizing-signal generators are synchronized to a common tone distributed over telephone circuits. A phase-shifting goniometer in the feed to each generator is used to ensure that the pictures associated with the different generators reach the central switching point in correct relation.

621.397.7 284
Operating Experiences at the Lime Grove Television Studios of the British Broadcasting Corporation, London—D. C. Birkinshaw. (*Arch. elekt. Übertragung*, vol. 9, pp. 311–325; July, 1955.) See 1504 of 1955.

621.397.7:621.396.11 285
Television Coverage of Great Britain—R. A. Rowden. (*J. Telev. Soc.*, vol. 7, pp. 457–461, 464–476; July/September, 1955.) Standards of field strength necessary for satisfactory reception are indicated; properties of the transmitter and of the propagation path affecting coverage are considered. A full account is given of the distribution of field strength in the British television service as at February, 1955; planned and possible developments are discussed.

TRANSMISSION

621.376.32:621.396.41.029.6 286
A Frequency Modulator for Broad-Band Radio Relay Systems—I. A. Ravenscroft and R. W. White. (*P.O. elect. Engrs' J.*, vol. 48, Part 2, pp. 108–109; July, 1955.) An if modulator based on the ladder-network type of *RC* phase-shift oscillator is described, in which the dynamic input resistances of two grounded-grid tubes serve as variable resistance elements. The performance is adequate for monochrome

television transmission, or for 240-channel telephony signals.

621.376.4 287

A New Method of Phase Modulation—A. D. Artym. (*Radiotekhnika, Moscow*, vol. 10, pp. 53–60; January, 1955.) A method is proposed in which nonlinear modulation of three hf voltage vectors is transformed into phase modulation. The theory of the method is discussed and a circuit is described providing phase deviations up to $\pm 300°$; for deviations up to 45° the coefficient of nonlinear distortion does not exceed 0.4 per cent. The parasitic anode modulation is of the order of 2 per cent.

621.396.61:621.372.542.2 288

A Ten-Kilowatt Low-Pass Filter—Broad and May. (See 47.)

TUBES AND THERMIONICS

537.5:538.56 289

Plasma Oscillations in Electron Beams—K. G. Hernqvist. (*J. appl. Phys.*, vol. 26, pp. 1029–1030; August, 1955.) "Self-sustained ion and electron plasma oscillations have been observed simultaneously in an ion neutralized electron beam traveling in a transverse magnetic field. The observed frequencies of oscillation agree with the Langmuir-Tonks theory for plasma oscillations. Electron plasma oscillations occur when the electron plasma frequency equals the gyro frequency of a circular orbit in the magnetic field."

621.314.63:621.383.5:621.396.822 290

Low-Frequency Noise in Illuminated Germanium Diodes—R. E. Burgess. (*Proc. phys. Soc.*, vol. 68, pp. 569–571; August 1, 1955.) It is shown theoretically that the current increase in a Ge diode under a given reverse bias when illuminated is independent of the bias voltage and is accompanied by an addition of shot noise which is negligibly small at low frequencies. The comparison of shot-noise behavior between a dark and an illuminated diode at a given reverse current is inappropriate.

621.314.632:546.289 291

Forward Characteristic of Germanium Point Contact Rectifiers—M. Cutler. (*J. appl. Phys.*, vol. 26, pp. 949–954; August, 1955.) The problem is treated by combining the flow equations for the barrier region, derived from emission theory (771 of 1955), with the corresponding equations ("spreading" or "diffusion" equations) for the flow of carriers in the region beyond the barrier. Numerical solutions are obtained for typical values of the contact parameters. Swanson's assumption (2536 of 1954), that the flow of holes in the barrier region is controlled by diffusion, is discarded; in consequence, the value found for γ at large currents is smaller, the hole concentration at the contact approaches a maximum value proportional to the equilibrium concentration of holes at the surface, and the spreading voltage becomes a linear function of the current.

621.314.632:546.289:537.312.6 292

Thermal Effects in Point-Contact Rectifiers—R. E. Burgess. (*J. appl. Phys.*, vol. 26, p. 1058; August, 1955.) Critical comment on notes by Armstrong (1242 of 1954 and 881 of 1955). See also 1948 of 1954 (Armstrong).

621.314.7 293

Alloyed-Junction Avalanche Transistors—S. L. Miller and J. J. Ebers. (*Bell Syst. tech. J.*, vol. 34, pp. 883–902; September, 1955.) Minority carriers accelerated in the high-field-strength region of a reverse-biased junction produce hole-electron pairs by collision with atoms. The action may be made cumulative, resulting in avalanche multiplication, which may be controlled by an emitter junction placed close to the multiplying collector junction. The theory of the process is presented and applications to circuits for switching and transmission are discussed. See also 2781 of 1955 (Kidd et al.).

621.314.7 294

Variation of Junction-Transistor Current-Amplification Factor with Emitter Current—L. J. Giacoletto. (PROC. IRE, vol. 43, p. 1529; October, 1955.) Using suitably chosen constants, the theory presented by Webster (2798 of 1954) can be experimentally verified for n-p-n as well as for p-n-p transistors.

621.314.7:537.311.33 295

The Theoretical Temperature Coefficient of a Junction Transistor—E. Groschwitz. (*Z. angew. Phys.*, vol. 7, pp. 280–282; June, 1955.) The p-n-p junction transistor is considered on the basis of Shockley's theory. If the collector voltage is chosen so that the collector operates in the saturation region, the emitter and collector currents are functions of the emitter voltage only and hence the temperature coefficient of the resistances can be determined. Calculations lead to results similar to those obtained for the p-n junction (3298 of 1955), where the principal term in the expression for the temperature coefficient is negative and voltage dependent, and the second term is positive and dependent on the carrier lifetime and the width of the base zone.

621.383.27+621.385.15 296

Statistical Problems of the Electron Multiplier—L. Yanoshi (Jánossy). (*Zh. eksp. teor. Fiz.*, vol. 28, pp. 679–694; June, 1955.) Two problems are considered: (*a*) the probability $P_N^{(k)}(\nu)$ of ν electrons being emitted by the Nth electrode if k primary electrons are incident on the first electrode, and (*b*) the distribution of $P(\nu)$, the probability of ν secondary electrons being emitted in response to the incidence of one primary electron, required to obtain a given distribution $P_N(\nu)$ after N steps.

621.383.27 297

The Characteristics of Photomultiplier Tubes and their Use for Absorption Measurements—K. W. Keohane, and W. K. Metcalf. (*J. sci. Instrum.*, vol. 32, pp. 259–260; July, 1955.) The cathode uniformity of Type-1P21 photomultipliers was examined by using a calibrated electrical attenuator to adjust the output of a comparison photomultiplier to equality with that of the tube under test, which was moved past a slit. The signal strengths used were sufficiently low to avoid fatigue effects. Variations in the characteristics were found to be within the experimental error (of the order of 0.5 per cent); the area of maximum sensitivity of the photocathode was determinable to the same accuracy and the input/output characteristics, in the range 2–0.05μA, were linear. The greater nonuniformity indicated in the results obtained by Edels and Gambling (*J. sci. Instrum.*, vol. 31, p. 121; 1954) is considered due to the experimental methods adopted.

621.383.27 298

A Method of Estimating Photomultiplier Pulse Durations and Shapes—B. Meltzer, J. A. Lodge, and P. L. Holmes. (*J. sci. Instrum.*, vol. 32, pp. 270–271; July, 1955.) The spectral output of a photomultiplier being given by the Fourier transforms of the current pulses initiated by individual photons incident on the photocathode, measurements of the output frequency spectrum may be used to show the average shape and duration of the pulses. Some experimental tests are described.

621.383.27 299

A Photomultiplier Tube for Scintillation Counting—R. Champeix, H. Dormont, and E. Morilleau. (*Philips tech. Rev.*, vol. 16, pp. 250–257; March, 1955.) The tube described has ten stages of secondary emission, giving an overall current amplification of 500000. The area of the $SbCs_3$ photocathode is 5 cm^2; a Wehnelt cylinder focuses the photoelectrons on the first dynode; a staggered arrangement of curved dynodes is used. Steps are taken to keep the inherent noise level low. The tube is suitable for spectroscopy as well as scintillation counting.

621.385.029.6 300

Power Flow in Electron Beams—L. R. Walker. (*J. appl. Phys.*, vol. 26, pp. 1031–1033; August, 1955.) An alternative approach to that used by Louisell and Pierce (2145 of 1955) is indicated for determining the flow of microwave power in an electron beam in a weak field.

621.385.032.216 301

Measurement of Excess Ba [and/or Sr] in Practical Oxide Coated Cathodes—L. A. Wooten, G. E. Moore, and W. G. Guldner. (*J. appl. Phys.*, vol. 26, pp. 937–942; August, 1955.) Over 300 cathodes of various designs were aged for periods up to 50,000 h, tested for emission and then analyzed chemically. The complexities and limitations of the available methods of analysis are discussed. The measure of Ba content significant for emission is taken as the amount of H_2 formed on 16 h exposure.

621.385.032.216 302

Excess Ba Content of Practical Oxide Coated Cathodes and Thermionic Emission—G. E. Moore, L. A. Wooten, and J. Morrison. (*J. appl. Phys.*, vol. 26, pp. 943–948; August, 1955.) Measurements on 125 indirectly heated and 15 directly heated cathodes are reported; methods described in 305 above were used. The evolution of H_2 by uncoated cathodes was also measured. No correlation was observed between the excess Ba Content and the emission, and it is inferred that in practice cathode performance is seldom limited by excess Ba.

621.385.1 303

On the Space-Charge-Limited Current between Nonsymmetrical Electrodes—G. D. O'Neill. (*J. appl. Phys.*, vol. 26, pp. 1034–1040; August, 1955.) "The validity of employing an equivalent symmetrical anode for expressing the space-charge-limited current between nonsymmetrical electrodes is examined. It is shown that when the equivalent anode is determined by the capacitance, the error in the expression for the current is usually quite small and its approximate magnitude may often be anticipated. Exact expressions for the capacitance of some basic electrode arrangements are given, followed by a brief resumé of corrections required for interpretation of experimental data."

621.385.832:621.374.4 304

Generation of Harmonics of a Given Fundamental—Katz and Rau. (See 61.)